AD_____

MIPR NO: 93MM3517

TITLE: METHOD FOR THE TECHNICAL EVALUATION OF RUGGEDIZATION OF A CT SCANNER

SUBTITLE: Linear Finite Element Analysis of a Prototype Ruggedized Commercial CT Scanner

PRINCIPAL INVESTIGATOR: Charles H. Robinson

CONTRACTING ORGANIZATION: U.S. Army ARDEC, Fuze Division
Applied Fuze Technology Branch
ATTN: SMCAR-AEF-T
2800 Powder Mill Road
Adelphi, Maryland 20783-1197

REPORT DATE: December 30, 1993

TYPE OF REPORT: Final Report

PREPARED FOR: U.S. Army Medical Research, Development, Acquisition, and Logistics Command, (Provisional), Fort Detrick, Frederick, Maryland 21702-5012

DISTRIBUTION STATEMENT: Approved for public release; distribution unlimited

The views, opinions and/or findings contained in this report are those of the author(s) and should not be construed as an official Department of the Army position, policy or decision unless so designated by other documentation.

REPORT DOCUMENTATION PAGE

Form Approved
OMB No. 0704-0188

1. AGENCY USE ONLY (Leave blank)	2. REPORT DATE	3. REPORT TYPE AND DATES COVERED
	30 December 1993	Final Report (1/1/93 - 12/31/93)

4. TITLE AND SUBTITLE Method for the Technical Evaluation of Ruggedization of a CT Scanner Subtitle: Lintar Finite Element Analysis of a Prototype Ruggedized Commercial CT Scanner

5. FUNDING NUMBERS

MIPR No.
93MM3517

6. AUTHOR(S)

Charles H. Robinson
Robert H. Wood

7. PERFORMING ORGANIZATION NAME(S) AND ADDRESS(ES)

U.S. Army ARDEC, Fuze Division
Applied Fuze Technology Branch, ATTN: SMCAR-AEF-T
2800 Powder Mill Road
Adelphi, Maryland 20783-1197

8. PERFORMING ORGANIZATION REPORT NUMBER

9. SPONSORING / MONITORING AGENCY NAME(S) AND ADDRESS(ES)

U.S. Army Medical Research, Development, Acquisition, and Logistics Command (Provisional)
Fort Detrick, Frederick, Maryland 21702-5012

10. SPONSORING / MONITORING AGENCY REPORT NUMBER

11. SUPPLEMENTARY NOTES

12a. DISTRIBUTION / AVAILABILITY STATEMENT

Approved for public release; distribution unlimited

12b. DISTRIBUTION CODE

13. ABSTRACT *(Maximum 200 words)*

A linear finite element model was created to predict the response of a prototype ruggedized CT scanner system's components when exposed to extremes of the logistical environment. Ruggedization consisted of mounting the three components (operator console, patient table, and gantry) of the commercial scanner individually on wire rope shock isolator assemblies inside a single-side-expandable ISO shelter in its stowed configuration. Clinical use requires expansion of the shelter, movement of the patient table into the expanded section, and lowering of the gantry down off its isolation mounts onto the shelter floor. The prototype's shock isolation system performance was characterized in the analysis. Dynamic response to three logistical inputs was calculated: vertical drop, rail impact, and lateral impact. The presence of gravity was modeled so that static offsets would be present prior to simulated shock exposures. The calculated responses included scanner component deflections and accelerations, shelter floor deflections and stresses, and stresses in the floor subframe. Issues such as adequacy of sway space zones, overtravel of the isolators, and damped vibration amplitudes in transportation vibration were analyzed.

14. SUBJECT TERMS	15. NUMBER OF PAGES
Ruggedization, CT Scanner, Linear Finite Element Analysis, Commercial, Analysis	16. PRICE CODE

17. SECURITY CLASSIFICATION OF REPORT	18. SECURITY CLASSIFICATION OF THIS PAGE	19. SECURITY CLASSIFICATION OF ABSTRACT	20. LIMITATION OF ABSTRACT
Unclassified	Unclassified	Unclassified	Unlimited

FOREWORD

Opinions, interpretations, conclusions and recommendations are those of the author and are not necessarily endorsed by the US Army.

____ Where copyrighted material is quoted, permission has been obtained to use such material.

____ Where material from documents designated for limited distribution is quoted, permission has been obtained to use the material.

CHR Citations of commercial organizations and trade names in this report do not constitute an official Department of Army endorsement or approval of the products or services of these organizations.

____ In conducting research using animals, the investigator(s) adhered to the "Guide for the Care and Use of Laboratory Animals," prepared by the Committee on Care and Use of Laboratory Animals of the Institute of Laboratory Resources, National Research Council (NIH Publication No. 86-23, Revised 1985).

____ For the protection of human subjects, the investigator(s) adhered to policies of applicable Federal Law 45 CFR 46.

____ In conducting research utilizing recombinant DNA technology, the investigator(s) adhered to current guidelines promulgated by the National Institutes of Health.

____ In the conduct of research utilizing recombinant DNA, the investigator(s) adhered to the NIH Guidelines for Research Involving Recombinant DNA Molecules.

____ In the conduct of research involving hazardous organisms, the investigator(s) adhered to the CDC-NIH Guide for Biosafety in Microbiological and Biomedical Laboratories.

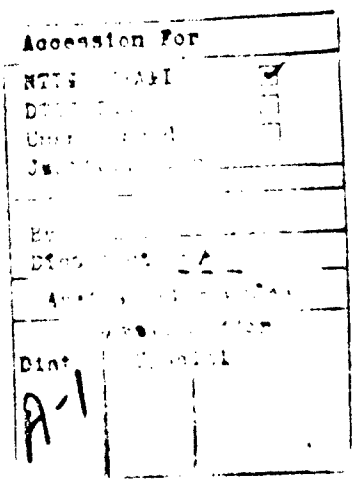

12-30-93

PI - Signature Date

ABSTRACT

A linear finite element model was created to predict the response of a prototype ruggedized CT scanner system's components when exposed to extremes of the logistical environment. Ruggedization consisted of mounting the three scanning components (operator console, patient table, and gantry) of the commercial scanner individually on wire rope shock isolator assemblies inside a single-side-expandable ISO shelter in its stowed configuration. Clinical use requires expansion of the shelter, movement of the patient table into the expanded section, and lowering of the gantry down off its isolation mounts onto the shelter floor. The prototype's shock isolation system performance was characterized in the analysis. Dynamic response to three logistical inputs was calculated: vertical drop, rail impact, and lateral impact. The presence of gravity was modeled so that static offsets would be present prior to simulated shock exposures. The calculated responses included scanner component deflections and accelerations, shelter floor deflections and stresses, and stresses in the floor subframe. Issues such as adequacy of sway space zones, overtravel of the isolators, and damped vibration amplitudes in transportation vibration were analyzed.

TABLE OF CONTENTS PAGE

1. Introduction

This report details the analysis of ruggedization of a prototype CT scanner system designed to withstand the logistical shock and vibration environment.

The ruggedized scanner under analysis was developed by Picker International Inc., as a demonstration prototype. It consisted of the three system units or "components" of the Picker IQ model scanner: the gantry, patient table, and the operator console, weighing 3800, 800 and 700 pounds, respectively. All three components were mounted inside a single-side-expandable ISO shelter. The gantry and console remained in fixed locations in the shelter, while the patient table was movable. To prepare the system for operation, the shelter was expanded and the patient table was moved into its operating position against the gantry. In its operating position, part of the table extended into the expanded portion of the shelter.

Picker's approach to ruggedization was to mount each component on its own system of helical wire rope isolators. Load spreader plates were used to interface the isolators to the ISO shelter floor without exceeding the floor point-load and distributed-load limits under dynamic loading during transportation. The console remained approximately 2 inches above the floor on its isolators even during operation, but the gantry operated while resting on the floor, and was screw-jacked up onto its isolator mounts in preparation for transport. When on the isolators, the base of the gantry was 2 to 3 inches above the floor. The patient table was similarly jacked up onto its isolators for transport, being normally fixed to the floor in position between the gantry and console, and then for operation was lowered about 2 inches onto the floor and moved into place perpendicularly against the gantry once the shelter was expanded. Figure 1 shows the layout in the stowed and operational configurations. The arrows in the figure indicate the direction of motion prior to the shocks or impacts that occurred later in model space. The axis conventions used throughout the analysis are also indicated. Figure 2 shows the actual prototype in its operating configuration.

This analysis stands on its own, but we originally planned to validate the model by comparing its predictions against the response of the actual prototype system in an instrumented test. Such a test was designed, and transducers were ordered, but we could not perform the test in advance of this writing because the prototype scanners were not available, being in nearly constant clinical use. An equally detailed analysis of another prototype, a ruggedized GE Sytec 3000 scanner system, was begun but was not completed when it was determined that a GE unit would not be available for model validation testing.

2. Objective

The purpose of the analysis was to determine whether the prototype ruggedized scanner system, as embodied in the ruggedized Picker IQ system, would survive the logistical environment. Various deployments, including a tour of operation in support of operation Desert Storm, already demonstrated that the Picker unit's ruggedization was adequate for many handling and transportation scenarios. However, it was necessary to go beyond this anecdotal evaluation. The objective was to more scientifically evaluate and define the prototype's shock isolation system performance to provide the basis for evaluating this and other systems against the ruggedization specification.

3. Approach

There were several possible approaches to evaluating ruggedization. One was to evaluate the ruggedization by subjecting the prototype system to steadily increasing shock inputs until either a failure occurred or the limits of the logistical environment were reached. But such an approach, though sufficient to show the first failure limit, would leave the situation indeterminate as to other limits or design margins, and would risk damaging unique prototype equipment.

Instead of risking the equipment in a full logistical level test, another approach was considered--it was proposed to create a finite element model of the system, then exercise the model to the limits of the logistical environment, to see what forces and deflections would develop. This would answer the question, "Is the isolation system adequate?"

A refinement to that approach was to perform an instrumented test of the prototype system under low-intensity (non-destructive) impacts, then compare observed response to predicted response to bring the computer model into line. The validated computer model could then be used to more accurately predict the outcome of testing at the full logistical levels. This concept is diagrammed in figures 3 and 4. This method of validating the model at low dynamic levels to enhance the model's prediction accuracy at the full dynamic levels had the best chance of predicting the outcome of the first article test (FAT) while avoiding the necessity of risking damage to the one-of-a-kind scanner system to find out.

As was stated earlier, however, the ruggedized scanner prototype was not available for testing prior to this writing. Instead of having the model validated by test data, we have proceeded with the analysis on its own. This analysis will

help to establish guideline values for parameters such as damped natural frequency, maximum allowable peak acceleration of the shelter, scanner component mass limitations, strength limits of the ISO shelter floor, and minimum sway space around each component. These values will allow competing ruggedized scanner prototypes to be evaluated against a system with characterized properties.

If the computer model predicts that the prototype ruggedized CT system will meet the ruggedization specification, it may be that no adjustments need to be made either to the scanner or to the FAT. This cannot be determined until the model is validated by testing. But if the model predicts failure--i.e., that structural limits or sway space limits will be exceeded, the ruggedization will have to be improved, or a reduced-level test can be written. In any case, the computer model makes it possible to more scientifically evaluate the ruggedization--to estimate how closely the installed ruggedization of the prototype comes to meeting the specification, or to evaluate design tradeoffs for improved ruggedization.

4. Model Construction

The ruggedized scanner system was analyzed using a linear finite element analysis (FEA) program called GIFTS. The analysis was accomplished in the following steps:

1. mass, structural, and geometric data were gathered on the scanner components and the ISO shelter structure.
2. a finite element model was made of the ISO shelter structure with particular detail devoted to the floor panel, its structural subframe, and the boundary conditions at its interfaces with the wall panels.
3. modes and natural frequencies of the unloaded shelter floor were calculated.
4. "rigid body" finite element models of each scanner component were constructed, striving to match mass, center of gravity, and moments of inertia.
5. spring, mass, and damping equivalents of the shock isolators were developed, paying attention to the differing load deflection curves of each isolator in its different axes.
6. dynamic loading functions simulating vertical drop, rail impact, and lateral impact from the logistical environment were developed.
7. shelter floor stresses resulting from the above dynamic loadings on the assembled model were calculated.
8. each scanner component's natural modes and frequencies were calculated and depicted.
9. component stress and deflection histories under the three dynamic loadings were calculated and compared.

10. one-degree-of-freedom free-vibrational response (frequency response function) was calculated for each component, to determine response to transportation vibration inputs.

a. ISO Shelter Modeling

The ISO shelter model is shown in figure 5. The wall and ceiling panels of the shelter are not explicitly modeled, but their effects are taken into account in the specification of the boundary conditions applied to the perimeter nodes of the floor structure, which was itself modeled in some detail. The floor structure consists of a subframe and a sandwich-composite floor panel. The shelter model simulates the aluminum subframe using defined beam sections, and simulates the honeycomb-core/aluminum-skin sandwich floor panel using horizontal plate elements for the aluminum skin and a network of small vertical plate elements to model the honeycomb core. To model the shelter floor panel accurately, additional nodes and elements were added to the regular floor grid where scanner component baseplate attachment points did not match the existing node structure.

The boundary conditions applied to the edges of the floor panel were as follows: the floor panel was allowed to expand laterally, because the walls would not be able to strongly constrain this, but the floor panel edges were completely restrained from vertical motion. Pivoting was allowed at the joint between the floor panel and the wall panels. The four corner nodes of the floor panel were clamped in five of the six freedoms. The only freedom allowed at the corner nodes was rotation about a vertical axis.

It was necessary to include damping in the model--all real objects in flexure experience viscous, structural or Coulombic (frictional) damping. A structure such as the floor panel typically exhibits "structural" damping, which requires complex variables (imaginary numbers) to define. The GIFTS program could not model true structural damping, so the effect was approximated by simulating it as viscous damping, distributed evenly among the nodes in the floor panel mesh. An approximate value for the damping was obtained by calculations based on information presented in reference 1, whose investigator concluded from test data that the floor of a fully loaded ISO shelter was near-critically damped. Some of that damping may have been "borrowed" from the unspecified payload (probably sandbags), but a reasonably high amount of damping is still plausible, considering the construction materials used in the floor panel--which was constructed of two 0.63 inch aluminum sheets, press-bonded by an epoxy-melt later to a three-inch paper/epoxy composite honeycomb core.

The above considerations provided only an approximate value of damping for the floor panel, but that was all that was necessary because the influence of this value was minimal, for two reasons. First, the floor's own first natural frequency was more than ten times higher than those of the isolated components, as will be shown later. This means that the floor panel would go through at least five vibrational cycles with damping before even the fastest of the isolated components would complete a half vibrational cycle. This meant that floor vibrations would be significantly attenuated before they affected the isolated components. Second, the amplitude of floor motion was negligible compared to motion of the isolated masses.

b. Scanner Component Modeling

Each of the three scanner components was modeled by defining and arranging plate elements such that for each component, the mass and center of gravity matched those of the real one, and the moments of inertia were approximately the same as those of the real ones. The overall arrangement of the components is shown in figure 6. Figure 7 shows increased detail, including the shock absorber elements, and figures 8 and 9 give the node numbers which are referred-to later to analyze motion.

All three components were treated as rigid bodies. This rigid-body approximation was acceptable in this analysis because, with the relatively much larger deflections allowed by the shock isolators, it was not necessary to model the components as flexible structures. All component flexures would be negligibly small compared with their own gross motions on the isolators.

c. Shock Isolator Modeling

Picker used Aeroflex helical wire rope isolators, four of model CB1700-15 under the gantry, and four each of model CB1400-17 under both the console and patient table. These isolators are relatively insensitive to changes in temperature, and they exhibit a high amount of damping due to flexural hysteresis (rubbing between the strands of the wire rope). The hysteretic damping was approximated as viscous damping in the computer model. The damping values used in the model were calculated from dimensionless damping ratios (C/Cc) given in the product catalog.

d. Vibrational Response: Single Degree of Freedom Model

A simple one-degree-of-freedom damped free-vibrational response was calculated for each component using application software from Barry Controls, of Barry Wright Corp. On the basis of input parameters such as component weight, isolator springrate (the sum of the four isolators under each component), and isolator damping ratio, the resonant frequencies were calculated and are shown in table 1 below. Values for isolator spring rates were obtained from Aeroflex product catalogs, and damping ratios were calculated from figures presented in the same source. The results of this simple model were useful as a check on the more detailed analysis which follows.

Component weight values given in table 1 differ somewhat from the weights listed in the Picker IQ model brochure. The values used here were obtained from the ruggedization design analysis report written by Aeroflex International, Inc., for Picker. We do not know why the somewhat lighter values were used, but perhaps they can be attributed to changes which Picker made in the hardware used in the prototype, such as replacing the console top with a smaller and lighter one.

Table 1. Tabulation of results of simple one-degree-of-freedom damped free-vibrational response calculation.

Scanner Component	Component Weight, (lb.)	Isolator Springrate, (lb./inch)	Damping Ratio, C/C_c	Calculated Resonant Frequency, (Hz)	Resonant Amplitude in Secured Cargo Basic Transportation (vertical)
Operator Console	400	4120	0.19	9.71	.092 inch rms
Patient Table	660	4120	0.15	7.65	.148 inch rms
Gantry	3400	15680	0.09	6.66	.236 inch rms

5. Load Idealization

The three dynamic input conditions being modeled were 12-inch flat drop impact, 10-mph rail impact (yielding a net velocity change of 8.5 mph), and 4.8 mph lateral impact, consistent with the extremes of the logistical environment. Each impact acceleration was modeled as a time-varying acceleration field applied to the shelter. Applying an acceleration impulse to the static, constrained shelter is the same, so far as the internal components are concerned, as bringing the moving shelter abruptly to rest.

The effects of gravity were included in the simulation. Normally, shock-isolated objects have a certain "static deflection" on their supports based on their weight, center of gravity, geometry, and the spring-rate of their isolators. It was advantageous to model, from the beginning, the static deflection due to gravity because it means that the calculated

and plotted outputs automatically incorporate the static deflection.

In real life, this static deflection already exists at the time an inadvertent rail impact or lateral impact occurs. But it is a limitation of the simulation model that it begins with its geometries defined ideally, in other words, with zero deflection at time t=0. This does not match reality, so gravitation must be expressly applied before applying the intended shock loads.

But applying gravity suddenly at t=0, in order to accomplish this, puts each component into a vertical oscillation at its damped natural frequency at the beginning of the simulation. It would obscure the results if the intended shock loads were applied at the same time t=0, before the gravity-transient response damped out. Therefore, gravity was applied as necessary, and the models were run from t=0 to t=0.8 seconds to allow the gravity-induced oscillation to damp out, before the idealized shock loads were applied.

a. Longitudinal and Lateral Impact Idealization

Lateral impact involved a velocity change of 85 in/sec (4.8 mph), and longitudinal impact involved a velocity change of 150 in/sec (8.5 mph). These idealized load sequences are depicted in figures 10a and 10c for the lateral shock and rail shock inputs. Direction of motion prior to impact is indicated by the arrow markings in figure 1. A time step of 5 msec was selected for the analysis. One and a half seconds of response output was needed, giving a total of 300 saved time steps per loading case. Of the 1.5 seconds, 0.7 sec was to observe the impact response, and 0.8 sec was available at the beginning to allow the gravitation pulse response to occur and damp out. These 0.8 and 0.7 sec response windows will be apparent later when the time traces are shown.

b.Vertical Impact Idealization

The situation was more complicated with 12-inch drop shock, as shown in figure 10b, because a dropped object goes from experiencing 1g when static to experiencing 0g as it accelerates from release until impact, when it also experiences 1-g again. So the loading simulation began in the same way as above, with gravity applied at t=0, and the resulting transient response settling out for only 0.75 sec in this case. But upon being dropped at t=0.75 sec, the shelter saw 0g again, for the time required to fall from 12 inches. Then gravity resumed at the same time the impact acceleration was applied, as shown. The

remainder of the time out to 1.50 sec was the oscillation "response" of the isolated system.

Vertical impact involved a velocity change of 95 in/sec (5.5 mph), assuming no rebound (bounce).

6. Predicted Mode Shapes and Vibrational Response

Mode shapes and natural frequencies are shown in figures 11 through 31. These include the first six vibrational modes of each of the three shock-isolated scanner components, and the first two modes of the non-loaded floor panel.

Mode shapes depict the ways a flexible or flexibly mounted body "likes" to vibrate, and they occur at the body's "natural frequencies." Any dynamic input to a system will tend to set the bodies into motions that will be resolved into the nearest available modes at the nearest available natural frequencies. For example, a rail impact is likely to excite or favor certain modes, and a vertical drop is likely to excite certain other modes. A steady vibrational input will tend to excite bodies in natural frequencies near the vibrational input frequencies.

When the center of gravity of an isolated body is not co-located with its center of geometry or lying directly above the center of influence of the isolation system, there is a certain amount of complex motion that occurs. This is because every induced motion is not resisted symmetrically by the isolation devices, creating twisting moments that tend to couple the motion into other natural modes. The console is fairly symmetric, but the gantry and particularly the patient table exhibit this asymmetry in their responses.

a. Console Modes

Mode 1 occurs at 1.99 Hz (figure 11). It is a simple rocking motion, occurring in the longitudinal (shelter axis) direction about the console base, and appears to work the isolators out of phase in tension and compression. This mode presents a risk of damage due to interference of the console top with the patient table, if excited to too great an amplitude. Rail impact is likely to excite this mode quite easily.

Mode 2, at 3.87 Hz, appears to be more of a combination of gliding and rocking, in the lateral (shelter axis) direction, working the isolators in phase in shear, and out of phase in tension/compression (figure 12). A lateral impact is likely to excite this mode.

Mode 3 occurs at 7.23 Hz (figure 13), and is a twisting or "yaw" motion about the console's vertical center axis, working the isolators in phase in both shear and tension.

Mode 4, at 9.68 Hz, is a pure up and down bouncing motion, working the isolators in phase vertically (figure 14). This mode is likely to be excited in a vertical drop situation. The one-degree-of-freedom model cited earlier predicted a very similar frequency for this mode, 9.71 Hz.

Mode 5 occurs at 11.9 Hz, and appears to be a sweeping motion in the lateral (shelter axis) direction, with the top and base moving in opposite directions (figure 15). The isolators are worked in phase in shear and tension.

Mode 6 appears similar to Mode 5, but is a sweeping motion in the longitudinal (shelter axis) direction, occurring at 12.7 Hz (figure 16).

b. Patient Table Modes

Mode 1 occurs at 2.58 Hz (figure 17), as a rocking motion about the base on the table's long axis. The patient table's being mounted at an oblique angle to the shelter axes makes it unclear which modes will be excited by certain inputs. However, this one is likely to be excited by a lateral or longitudinal impact.

Mode 2, at 6.76 Hz, appears to be a combination endwise gliding and rocking motion, working the isolators in shear, in-phase with tension (figure 18).

Mode 3, at 7.47 Hz, is a vertical bouncing motion, working the isolators in phase (figure 19). There is some endwise motion in this mode, probably caused by the center of gravity not being located above the center of the isolation system. This mode is likely to be excited in a vertical drop. The single-degree-of-freedom model predicted this mode at 7.65 Hz. It is probable that the GIFTS model predicts a lower frequency because of the slight compliance of the shelter floor.

Mode 4, at 8.73 Hz (figure 20), is a twisting or "yaw" type motion about the patient table's vertical center axis, working the isolators in phase in both shear and tension.

Mode 5 occurs at 9.90 Hz as a see-saw rocking motion. Figure 21 shows the isolator and table-end actually going *below* the shelter floor. This is only an appearance because of the large scale factor used to dramatize the motion.

Mode 6 occurs at 11.2 Hz as a sweeping or "roll" motion about the table's long axis. Isolators are worked in phase in both shear and tension (figure 22).

With the center of gravity of the patient table not located at the center of geometry or above the isolation system's center, it is easy to see how these modes might interrelate, where the energy from one mode may be able to excite motion with another near-frequency mode. For example, a motion that starts out as primarily Mode 1 motion might couple some of its energy into modes 4, 5, or 6 motion.

c. Gantry Modes

Mode 1 (figure 23) occurs at 6.28 Hz as a vertical bouncing motion. This is likely to be excited by a vertical drop situation. The single-degree-of-freedom model predicted this mode would occur at 6.66 Hz. Again, the difference in frequency is due to the compliance of the shelter floor.

Mode 2, at 7.26 Hz, appears as a lateral glide (figure 24). The motion of the top is shown by the deformation of the two motion limiter elements placed on top of the gantry to limit sway. They look like TV antennas in the figures, with the far ends attached to the ceiling panel. Again, the deflections are exaggerated for viewing.

Mode 3, at 7.34 Hz, appears as a gliding endwise motion without much rocking (figure 25). The whole gantry appears to oscillate by moving back and forth parallel to the x-ray imaging plane. The motion-limiter elements on the top of the gantry show deformation in the same direction and phase as the base, with no vertical movement, which supports the gliding interpretation. The isolators are worked in shear and tension.

Mode 4, at 9.49 Hz, is a twisting motion about a vertical axis through the center of the gantry (figure 26).

Mode 5, at 10.8 Hz, is a sweeping or roll motion about an axis parallel to the gantry tilt axis (figure 27). The isolators are worked in phase with one another, but out of phase with the motion limiter on top of the gantry.

Mode 6 occurs at 10.9 Hz as a see-saw rocking motion (figure 28) about the gantry rotor axis.

It is significant that the frequencies of modes 2 and 3, and modes 5 and 6 are almost right on top of one another. It is likely that energy can pass easily between modes so nearly co-located on the frequency spectrum.

d. ISO Shelter: Floor Panel Modes

Mode 1 occurs at 91.6 Hz, as a "trampoline" mode (figure 29).

Mode 2 occurs at 100 Hz, in a symmetrical out-of-phase dual trampoline mode deflection (figure 30).

When loaded down with the scanner elements and the isolation system, the shelter floor first mode occurs at 90.3 Hz, as shown in figure 31. Notice the floor reaches its bottom position (exaggerated scale) with no apparent movement of the scanner components. This is due to the isolation. The floor oscillates at a frequency well into the isolation region of the scanner components.

This analysis shows that the shelter floor is sufficiently rigid to allow the scanner component motions to be analyzed independently--as "uncoupled." In other words, there is not enough flex in the floor, relative to the motions of the components on their isolators, to allow, for example, the motions of the gantry to be significantly affected by the motions of the patient table or of the patient table to be affected by motions of the console, etc.

7. Predicted Response to Mechanical Shock

Mechanical stresses discussed in this section are titled "von Mises Criteria" in the figures. The Huber-Henchy-von Mises theory (also called the maximum-distortion-energy theory) gives the best predictions of failure in ductile materials. The aluminum floor-panel skin material and the welded aluminum subframe are examples of ductile materials. Von Mises criterion values given in the figures are to be read as "percentage of yield strength for the material." In other words, an isostress line valued at 1.600E+01 corresponds to a stress contour at 16 percent of the yield stress. Displacements are given in units of inches.

Acceleration time trace predictions are to be read in acceleration units of inches/sec^2. The charts must be read carefully, as the amplitude scales on the time trace plots may be different for each trace.

a. 12-inch Vertical Flat Drop

Figure 32 shows the response of the scanner components to the vertical drop impact (exaggerated scale), at 1.050 sec into the simulation, or 50 msec after beginning of impact. Figure 33 shows the same thing but with the component deflections plotted in scale. The time frame at t = 1.050 sec was se-

lected to correspond roughly to the moment of greatest average stress or acceleration of the three scanner components under this loading.

The deflections and stresses induced in the shelter floor at the selected time are elaborated in figures 34 to 36. The figures show that the greatest displacements and stresses occur under the inboard footing of the gantry. The stress detail in figure 36 shows that stresses reached a maximum of 65 percent of yield strength in the floor panel surface, assuming no load-spreader plate is used. If some contours in the figure appear to be redundant, it is because the figure shows stresses on both the top and bottom surfaces of the floor panel in the same view.

Figure 37 shows the deflection of the subframe (exaggerated scale) at the same moment in the simulation. Figure 38 gives the maximum normal and shear stresses found in the beams of the floor substructure. In one place in the subframe, stress is predicted to reach 61 percent of yield stress.

In figures 39 through 48 are shown the time traces of deflection and acceleration at selected representative nodes. The node locations were shown earlier in figures 7 through 9. For the time traces, the alluded-to "freedoms" are:

freedom 1 = x, or parallel to the shelter longitudinal axis
freedom 2 = y, or vertical
freedom 3 = z, or lateral to the shelter main axis

In the time traces, as was mentioned before, the first part of the response is due to the application of gravity acceleration at the beginning of the simulation. That response is meant to damp out sufficiently by the time the intended load is applied.

In reading these charts it is important to pay attention to both the "scale" and to the "freedom." In figure 39, the trace for point 306, freedom 1, appears to have a significant motion prior to the impact, which occurs at t = 1.0 sec. But using the scale, this motion is observed to have a zero-to-peak amplitude of only 0.001 inch, and even after the impact the motion in the "1" direction is small. However, the trace for point 306, freedom 2, has a different scale, and the static offset after gravity is applied is seen to be about 0.1 inch, the response after gravity is removed (free fall) is seen to damp out, and the dynamic response upon impact has a peak value of about -1.3 inches.

b. 10-mph Rail Impact

Figure 49 shows the response of the scanner components to the rail impact, at 0.84 sec into the simulation (40 msec after beginning of impact). A rail car impact at 10 mph leads to a combined-mass velocity of 1.5 mph, meaning the CT scanner system undergoes an 8.5 mph net change in velocity during the impact. Figure 50 is the same response as in figure 49, but without the exaggerated deflection scale. The time frame at 0.84 sec was chosen to correspond to the moment of greatest average deflection of the three components, which all appear to be near the extreme left extent of their travel. The three components do not reach maximum deflection at the same time, however. Notice that the motion limiters on top of the gantry have minimized its ability to heel over the way the console has.

Figures 51 and 52 show the longitudinal and vertical displacement contours in the floor panel, with a maximum vertical displacement of -.02 inches and a maximum longitudinal displacement of -0.14 under the inboard gantry footing. Figures 53 and 54 show floor panel stresses under the deflected components. The stresses are greatest around the console footings, and around the outboard gantry footing, where the maximum 22 percent of yield stress was reached. Figure 55 shows the floor panel subframe deflections, with an exaggerated scale. Figure 56 gives the maximum normal and shear stresses found in the floor substructure beams at the selected time "snapshot". These amount to 24 percent of the yield stress.

Figure 57 shows the rail impact response at a later time in the simulation, at 0.930 seconds (130 msec after impact). Figure 58 is the same response without the exaggerated scale. These figures provide an interesting contrast to figure 49. In the figure 49 snapshot, all three components were deflected to the left, and their motions appeared to be "in phase." But in this frame, at 0.93 seconds, the components have bounced back at different rates (because they each have different natural frequencies and modes), so that now they appear somewhat out of phase. The console and the patient table, in particular, may be in some danger of colliding as they are closely placed and are starting to move out of phase with one another. When the console has gone through only three quarters of its first cycle, the patient table has gone through 1.25 cycles, putting them 180 degrees out of phase while their motion is still at fairly high amplitudes. The same situation exists between the couch and the gantry. It is this condition (out-of-phase motion, and near proximity) that should be used to set sway-space allocations in the design.

Figures 59 and 60 show floor panel stresses under the deflected components, 130 msec after impact. The stresses are

greatest around the console footings, where the maximum of 24 percent of yield stress was reached. Note that this stress figure exceeds the stress level under the gantry footings in the earlier time "snapshot." Figure 61 shows the floor panel subframe deflections, with an exaggerated scale. Figure 62 gives the maximum normal and shear stresses found in the floor sub-structure beams at the selected time "snapshot". These amount to a maximum of only 6 percent of the yield stress.

Fortunately, damping in the isolators quickly reduces the amplitude of the motions, which means that any time after the components have completed their first one or two cycles of motion, amplitudes are down and the risk of collisions or overstress is gone. The critical period is in the first full cycle of the slowest component (the console). The fact that the stresses have gone down is apparent in the stress numbers given in figures 63 and 64.

An observation from this analysis is that sway space must be specified in a coordinated manner that takes into account the possibility that the dynamic response of adjacent components may become out of phase with one another. Sway space should be at least as large as the arithmetic sum of the maximum component deflections after one cycle of damping of each component.

In figures 63 through 77 are shown the time traces of deflection and acceleration at selected representative nodes. The node locations were shown earlier in figures 7 through 9.

c. Lateral Impact

Figure 78 shows the response of the scanner components 35 msec after lateral impact at 4.5 mph, deflections are to an exaggerated scale. Figure 79 shows the same response without the exaggerated scale. Stress contours are shown in figures 80 and 81. The maximum stress in the floor panel was 28 percent of yield, which exceeded by a few percent the maximum stress reached in the floor panel after rail impact. Deflections and stress maximums in the ISO-shelter floor substructure are shown in figures 82 and 83. Figures 84 through 98 show the time traces of deflection and acceleration at selected representative nodes.

Of greatest concern with the lateral impact response is the potential for inducing impact of the gantry or of the console against the shelter walls on the stowed-panel side of the shelter. Calculations showed that lateral motion was as great as 3.20 inches for the console top and 1.75 inches for the gantry.

8. Discussion/Summary

a. The Model

(1) When the gravity field was applied at time zero in the model simulations, to set up the "static offset" that exists in real systems before shock inputs are experienced, the time traces showed (in section 7), that the settle-out time for the gravity-induced transient was adequate. This can be seen, for example, in figure 45, the second and third traces. These traces are deflection versus time in the vertical direction at the inboard footing of the gantry. Viewing each trace from left to right, the bounce due to the sudden application of gravity (acceleration field) is shown to be about -0.5 inch in the first cycle. This motion damps out and settles, in about five cycles, at a static deflection of -0.25 inches. Almost nothing is left of the original gravity-induced transient by the time gravity is released, at about 0.75 sec, when free fall begins. At this point a similar transient is initiated, this time by the release of gravity (at the beginning of free fall). This second gravity-induced transient, however, does not have time to damp out before the shelter impacts the floor. Thus the observed response after impact is the combined result of the ongoing gravity-release transient response and the impact transient response. This matches reality.

(2) Hardware and Software Limitations: several adaptations or consequences resulted from characteristics or limitations in the analysis software and hardware.

First, the software could not model true structural damping (which is described by complex variables), so, as was said earlier, the structural damping in the floor panel was approximated as viscous damping. As it turned out, the actual value of damping used in the analysis turned out to be of little importance, as floor motion had negligible influence on the motion of the shock-isolated scanner components.

Second, practical limitations in the modeling software and hardware made it desirable to model the scanner components as rigid bodies. To model the components as flexible structures would have required a much larger computer model and considerably more engineering and manufacturing data than was available. The analysis showed, anyway, that component flexures would have been negligible compared to the much larger gross motions of the components on the shock isolators. Larger modeling capacity including the effects of component flexures would have returned essentially the same results in terms of gross body deflections and peak accelerations, which was our primary interest.

Third, there were tradeoffs among practical issues that had to do with making the calculations and storing and viewing the results, as follows:

(a) the first issue was disk storage capacity and computation time. Many data files were to be generated and stored, and load case computation cycle time had to be reasonable in order to cover the many load cases. This set practical limits on the total number of iteration steps to be used in each calculation.

(b) the second issue was output resolution. The shock responses had to plot smoothly, but going overboard on resolution would only translate into burgeoning computation time and dwindling disk storage.

(c) the third issue was the need to apply simulated gravity at time zero and allow enough time (three to five cycles of motion) for the response to settle at the static offset.

These tradeoffs led to the selection of an analysis time window of 1.50 seconds, with the first 0.8 seconds (or 0.75 sec in the vertical-drop case) for settling time after the application of gravity, and the remainder of the time (about 0.7 sec) devoted to observing the intended shock response. This 0.7 seconds was enough to observe from 3 to 5 complete cycles of motion of the isolated components. This was sufficient to note the amplitude and phase of component motions as they damped out, and to observe possible interferences between the components in motion and to determine the required sway space to prevent collisions against the shelter walls.

(3) Shelter Floor Panel: it was apparent from the analysis that the ISO shelter floor panel could be treated as rigid as far as component response was concerned. Due to the rigidity of the floor panel, the shock isolated scanner components are essentially dynamically uncoupled from one another. If the floor panel were more compliant, the scanner components' motions would begin to be influenced by one another through induced floor-panel motion, and it would be inaccurate to examine their motions as unrelated.

b. Load Idealization

A close analysis of the acceleration traces which apply to accelerations in the freedom-2 (vertical) direction will show an apparent anomaly. The applied acceleration fields (inputs) are superimposed on the acceleration output plots, an undesirable effect inherent in the software. This has to do with the way the modeling program, GIFTS, obtains the acceleration traces--it does so by twice differentiating the displacement traces. If an object experiences acceleration without displacement, GIFTS will produce an acceleration trace showing zero acceleration. But an object can be at rest and

still experience an acceleration due to gravity. The effect is that to be completely correct, 1-g needs to be added to all the vertical (freedom 2) acceleration traces, but only during the moments when gravity is being applied, i.e., not during free-fall. These vertical acceleration traces appear in figures 40, 42, 44, 46, 48, 64, 67, 69, 74, 76, 85, 88, 90, 95 and 97. The analysis is not adversely affected by this. The similar effect corresponding to the applied impact accelerations fields has been corrected-for in the traces as they are shown.

c. Mode Shapes and Vibrational Response

The first six (free vibrational) mode shapes and natural frequencies were calculated for all three scanner components. The first two mode shapes and natural frequencies were calculated for the shelter floor, and one for the loaded shelter floor. Observations from the mode shapes and resonance frequencies:

(1) All the component natural modes occur at frequencies within the transportation vibration spectrum, and some of them occur at frequencies below the effective isolation region of the isolation system. The main concern here is with the vertical modes, which are aligned with the dominant transportation vibrational input. This would be a grave concern, as these modes could gain large amplitudes in resonance, except that the amount of damping in the isolators and the large sway zones specified for the shock environment are more than sufficient to make the transportation vibration input not a threat. The resonant vertical vibration amplitudes of the components under basic transportation vibration was given in the last column of table 1.

(2) It is likely that energy will be traded among modes occurring at nearly the same frequencies, since centers of gravity are not co-located with centers of geometry of the scanner components. This means that a longitudinal rocking motion may quickly metamorphose into a sideways rocking motion. The implications are that shock input in one axis can lead to large deflections in an unrelated axis. This effect was seen in the animation video of scanner component motions presented to USAMMA in May 1992.

d. Response to Mechanical Shocks

(1) 12-inch Vertical Drop

A summary of the relevant extremes of motion and acceleration resulting from the vertical drop impact is given in table 2.

These data are gleaned from the information in figures 32 through 48, and from the mode shape predictions. Certain data are signified with ellipses, in the "maximum isolator travel" column. In those cases, the predicted amount of component travel exceeded the design limits of the associated isolator or motion limiter. A study of these design limits and a breakdown of motions in the isolator's own axes are given in table 3, which will be explained in more detail later.

In table 2, for the vertical drop, the analysis shows that shock isolation of all three components was sufficient to prevent acceleration peaks in excess of 15 g's, as shown in the first major column. This indicates the analyzed isolation system accomplishes an important goal. In the next major column are the "primary excited modes." It was noted earlier that imposed mechanical shocks will tend to excite certain of the natural vibration modes of shock-isolated components. Thus the vertical drop shock tends to excite console mode 4, see figure 14, which is "mode 12" among all the modes computed, and which occurs at 9.68 Hz. The amplitude of this excited mode on the first cycle (before attenuation due to damping) is 6.7 g-peak, as shown in the third sub-column.

In the next major column of table 2, values are given in the three shelter axes for "minimum sway-space required," in inches. This is the zone of space needed around each component to prevent collisions with other components or with the shelter walls under the given dynamic inputs.

In the vertical drop, of course, the sway space is needed primarily in the vertical direction. It can be seen looking down the "minimum sway-space required" column of table 2 that the maximum vertical "sway" of the gantry in the vertical direction is 2.36 inches (absolute value). This same number can be found in Table 3, column 2, under the "y" sub column, also for the gantry.

Table 3 summarizes only the extreme maximum conditions experienced in all the mechanical shock environments. Note that the figure for the maximum vertical sway of the console as a result of the vertical drop, 1.25 inches, does not appear in table 3. This is because it is exceeded by a 1.90 inch maximum isolator displacement in the rail impact. Table 3 only summarizes the most extreme of the entries in table 2, i.e., it gives only the maximum accelerations experienced and the overall minimum required sway space for each scanner component.

As said before, those sway space requirements translate to zones around each component that must be vacant under these impact environments for no collisions to occur. A depiction of these minimum required sway zones is given in figure 99. Where each zone is defined, a second number is given in ellip-

ses which is the size of the zone in the prototype system, based on drawings and estimates. It will be noted that in four places, the sway zones of the prototype system are insufficient. Note, also, the zones apply in both the plus and minus directions along each axis--there is a rebound after each impact, and impacts to the shelter can come from any direction.

The next major column in table 2 gives "maximum isolator travel" in directions corresponding to the shelter axes. These numbers can differ from "sway space" when there is tilting of the components, as can be seen in the rail and lateral impact cases.

In the vertical drop condition, however, there is a different problem. The calculated vertical displacements of 1.87 inches (couch) and 2.36 inches (gantry) exceed the design limits of the isolators. The isolator design limits are given in the last major column of table 3, where the rated vertical (compression) travel limits are 1.6 inch for the couch and 2.0 for the gantry. Thus, the real isolators will "bottom out" in the vertical drop. In the simulation, the isolators are treated as linear for any amount of deflection. Hence, the peak acceleration values given in table 2 are assuming the isolators do not "bottom out." Bottoming out would result in higher acceleration peaks than this linear model predicts. If they did reach their limits, it is possible the isolators could be permanently deformed, or that the motion resistance (effective spring rate) could go up dramatically as the stops are approached, imparting much higher acceleration peaks to the isolated components than this analysis predicts.

In the third and fourth columns of table 3, the maximum isolator travel values are translated from the shelter axes (x,y,z) into the isolator's own axes (roll, compression, shear). This re-orientation is necessary because component motions, which are viewed in table 2 with reference to the shelter axes to determine interferences with the shelter walls and among the components, must also be viewed in terms of their effects on the isolators themselves. Since isolator force curves are only published in the isolator's own axes, the motions should be examined in that frame. Thus the telling comparison, so far as isolator overtravel is concerned, is between the fourth and fifth columns in table 3, where maximum predicted isolator travel in the isolator's own axes can be compared with maximum rated (allowed) dynamic travel of the isolators. On this basis, it is easy to see that at least some overtravel occurs with all three components, when the extreme environmental inputs are experienced.

A final problem must be considered. In the vertical drop environment, the predicted vertical compression of the gantry

isolators is 2.36 inches, which is enough to allow the pin-in-cup motion limiters to disengage (assuming the pins' insertion into the limiter cups is 1.7 to 2.25 inches vertically when the gantry is elevated onto its isolators). If lateral motion were present when such a vertical disengagement occurred, the pins could be diverted away from the limiter cups on the return trip, and remain outside the limiter cups, thus nullifying the motion restraint on top of the gantry. This would result in metal-to-metal contact and possible damage to the gantry structure or the shelter roof panel, and would markedly increase vulnerability of the gantry to ensuing shocks.

(2) 10-mph Rail Impact

Summary information similar to that covered for part (1) above is given in tables 2 and 3 for the 10-mph rail impact response. These data are obtained from the information in figures 49 through 77, and from the mode shape predictions. Maximum accelerations are predicted to slightly exceed the 15-g design goal in all three components at the baseplates, and in the gantry at the top.

In table 2, for the rail impact, shock isolation was not sufficient to prevent acceleration peaks in excess of 15 g's, as shown in the maximum acceleration column. A distinction was made between acceleration levels experienced at the base or at the top of each component ("high" or "low" in the table), as this sometimes made a large difference in the values obtained. For example, the console baseplate experienced 20.7 g's, while the top saw only about 5 g's in the rail impact. Figures for the top and bottom of the gantry are about the same because of the restraining action of the pin-in-cup limiters.

The primary modes excited by the rail impact are different from those excited by the vertical drop. Figures 11, 17, and 25 correspond to the modes cited in table 2. Note that the rail impact primarily excites the console in a longitudinal rocking mode, and the couch starts out as a lurching across the corner but resolves itself primarily into a lateral rocking motion at a considerable angle from the impact direction. Both modes are very low frequency, hence, their displacements have large magnitudes, as evidenced by the sway space requirements cited in table 2, "minimum sway-space required" column. The isolators for the patient couch are worked beyond the design limits in all three axes. The console isolators are overworked in compression. The pin-in-cup limiters at the top of the gantry are greatly over-traveled. In the real system, as presently designed, under 10 mph rail impact the gantry would experience acceleration peaks higher than those given in table 2, and the pin-in-cup motion limiter would probably experience failure.

The console rocking motion mentioned above is of some concern, with the top swaying 12.3 inches. While x-axis travel may be only 1.2 inches at the isolator (console baseplate), and acceleration peaks may be high, at 20.7 g's, the reverse is true at the top of the console, where in this case the x-axis motion is 12.3 inches and the acceleration peak is only 5 g's. The calculated minimum sway zones from table 3 are depicted in figure 99. Only 10.7 inches of space is required between the console and the couch. This number is the result of geometric calculations, and takes into account the motion of both components being simultaneously excited by a single rail impact. If one considered the sway-space required for each of the components separately, it would actually lead to a larger number than 10.7 inches, but when the phase of motion and the influence of damping were factored in, a less conservative amount of sway space could be used.

(3) Lateral Impact

Summary information similar to that covered in parts (1) and (2) above is given in table 2 for the lateral impact response. These predictions are obtained from the information in figures 78 through 98, and from the mode shape predictions. Maximum accelerations did not exceed the 15-g design goal in any of the components, but it was predicted that the design limit of the pin-in-cup motion limiters on top of the gantry would be exceeded. This would result in higher accelerations than the predictions show and possible failure of the pin-in-cup system.

The primary mode excited by the lateral impact was the same for the couch as in the rail impact. Figures 12, 17, and 24 correspond to the modes cited in table 2. The lateral impact excites the console in a lateral rocking mode, and the couch is predicted to adopt a lateral rocking motion at a considerable angle from the initial impulse direction. Both are very low frequency, hence, they have large magnitudes, as evidenced by the associated sway space cited in table 2.

The calculated minimum sway zones from table 3 are depicted in figure 99. The greatest concern with the lateral impact is contact of the gantry or of the console against the shelter walls on stowed-panel side. The lateral impact imparts a maximum sway of 3.2 inches for the console and 1.75 inches for the gantry, both of which will result in impacts against the stowed shelter panels.

e. General Discussion

It was said earlier that sway space must be specified to take into account that oscillations of adjacent components may become out of phase with one another after a shock input. A conservative approach would require specifying the sway-space between adjacent components as the arithmetic sum of the maximum expected individual component deflections. That may lead to impractically large sway zones being specified. A better approach is to observe the sway behavior in the time traces and specify the sway zones based on the combined motions of adjacent components at the first moment that they are nearly 180 degrees out of phase (they start motion in-phase after a single impact). By the time they are out of phase, damping may have reduced the amplitudes significantly. This approach leads to reduced and potentially more achievable sway zones without risk of collisions from a single shock input to the shelter.

There was good agreement between the simple one-degree of freedom analysis and the finite element analysis in terms of damped natural frequency. The small discrepancies are attributed to the compliance of the shelter floor, yielding slightly lower predicted natural frequencies. Accuracy of the model predictions could be enhanced by comparing or validating them against the response of the actual prototype system in an instrumented test.

It was predicted earlier that the shelter floor will under certain dynamic inputs be exercised to more than sixty percent of its yield strength. This is not likely, since in the actual prototype there was some load-spreading by the plates to which the isolators were mounted. The load applied to the spreader plates can be obtained by multiplying the maximum isolator deflection by the isolator spring rate, given earlier.

9. Conclusions

The analysis showed that the ruggedized CT scanner prototype studied in this report has attained a significant degree of ruggedness through application of shock and vibration isolation techniques. The system meets the ruggedization requirements in all but the most extreme conditions of lateral impact, rail impact, and vertical drop. When these inputs are at their extreme levels, it is predicted that shock isolators are slightly overtraveled, some sway spaces are exceeded, and the pin-in-cup motion limiter is greatly overloaded.

Some changes must be made in the existing design, or verification testing must be done, before the system can be considered

fully ruggedized to the mil spec levels. It is not realistic to reduce the maximum allowable environmental inputs to a level where the analyzed system will not experience exceeded isolator limits or sway zones.

Analysis shows that under the extreme shock inputs, acceleration peaks as high as 17-20 g's are reached at the baseplates of the isolated components. Therefore, the objective of limiting peak acceleration to $\pm$15 g's in the gantry during these extreme shock inputs was not met. However, it is still not known whether this necessarily will lead to a failure of the scanner components, as they themselves have not been characterized in the shock environment.

The analysis also shows that shelter floor panel and subframe stress limits are not exceeded. However, the load spreader plates and methods of attachment to the ISO shelter floor must be validated.

Some straightforward and relatively minor changes to the present system could yield significant improvements to the ruggedization which would then approach accommodating the most extreme input levels. These measures are outlined in the next section.

To correctly specify sway zones between components, one must take into account the possibility that the dynamic response of adjacent shock-isolated components may become out of phase with one another in the first one or two oscillations. A conservative specification of sway zones would involve the arithmetic sum of maximum amplitudes of adjacent bodies in a given axis. However, damping is present and, when taken into account, will reduce the sway zone requirements.

Helical wire rope isolators have many desirable properties for fielded equipment ruggedization, including temperature insensitivity, high damping, strength, and nearly uniform omnidirectional spring rates.

The two major approximations in this analysis were the estimation of moments of inertia of the CT scanner components and the linear representation of the isolator load-versus-deflection curves. This analysis can form a basis for evaluating future proposed CT scanner systems against the ruggedization specification.

An improved design for the gantry top pin-in-cup motion limiter was conceived by the writers and is recommended below, but its performance when applied to the studied system was not analyzed.

10. Recommendations

Adequate isolation system performance under the extreme impact loadings may be attainable with the present system if sway-space allocations are changed to accord with those in figure 99, and if the pin-in-cup motion limiter system were replaced with a system like the one shown conceptually in figure 100.

This analysis should be calibrated using the measured response of the actual prototype system in an instrumented test at low dynamic input levels, before it is used for binding predictions of equipment survival at logistical dynamic input levels.

If future efforts are made using this model or one like it, phantom lines or plate elements should be incorporated that describe the true outside contours of the scanner components. This would facilitate the on-terminal viewing and plotting of predicted interferences, to more readily establish safe sway space zones. Also, in the future, it would be preferable to employ a non-linear analysis tool using verified values for component weights, centers-of-gravity, and mass moments of inertia, and one able to model the non-linear characteristics of the isolators. If such mass and inertia data were not available from the scanner manufacturer, a more accurate and direct method than was used in the present analysis should be used to establish component moments of inertia. This could be done by solids modeling of the components or by direct measurement.

The performance of the isolation system after implementation of the changes recommended above could be very easily predicted using the existing computer model, once appropriate modifications were made to the model to account for the changes.

11. References

1. "Analysis of Accelerations in a Dynamically Loaded Tactical Shelter," Arthur R. Johnson, NATICK/TR-83-007, US Army Natick Research and Development Laboratories, July 1982.

2. "Specification, Design, and Response of a Transportation Isolation System for Equipment Mounted in Army (MASH) ISO Shelters," Robert Wood, 22 May 1990.

DISTRIBUTION:

J. Beard, SMCAR-AEF-T
C. Campagnuolo, AMSRL-SS-SL
R. Christopherson, SMCAR-AEF-P
P. Emmerman, AMSRL-SS-IC
A. Frydman, AMSRL-WT-PD
R. Goodman, SMCAR-AEF-M
J. Hartranft, SMCAR-AEF-T
G. McNally, SMCAR-AEF-A
J. Miller, AMSRL-SS-S
J. Pellegrino, AMSRL-SS-I
R. Shaffer, SMCAR-AEF

Table 2. Summary of Results

TEST CONDITION (Type of Dynamic Input)	CT Scanner System Component	Max. Accel., Internally Mounted Equipment, G's		Primary Excited Mode, (Post Transient)			Minimum Sway-Space Required (inches, 0-pk)			Location on Component	Maximum Isolator Travel (inches, 0-pk)			Maximum Floor Stress, % Yield	
		Mounted High	Mounted Low	Freq (Hz)	Mode (#)	Ampl. (G-pk)	(x)	(y)	(z)		(x)	(y)	(z)	Panel	Frame
Vertical Drop	Console	12.9	12.9	9.68	12	6.7	0.01	1.25	0.05		0.01	1.25	0.02		
	Couch	11.4	11.4	7.47	9	5.2	0.12	1.87	0.11		0.11	(1.87)	0.08	65	61
	Gantry	10.3	10.3	6.28	4	7.3	0.12	2.36	0.03	top:	0.03	(2.36)*	0.02		
										bottom:	0.12	(2.36)	0.07		
Rail Impact	Console	5.2	20.7	2.00	1	6.0	12.30	1.90	0.02		1.20	(1.90)	0.01		
	Couch	10.4	15.3	2.58	2	5.2	3.50	1.75	4.70		(2.45)	(1.65)	(1.65)	22	24
	Gantry	17.6	15.3	7.34	8	10.4	3.00	0.50	0.18	top:	(3.0)	0.50	0.18		
										bottom:	2.60	0.50	0.12		
Lateral Impact	Console	5.2	10.4	3.87	3	3.9	0.01	1.10	3.20		0.01	1.10	0.88		
	Couch	4.2	9.8	2.58	2	2.6	2.65	1.30	3.30		0.90	1.30	1.20	28	8
	Gantry	10.1	7.9	7.26	7	6.5	0.04	0.38	1.75	top:	0.04	0.38	(1.75)		
										bottom:	0.04	0.38	1.55		

KEY: x.xx [underscore] these figures exceed the 15-G design objective.

(x.xx) [ellipses] this amount of travel exceeds the design limits of the isolator or motion limiter.

* this may be sufficient vertical travel to disengage the pin-in-cup motion limiter.

Table 3. Summary of Maximum Values and Limits-Exceeded.

CT Scanner System Component	Overall Maximum Acceleration Experienced, (G's)			Overall Minimum Required Sway-Space, (inch, 0-pk)			Overall Maximum Isolator Travel, (inches, 0-pk)				Overall Maximum Isolator Travel in Isolator's Own Axes, (inches, 0-pk)			Maximum Rated Dynamic Travel of Isolator, (inches, 0-pk)		
	x	y	z	x	y	z		x	y	z	Roll	Compr.	Shear	Roll	Compr.	Shear
CONSOLE	20.7	12.9	10.4	12.30	1.90	3.20		1.20	1.90	0.88	0.88	(1.90)	1.20	1.3	1.6	1.3
COUCH	15.3	11.4	9.8	3.50	1.87	4.70		2.45	1.87	1.65	(2.05)	(1.87)	(1.38)	1.3	1.6	1.3
GANTRY	17.6	10.3	10.1	3.00	2.36	1.75	top:	(3.00)	(2.36)	(1.75)	(3.00)	(2.36)	(1.75)	1.2	1.75	1.2
							bottom:	2.60	(2.36)	1.55	(2.18)	(2.36)	1.42	2.1	2.0	2.1

KEY: x.xx [underscore] these figures exceed the 15-G design objective.

(x.xx) [ellipses] this amount of travel exceeds the design limits of the isolator or motion limiter.

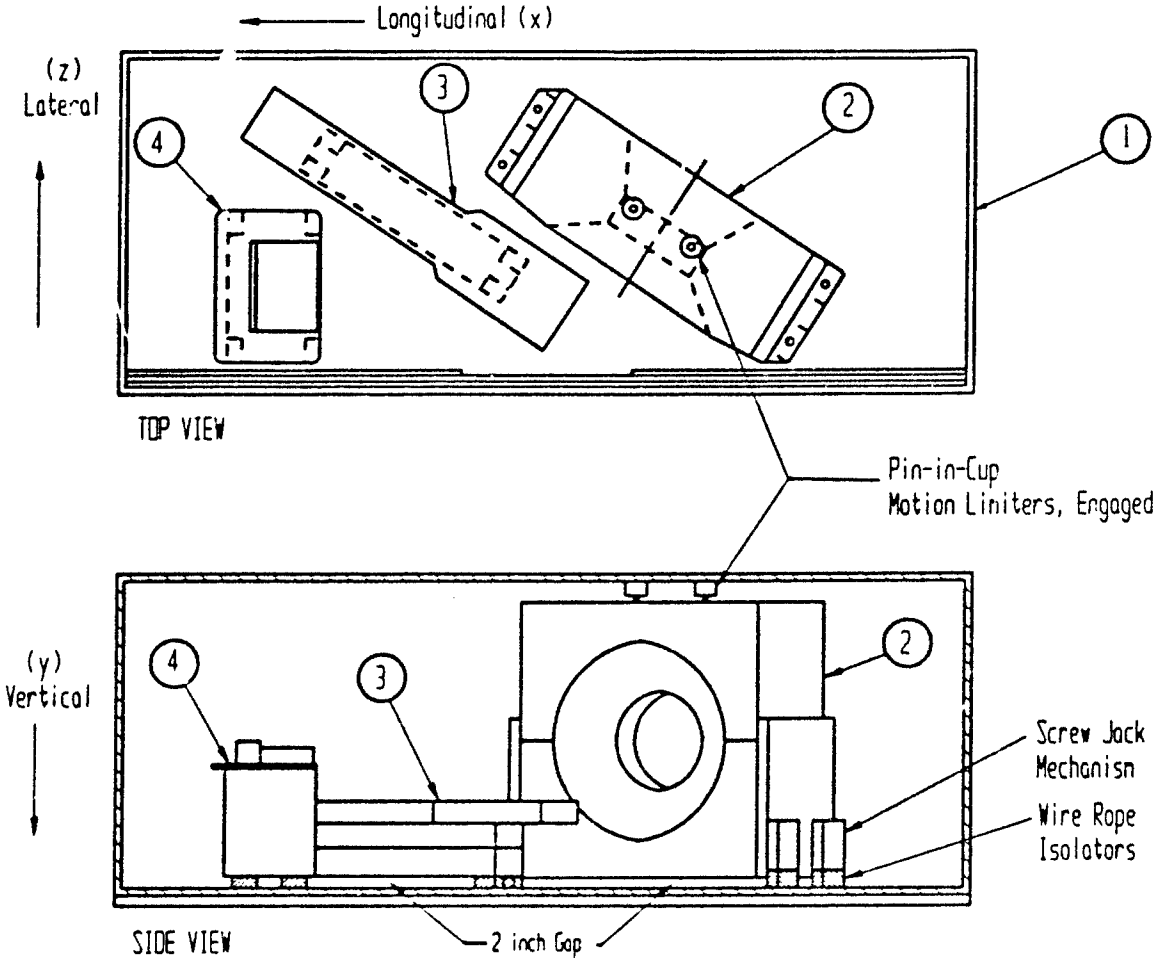

FIGURE 1a. Layout of Ruggedized Picker IQ Scanner Components in a 2:1 ISO Shelter, Stowed configuration.

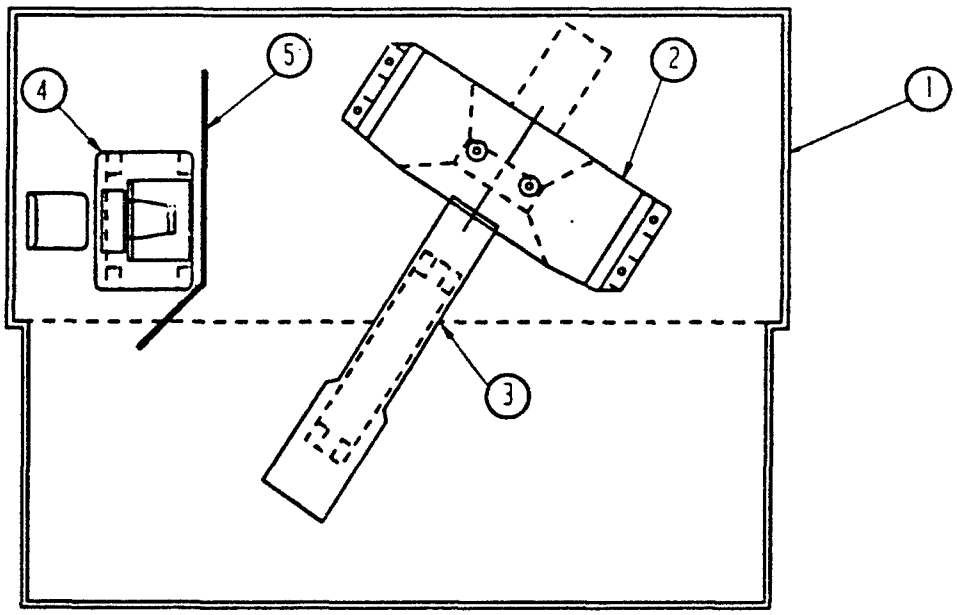

TOP VIEW

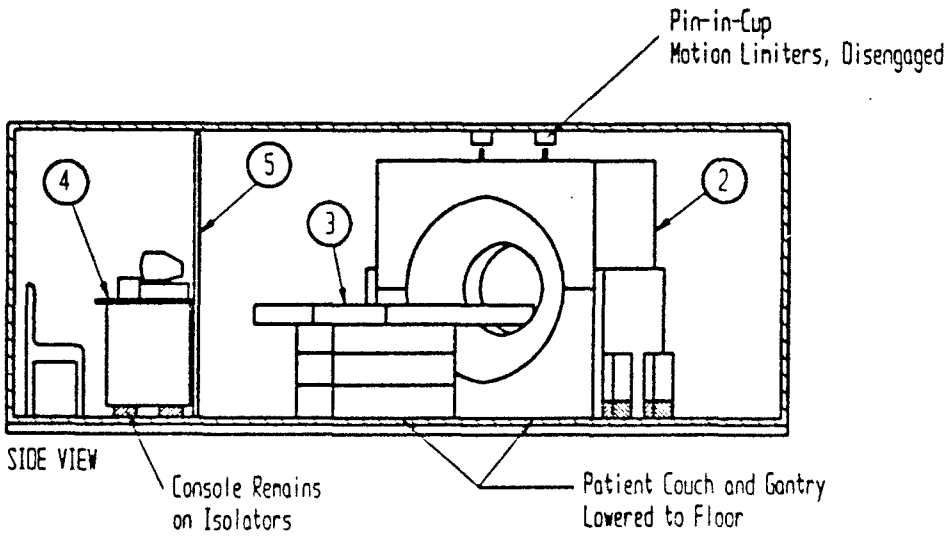

(1) One-Side Expandable Shelter (3) Patient Couch (5) Shield

(2) Gantry (4) Operators Console

FIGURE 1b. Layout of Ruggedized Picker IQ Scanner Components in a 2:1 ISO Shelter, Operational configuration.

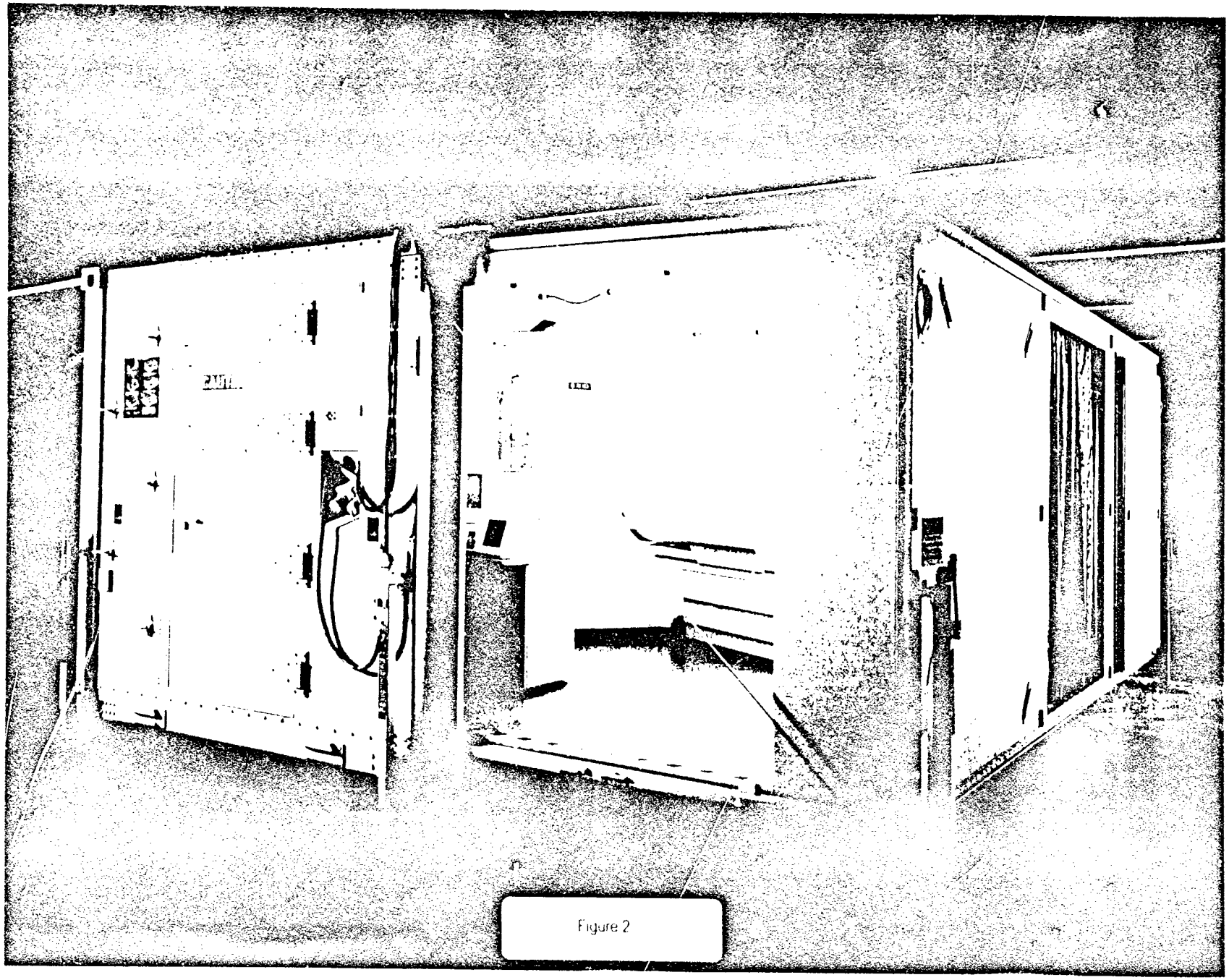

Figure 2

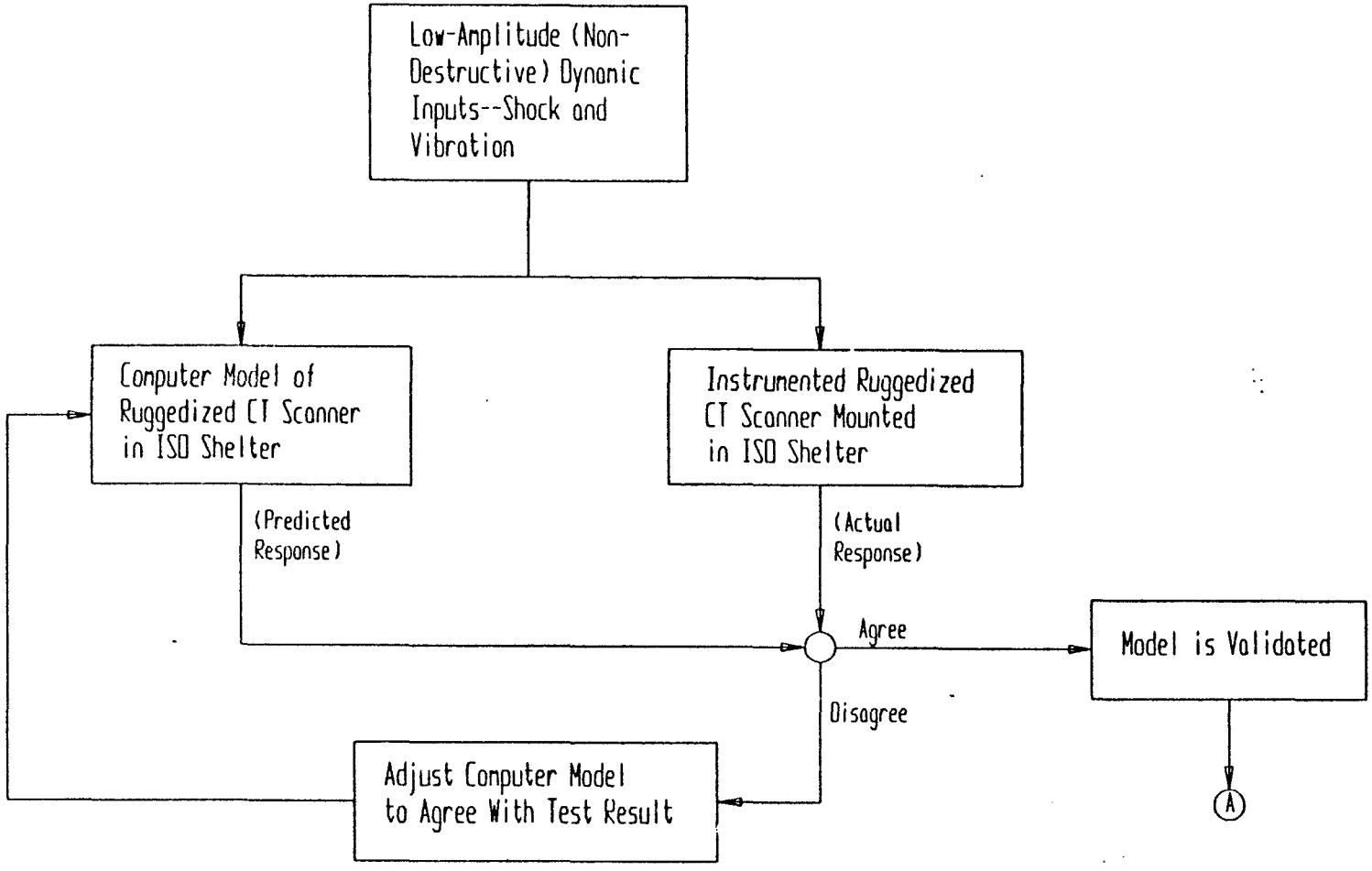

Figure 3. Low-Anplitude Dynanic Test for Model Validation or Adjustment

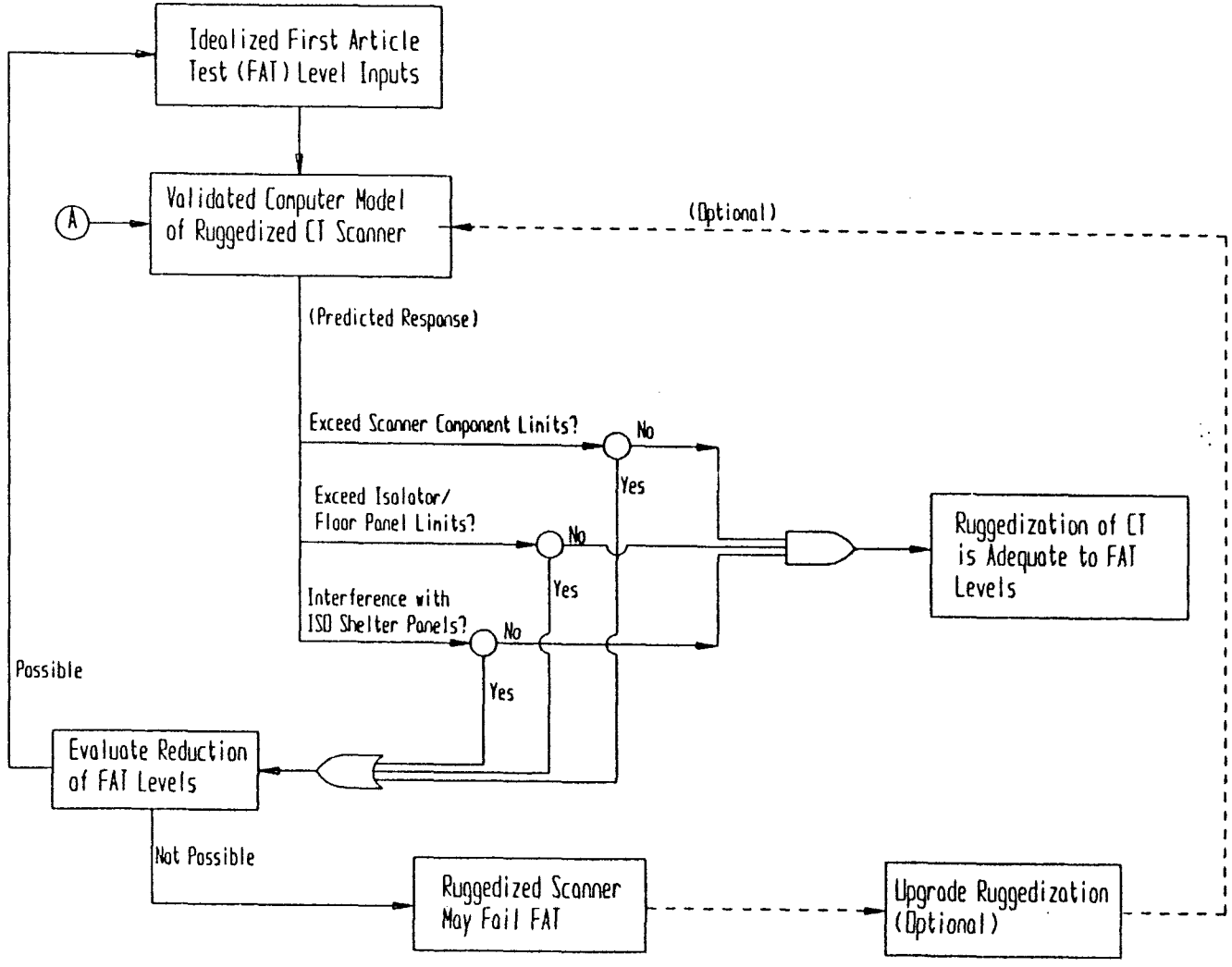

Figure 4. Using the Computer Model to Predict Outcome of First Article Test.

Boundary Conditions/Freedoms:

[A] Constrained in vertical direction and constrained from rotating about an axis perpendicular to the associated wall structure.

[B] Free to rotate about a vertical axis, otherwise constrained.

Note: ISO Shelter Wall Panels and Ceiling Panel are Not Explicitly Modeled, But Their Structural Effects are Included in the Imposed Boundary Conditions and Element "Freedoms"

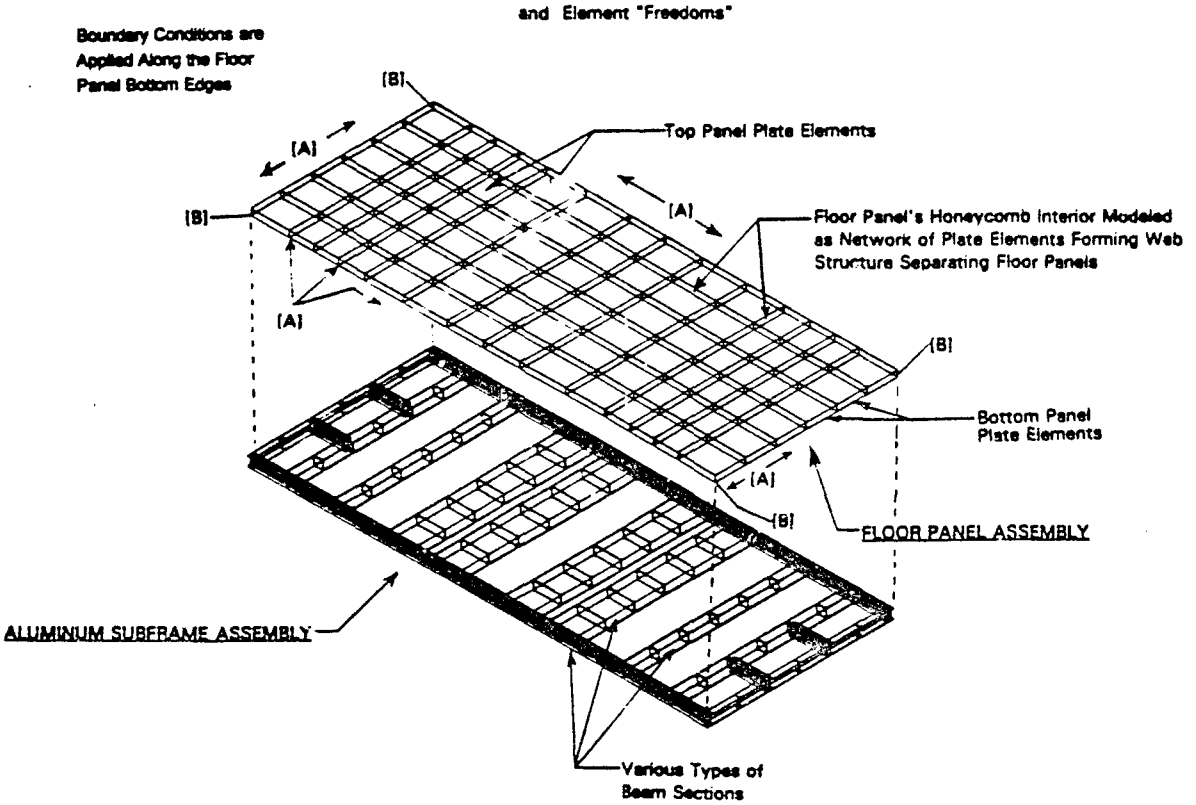

Figure 5. ISO Shelter Model

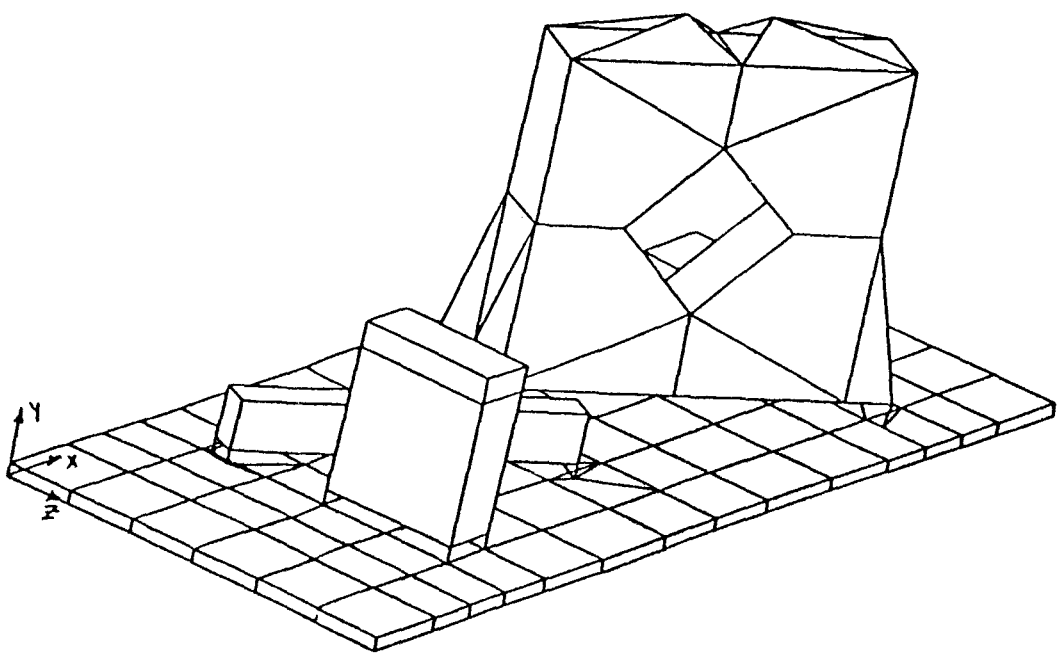

Figure 6. Arrangement of CT-Scanner operator consule, patient table, and gantry rigid-body models upon ISO shelter floor grid. Corner detail shows axis conventions.

JOB: PLOT3H
22-APR-92 17:49

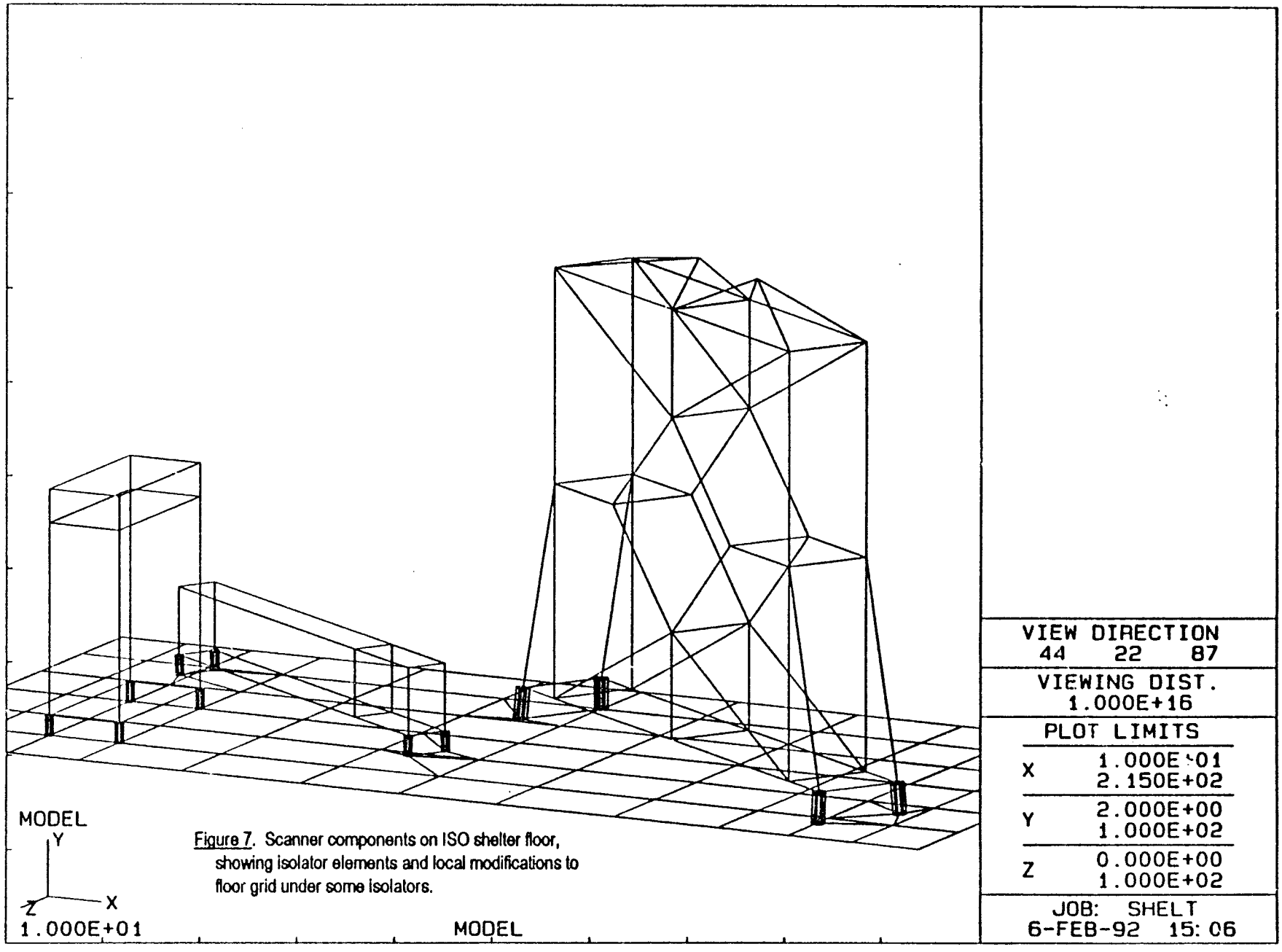

Figure 7. Scanner components on ISO shelter floor, showing isolator elements and local modifications to floor grid under some isolators.

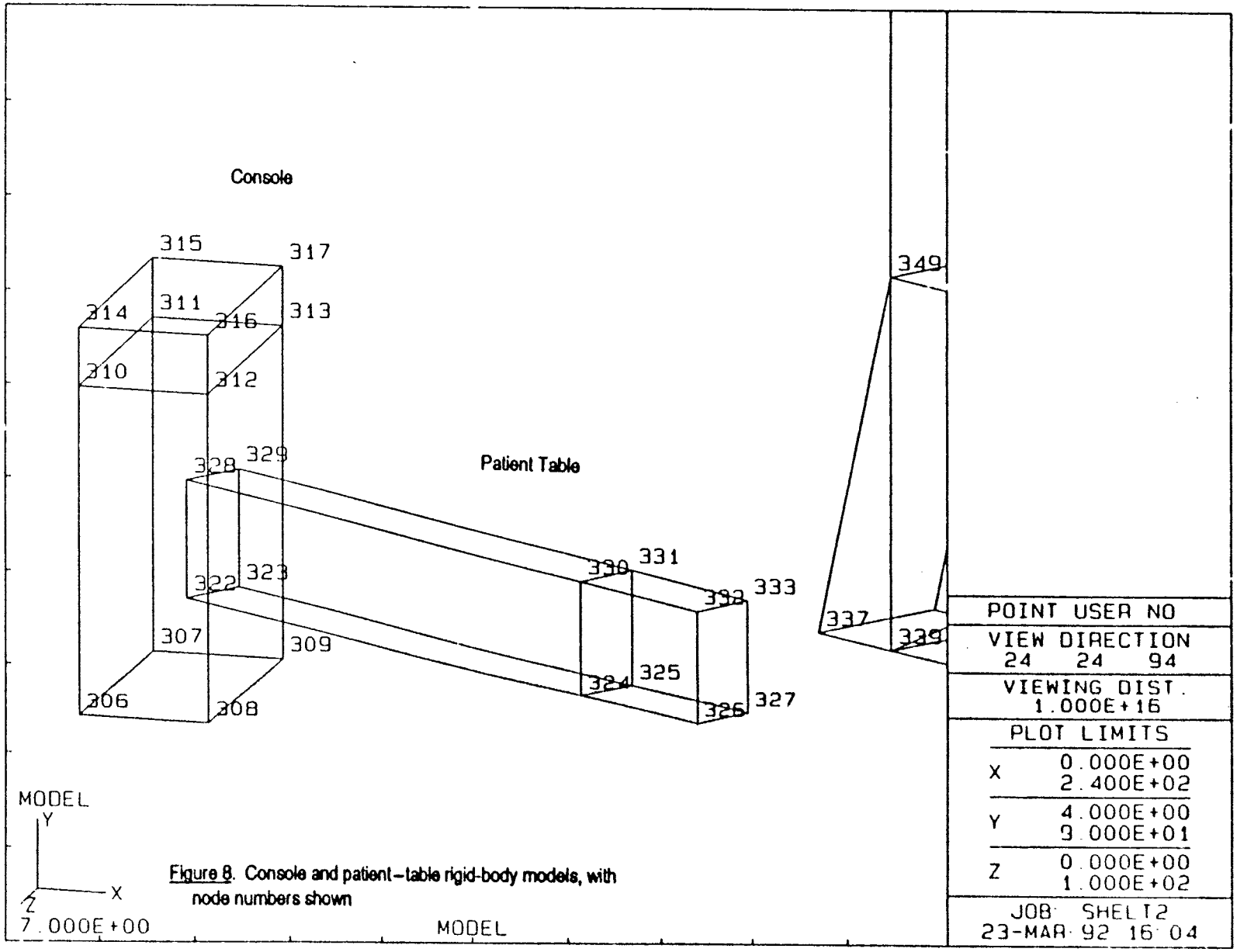

Figure 8. Console and patient-table rigid-body models, with node numbers shown

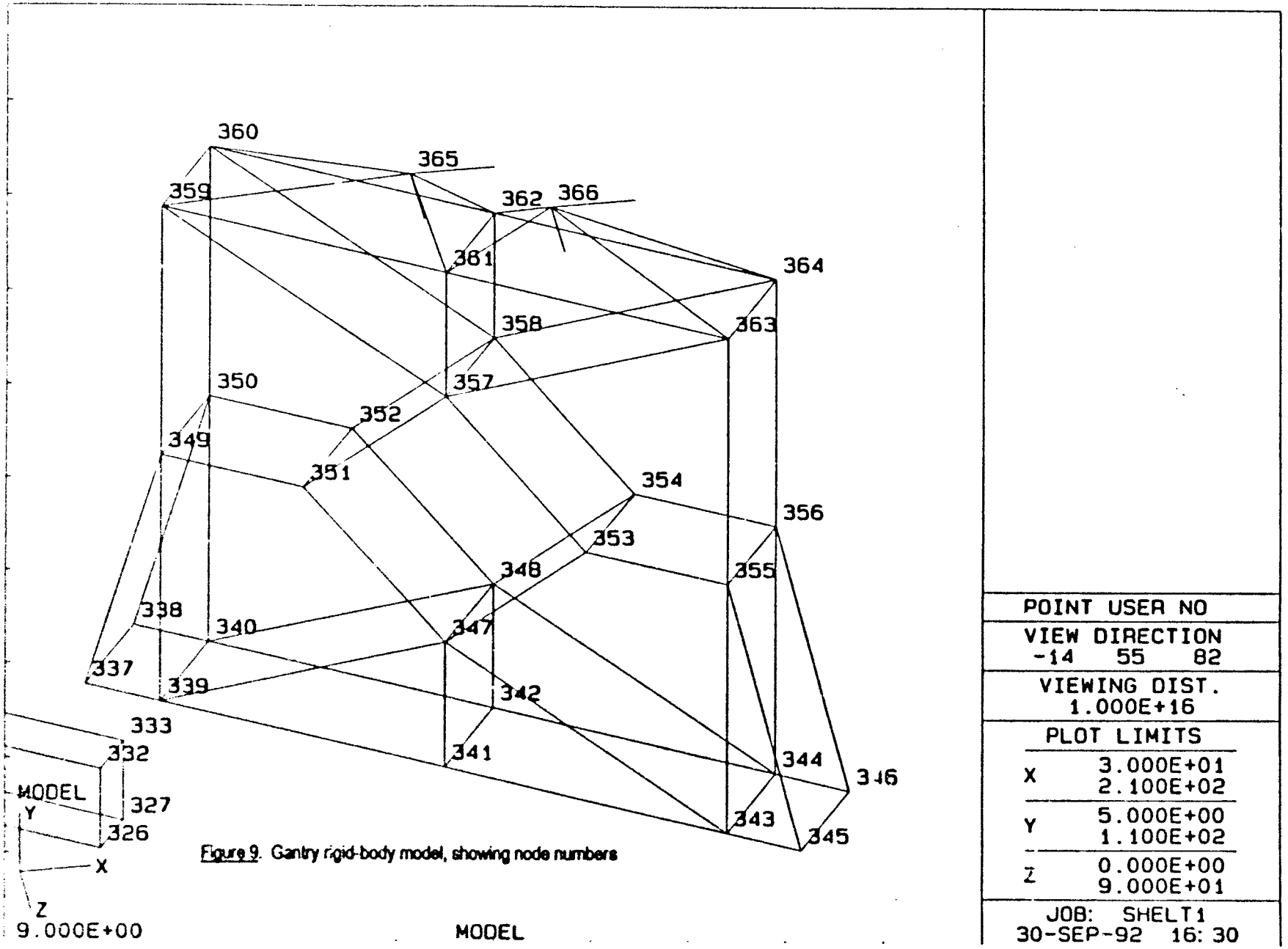

Figure 9. Gantry rigid-body model, showing node numbers

a)

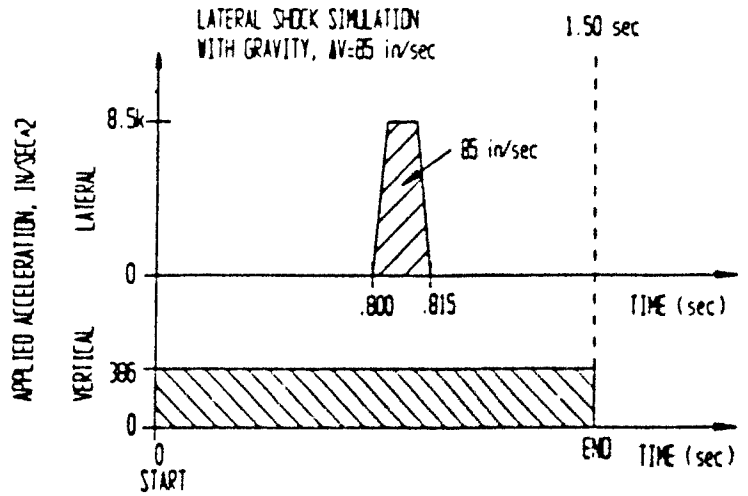

b)

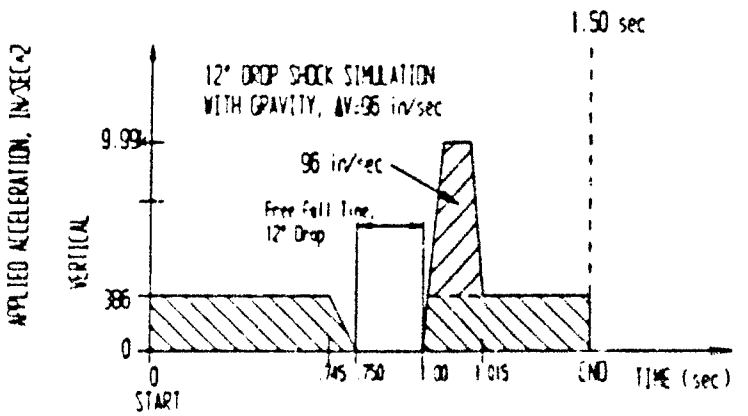

c)

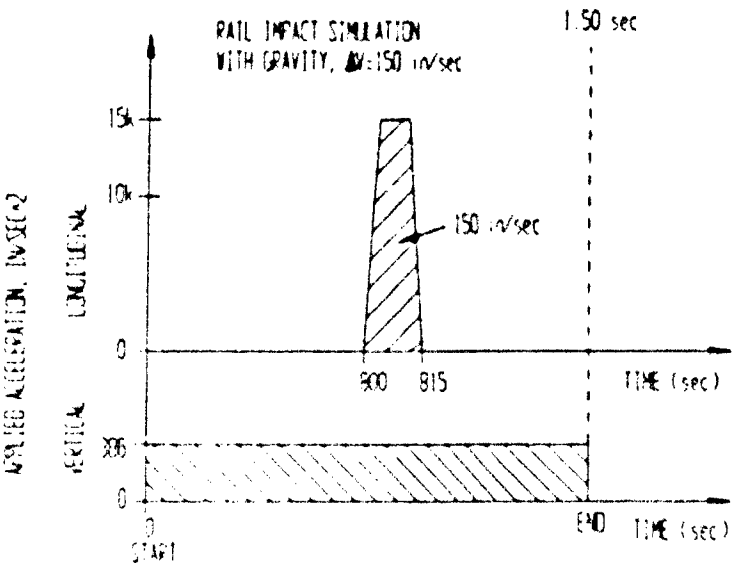

Figure 10. Load Realizations for Lateral, Drop, and Rail Impacts

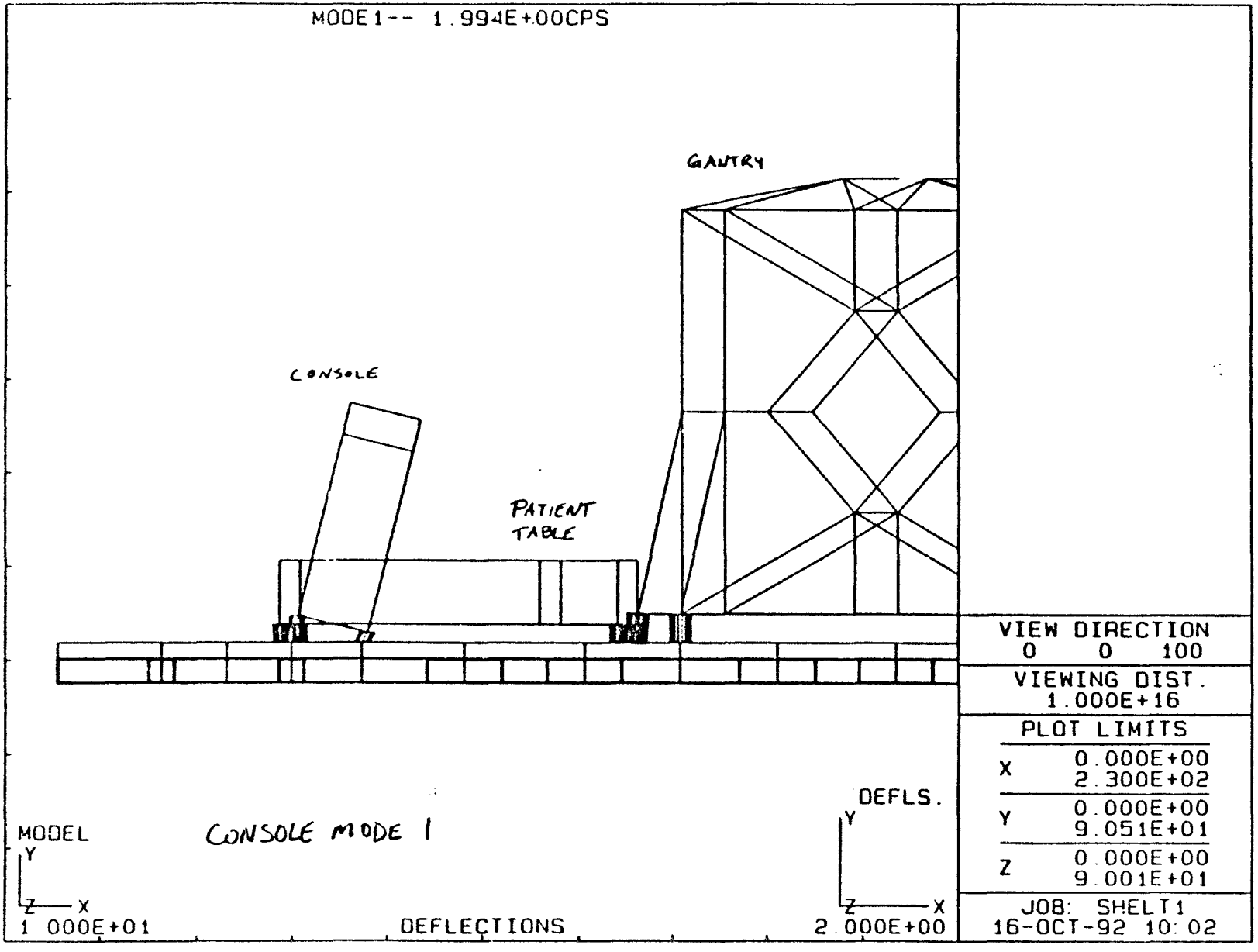
MODE 1 -- 1.994E+00CPS
GANTRY
CONSOLE
PATIENT TABLE
VIEW DIRECTION
0 0 100
VIEWING DIST.
1.000E+16
PLOT LIMITS
X 0.000E+00
2.300E+02
Y 0.000E+00
9.051E+01
Z 0.000E+00
9.001E+01
JOB: SHELT1
16-OCT-92 10:02
MODEL
CONSOLE MODE 1
DEFLS.
Y
Z
X
1.000E+01
DEFLECTIONS
2.000E+00

Figure 11

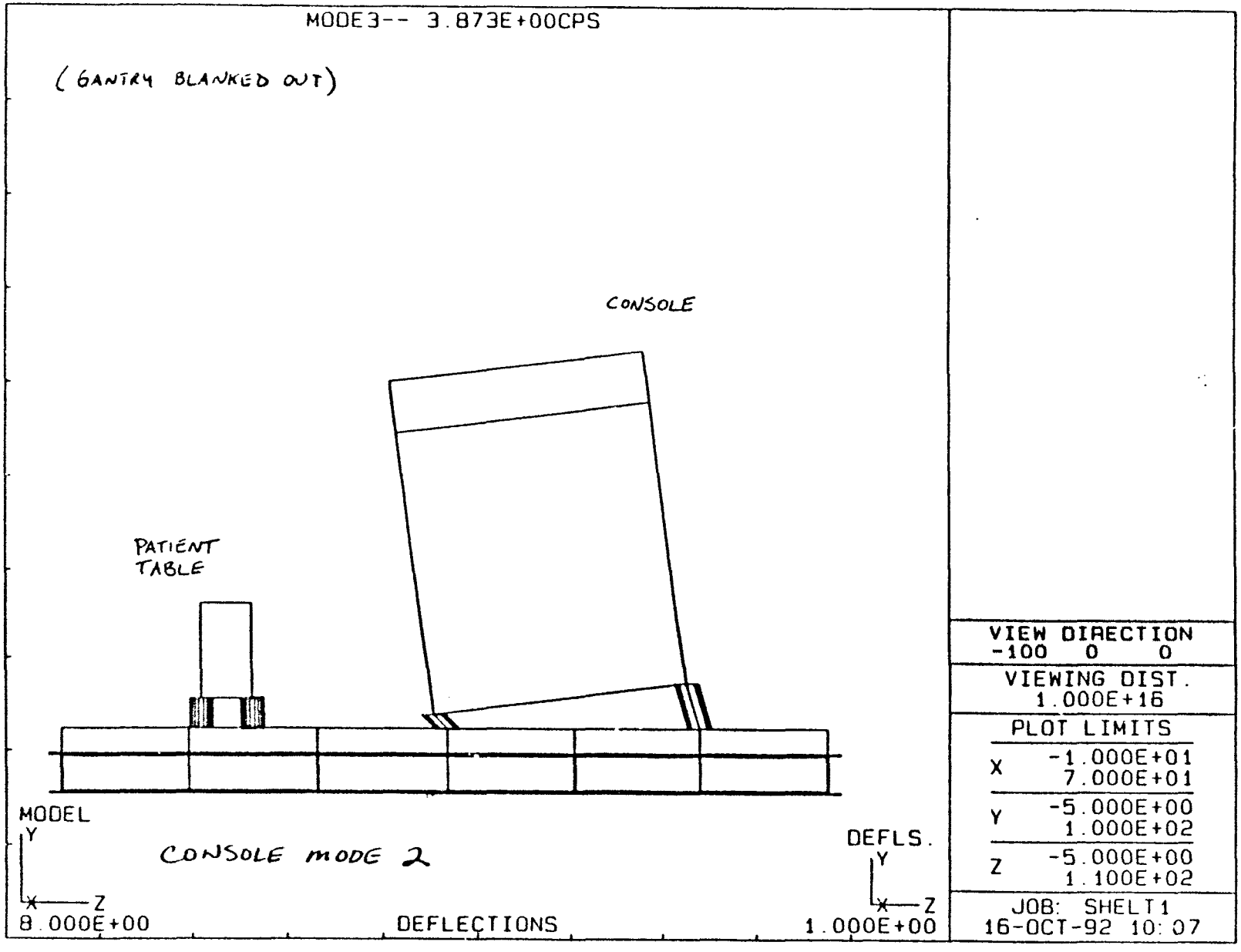
MODE3-- 3.873E+00CPS
(GANTRY BLANKED OUT)
CONSOLE
PATIENT TABLE
MODEL
Y
Z
CONSOLE MODE 2
DEFLS.
Y
Z
8.000E+00
DEFLECTIONS
1.000E+00
VIEW DIRECTION
-100 0 0
VIEWING DIST.
1.000E+16
PLOT LIMITS
X -1.000E+01 7.000E+01
Y -5.000E+00 1.000E+02
Z -5.000E+00 1.100E+02
JOB: SHELT1
16-OCT-92 10:07

Figure 12

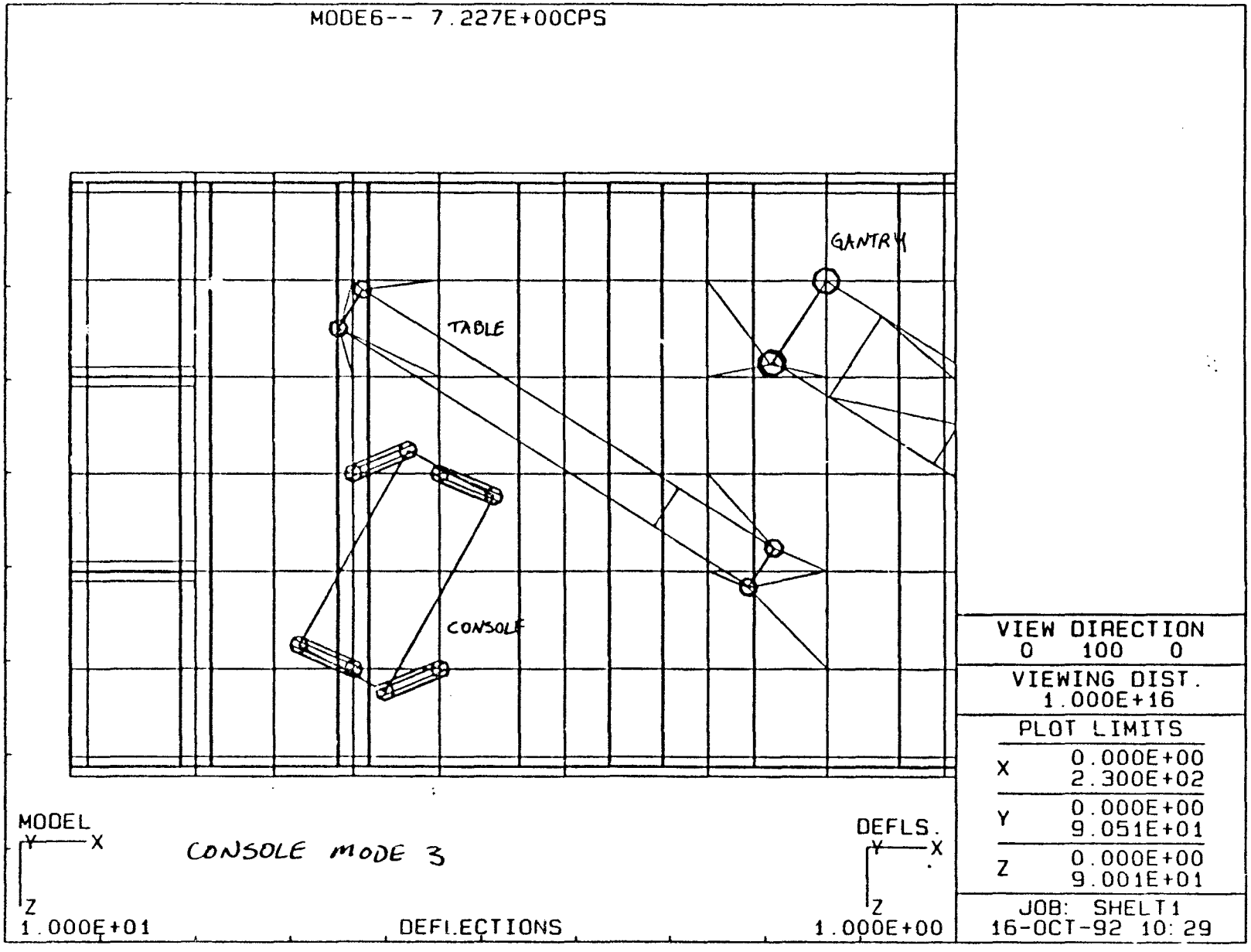
MODE6-- 7.227E+00CPS
GANTRY
TABLE
CONSOLE
MODEL
Y
X
Z
1.000E+01
CONSOLE MODE 3
DEFLECTIONS
DEFLS.
Y
X
Z
1.000E+00
VIEW DIRECTION
0 100 0
VIEWING DIST.
1.000E+16
PLOT LIMITS
X 0.000E+00
2.300E+02
Y 0.000E+00
9.051E+01
Z 0.000E+00
9.001E+01
JOB: SHELT1
16-OCT-92 10:29

Figure 13

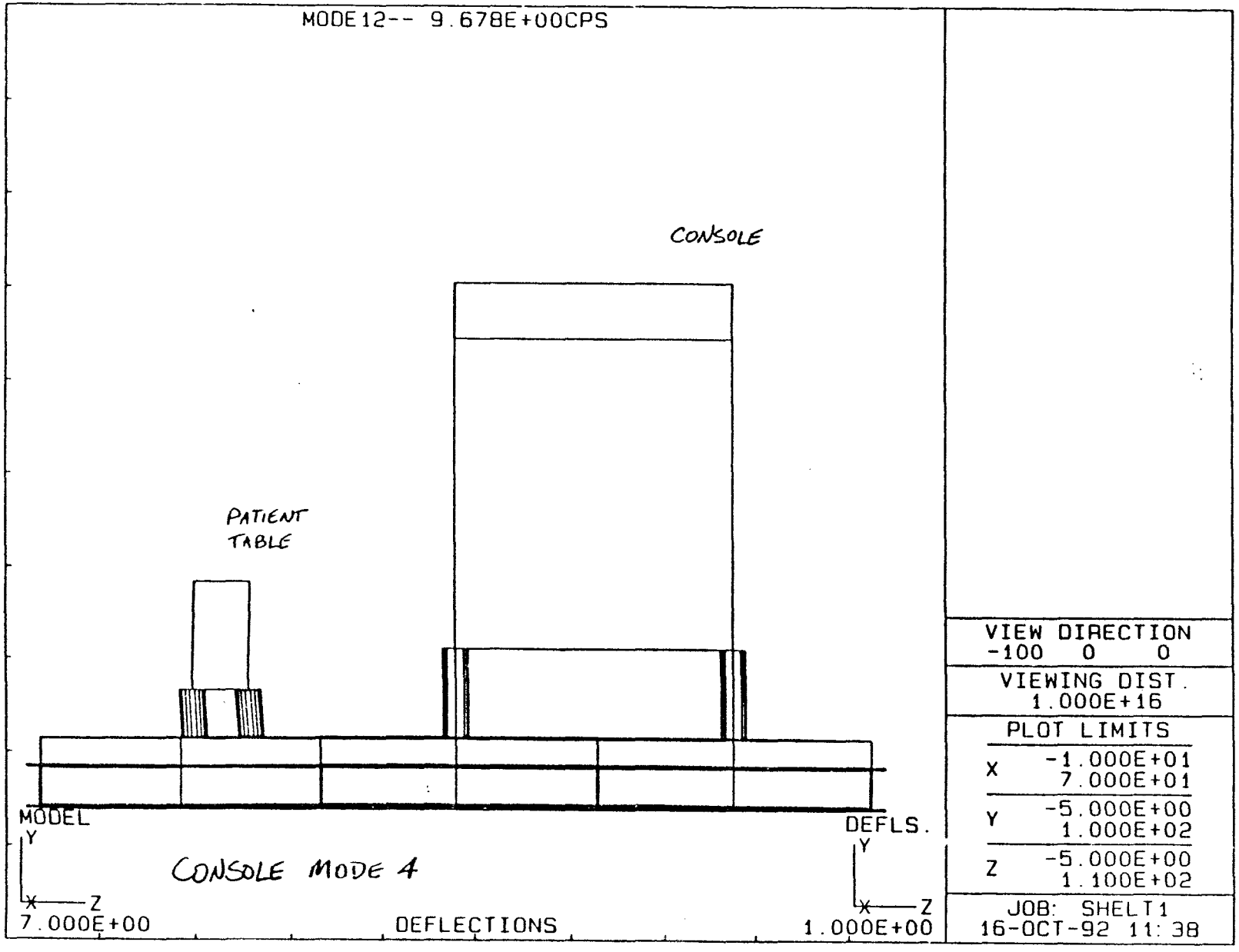
MODE12-- 9.678E+00CPS
CONSOLE
PATIENT TABLE
MODEL
Y
Z
7.000E+00
CONSOLE MODE 4
DEFLS.
Y
Z
1.000E+00
DEFLECTIONS
VIEW DIRECTION
-100 0 0
VIEWING DIST.
1.000E+16
PLOT LIMITS
X -1.000E+01 7.000E+01
Y -5.000E+00 1.000E+02
Z -5.000E+00 1.100E+02
JOB: SHELT1
16-OCT-92 11:38

Figure 14

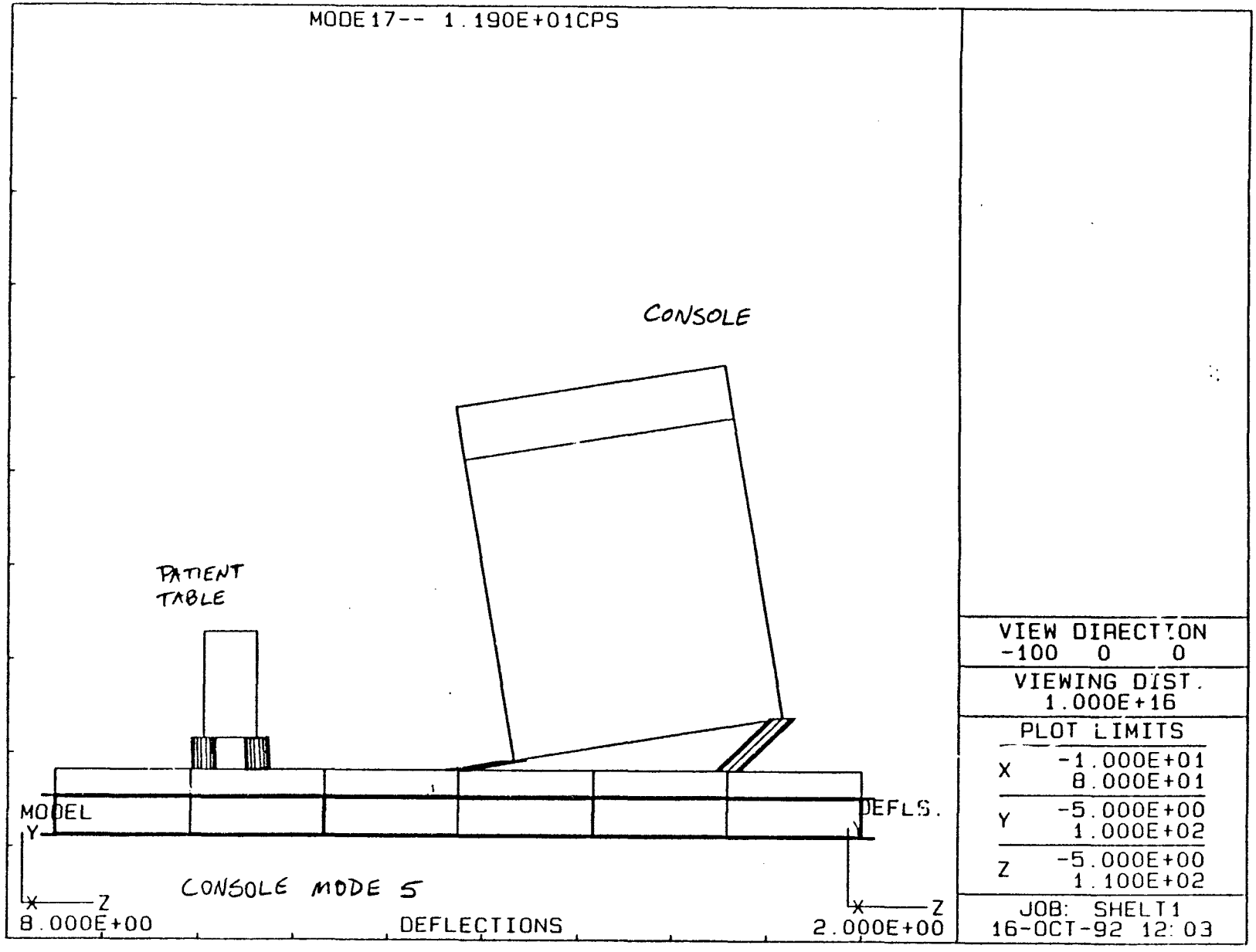
MODE 17-- 1.190E+01CPS
CONSOLE
PATIENT TABLE
MODEL
Y
Z
8.000E+00
CONSOLE MODE 5
DEFLECTIONS
DEFLS.
Z
2.000E+00
VIEW DIRECTION
-100 0 0
VIEWING DIST.
1.000E+16
PLOT LIMITS
X -1.000E+01 8.000E+01
Y -5.000E+00 1.000E+02
Z -5.000E+00 1.100E+02
JOB: SHELT1
16-OCT-92 12:03

Figure 15

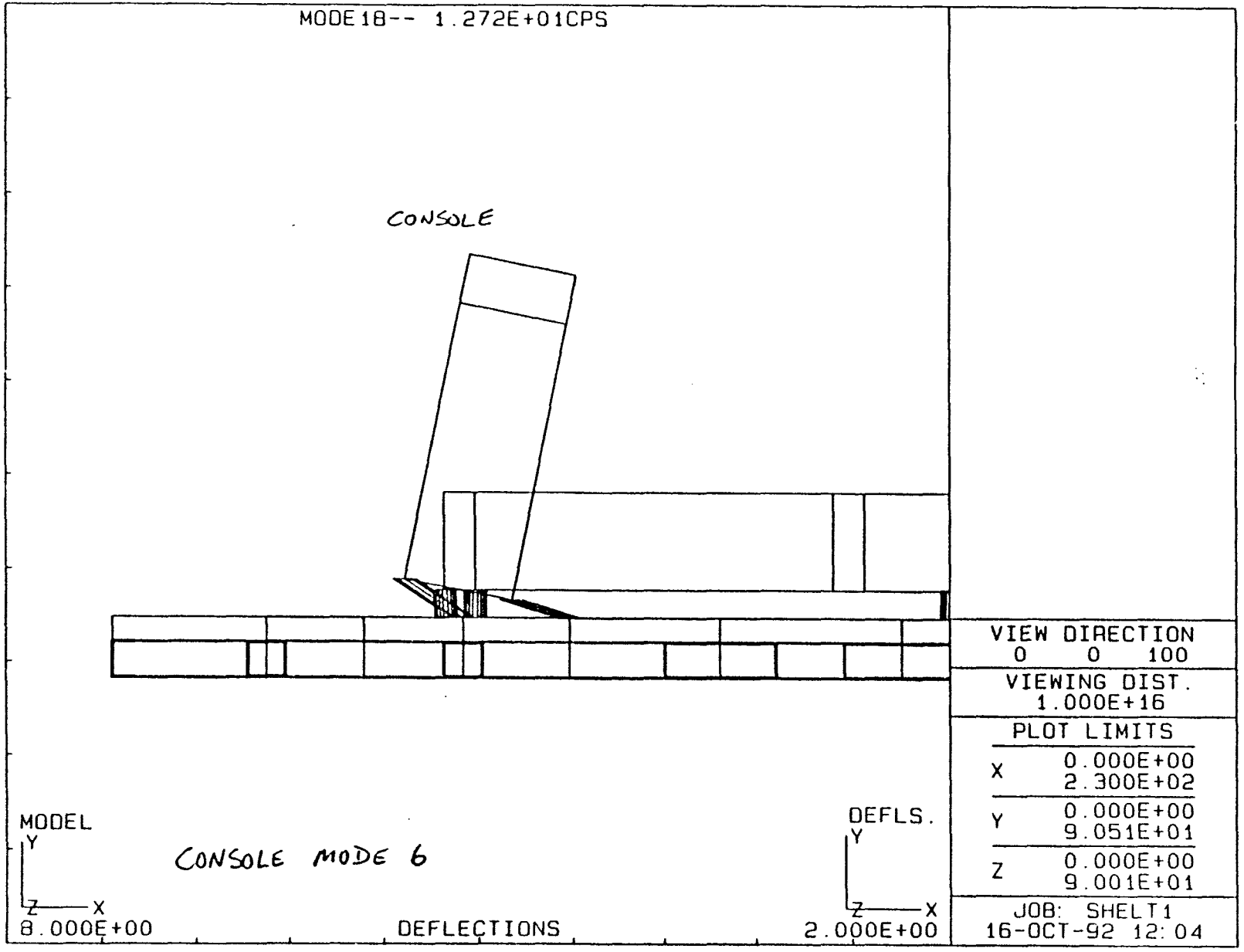
MODE 18-- 1.272E+01CPS
CONSOLE
VIEW DIRECTION
0 0 100
VIEWING DIST.
1.000E+16
PLOT LIMITS
X 0.000E+00
2.300E+02
Y 0.000E+00
9.051E+01
Z 0.000E+00
9.001E+01
JOB: SHELT1
16-OCT-92 12:04
MODEL
Y
Z
X
CONSOLE MODE 6
DEFLS.
Y
Z
X
8.000E+00
DEFLECTIONS
2.000E+00

Figure 16

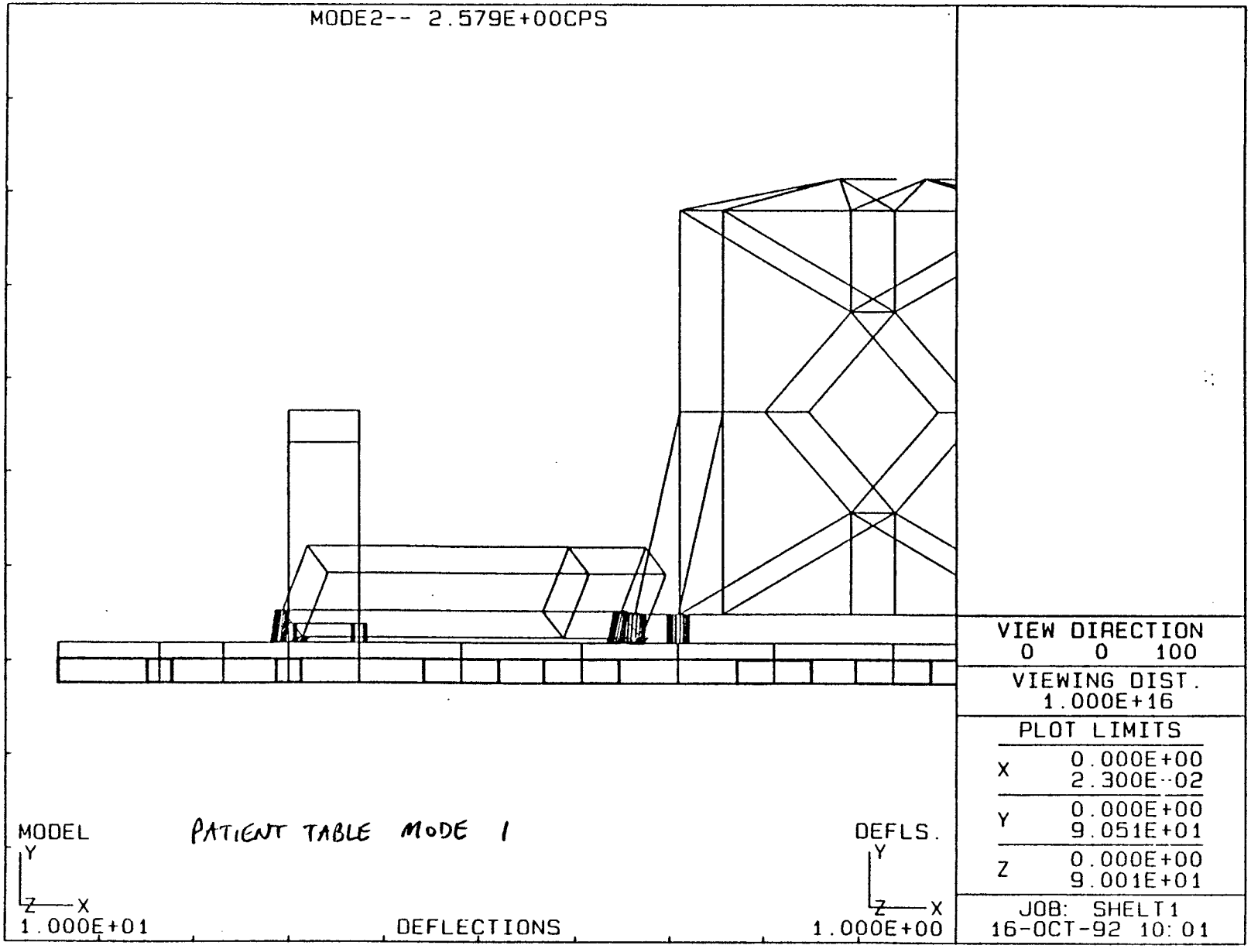
MODE2-- 2.579E+00CPS
VIEW DIRECTION
0 0 100
VIEWING DIST.
1.000E+16
PLOT LIMITS
X 0.000E+00
2.300E-02
Y 0.000E+00
9.051E+01
Z 0.000E+00
9.001E+01
JOB: SHELT1
16-OCT-92 10:01
MODEL
Y
Z X
1.000E+01
PATIENT TABLE MODE 1
DEFLS.
Y
Z X
1.000E+00
DEFLECTIONS

Figure 17

Figure 18

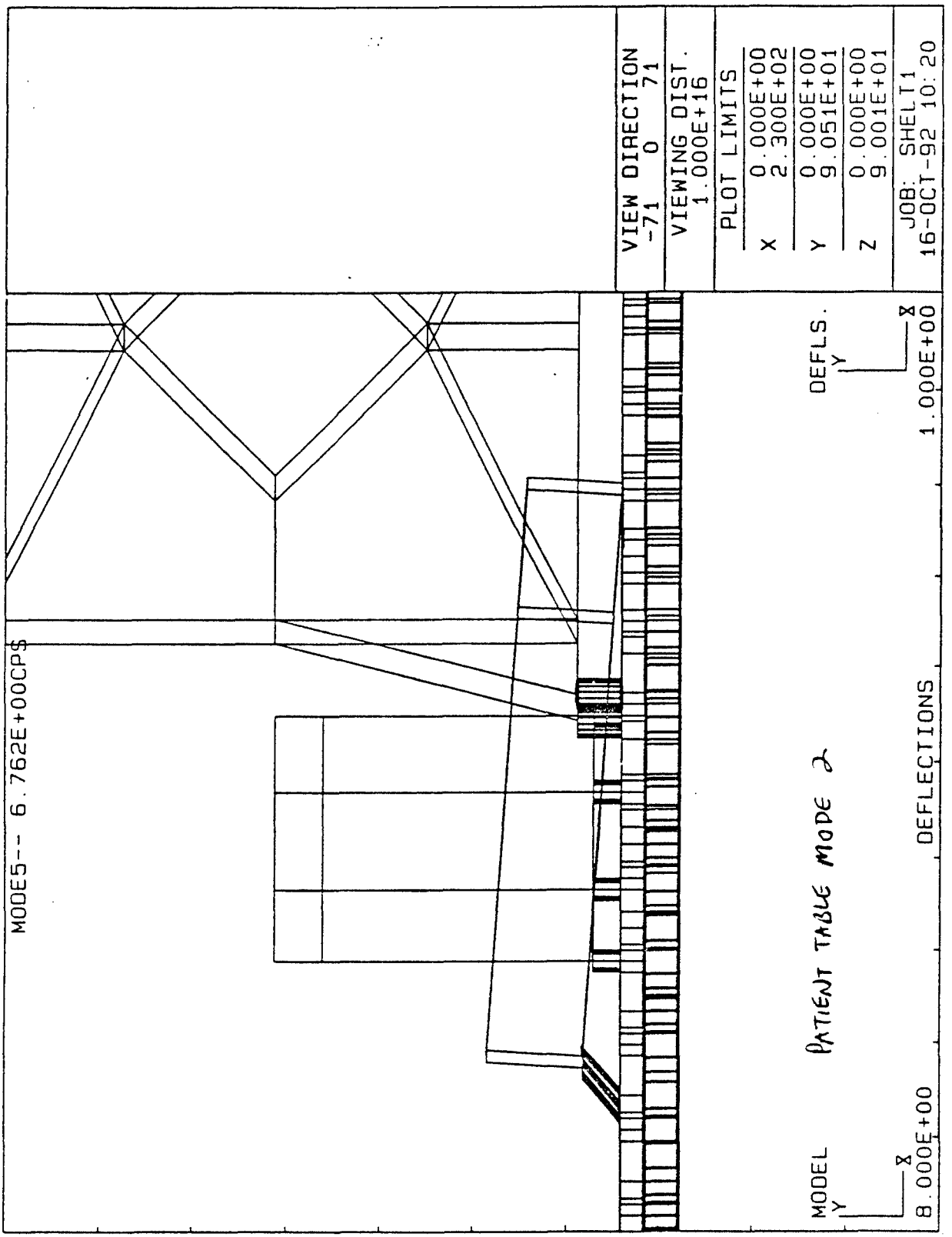
MODE5-- 6.762E+00CPS
VIEW DIRECTION
-71 0 71
VIEWING DIST.
1.000E+16
PLOT LIMITS
X 0.000E+00
2.300E+02
Y 0.000E+00
9.051E+01
Z 0.000E+00
9.001E+01
JOB: SHELT1
16-OCT-92 10:20
DEFLS.
1.000E+00
MODEL
8.000E+00
PATIENT TABLE MODE 2
DEFLECTIONS

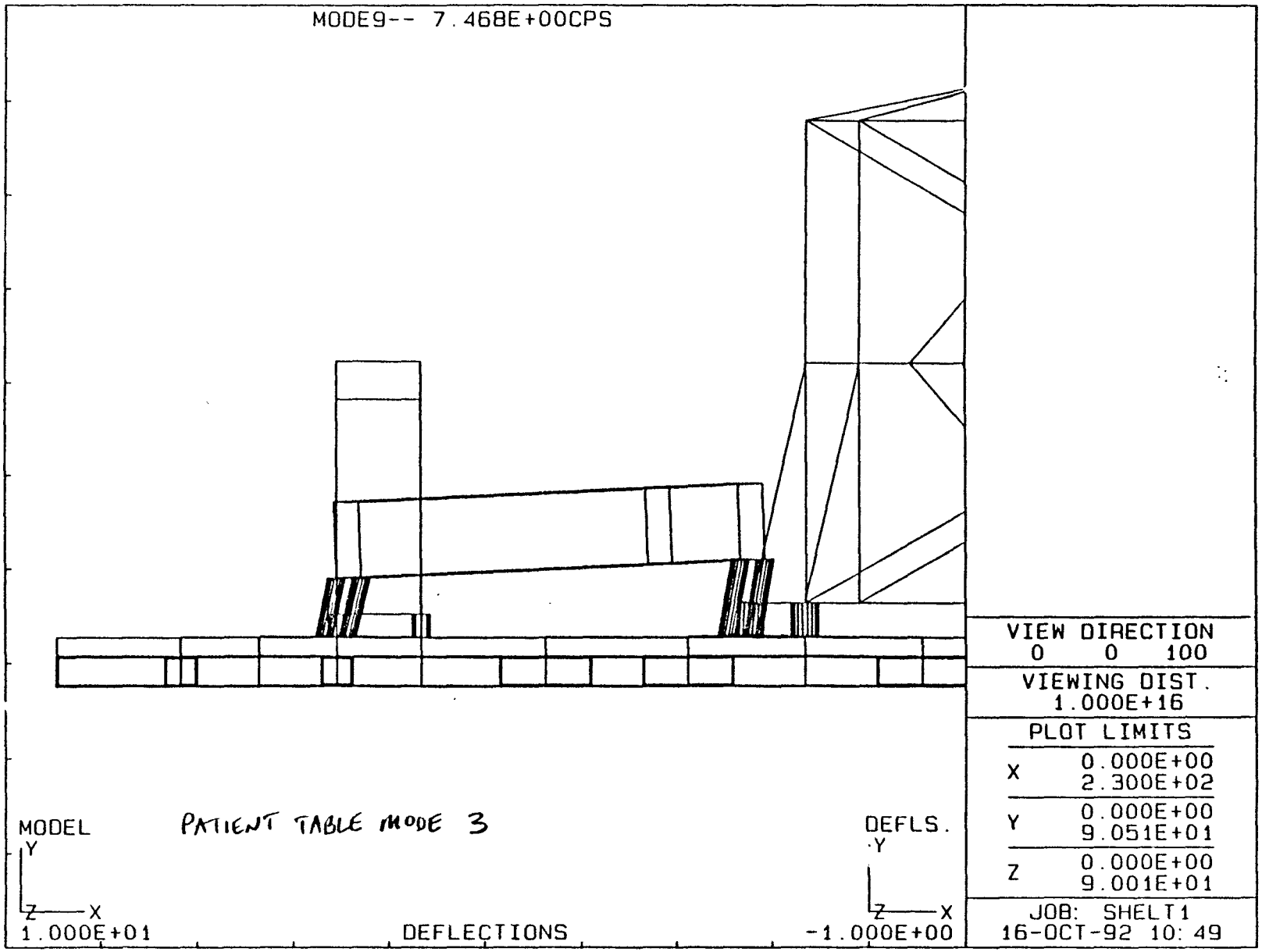
MODE9-- 7.468E+00CPS
VIEW DIRECTION
0 0 100
VIEWING DIST.
1.000E+16
PLOT LIMITS
X 0.000E+00
2.300E+02
Y 0.000E+00
9.051E+01
Z 0.000E+00
9.001E+01
JOB: SHELT1
16-OCT-92 10:49
MODEL
Y
Z
X
1.000E+01
PATIENT TABLE MODE 3
DEFLECTIONS
DEFLS.
Y
Z
X
-1.000E+00

Figure 19

Figure 20

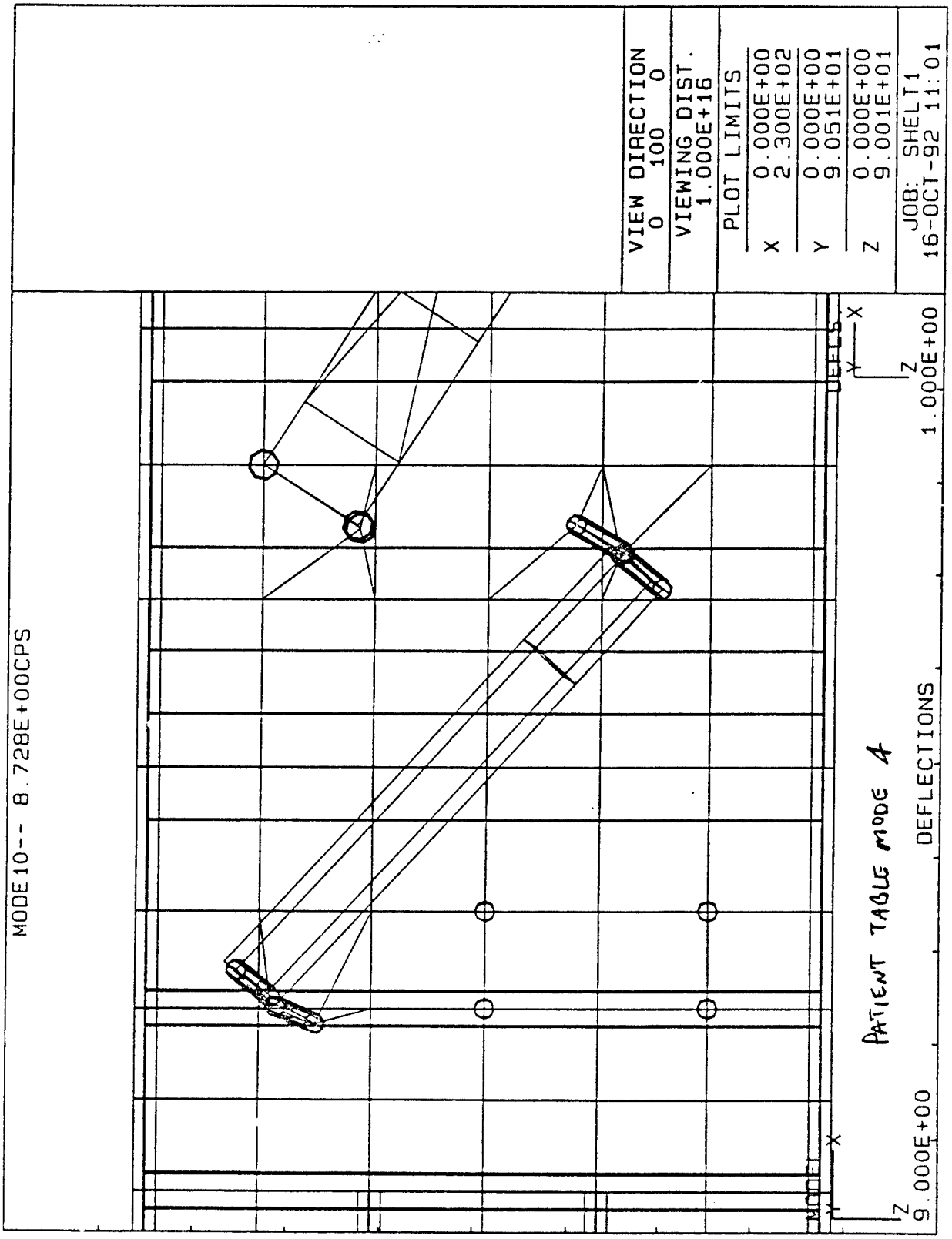
MODE 10-- 8.728E+00CPS
VIEW DIRECTION
0 100 0
VIEWING DIST.
1.000E+16
PLOT LIMITS
X 0.000E+00 2.300E+02
Y 0.000E+00 9.051E+01
Z 0.000E+00 9.001E+01
JOB: SHELT1
16-OCT-92 11:01
DEFLS
1.000E+00
PATIENT TABLE MODE 4
DEFLECTIONS
9.000E+00
MODEL

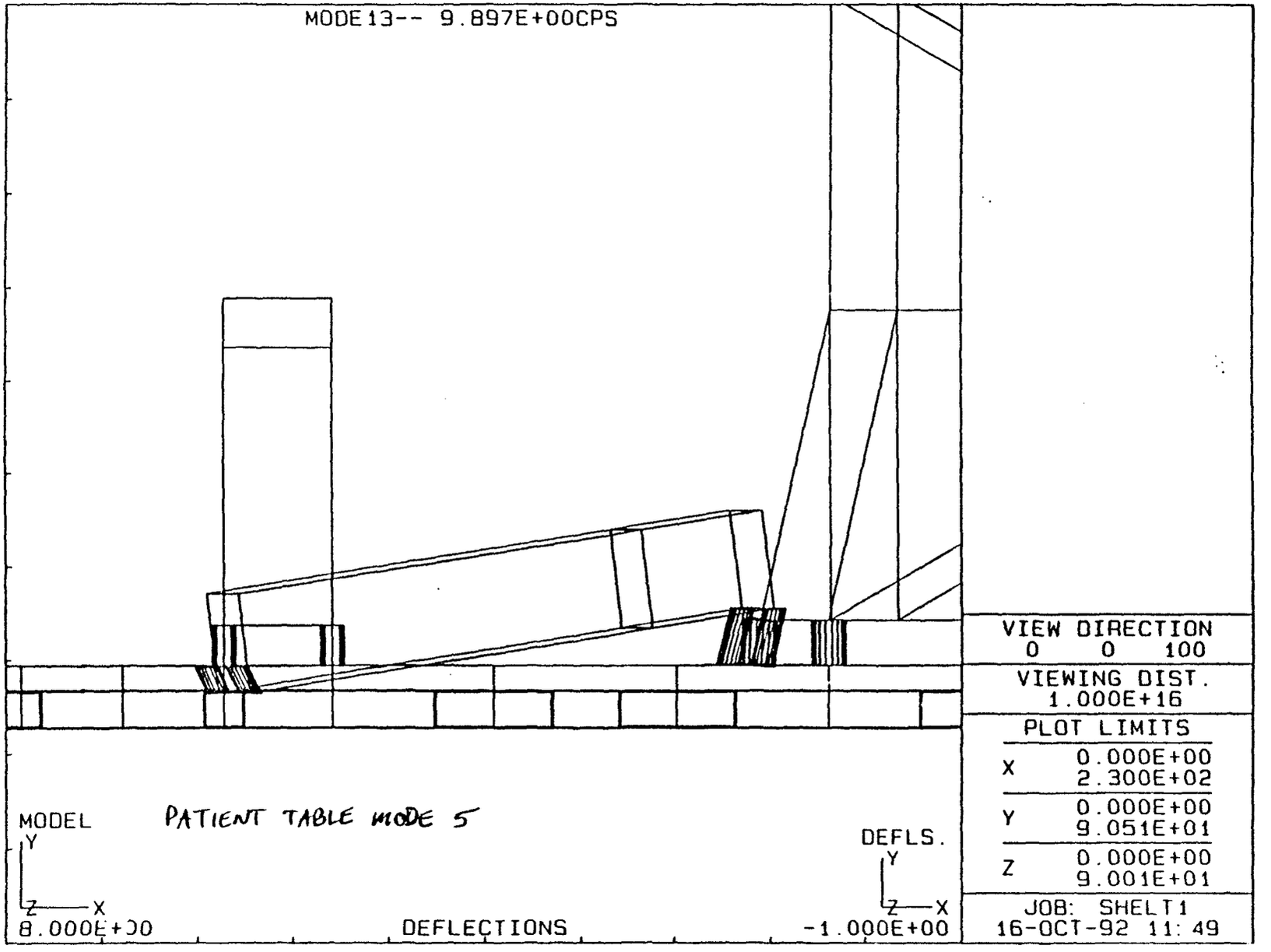
MODE 13-- 9.897E+00CPS
VIEW DIRECTION
0 0 100
VIEWING DIST.
1.000E+16
PLOT LIMITS
X 0.000E+00
2.300E+02
Y 0.000E+00
9.051E+01
Z 0.000E+00
9.001E+01
JOB: SHELT1
16-OCT-92 11:49
MODEL
PATIENT TABLE MODE 5
DEFLS.
Y
Z X
8.000E+00
DEFLECTIONS
-1.000E+00

Figure 21

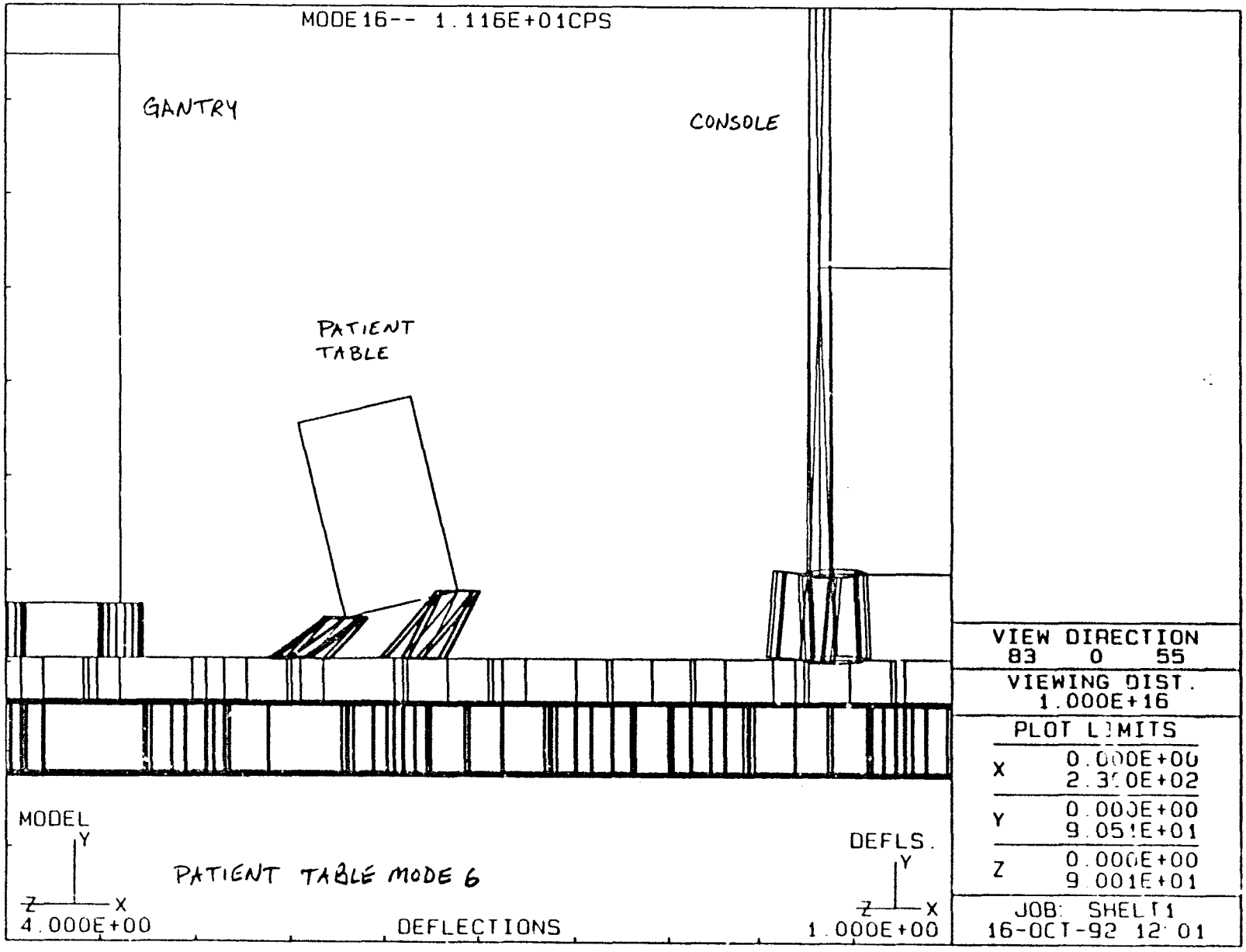
MODE 16-- 1.116E+01CPS
GANTRY
CONSOLE
PATIENT TABLE
MODEL
Y
Z
X
4.000E+00
PATIENT TABLE MODE 6
DEFLECTIONS
DEFLS.
Y
Z
X
1.000E+00
VIEW DIRECTION
83 0 55
VIEWING DIST.
1.000E+16
PLOT LIMITS
X 0.000E+00
2.300E+02
Y 0.000E+00
9.051E+01
Z 0.000E+00
9.001E+01
JOB: SHELL1
16-OCT-92 12:01

Figure 22

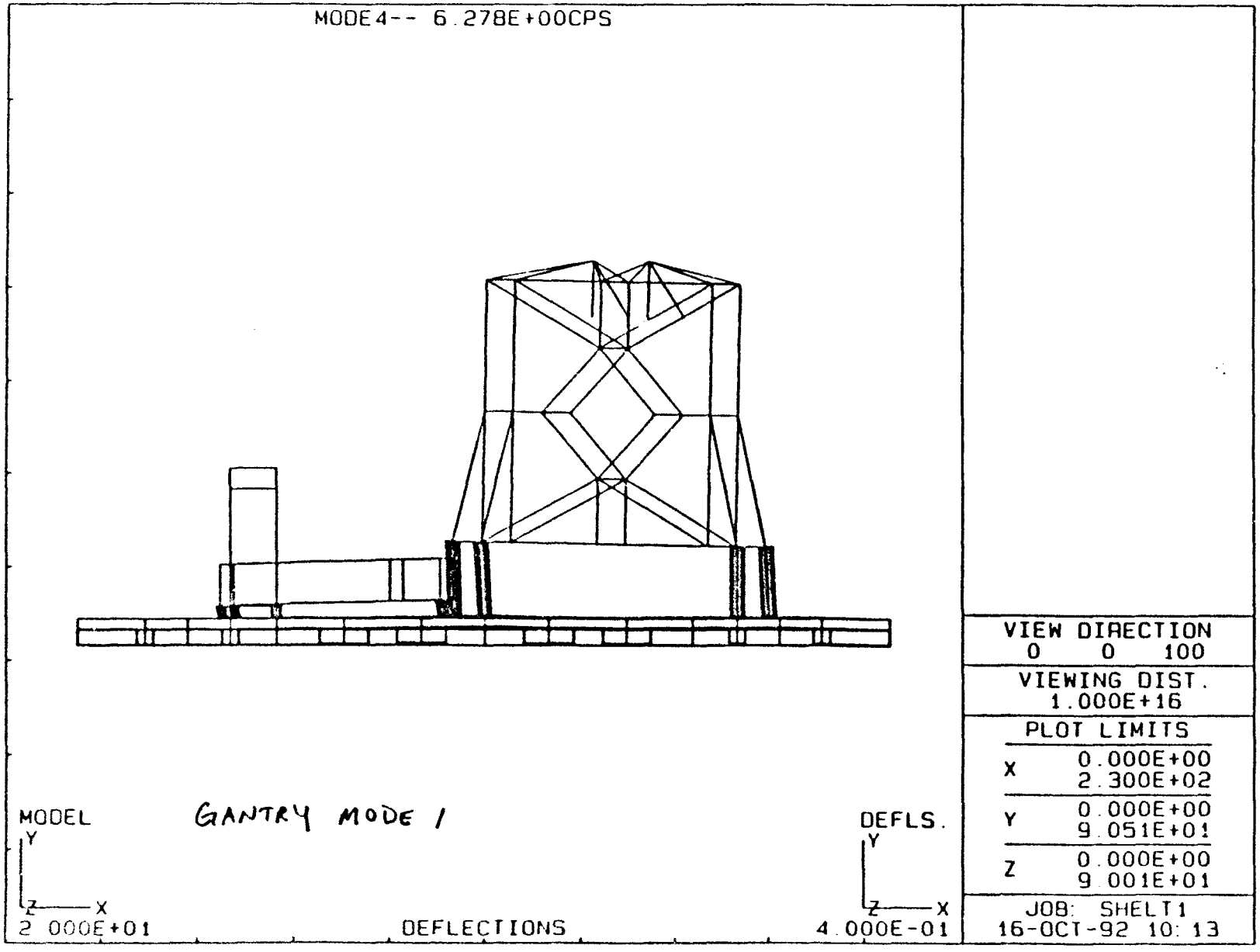
MODE 4-- 6.278E+00CPS
VIEW DIRECTION
0 0 100
VIEWING DIST.
1.000E+16
PLOT LIMITS
X 0.000E+00
2.300E+02
Y 0.000E+00
9.051E+01
Z 0.000E+00
9.001E+01
JOB: SHELT1
16-OCT-92 10:13
MODEL
Y
Z
X
GANTRY MODE 1
DEFLS.
Y
Z
X
2.000E+01
DEFLECTIONS
4.000E-01

Figure 23

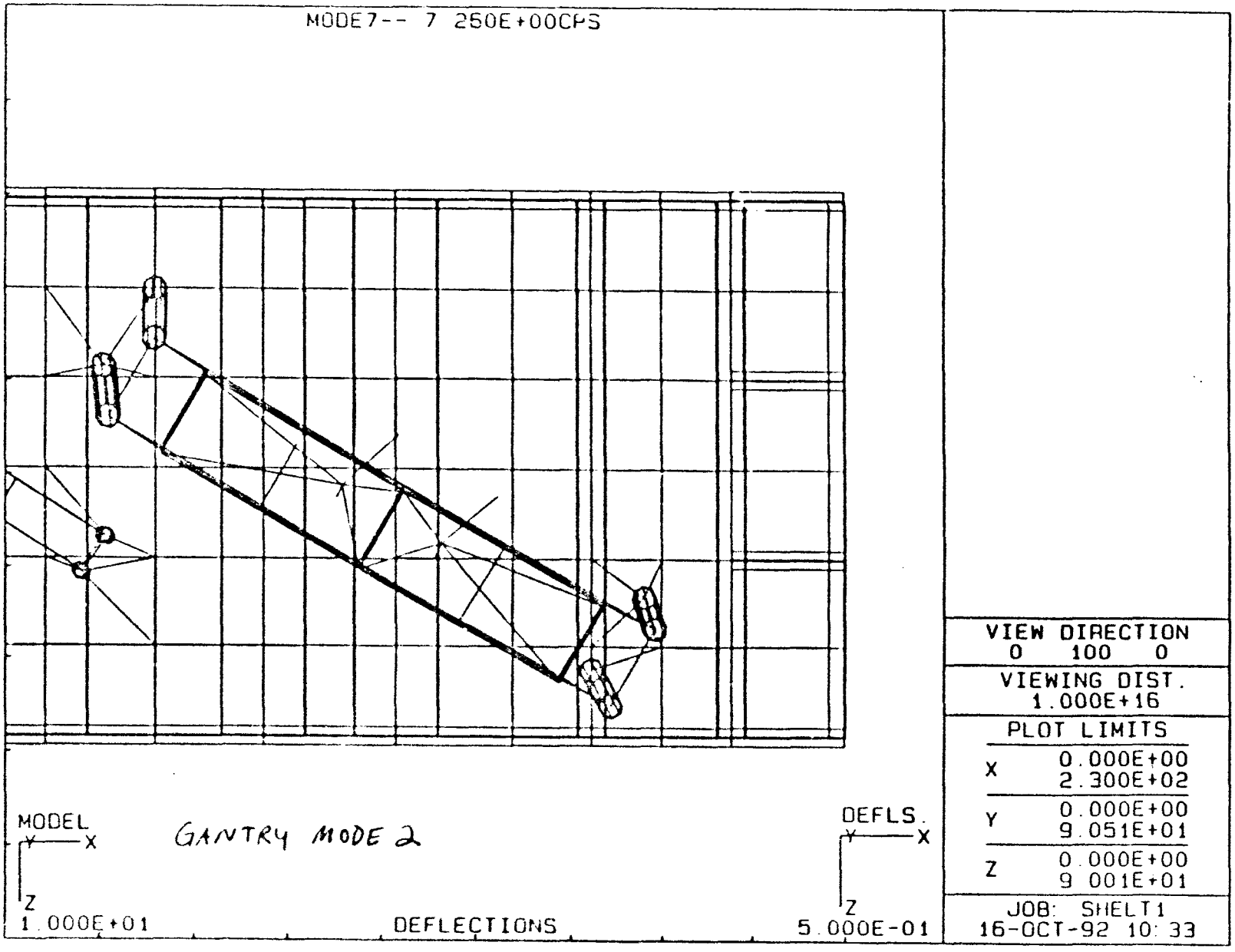
MODE7-- 7.250E+00CPS
MODEL
X
Z
GANTRY MODE 2
DEFLS.
X
Z
1.000E+01
DEFLECTIONS
5.000E-01
VIEW DIRECTION
0 100 0
VIEWING DIST.
1.000E+16
PLOT LIMITS
X 0.000E+00 2.300E+02
Y 0.000E+00 9.051E+01
Z 0.000E+00 9.001E+01
JOB: SHELT1
16-OCT-92 10:33

Figure 24

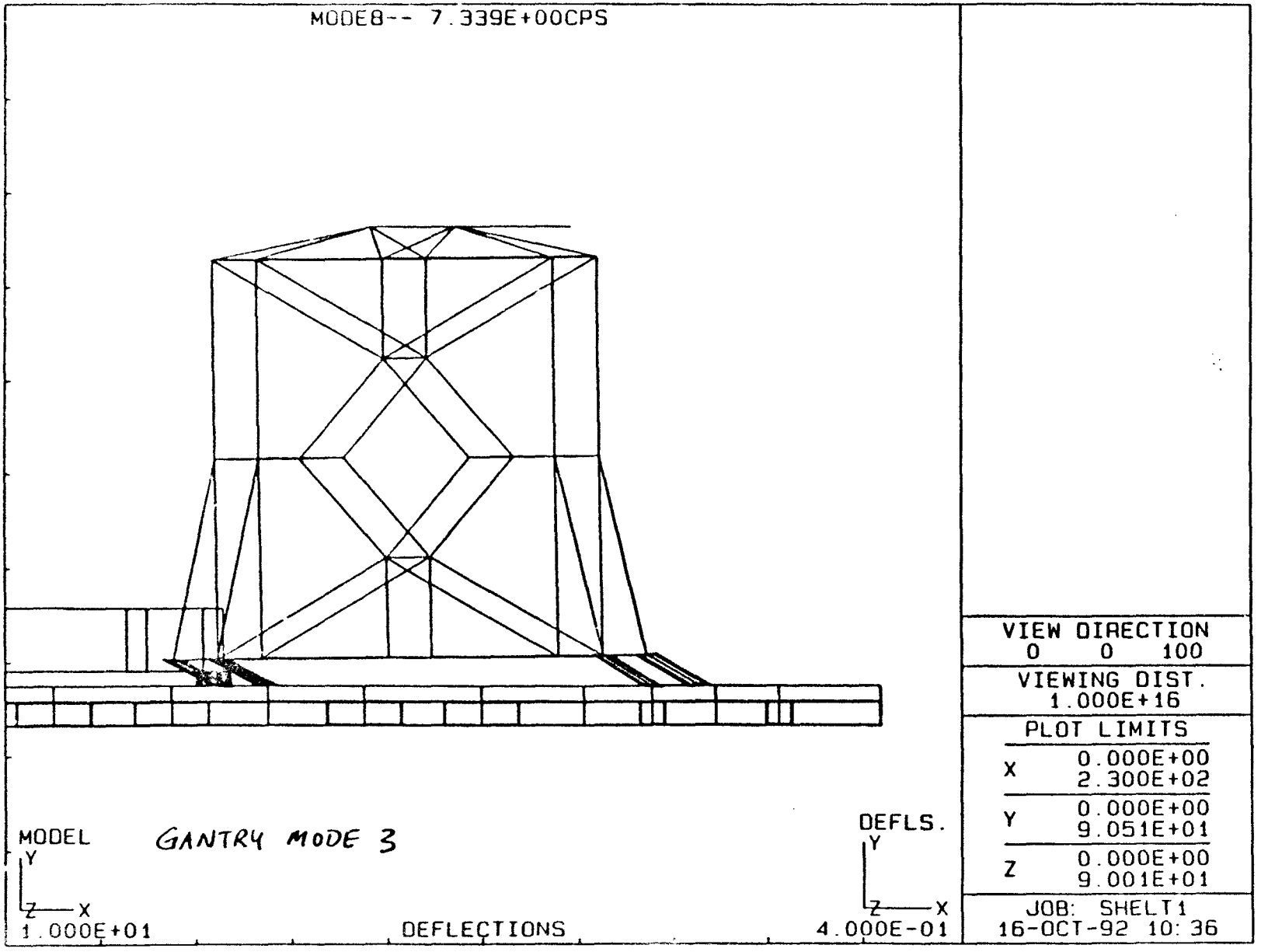
MODE8-- 7.339E+00CPS
VIEW DIRECTION
0 0 100
VIEWING DIST.
1.000E+16
PLOT LIMITS
X 0.000E+00
2.300E+02
Y 0.000E+00
9.051E+01
Z 0.000E+00
9.001E+01
JOB: SHELT1
16-OCT-92 10:36
MODEL
GANTRY MODE 3
DEFLS.
1.000E+01
DEFLECTIONS
4.000E-01

Figure 25

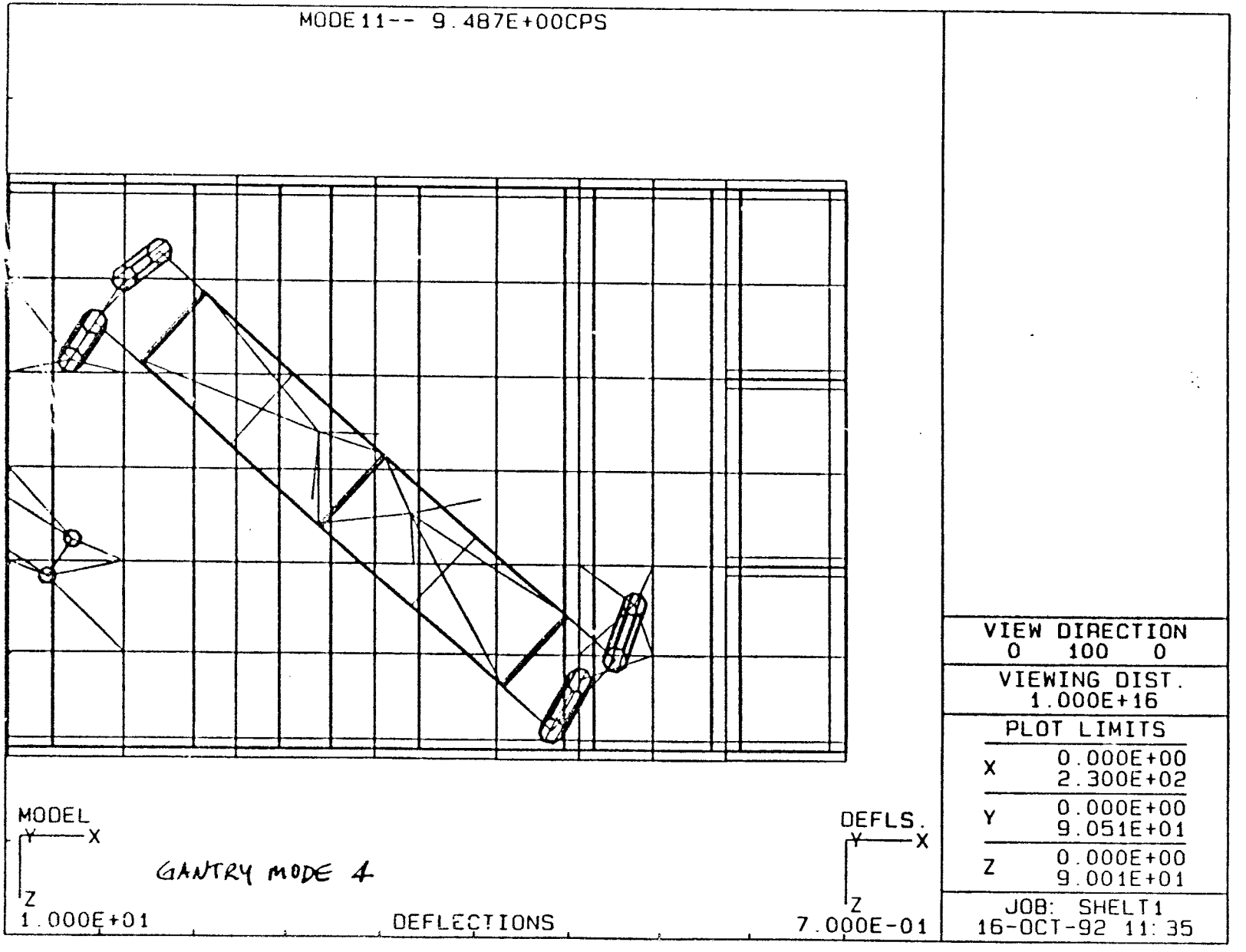
MODE 11-- 9.487E+00CPS
VIEW DIRECTION
0 100 0
VIEWING DIST.
1.000E+16
PLOT LIMITS
X 0.000E+00
2.300E+02
Y 0.000E+00
9.051E+01
Z 0.000E+00
9.001E+01
JOB: SHELT1
16-OCT-92 11:35
MODEL
Y X
Z
GANTRY MODE 4
1.000E+01
DEFLECTIONS
DEFLS.
Y X
Z
7.000E-01

Figure 26

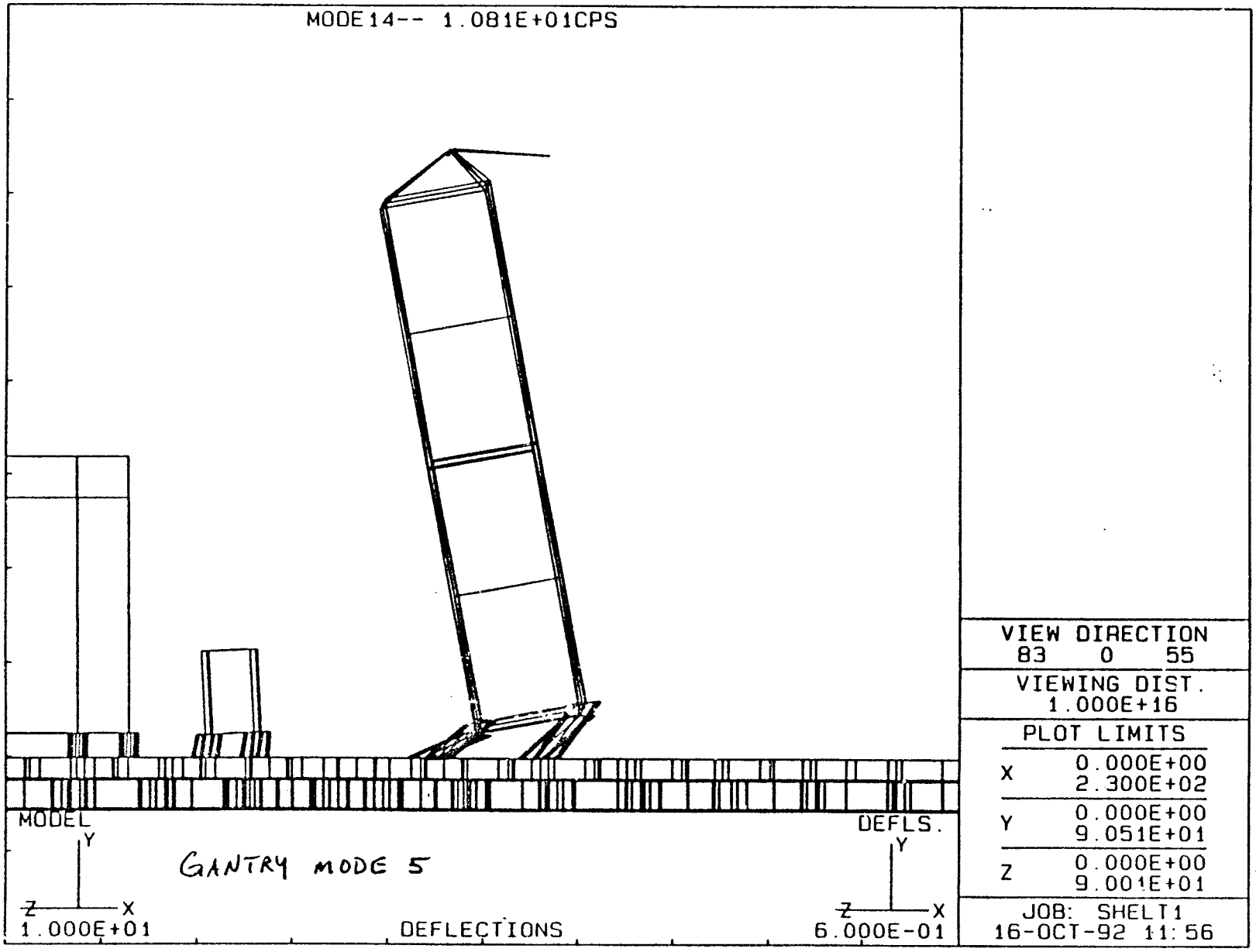
MODE 14-- 1.081E+01CPS
VIEW DIRECTION
83 0 55
VIEWING DIST.
1.000E+16
PLOT LIMITS
X 0.000E+00
2.300E+02
Y 0.000E+00
9.051E+01
Z 0.000E+00
9.001E+01
JOB: SHELT1
16-OCT-92 11:56
MODEL
Y
Z
X
1.000E+01
GANTRY MODE 5
DEFLS.
Y
Z
X
6.000E-01
DEFLECTIONS

Figure 27

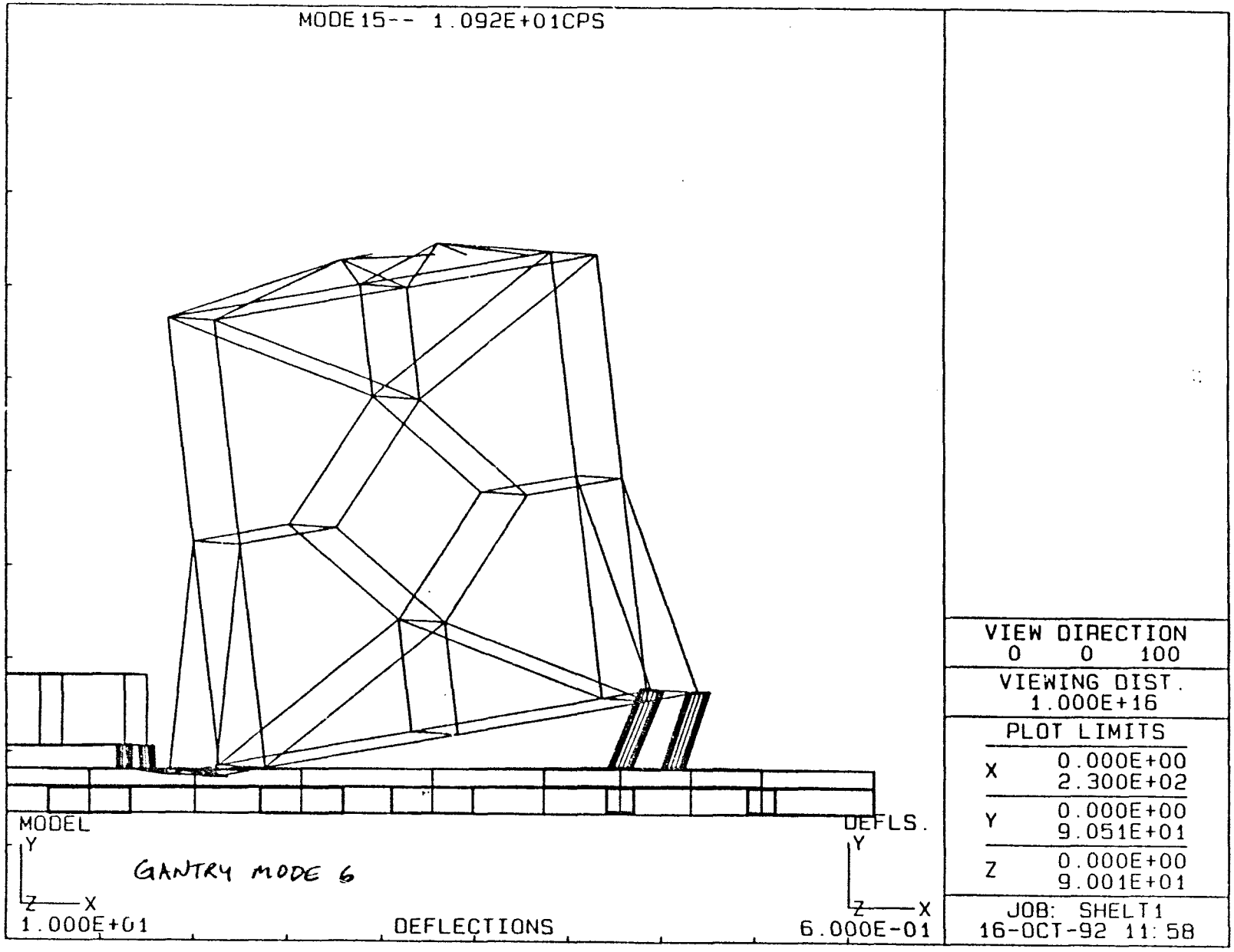
MODE 15-- 1.092E+01CPS
VIEW DIRECTION
0 0 100
VIEWING DIST.
1.000E+16
PLOT LIMITS
X 0.000E+00
2.300E+02
Y 0.000E+00
9.051E+01
Z 0.000E+00
9.001E+01
JOB: SHELT1
16-OCT-92 11:58
MODEL
Y
Z X
GANTRY MODE 6
DEFLS.
Y
Z X
1.000E+01
DEFLECTIONS
6.000E-01

Figure 28

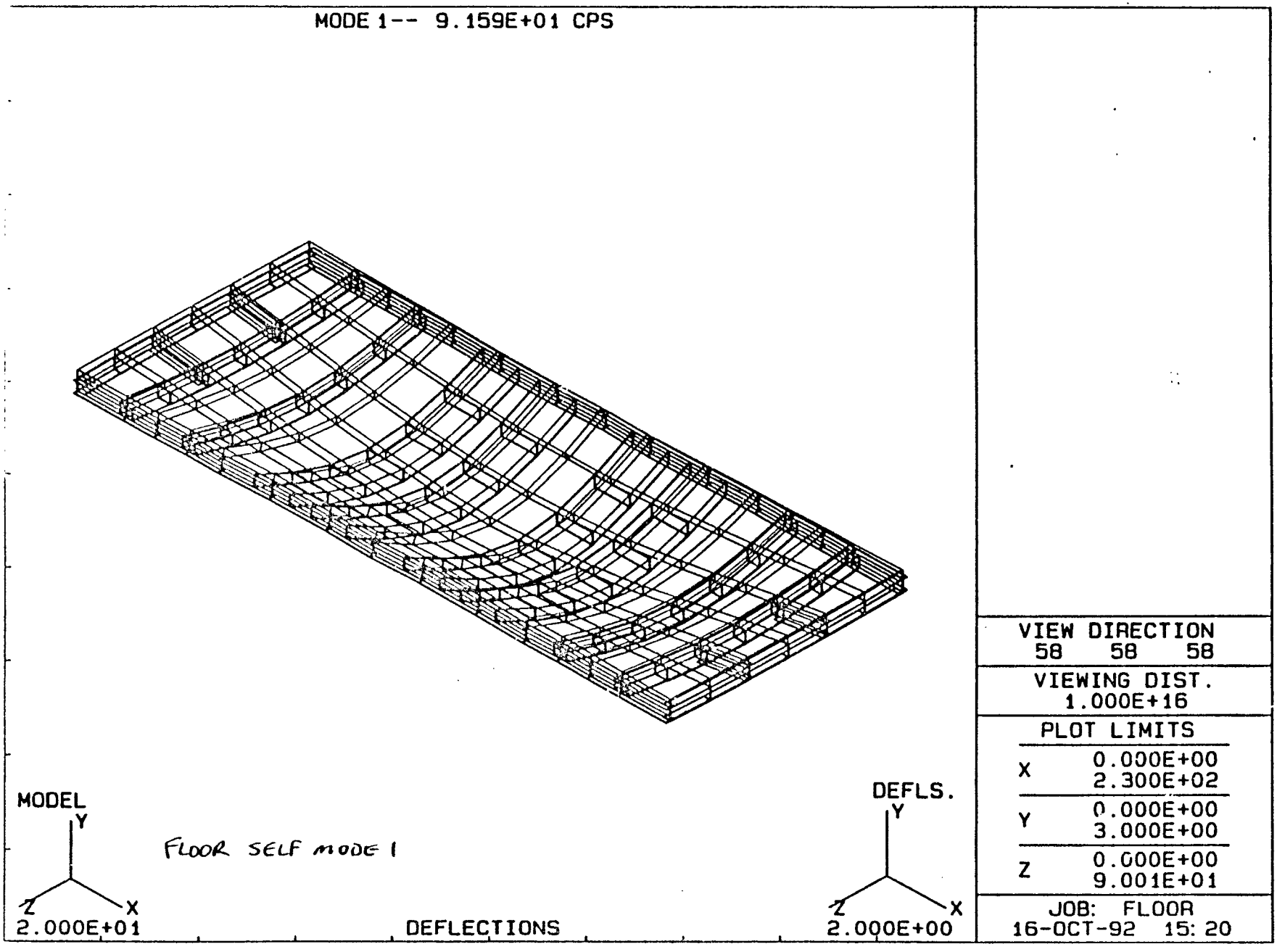
MODE 1-- 9.159E+01 CPS
MODEL
Y
Z
X
2.000E+01
FLOOR SELF MODE 1
DEFLECTIONS
DEFLS.
Y
Z
X
2.000E+00
VIEW DIRECTION
58 58 58
VIEWING DIST.
1.000E+16
PLOT LIMITS
X 0.000E+00
2.300E+02
Y 0.000E+00
3.000E+00
Z 0.000E+00
9.001E+01
JOB: FLOOR
16-OCT-92 15:20

Figure 29

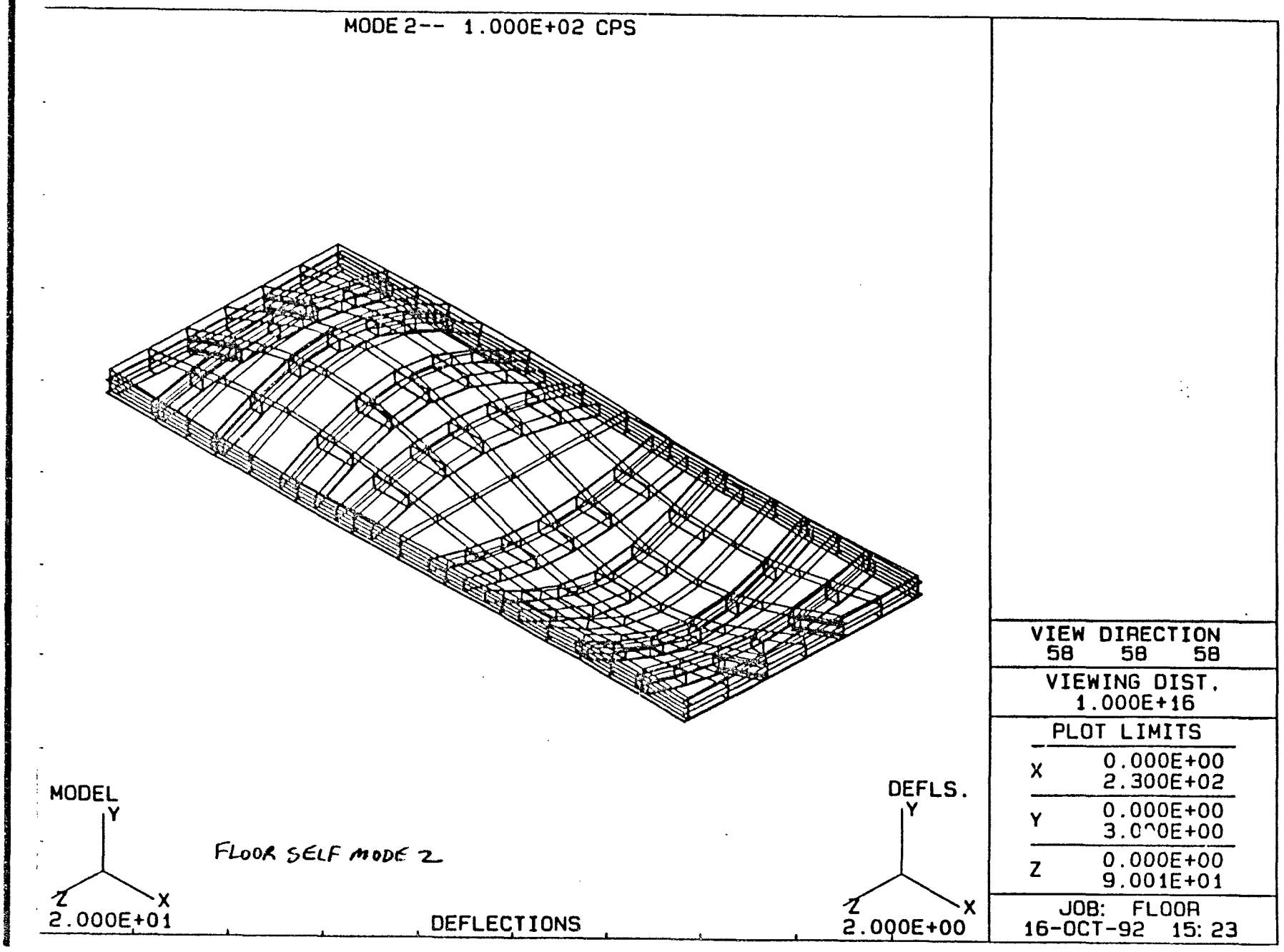
MODE 2-- 1.000E+02 CPS
VIEW DIRECTION
58 58 58
VIEWING DIST.
1.000E+16
PLOT LIMITS
X 0.000E+00
2.300E+02
Y 0.000E+00
3.0^0E+00
Z 0.000E+00
9.001E+01
JOB: FLOOR
16-OCT-92 15:23
MODEL
Y
Z
X
2.000E+01
FLOOR SELF MODE 2
DEFLS.
Y
Z
X
2.000E+00
DEFLECTIONS

Figure 30

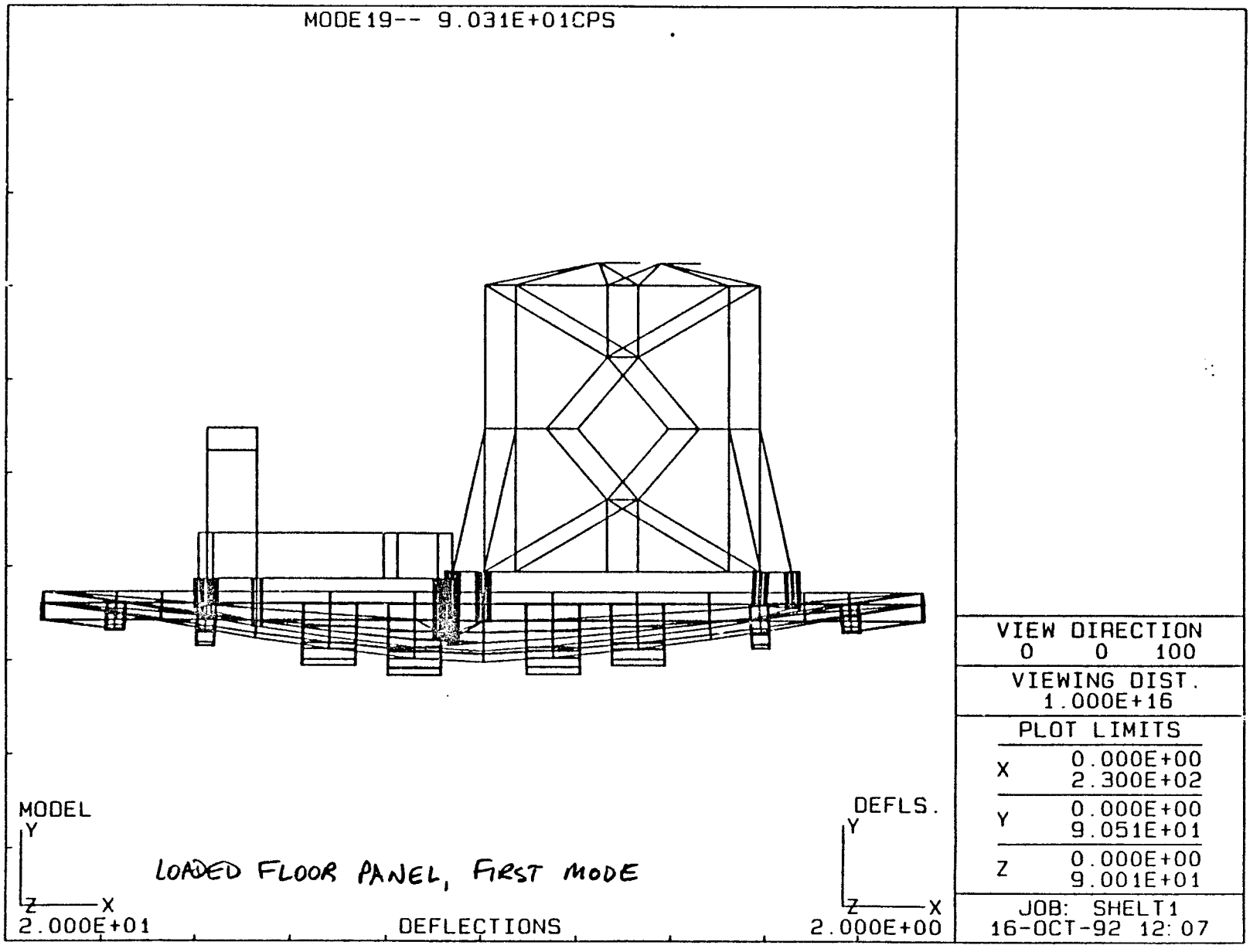
MODE19-- 9.031E+01CPS
VIEW DIRECTION
0 0 100
VIEWING DIST.
1.000E+16
PLOT LIMITS
X 0.000E+00
2.300E+02
Y 0.000E+00
9.051E+01
Z 0.000E+00
9.001E+01
JOB: SHELT1
16-OCT-92 12:07
MODEL
Y
Z
X
2.000E+01
LOADED FLOOR PANEL, FIRST MODE
DEFLECTIONS
DEFLS.
Y
Z
X
2.000E+00

Figure 31

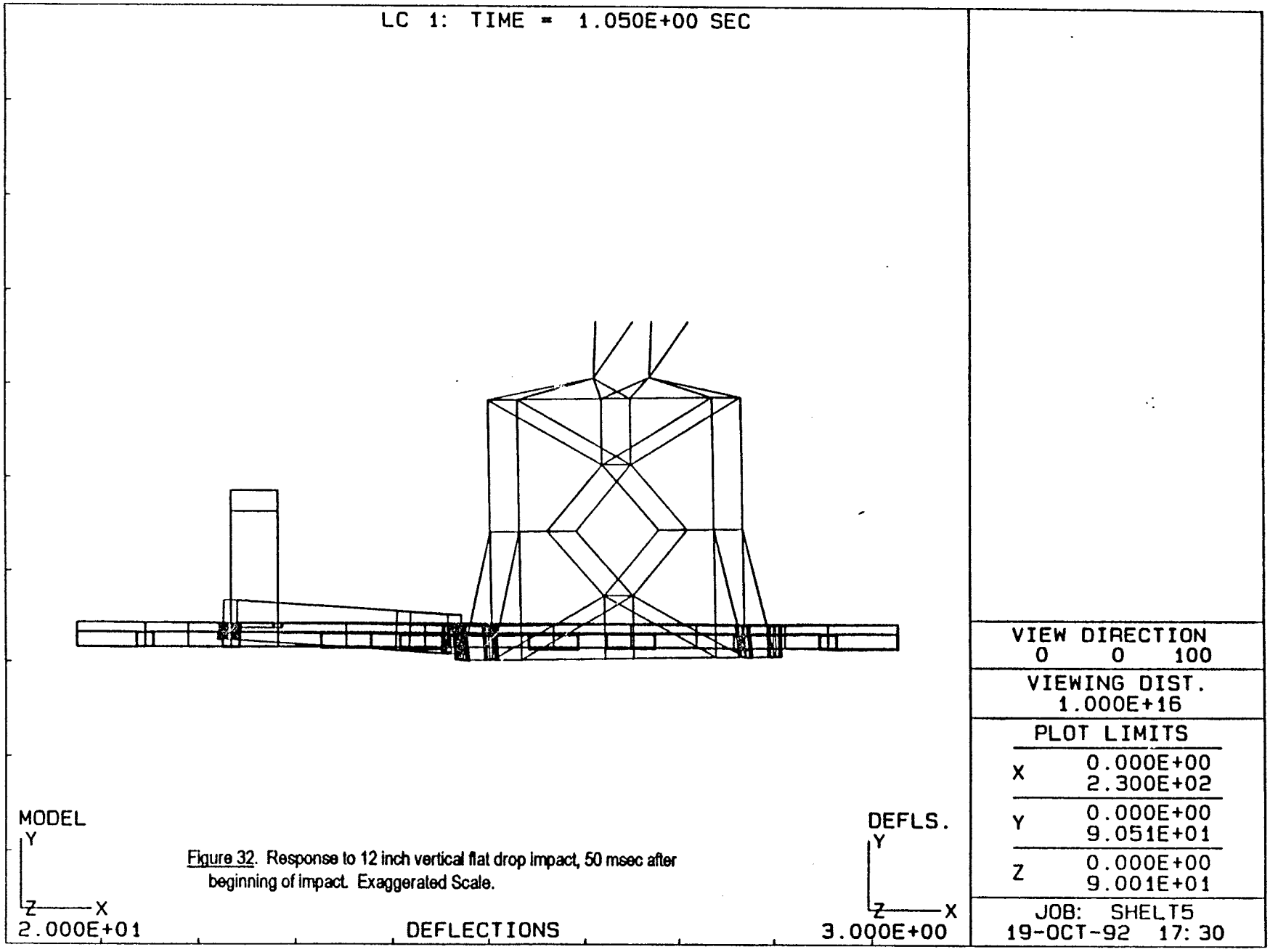

Figure 32. Response to 12 inch vertical flat drop impact, 50 msec after beginning of impact. Exaggerated Scale.

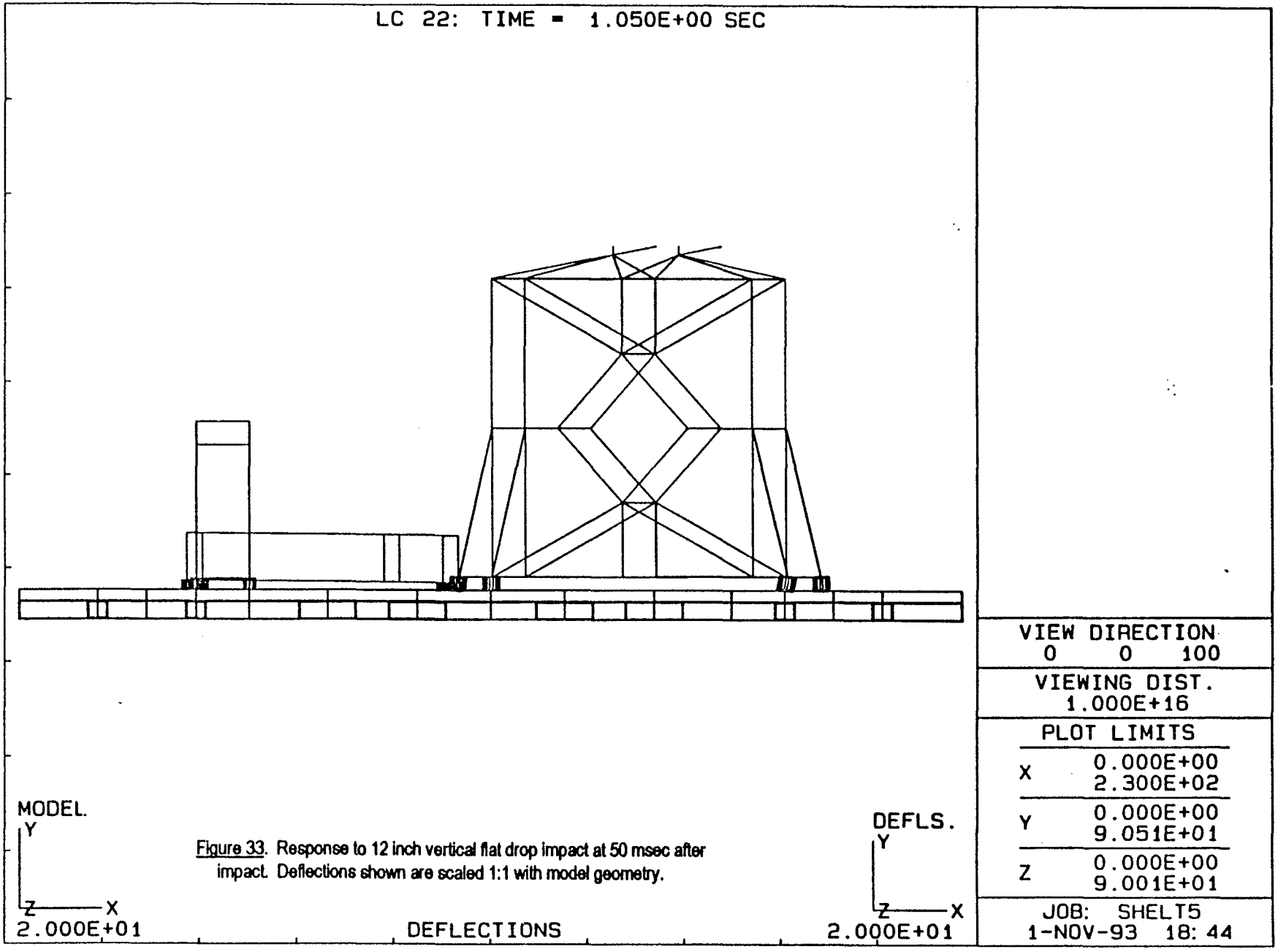

Figure 33. Response to 12 inch vertical flat drop impact at 50 msec after impact. Deflections shown are scaled 1:1 with model geometry.

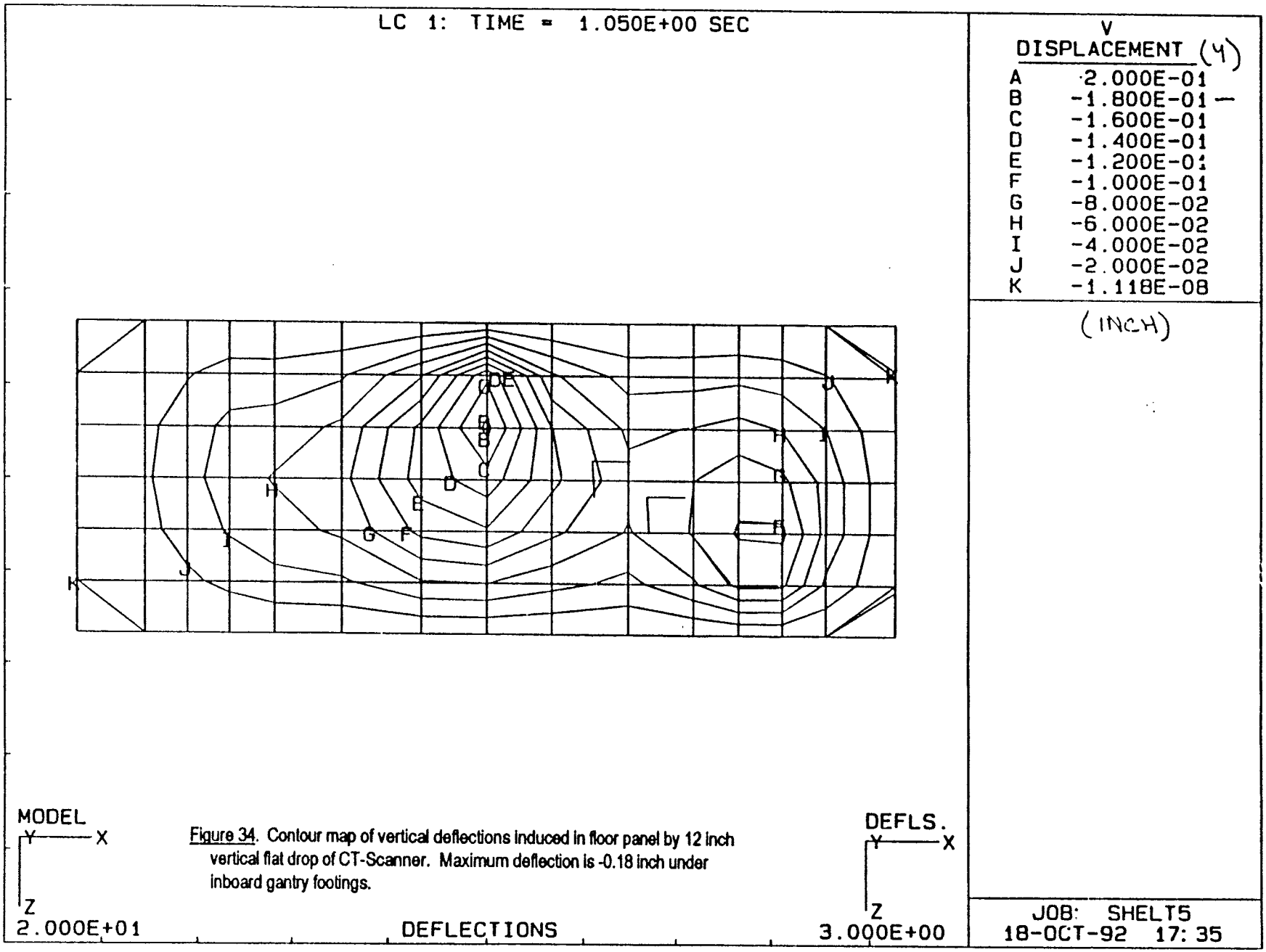

Figure 34. Contour map of vertical deflections induced in floor panel by 12 inch vertical flat drop of CT-Scanner. Maximum deflection is -0.18 inch under inboard gantry footings.

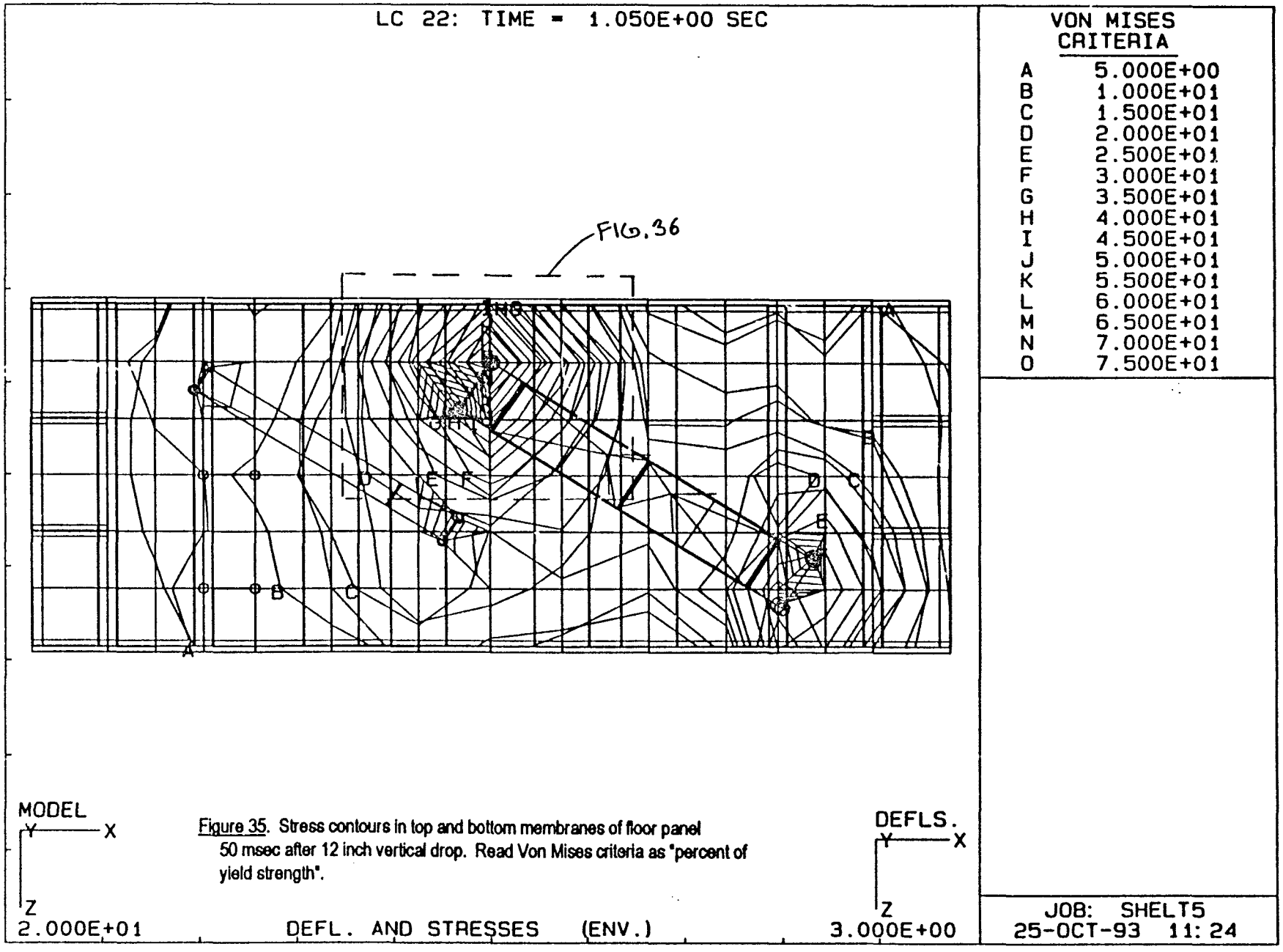

Figure 35. Stress contours in top and bottom membranes of floor panel 50 msec after 12 inch vertical drop. Read Von Mises criteria as "percent of yield strength".

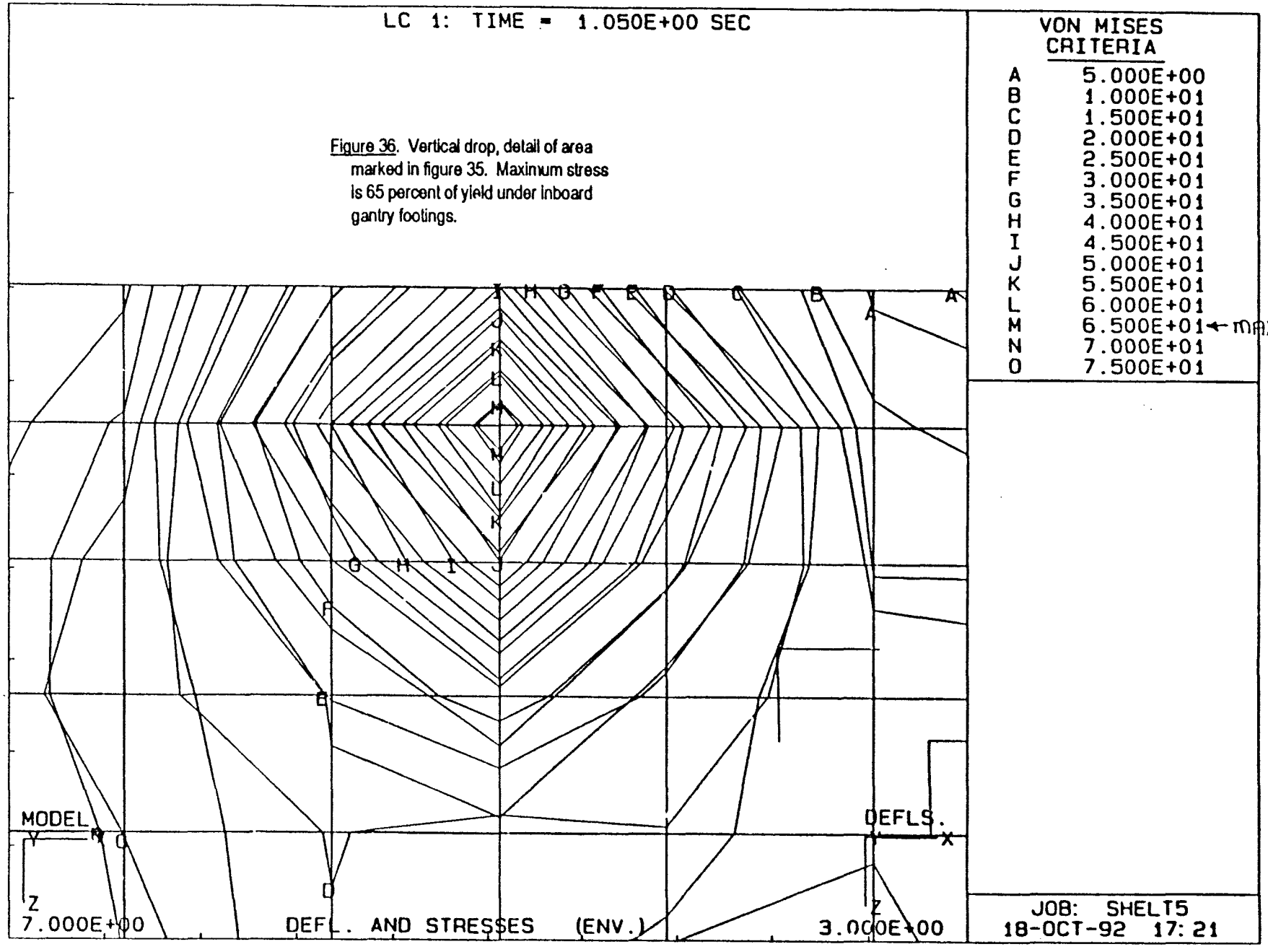

Figure 36. Vertical drop, detail of area marked in figure 35. Maximum stress is 65 percent of yield under inboard gantry footings.

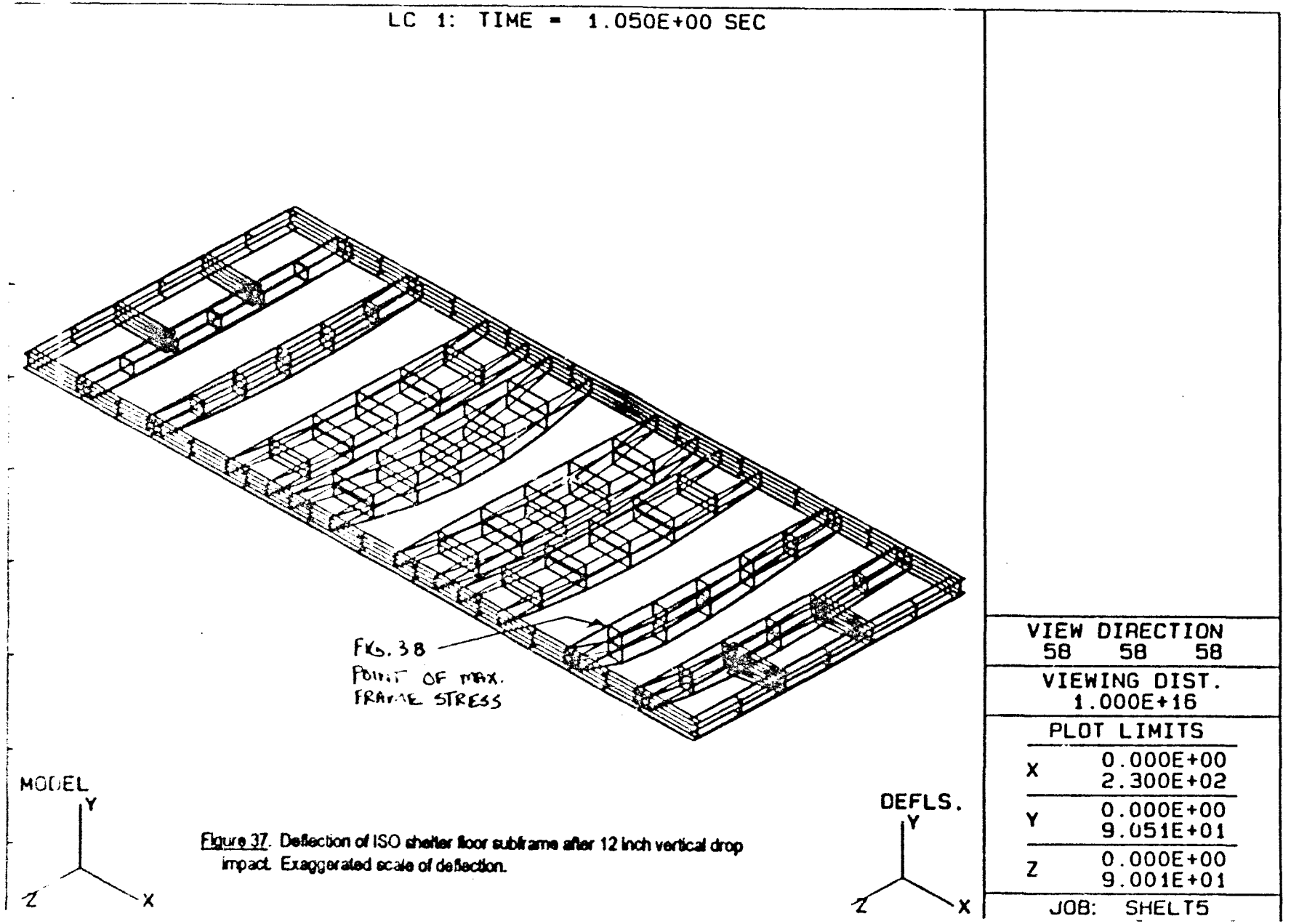

Figure 37. Deflection of ISO shelter floor subframe after 12 inch vertical drop impact. Exaggerated scale of deflection.

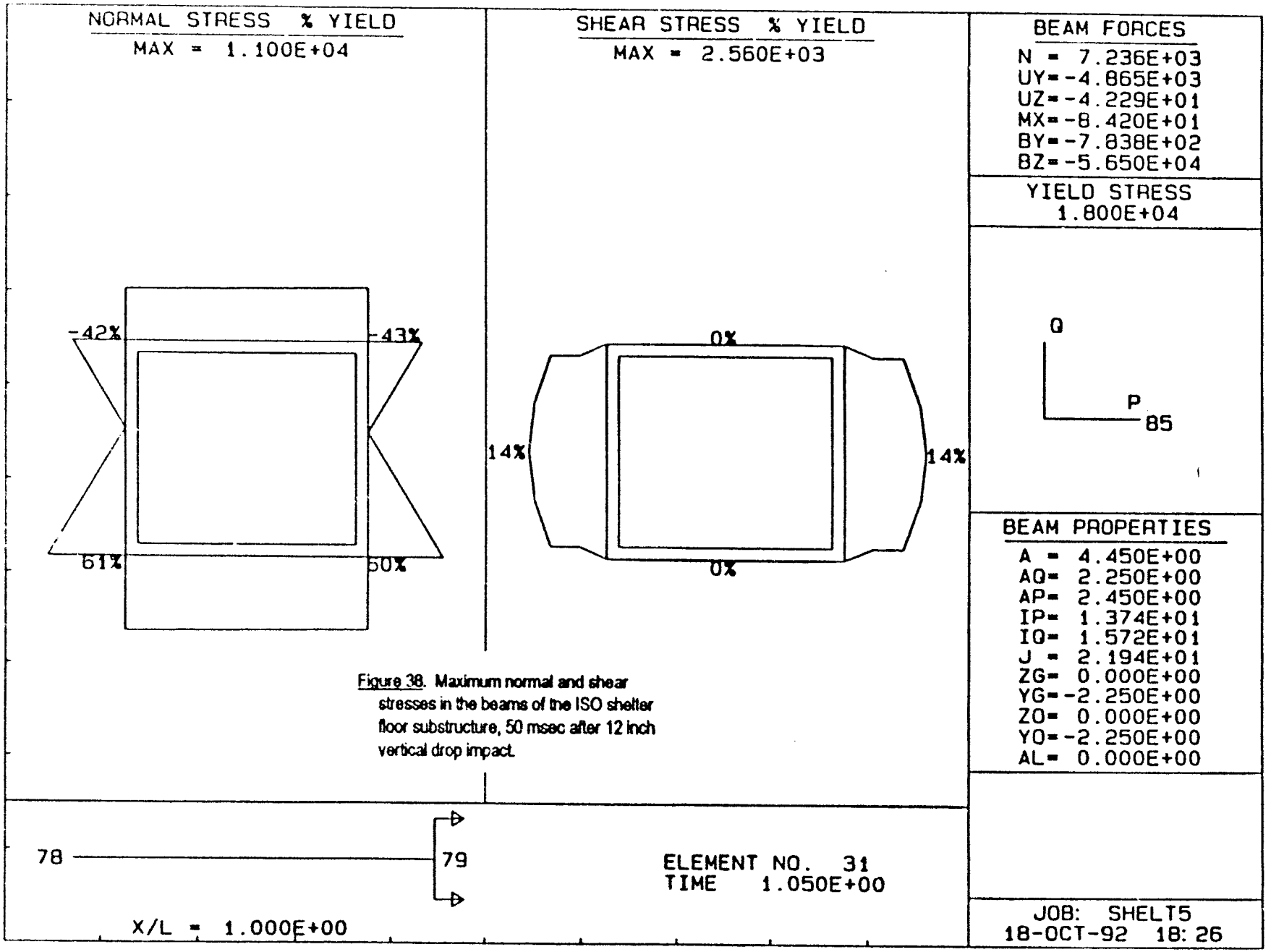

Figure 38. Maximum normal and shear stresses in the beams of the ISO shelter floor substructure, 50 msec after 12 inch vertical drop impact.

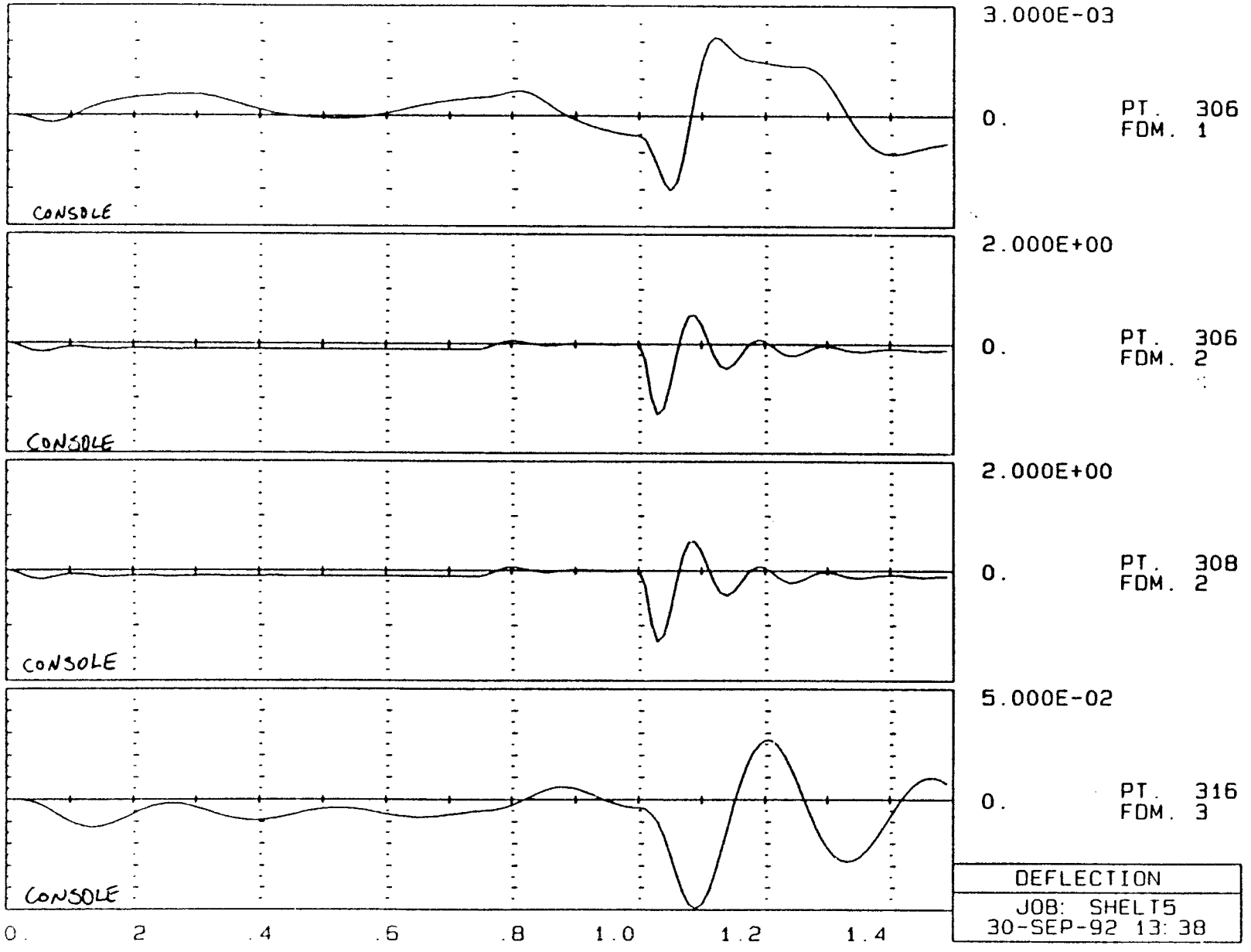
3.000E-03
0.
PT. 306
FDM. 1
CONSOLE
2.000E+00
0.
PT. 306
FDM. 2
CONSOLE
2.000E+00
0.
PT. 308
FDM. 2
CONSOLE
5.000E-02
0.
PT. 316
FDM. 3
CONSOLE
0.
.2
.4
.6
.8
1.0
1.2
1.4
DEFLECTION
JOB: SHELT5
30-SEP-92 13:38

Figure 39

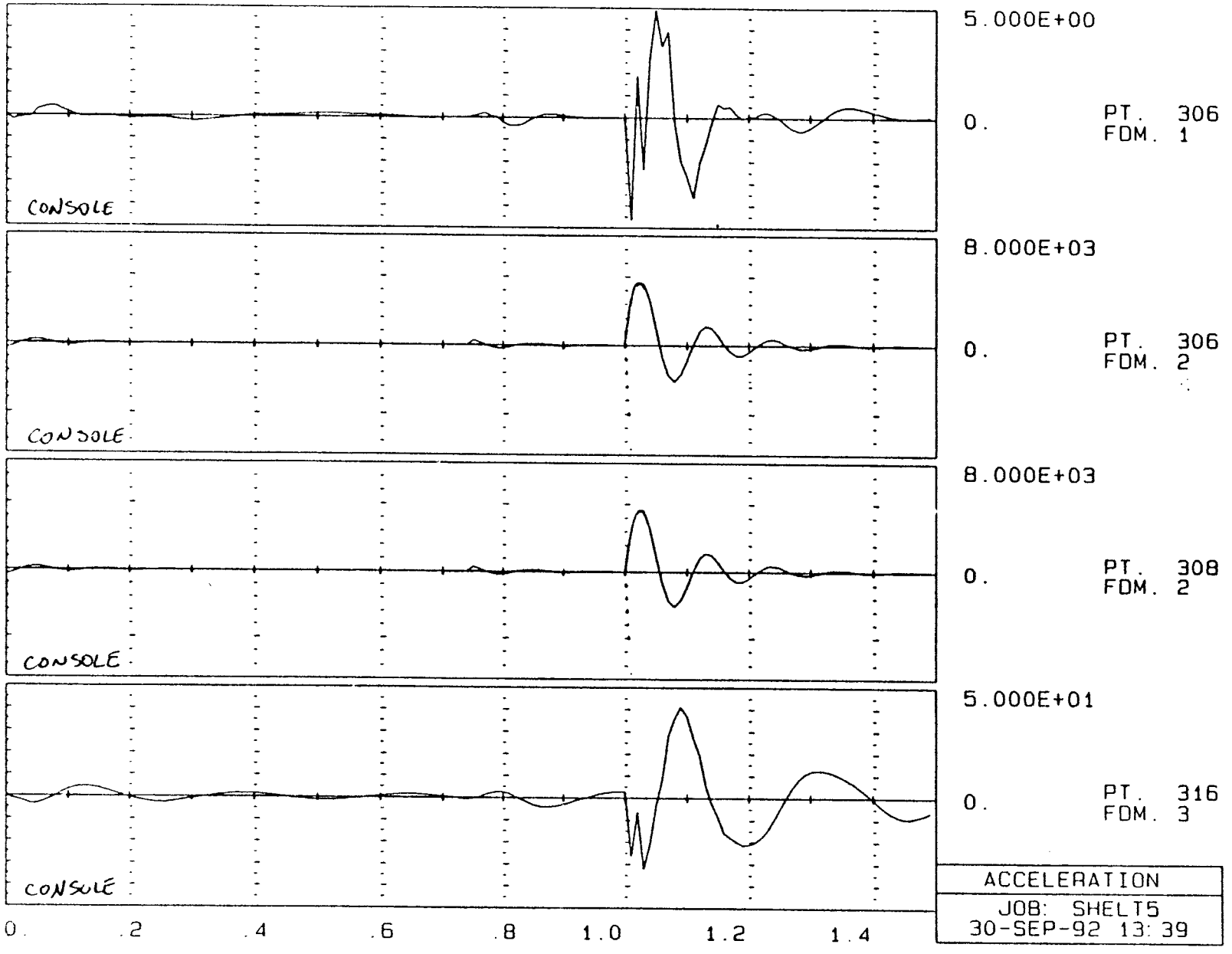
5.000E+00
0.
PT. 306
FDM. 1
CONSOLE
8.000E+03
0.
PT. 306
FDM. 2
CONSOLE
8.000E+03
0.
PT. 308
FDM. 2
CONSOLE
5.000E+01
0.
PT. 316
FDM. 3
CONSOLE
0.
.2
.4
.6
.8
1.0
1.2
1.4
ACCELERATION
JOB: SHELTS
30-SEP-92 13:39

Figure 40

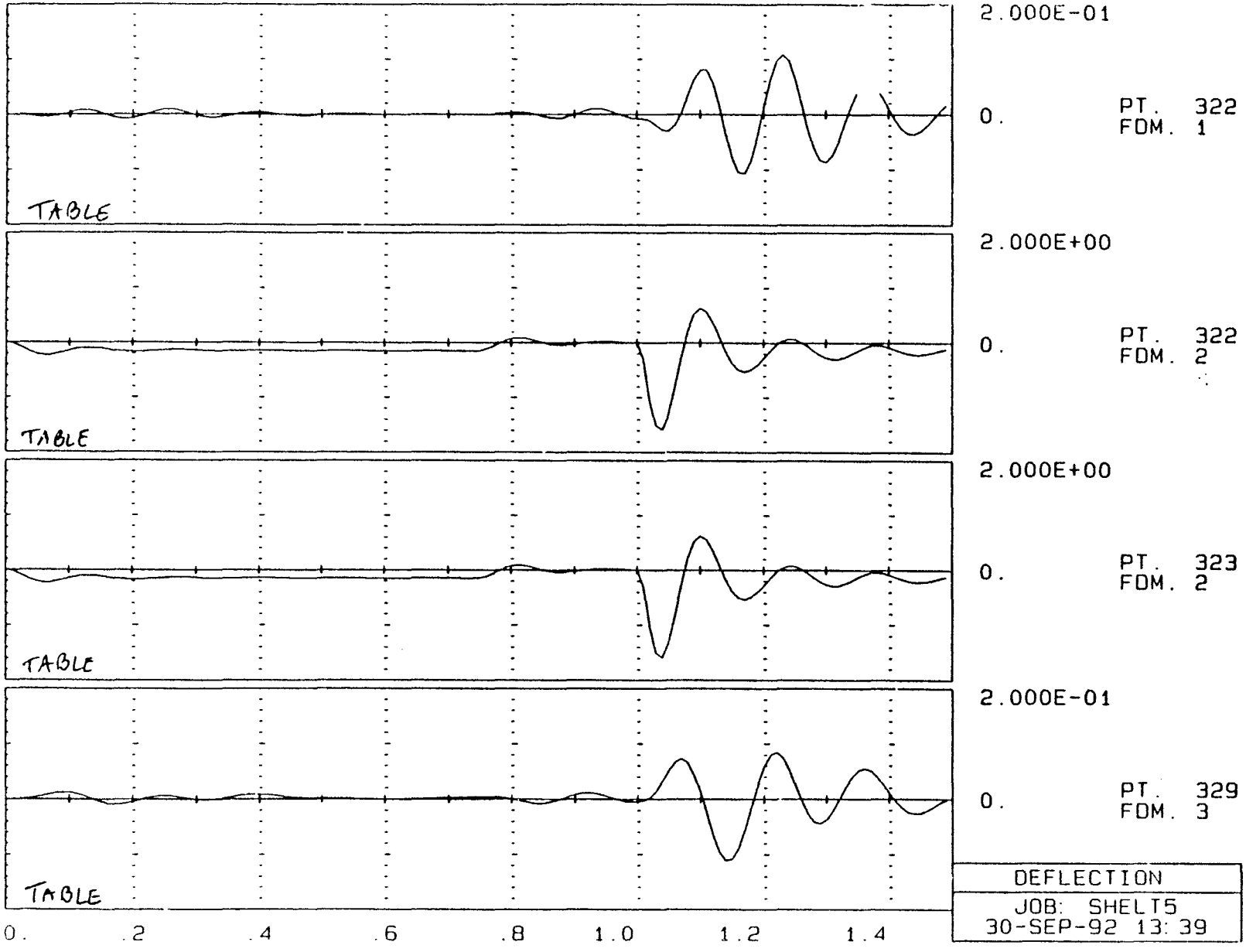
2.000E-01
0.
PT. 322
FDM. 1
TABLE
2.000E+00
0.
PT. 322
FDM. 2
TABLE
2.000E+00
0.
PT. 323
FDM. 2
TABLE
2.000E-01
0.
PT. 329
FDM. 3
TABLE
0.
.2
.4
.6
.8
1.0
1.2
1.4
DEFLECTION
JOB: SHELT5
30-SEP-92 13:39

Figure 41

Figure 43

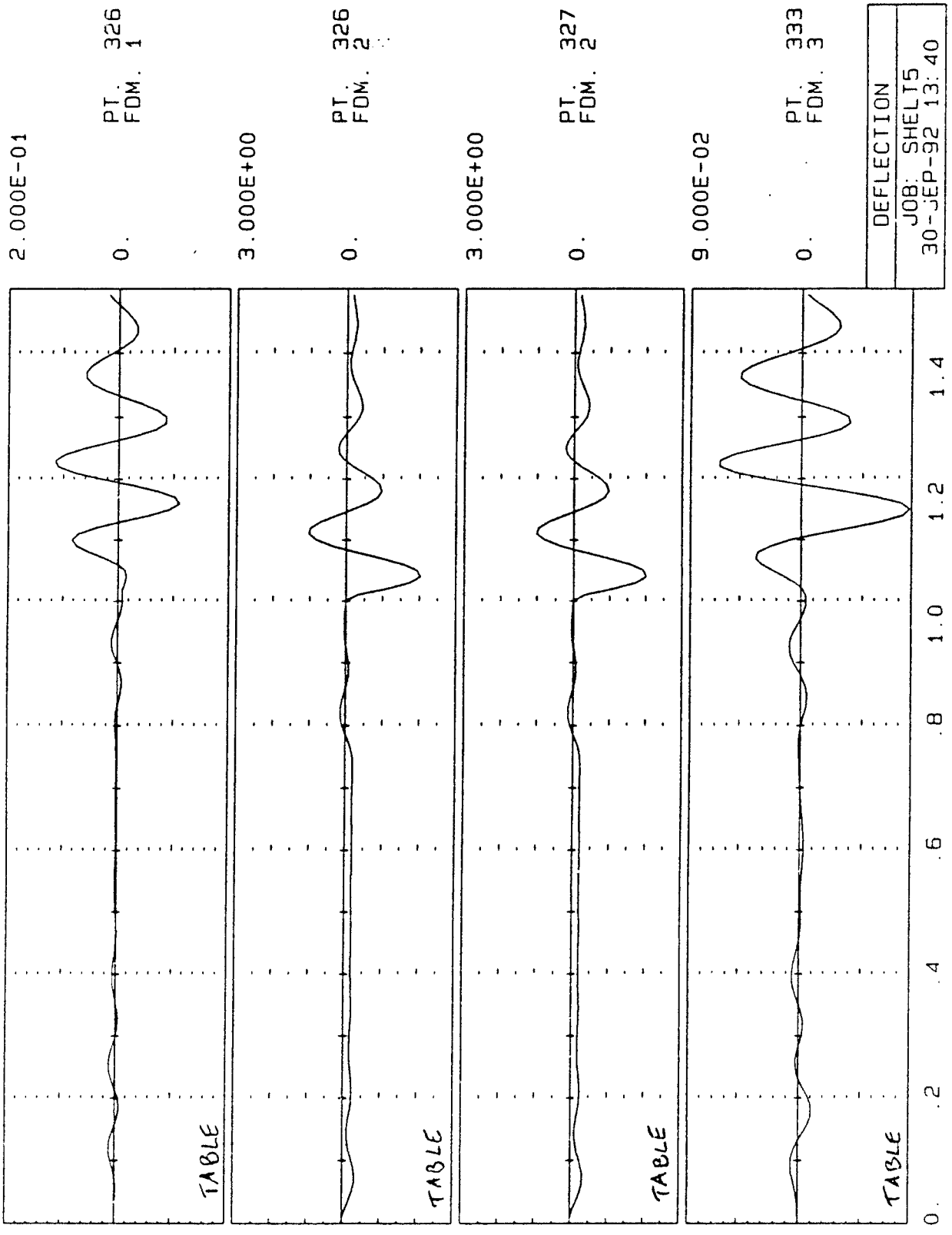
DEFLECTION
JOB: SHELT5
30-SEP-92 13:40
2.000E-01
PT. 326
FOM. 1
0.
TABLE
3.000E+00
PT. 326
FOM. 2
0.
TABLE
3.000E+00
PT. 327
FOM. 2
0.
TABLE
9.000E-02
PT. 333
FOM. 3
0.
TABLE
0. .2 .4 .6 .8 1.0 1.2 1.4

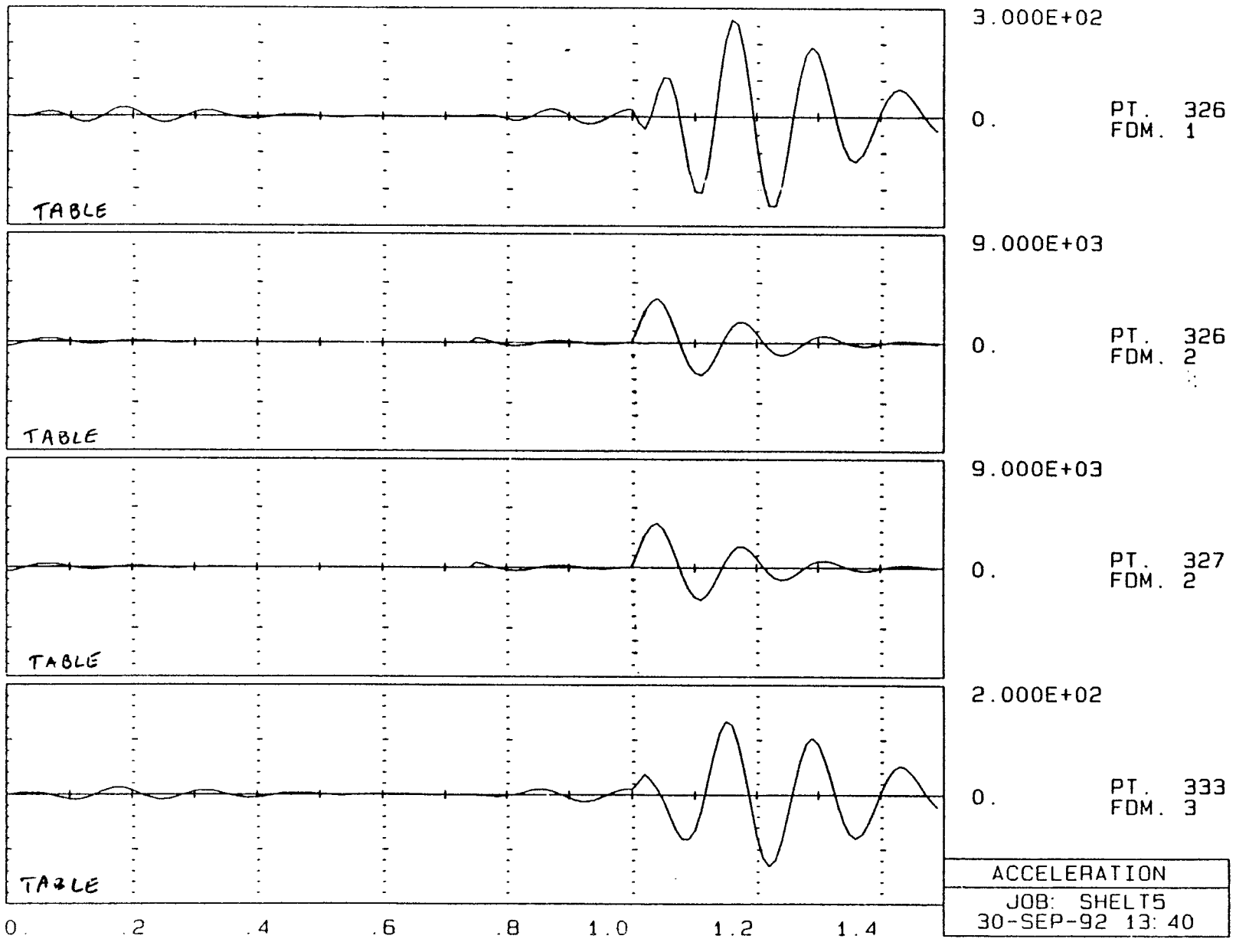
3.000E+02
0.
PT. 326
FDM. 1
TABLE
9.000E+03
0.
PT. 326
FDM. 2
TABLE
9.000E+03
0.
PT. 327
FDM. 2
TABLE
2.000E+02
0.
PT. 333
FDM. 3
TABLE
0.
.2
.4
.6
.8
1.0
1.2
1.4
ACCELERATION
JOB: SHELT5
30-SEP-92 13:40

Figure 44

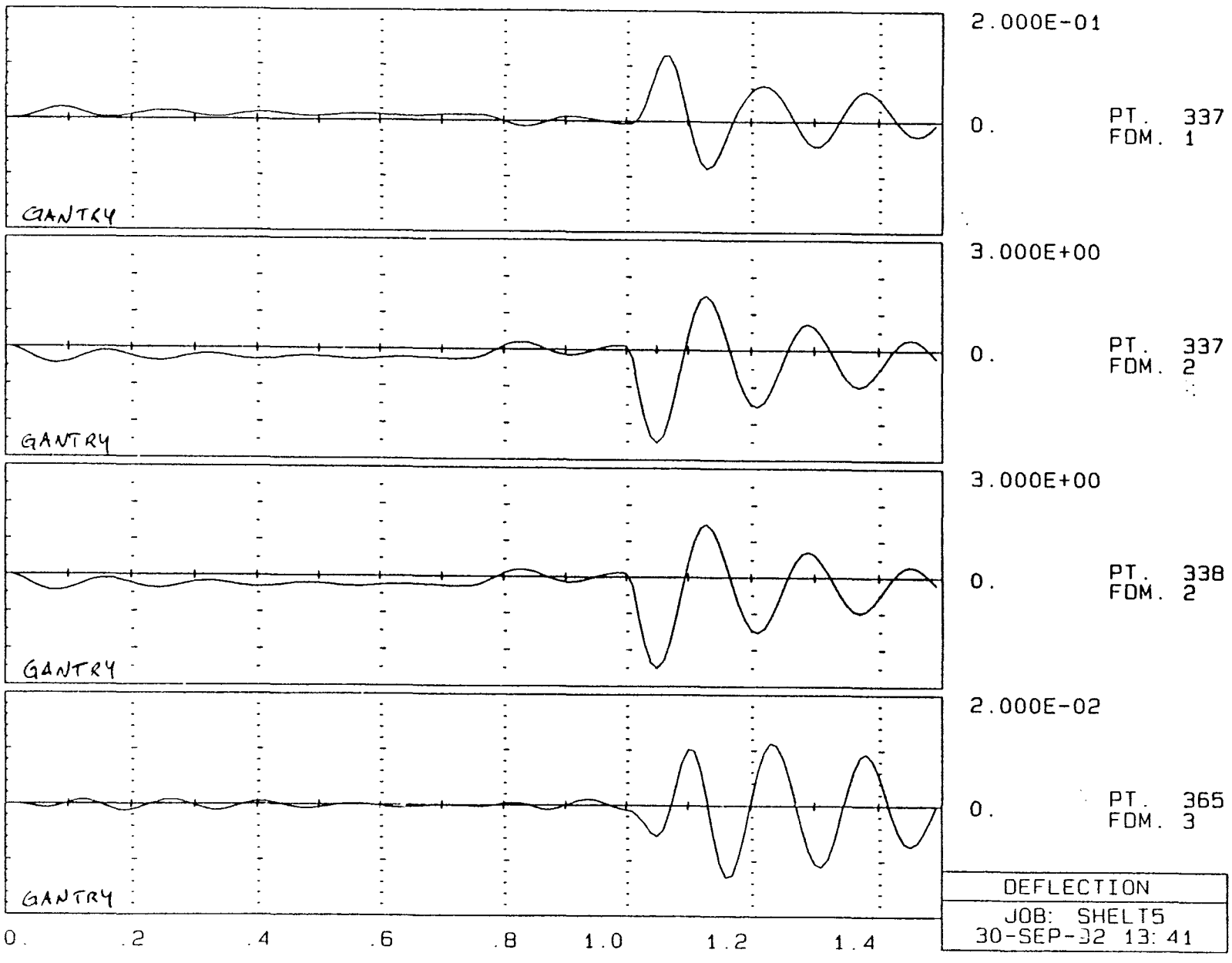
2.000E-01
0.
PT. 337
FDM. 1
GANTRY
3.000E+00
0.
PT. 337
FDM. 2
GANTRY
3.000E+00
0.
PT. 338
FDM. 2
GANTRY
2.000E-02
0.
PT. 365
FDM. 3
GANTRY
0.
.2
.4
.6
.8
1.0
1.2
1.4
DEFLECTION
JOB: SHELT5
30-SEP-32 13:41

Figure 45

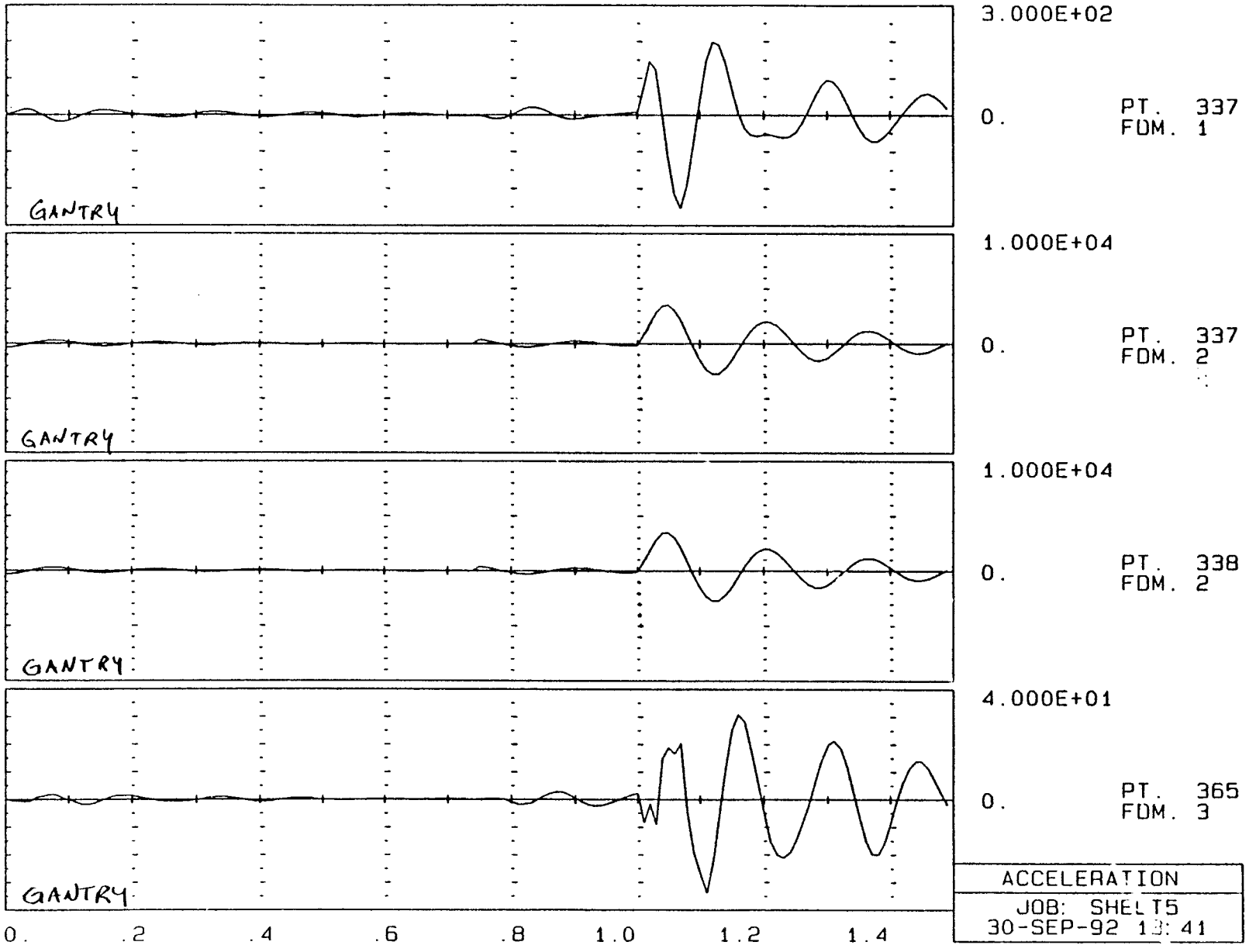
3.000E+02
0.
PT. 337
FDM. 1
GANTRY
1.000E+04
0.
PT. 337
FDM. 2
GANTRY
1.000E+04
0.
PT. 338
FDM. 2
GANTRY
4.000E+01
0.
PT. 365
FDM. 3
GANTRY
0.
.2
.4
.6
.8
1.0
1.2
1.4
ACCELERATION
JOB: SHELT5
30-SEP-92 13:41

Figure 46

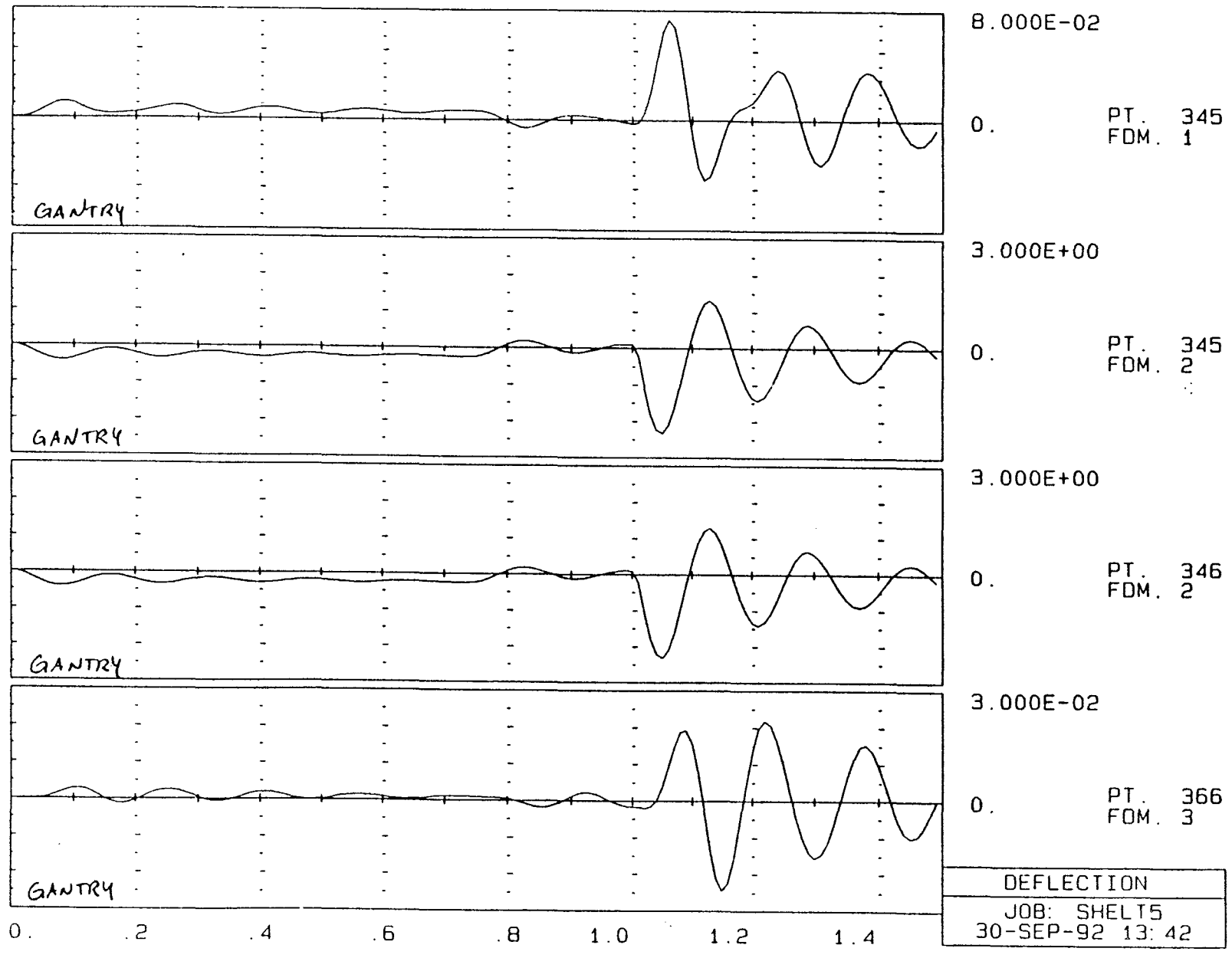
8.000E-02
0.
PT. 345
FDM. 1
GANTRY
3.000E+00
0.
PT. 345
FDM. 2
GANTRY
3.000E+00
0.
PT. 346
FDM. 2
GANTRY
3.000E-02
0.
PT. 366
FDM. 3
GANTRY
0.
.2
.4
.6
.8
1.0
1.2
1.4
DEFLECTION
JOB: SHELT5
30-SEP-92 13:42

Figure 47

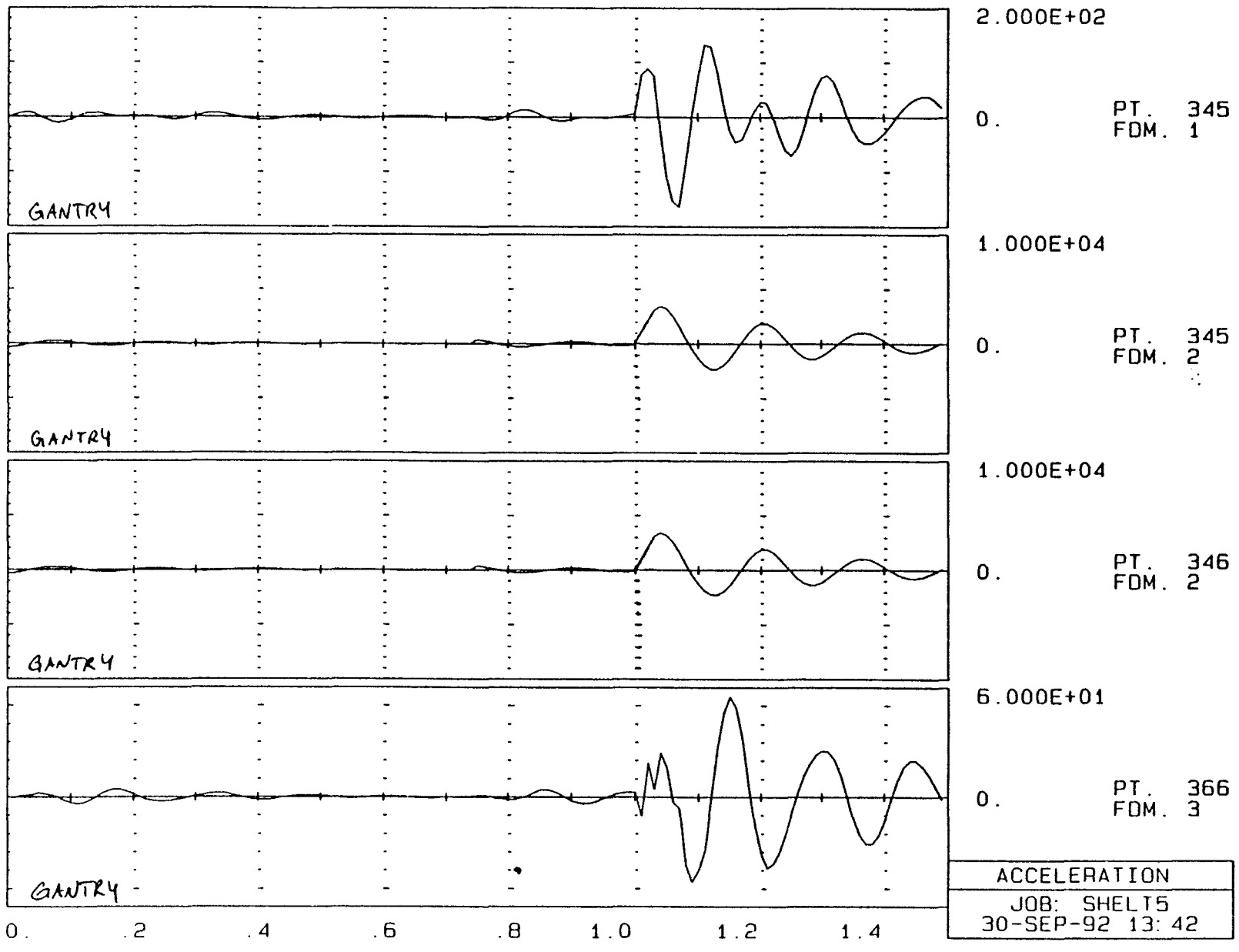
2.000E+02
0.
PT. 345
FDM. 1
GANTRY
1.000E+04
0.
PT. 345
FDM. 2
GANTRY
1.000E+04
0.
PT. 346
FDM. 2
GANTRY
6.000E+01
0.
PT. 366
FDM. 3
GANTRY
0.
.2
.4
.6
.8
1.0
1.2
1.4
ACCELERATION
JOB: SHELT5
30-SEP-92 13:42

Figure 48

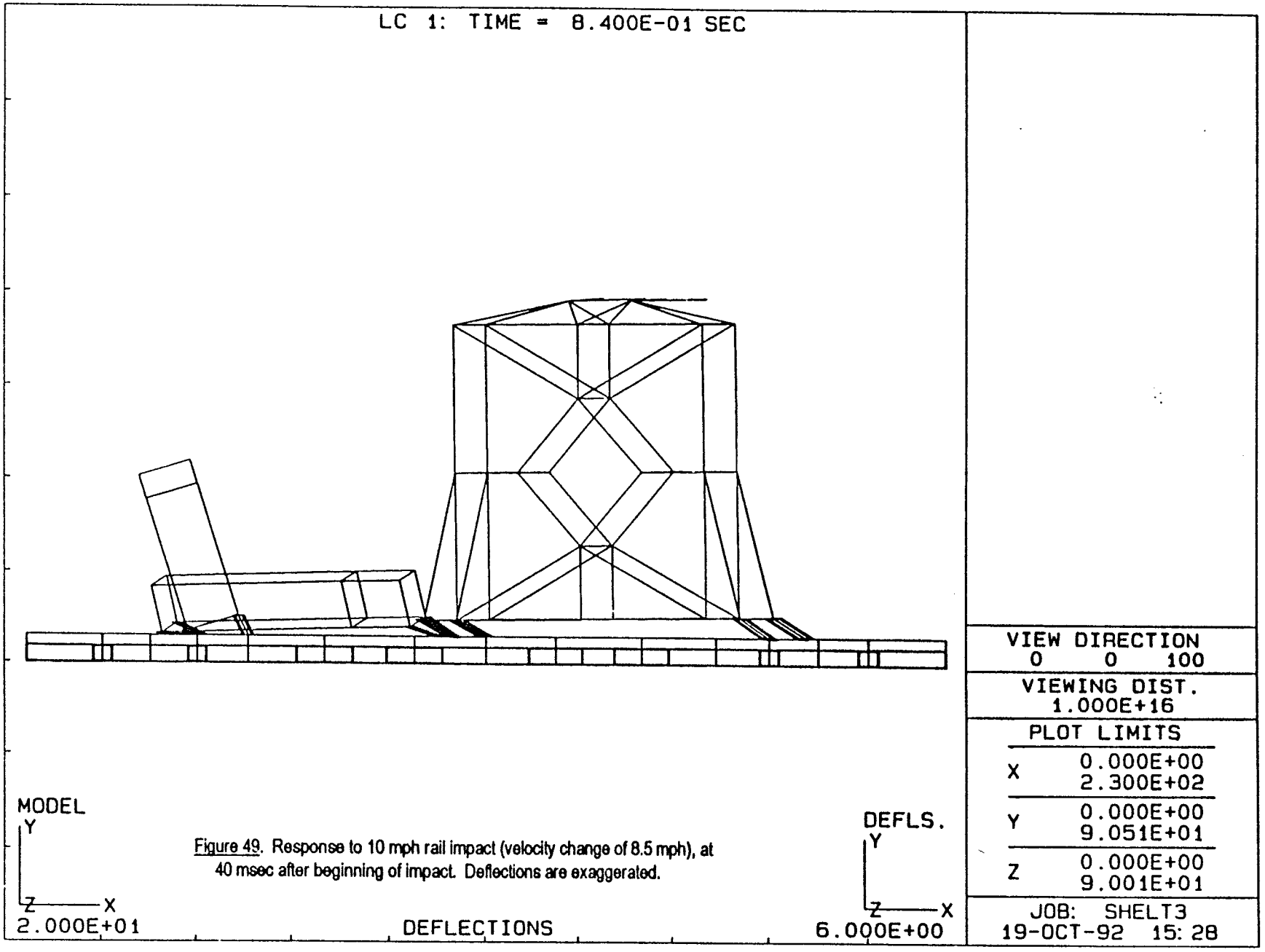

Figure 49. Response to 10 mph rail impact (velocity change of 8.5 mph), at 40 msec after beginning of impact. Deflections are exaggerated.

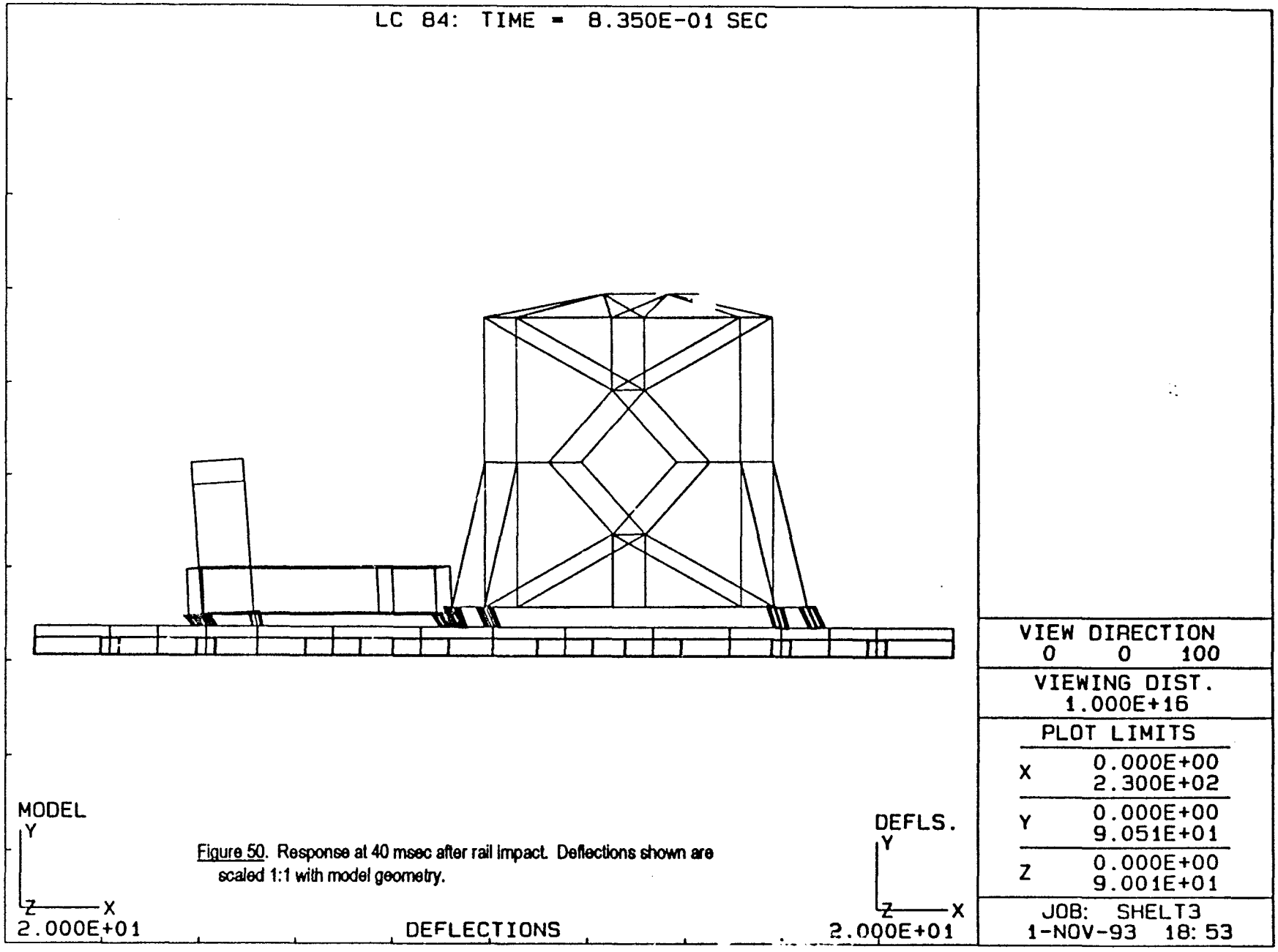

Figure 50. Response at 40 msec after rail impact. Deflections shown are scaled 1:1 with model geometry.

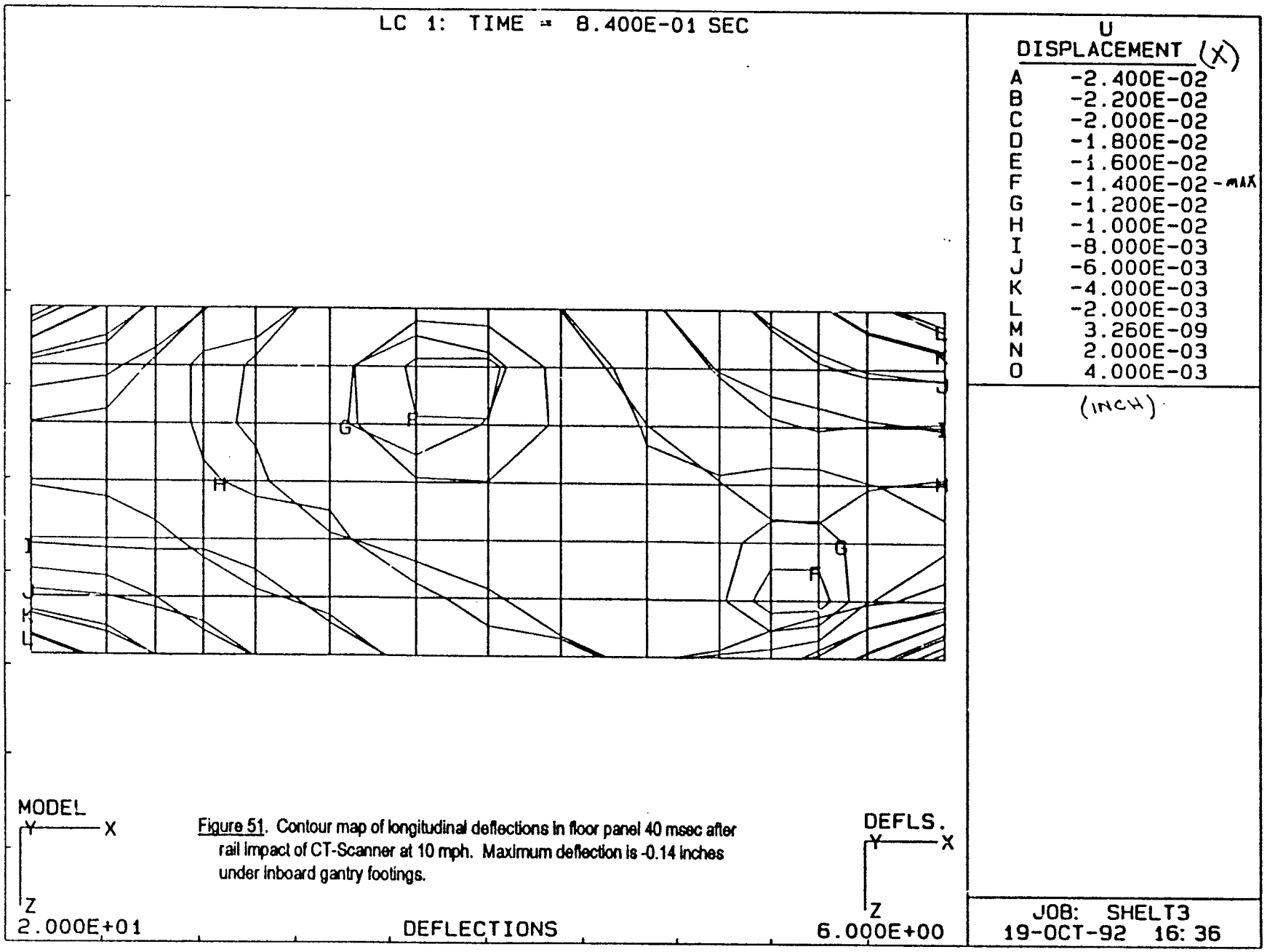

Figure 51. Contour map of longitudinal deflections in floor panel 40 msec after rail impact of CT-Scanner at 10 mph. Maximum deflection is -0.14 inches under inboard gantry footings.

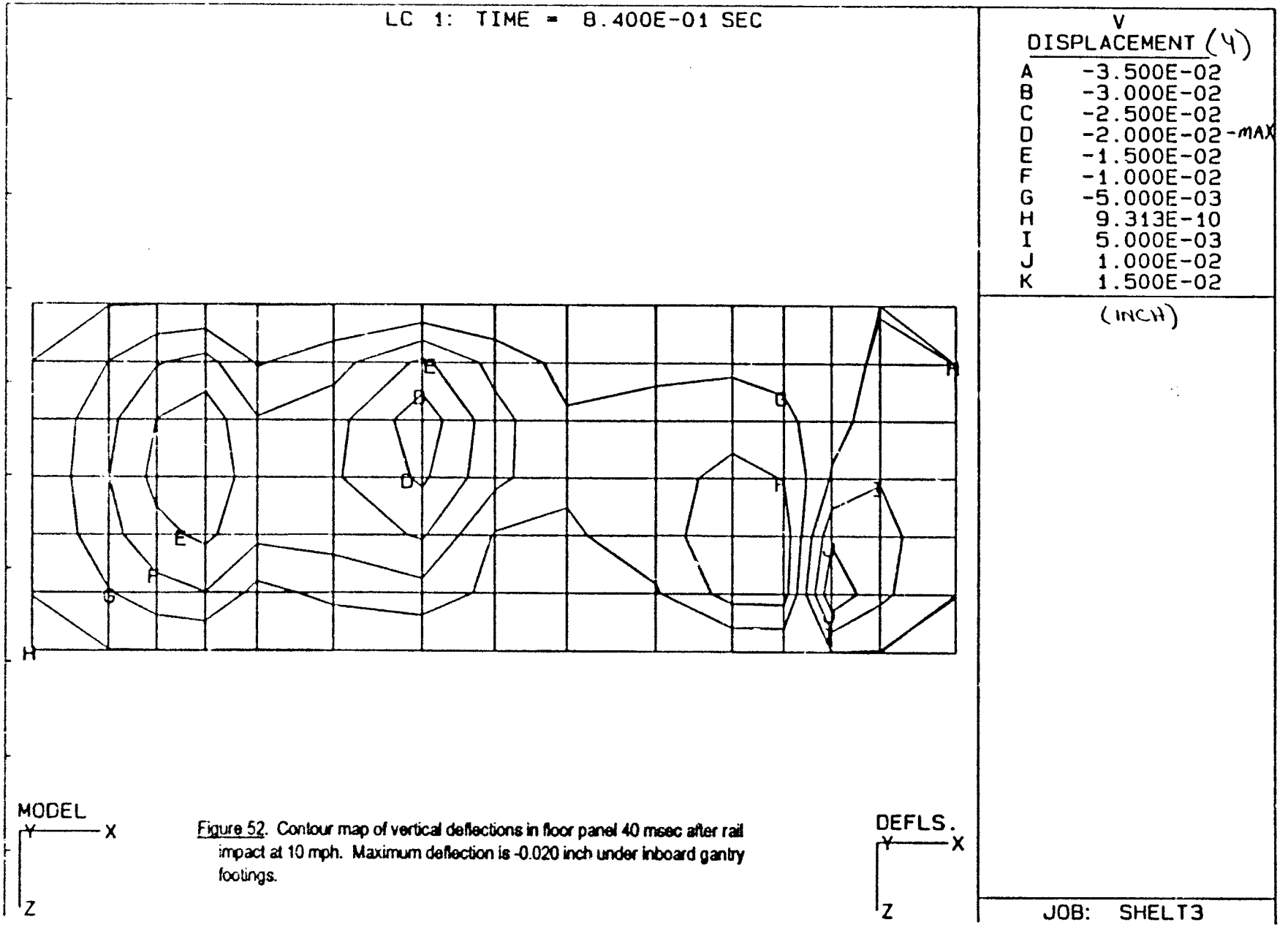

Figure 52. Contour map of vertical deflections in floor panel 40 msec after rail impact at 10 mph. Maximum deflection is -0.020 inch under inboard gantry footings.

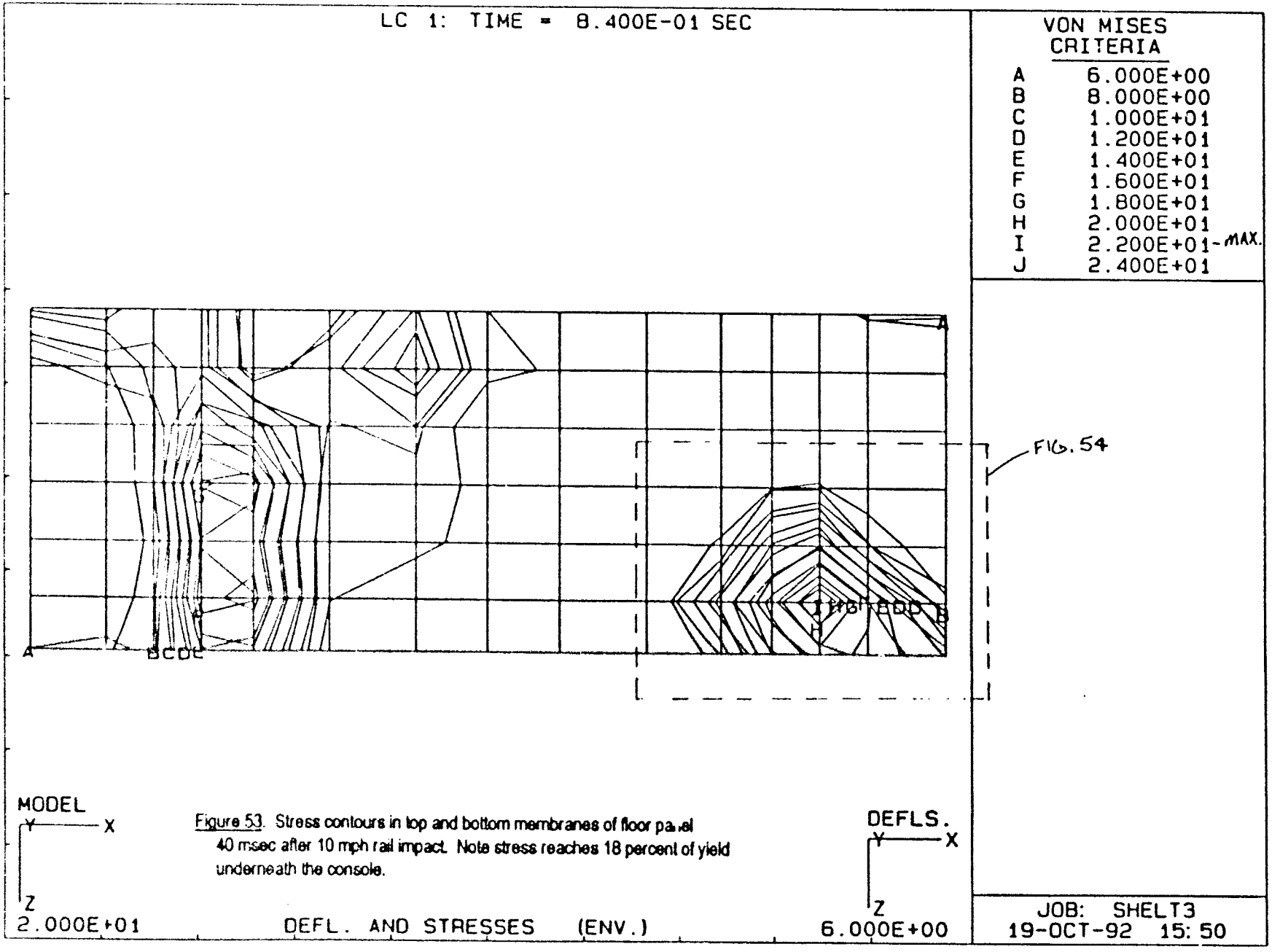

Figure 53. Stress contours in top and bottom membranes of floor panel 40 msec after 10 mph rail impact. Note stress reaches 18 percent of yield underneath the console.

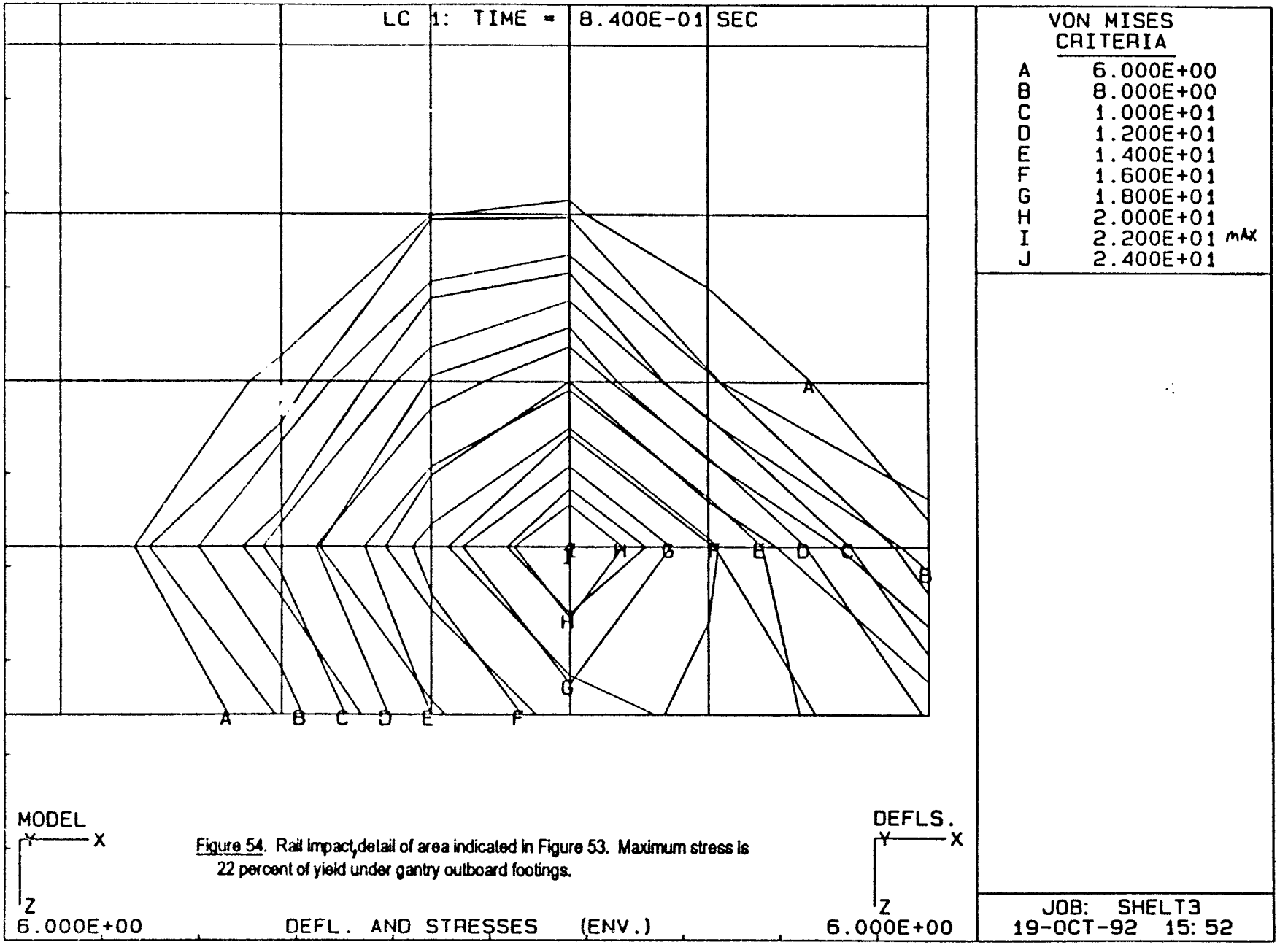

Figure 54. Rail impact, detail of area indicated in Figure 53. Maximum stress is 22 percent of yield under gantry outboard footings.

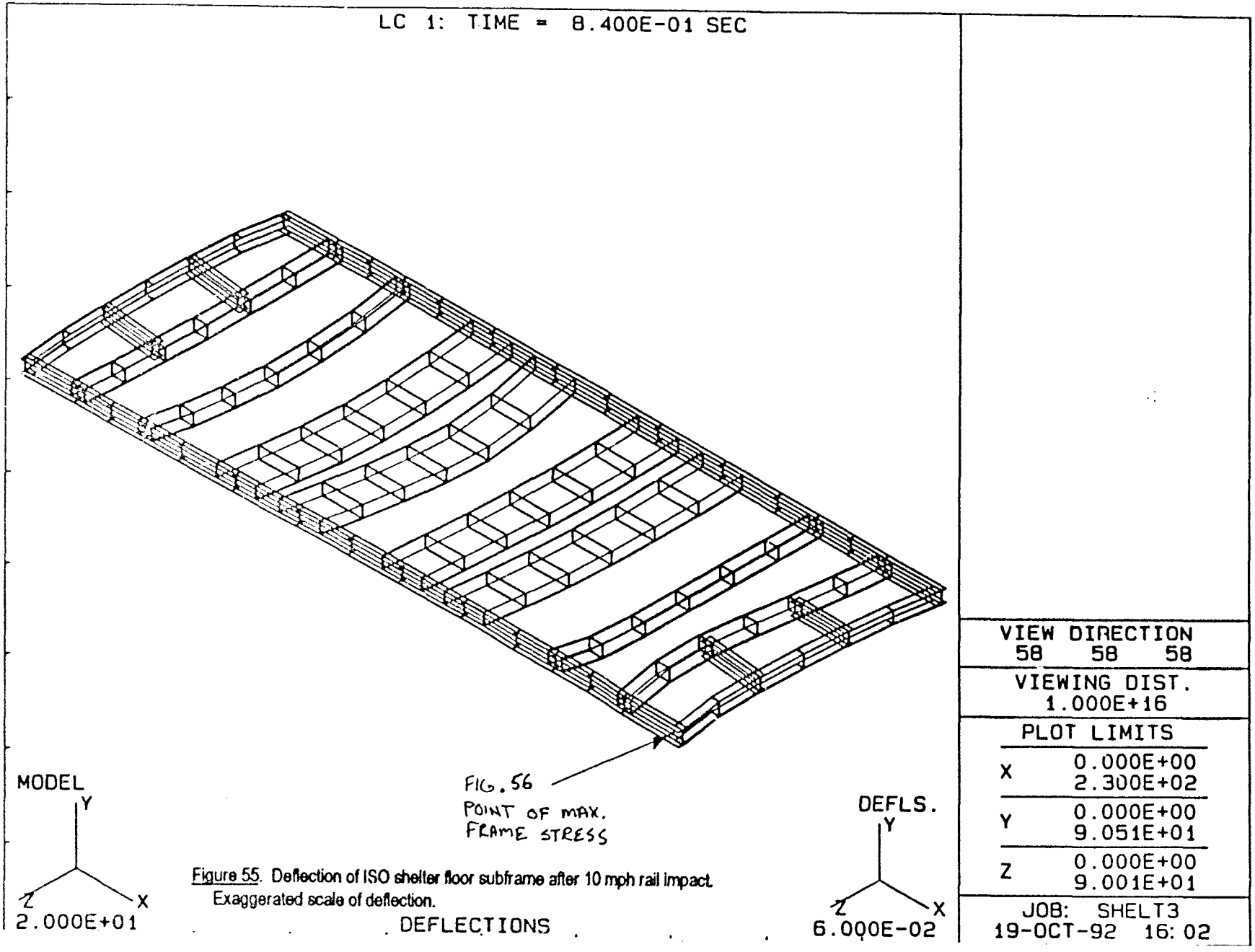

Figure 55. Deflection of ISO shelter floor subframe after 10 mph rail impact. Exaggerated scale of deflection.

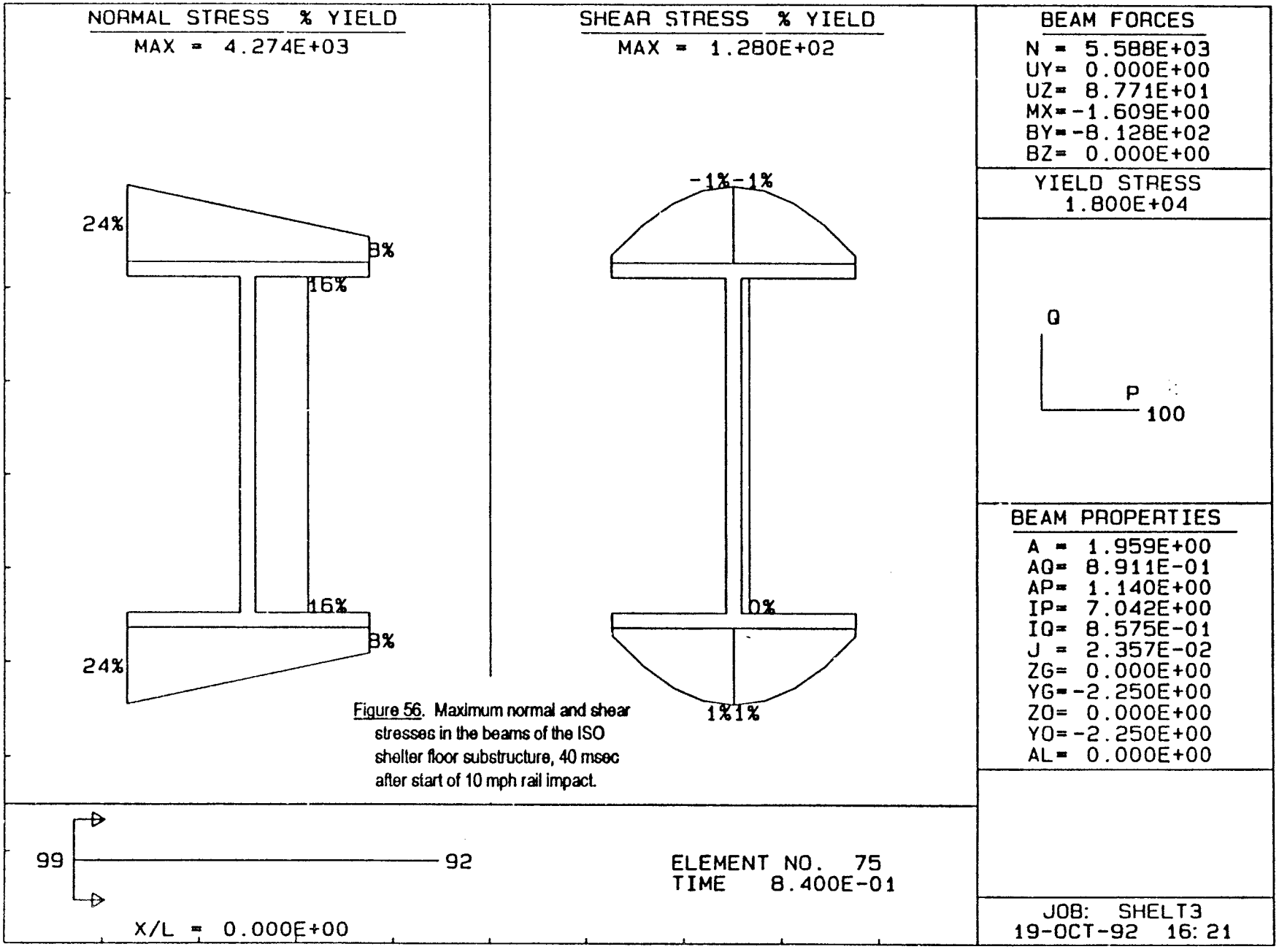

Figure 56. Maximum normal and shear stresses in the beams of the ISO shelter floor substructure, 40 msec after start of 10 mph rail impact.

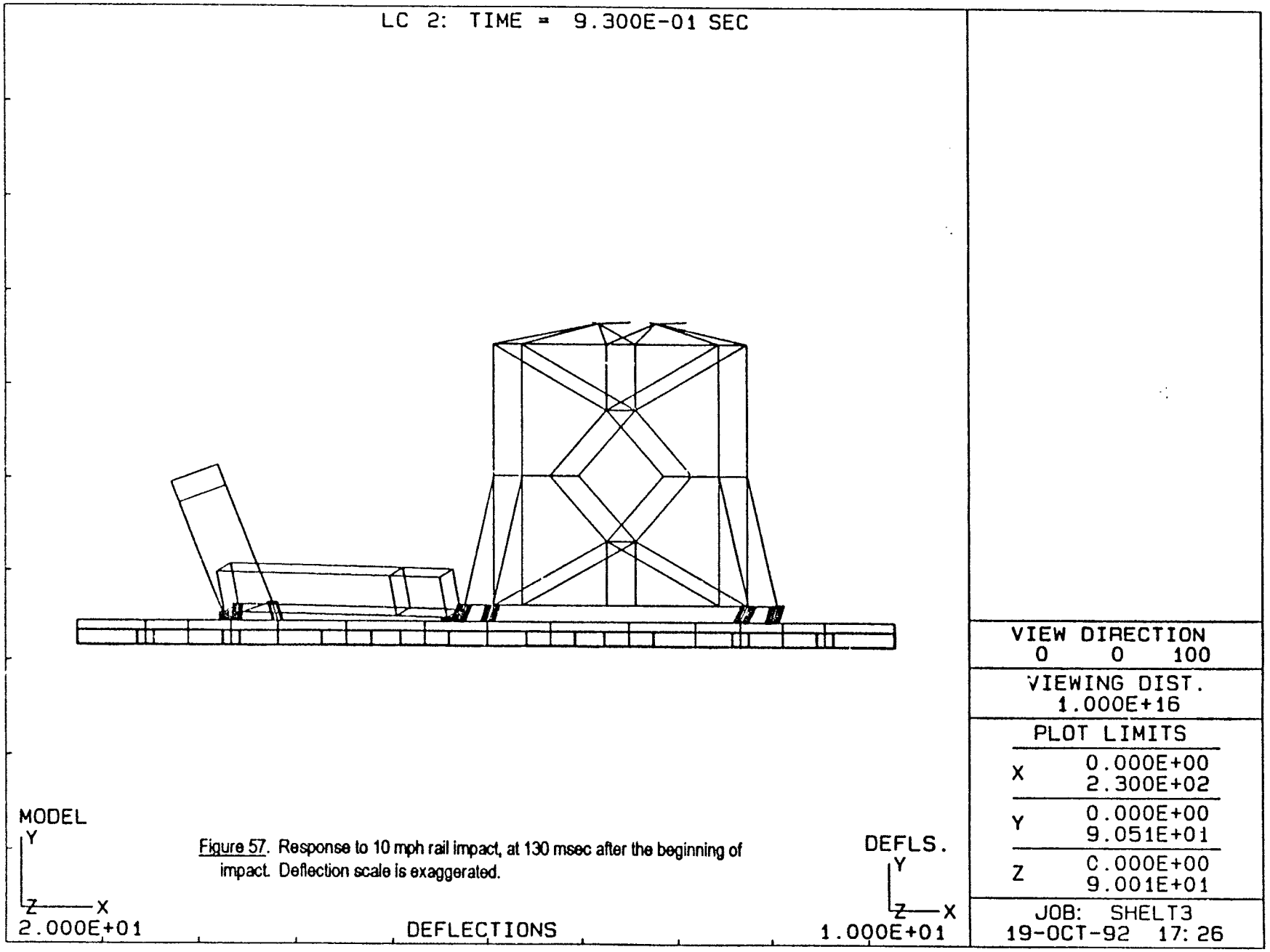

Figure 57. Response to 10 mph rail impact, at 130 msec after the beginning of impact. Deflection scale is exaggerated.

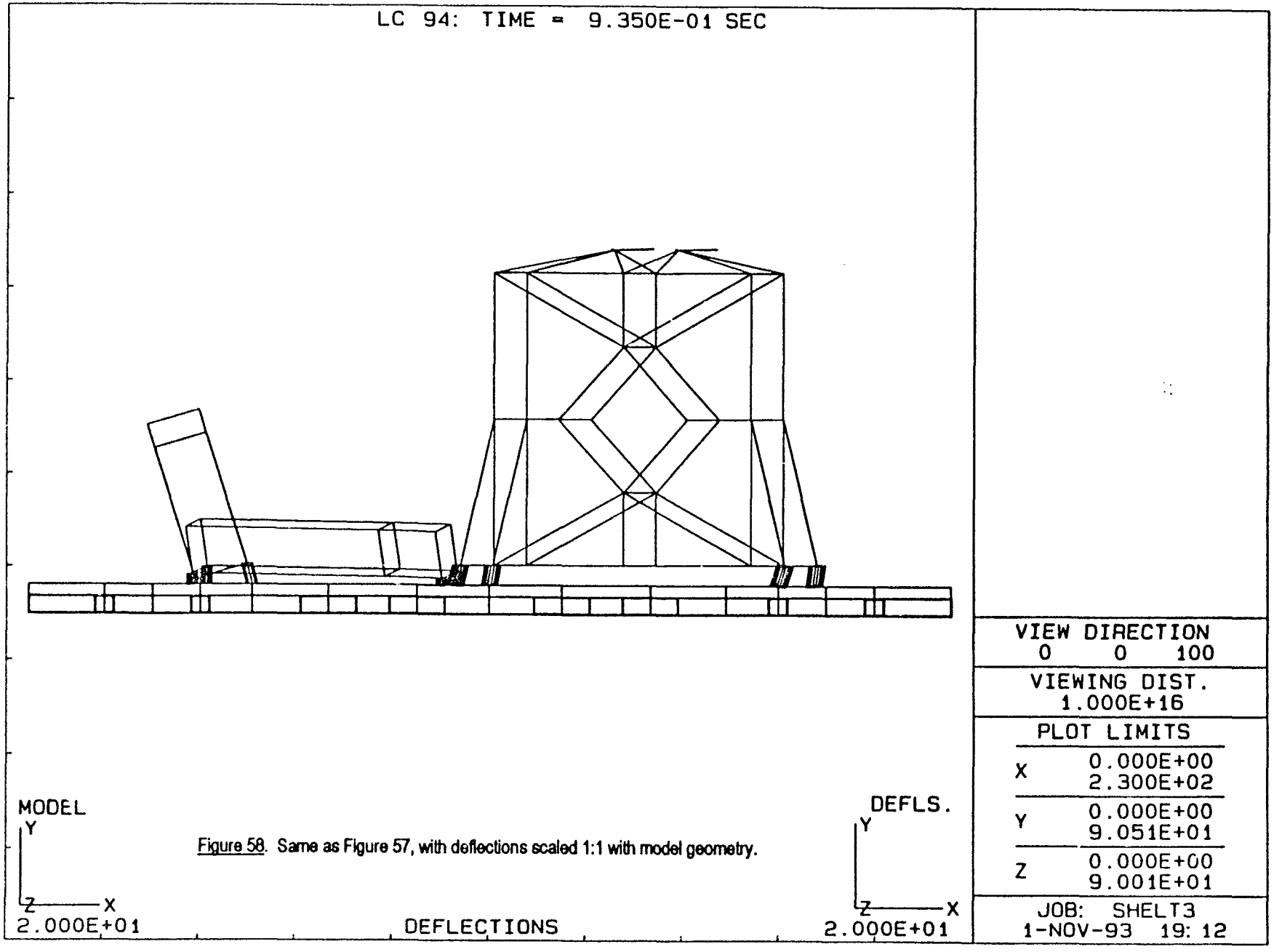

Figure 58. Same as Figure 57, with deflections scaled 1:1 with model geometry.

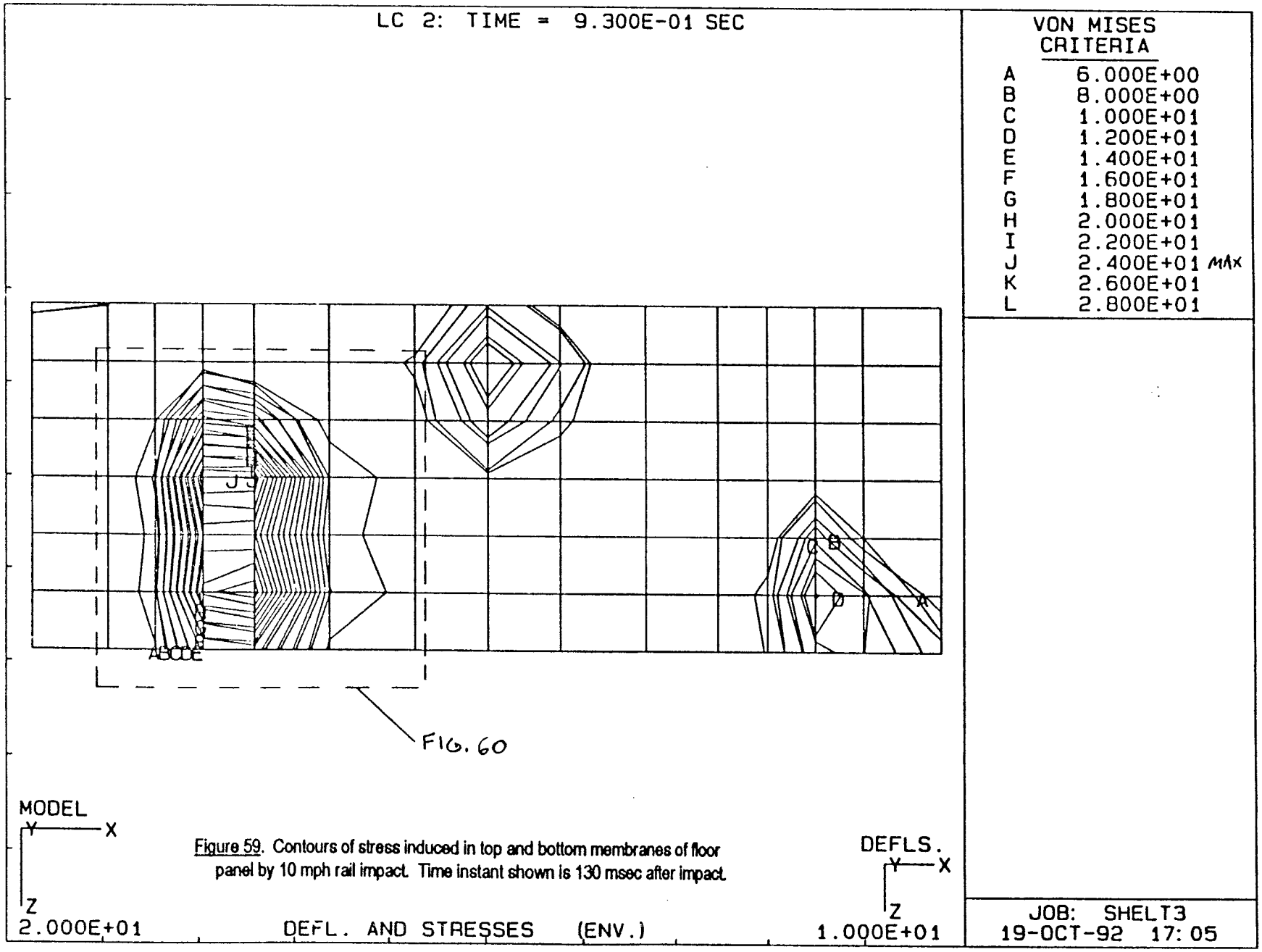

Figure 59. Contours of stress induced in top and bottom membranes of floor panel by 10 mph rail impact. Time instant shown is 130 msec after impact.

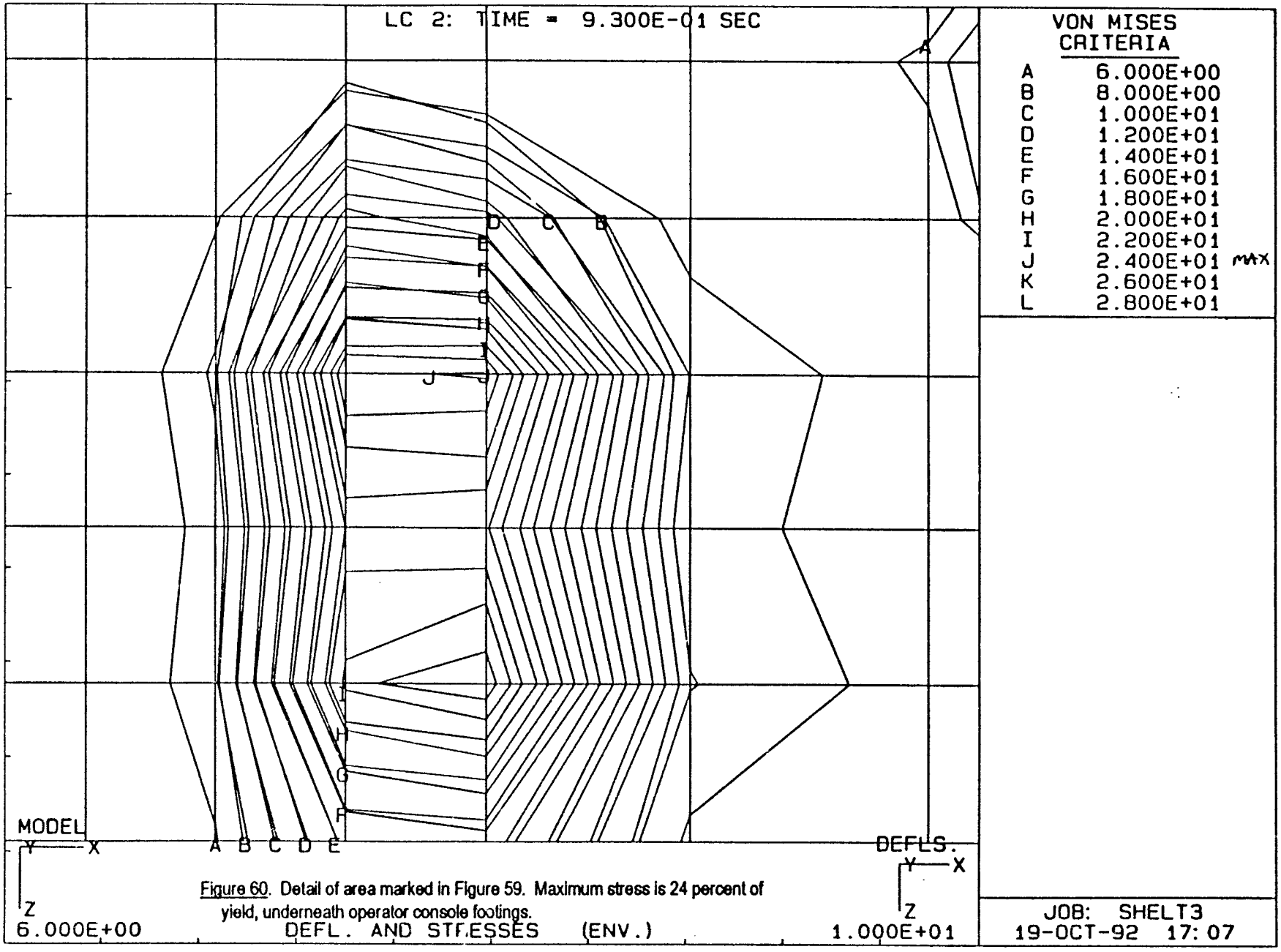

Figure 60. Detail of area marked in Figure 59. Maximum stress is 24 percent of yield, underneath operator console footings.

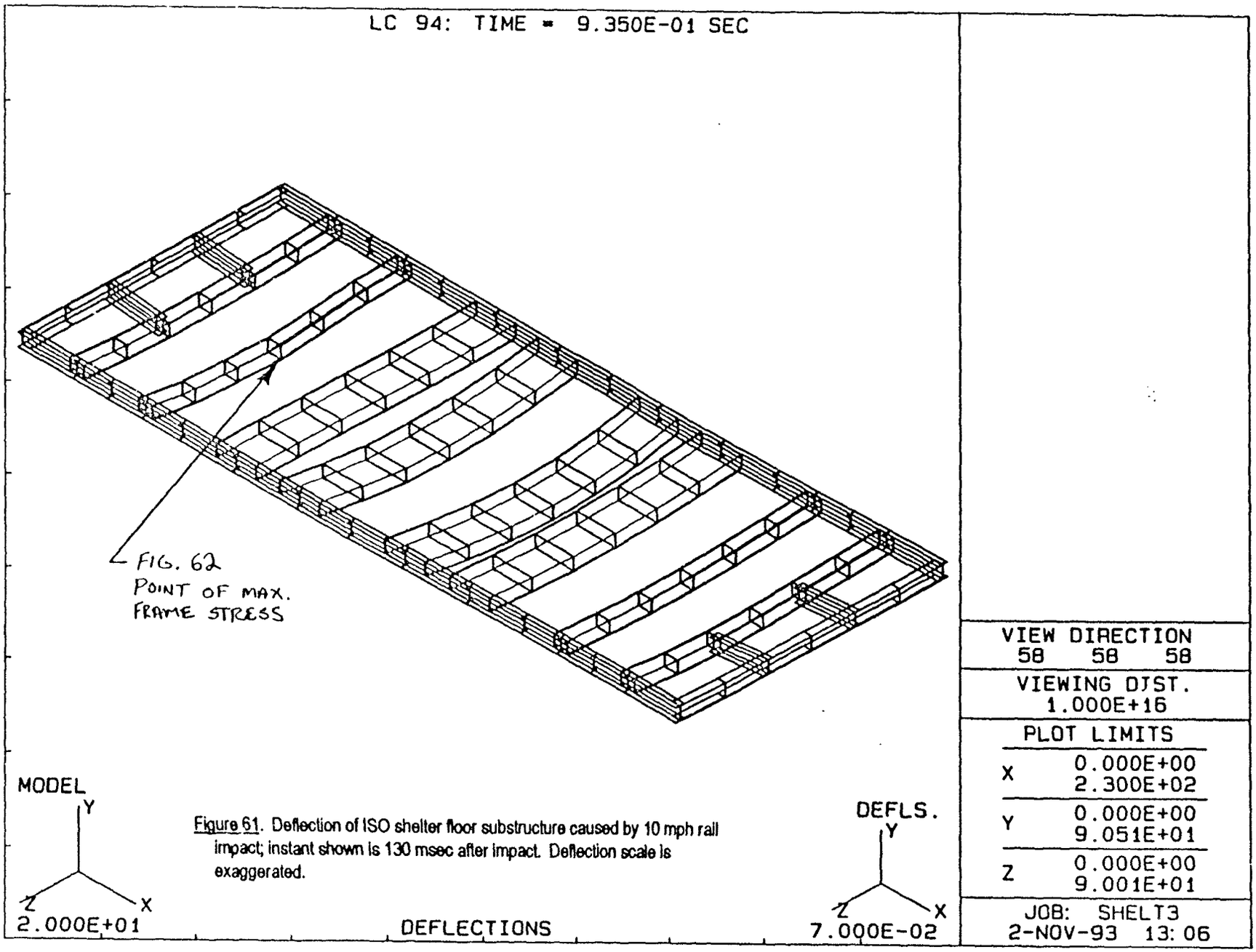

Figure 61. Deflection of ISO shelter floor substructure caused by 10 mph rail impact; instant shown is 130 msec after impact. Deflection scale is exaggerated.

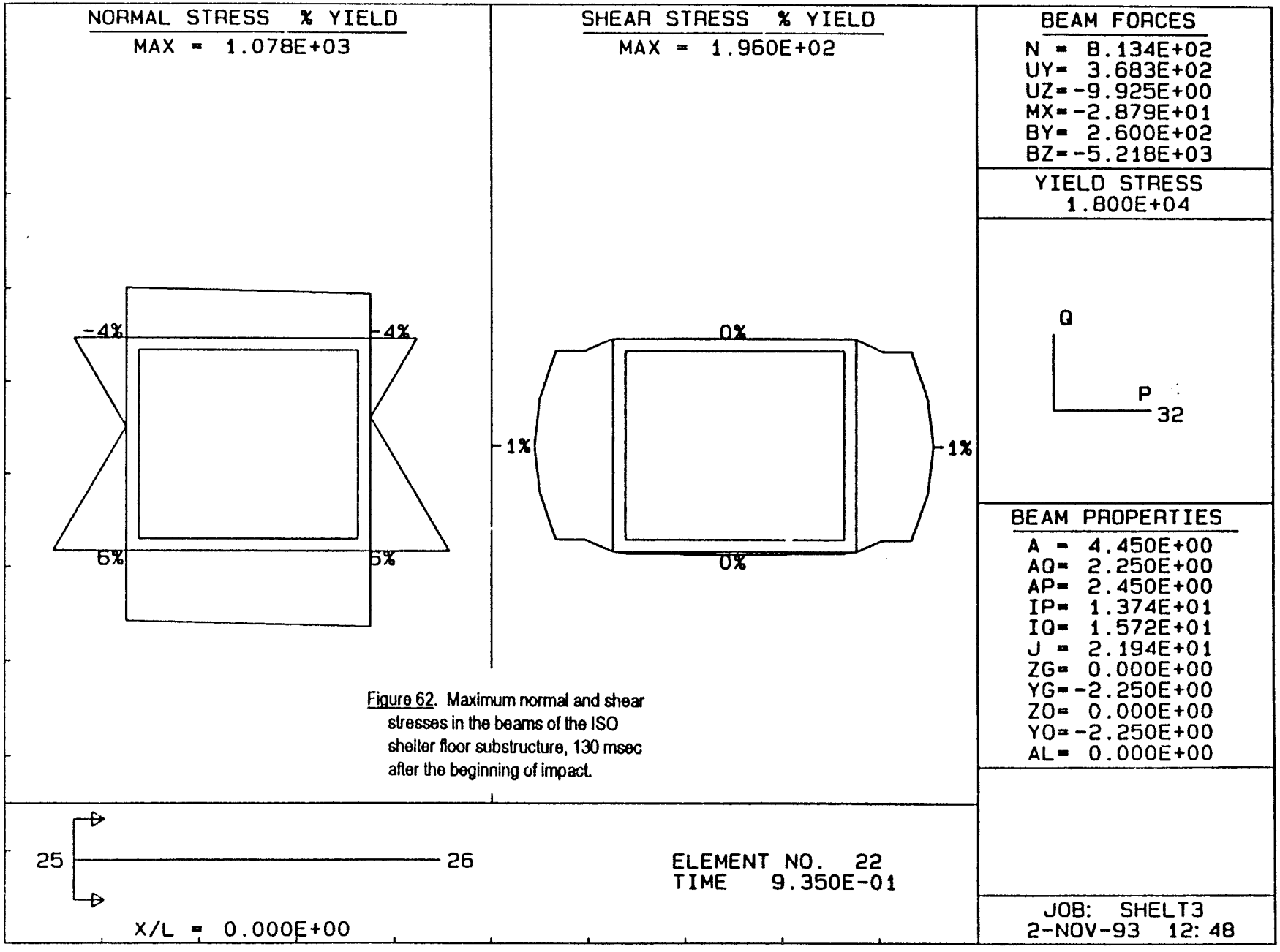

Figure 62. Maximum normal and shear stresses in the beams of the ISO shelter floor substructure, 130 msec after the beginning of impact.

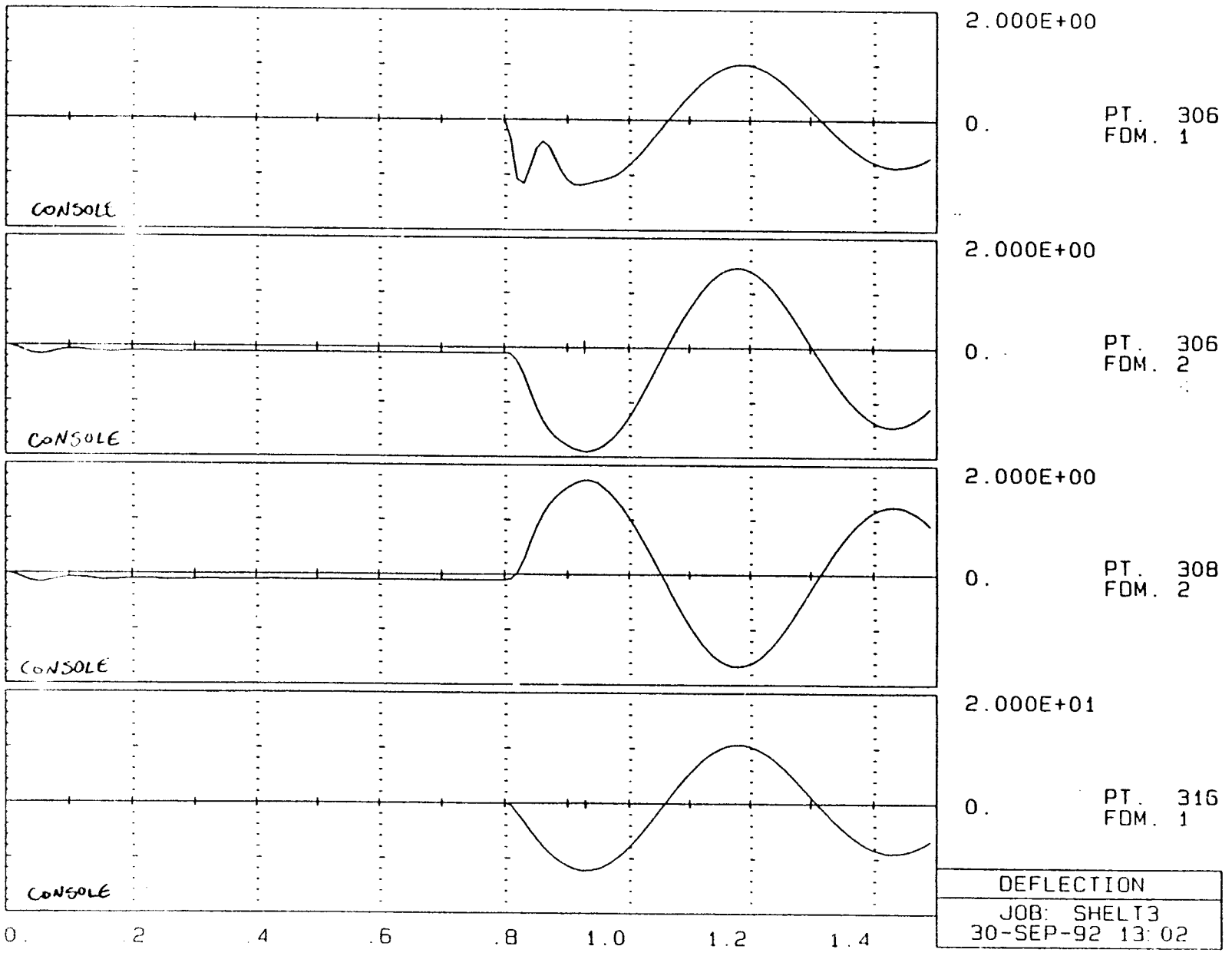
2.000E+00
0.
PT. 306
FDM. 1
Bottom Inside Corner of Console
CONSOLE
2.000E+00
0.
PT. 306
FDM. 2
CONSOLE
2.000E+00
0.
PT. 308
FDM. 2
CONSOLE
2.000E+01
0.
PT. 316
FDM. 1
CONSOLE
0.
.2
.4
.6
.8
1.0
1.2
1.4
DEFLECTION
JOB: SHELT3
30-SEP-92 13:02

Figure 63

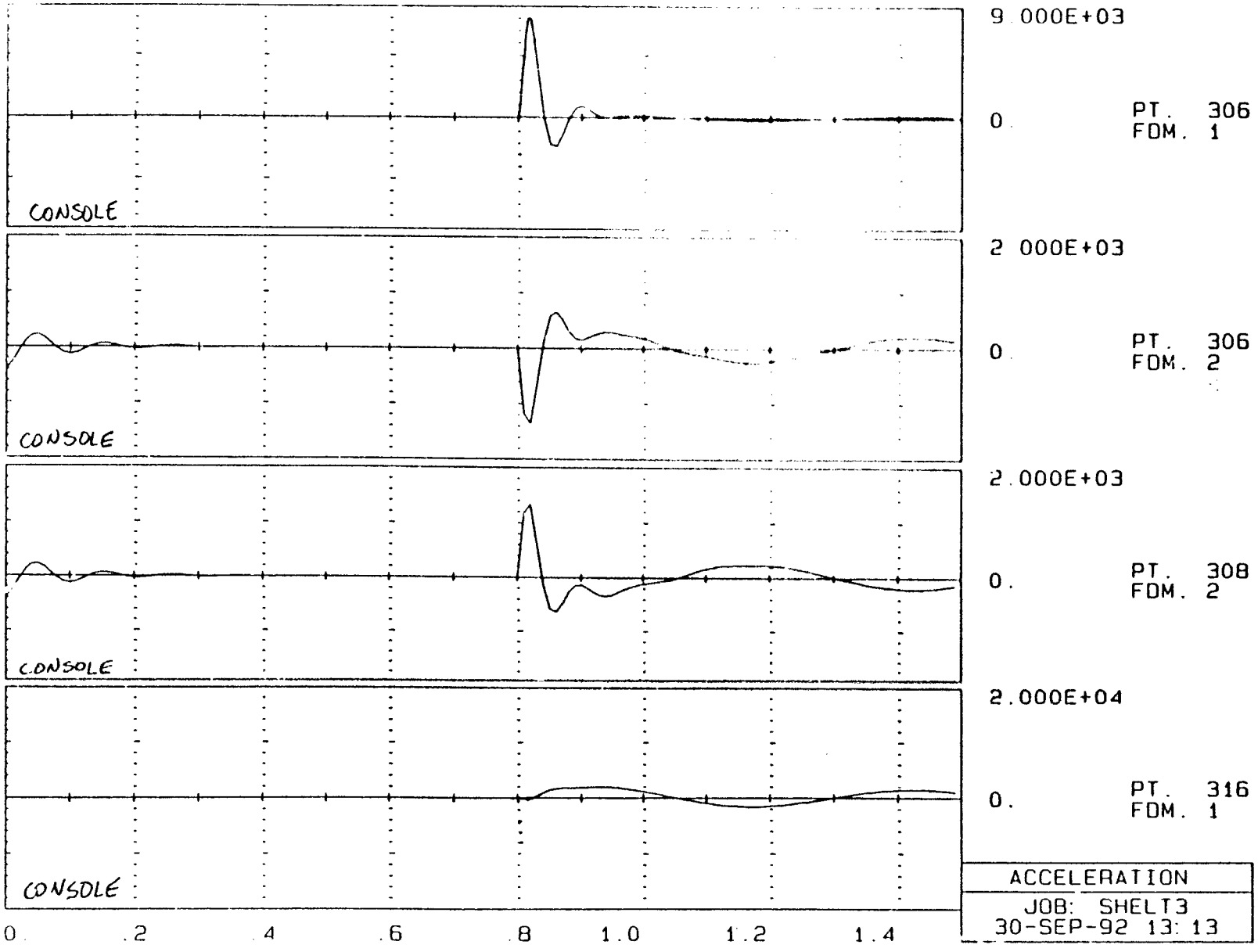
9.000E+03
0
PT. 306
FOM. 1
CONSOLE
2.000E+03
0
PT. 306
FOM. 2
CONSOLE
2.000E+03
0.
PT. 308
FOM. 2
CONSOLE
2.000E+04
0.
PT. 316
FOM. 1
CONSOLE
0
.2
.4
.6
.8
1.0
1.2
1.4
ACCELERATION
JOB: SHELT3
30-SEP-92 13:13

Figure 64

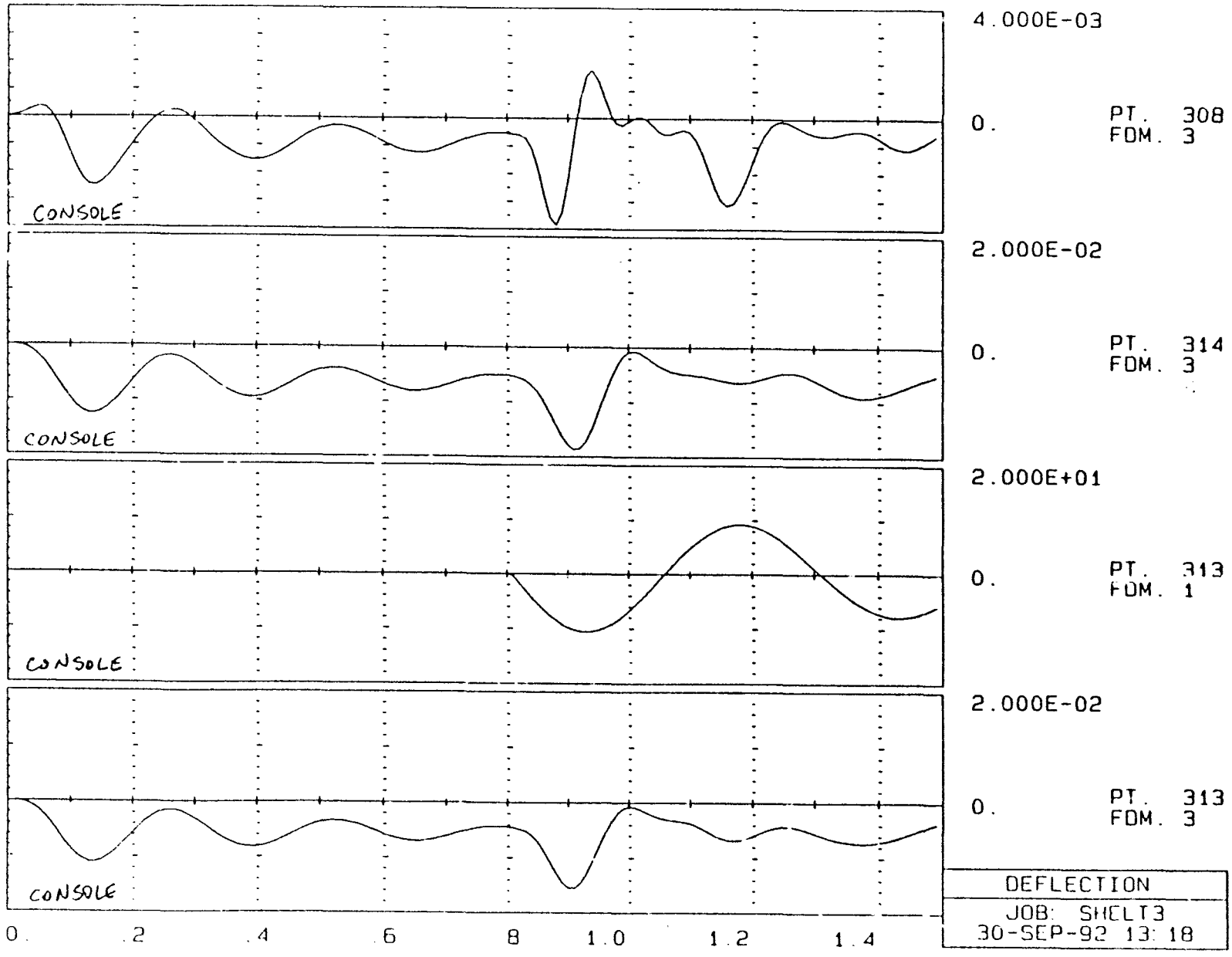
4.000E-03
0.
PT. 308
FDM. 3
CONSOLE
2.000E-02
0.
PT. 314
FDM. 3
CONSOLE
2.000E+01
0.
PT. 313
FDM. 1
CONSOLE
2.000E-02
0.
PT. 313
FDM. 3
CONSOLE
0
.2
.4
.6
.8
1.0
1.2
1.4
DEFLECTION
JOB: SHELT3
30-SEP-92 13:18

Figure 65

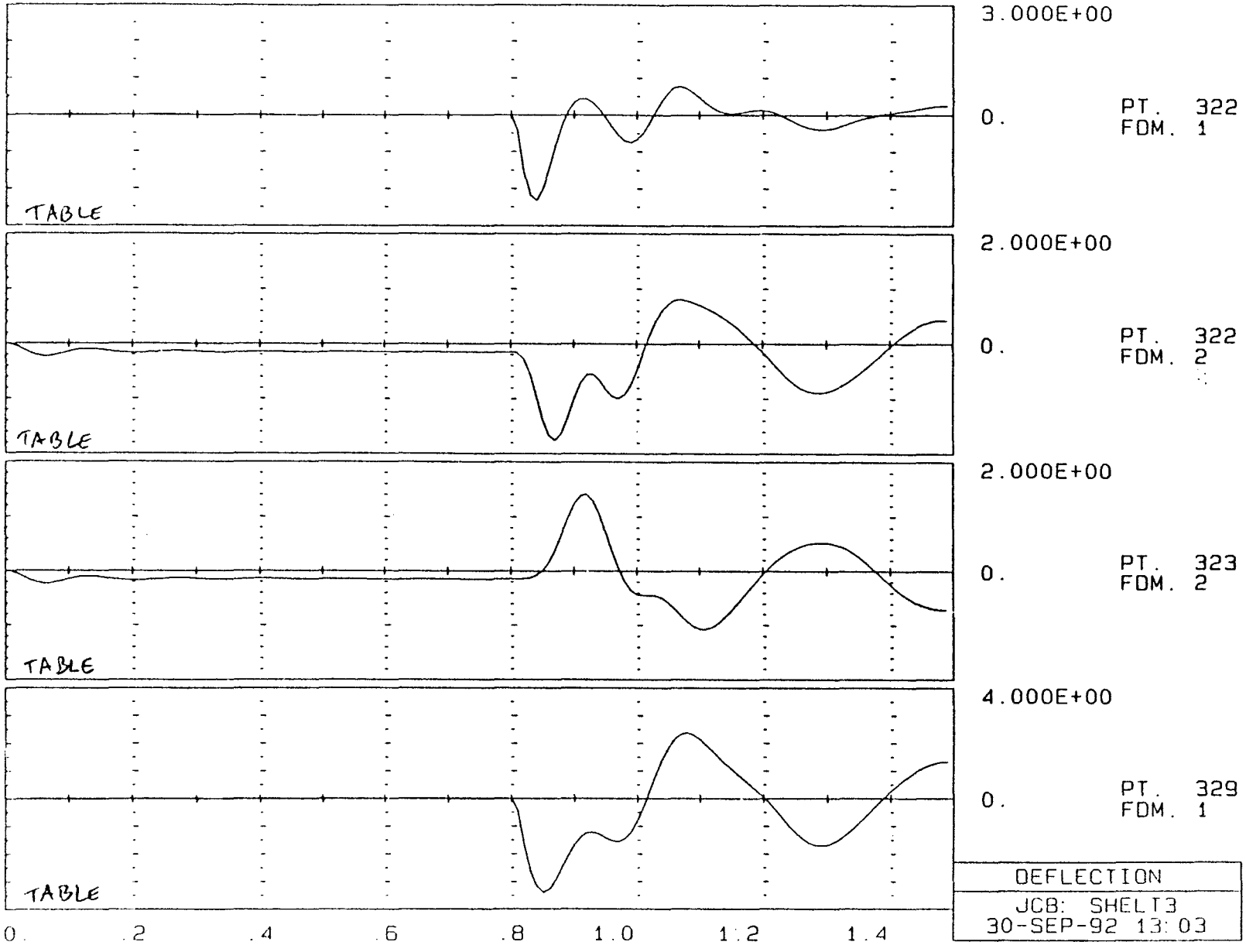
3.000E+00
0.
PT. 322
FDM. 1
TABLE
2.000E+00
0.
PT. 322
FDM. 2
TABLE
2.000E+00
0.
PT. 323
FDM. 2
TABLE
4.000E+00
0.
PT. 329
FDM. 1
TABLE
0.
.2
.4
.6
.8
1.0
1.2
1.4
DEFLECTION
JCB: SHELT3
30-SEP-92 13:03

Figure 66

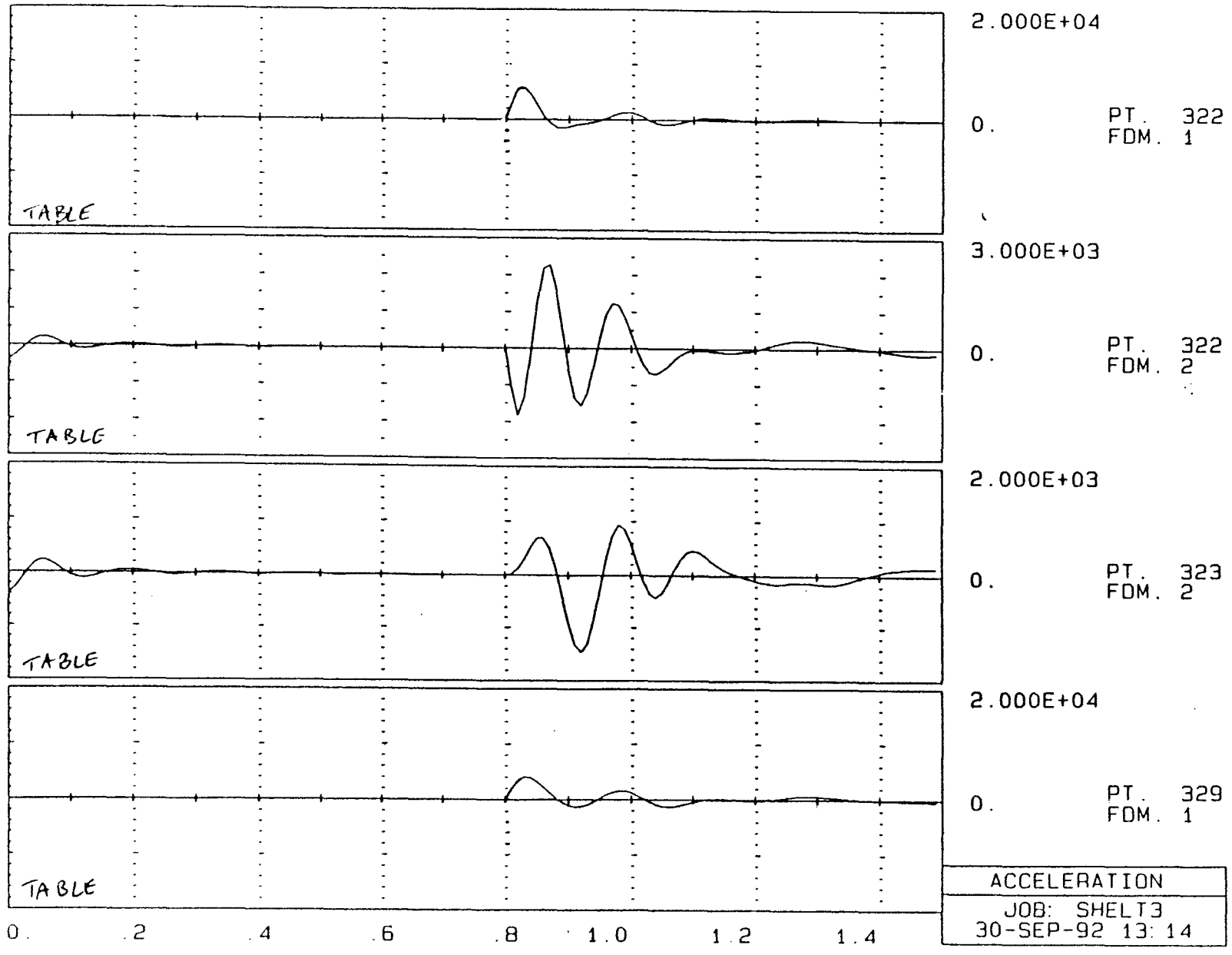
2.000E+04
0.
PT. 322
FDM. 1
TABLE
3.000E+03
0.
PT. 322
FDM. 2
TABLE
2.000E+03
0.
PT. 323
FDM. 2
TABLE
2.000E+04
0.
PT. 329
FDM. 1
TABLE
0.
.2
.4
.6
.8
1.0
1.2
1.4
ACCELERATION
JOB: SHELT3
30-SEP-92 13:14

Figure 67

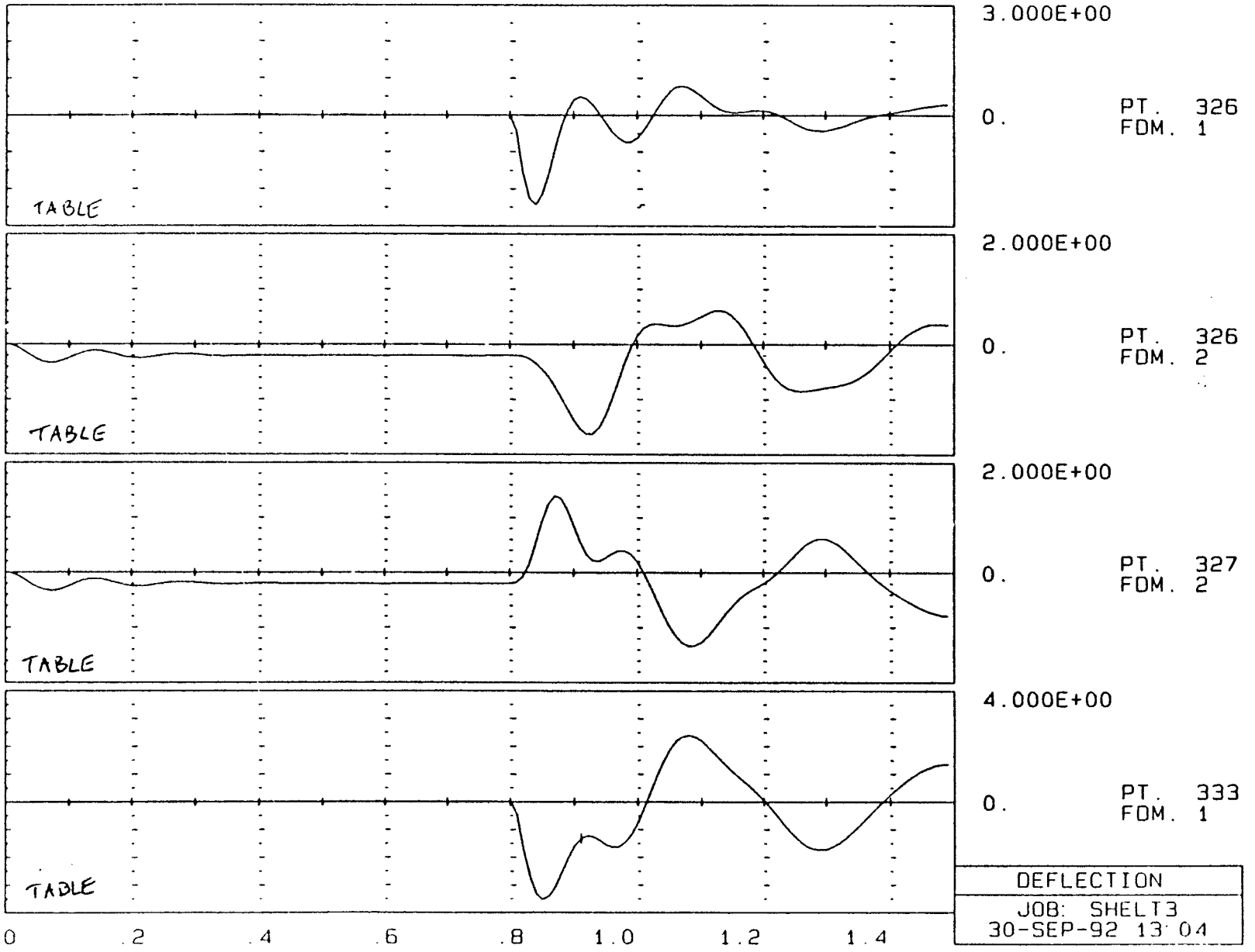
3.000E+00
0.
PT. 326
FDM. 1
TABLE
2.000E+00
0.
PT. 326
FDM. 2
TABLE
2.000E+00
0.
PT. 327
FDM. 2
TABLE
4.000E+00
0.
PT. 333
FDM. 1
TABLE
0
.2
.4
.6
.8
1.0
1.2
1.4
DEFLECTION
JOB: SHELT3
30-SEP-92 13:04

Figure 68

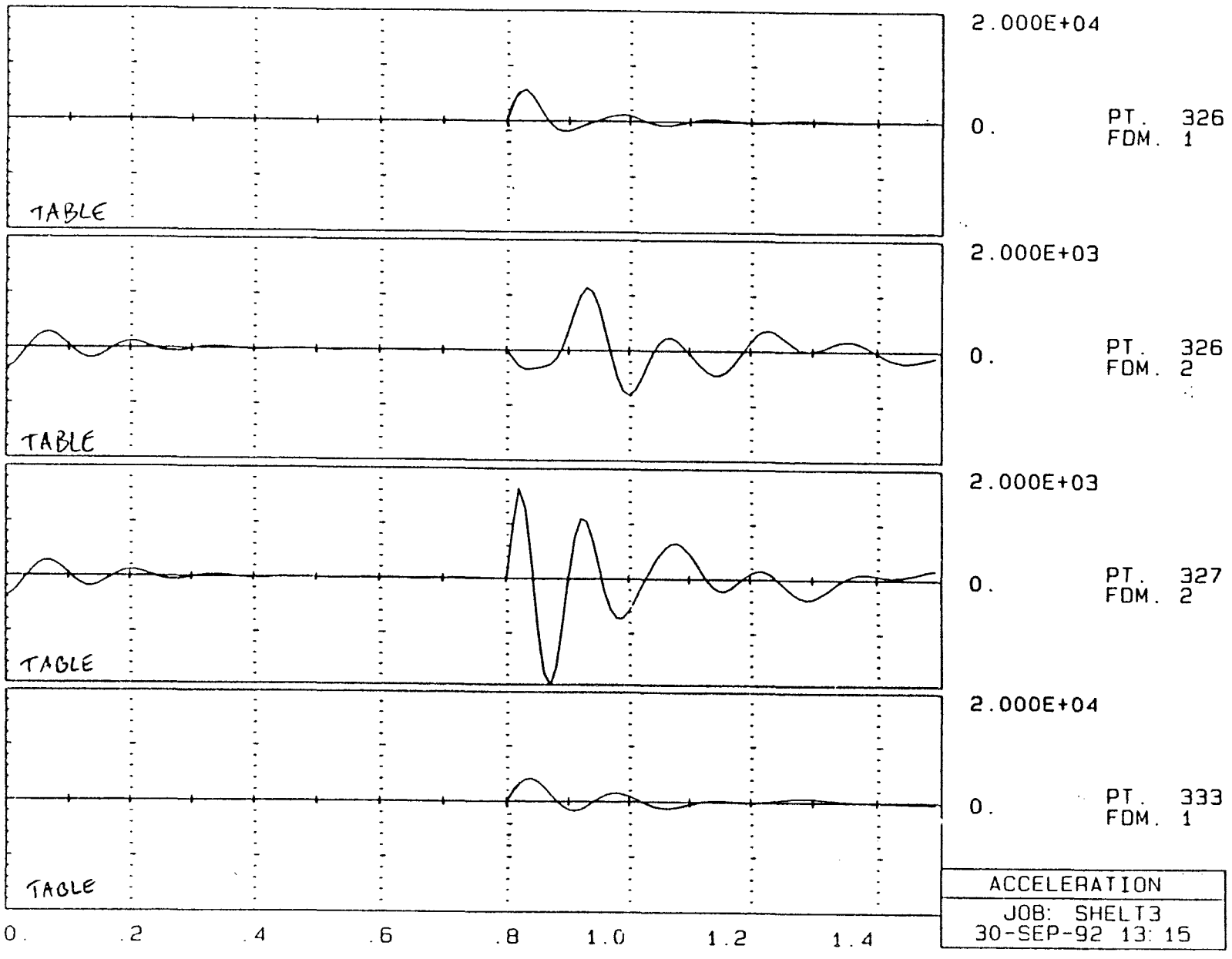
2.000E+04
0.
PT. 326
FDM. 1
TABLE
2.000E+03
0.
PT. 326
FDM. 2
TABLE
2.000E+03
0.
PT. 327
FDM. 2
TABLE
2.000E+04
0.
PT. 333
FDM. 1
TABLE
0.
.2
.4
.6
.8
1.0
1.2
1.4
ACCELERATION
JOB: SHELT3
30-SEP-92 13:15

Figure 69

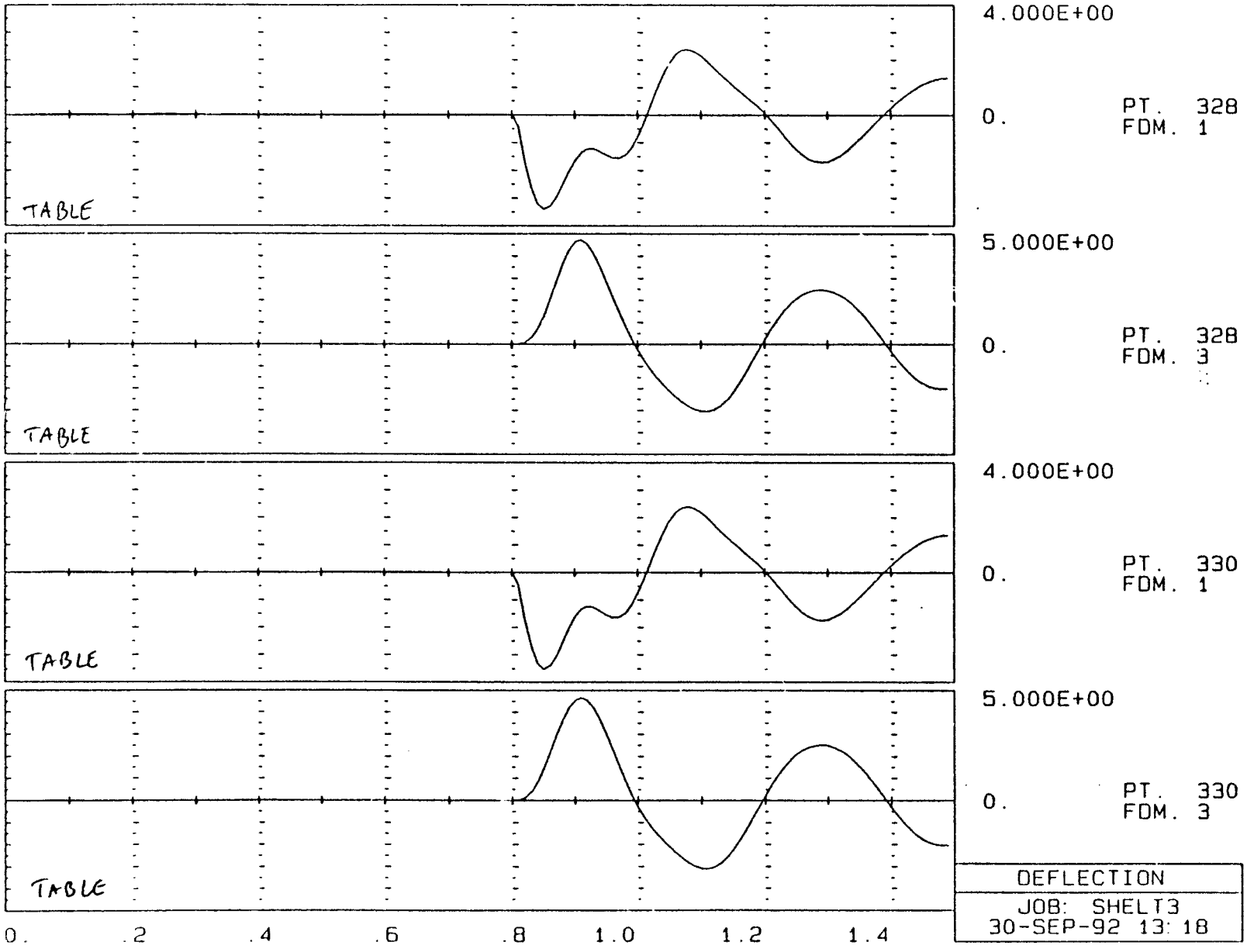
4.000E+00
0.
PT. 328
FDM. 1
TABLE
5.000E+00
0.
PT. 328
FDM. 3
TABLE
4.000E+00
0.
PT. 330
FDM. 1
TABLE
5.000E+00
0.
PT. 330
FDM. 3
TABLE
0.
.2
.4
.6
.8
1.0
1.2
1.4
DEFLECTION
JOB: SHELT3
30-SEP-92 13:18

Figure 70

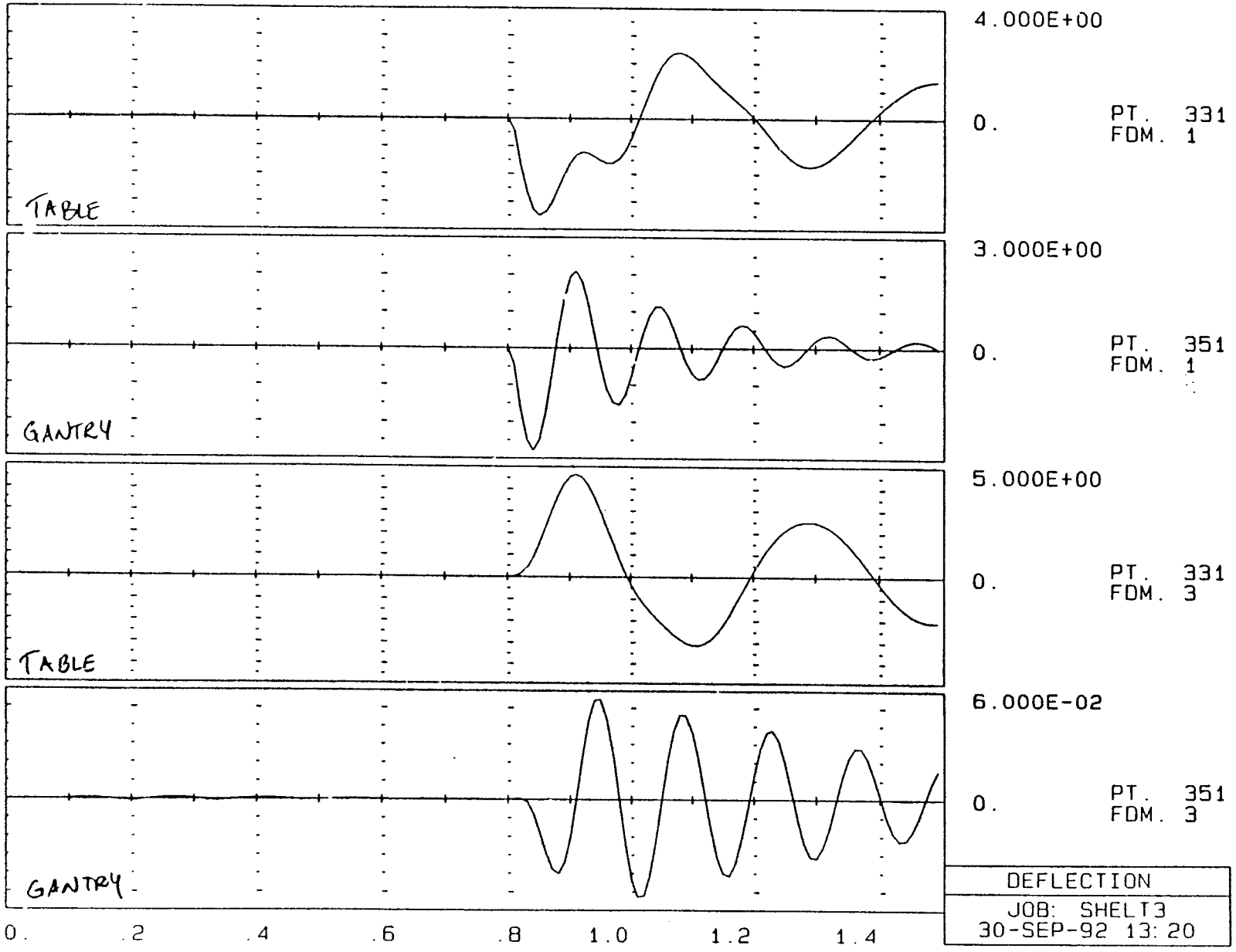
4.000E+00
0.
PT. 331
FDM. 1
TABLE
3.000E+00
0.
PT. 351
FDM. 1
GANTRY
5.000E+00
0.
PT. 331
FDM. 3
TABLE
6.000E-02
0.
PT. 351
FDM. 3
GANTRY
0.
.2
.4
.6
.8
1.0
1.2
1.4
DEFLECTION
JOB: SHELT3
30-SEP-92 13:20

Figure 72

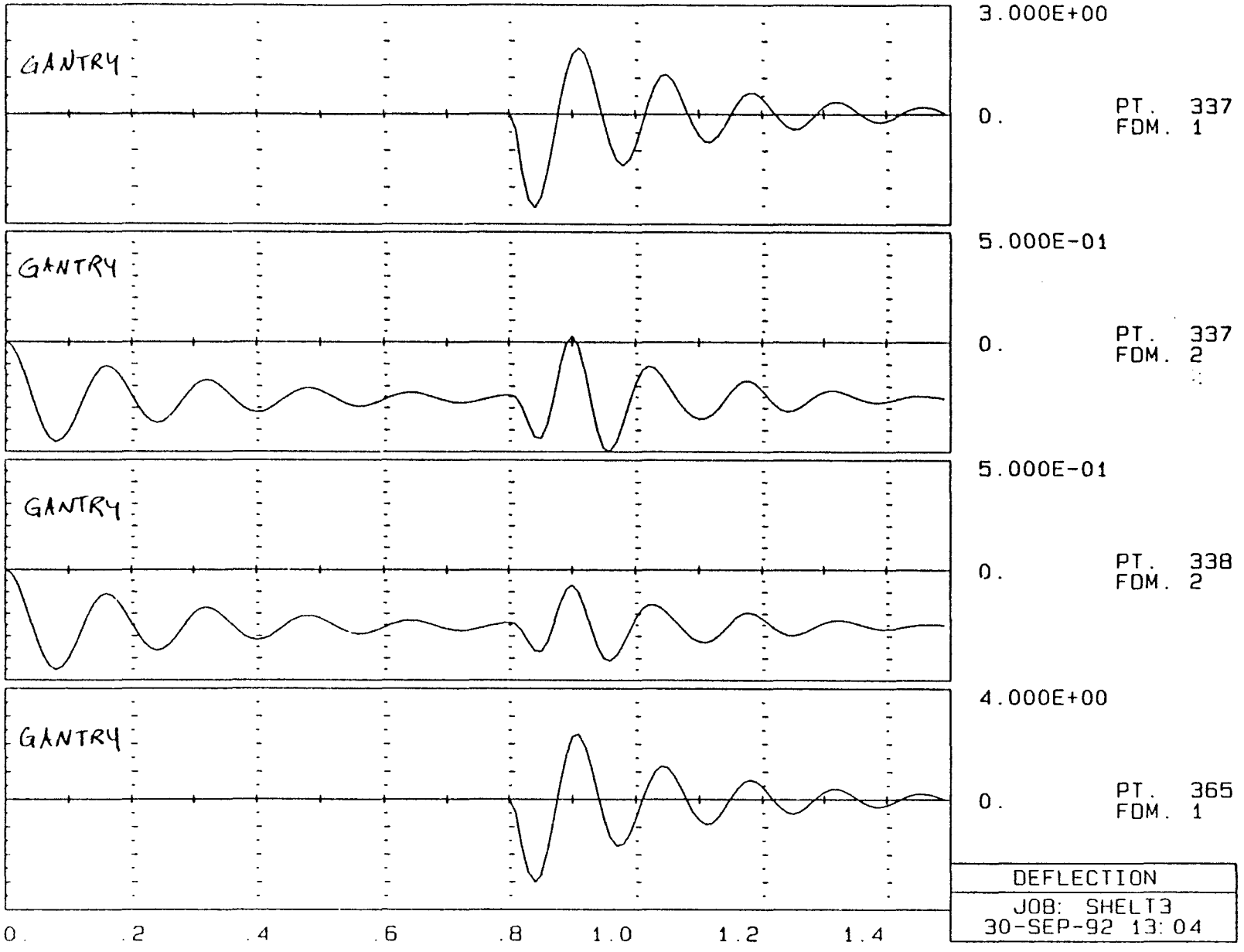
GANTRY
3.000E+00
0.
PT. 337
FDM. 1
GANTRY
5.000E-01
0.
PT. 337
FDM. 2
GANTRY
5.000E-01
0.
PT. 338
FDM. 2
GANTRY
4.000E+00
0.
PT. 365
FDM. 1
0.
.2
.4
.6
.8
1.0
1.2
1.4
DEFLECTION
JOB: SHELT3
30-SEP-92 13:04

Figure 73

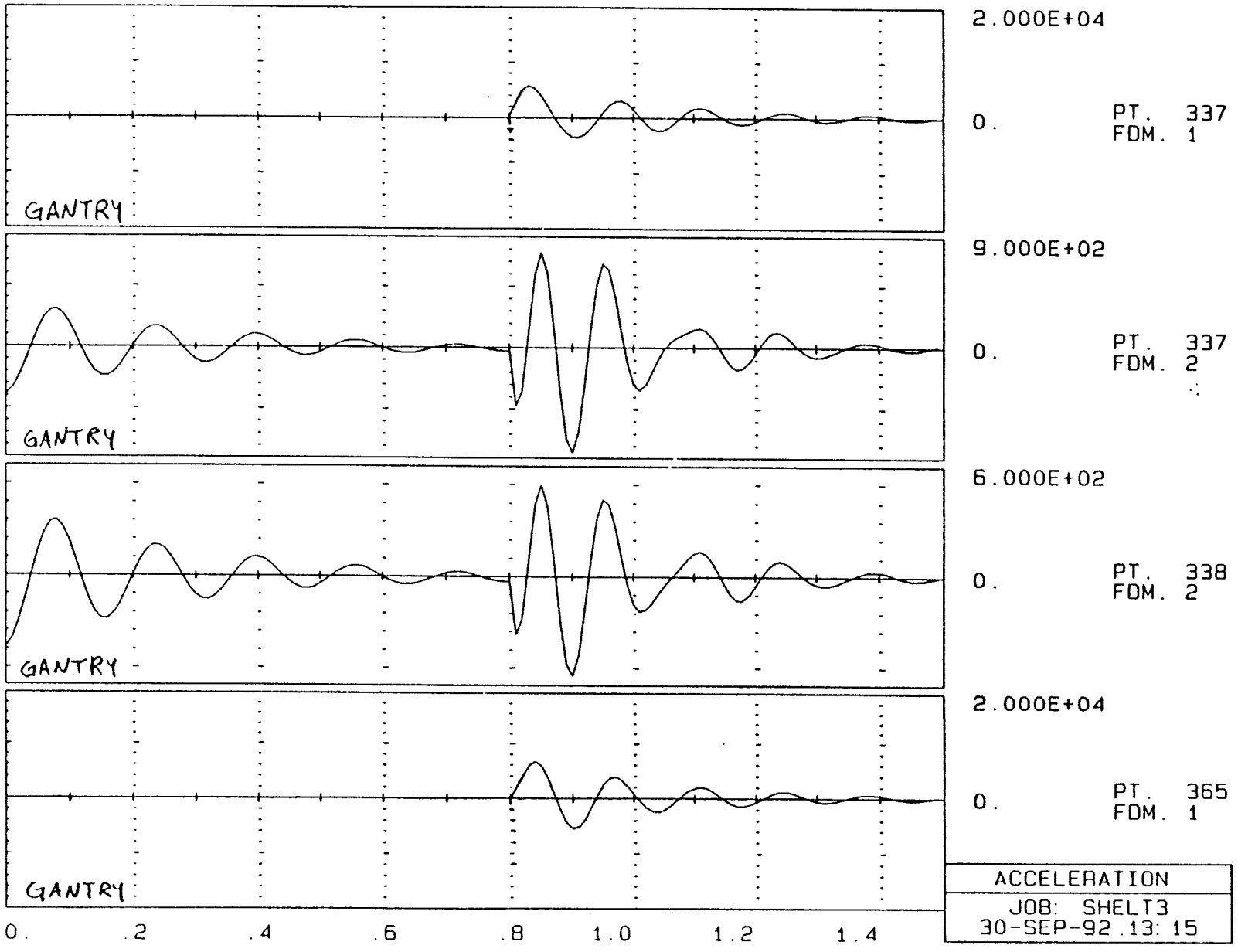
2.000E+04
0.
PT. 337
FDM. 1
GANTRY
9.000E+02
0.
PT. 337
FDM. 2
GANTRY
6.000E+02
0.
PT. 338
FDM. 2
GANTRY
2.000E+04
0.
PT. 365
FDM. 1
GANTRY
0.
.2
.4
.6
.8
1.0
1.2
1.4
ACCELERATION
JOB: SHELT3
30-SEP-92 13:15

Figure 74

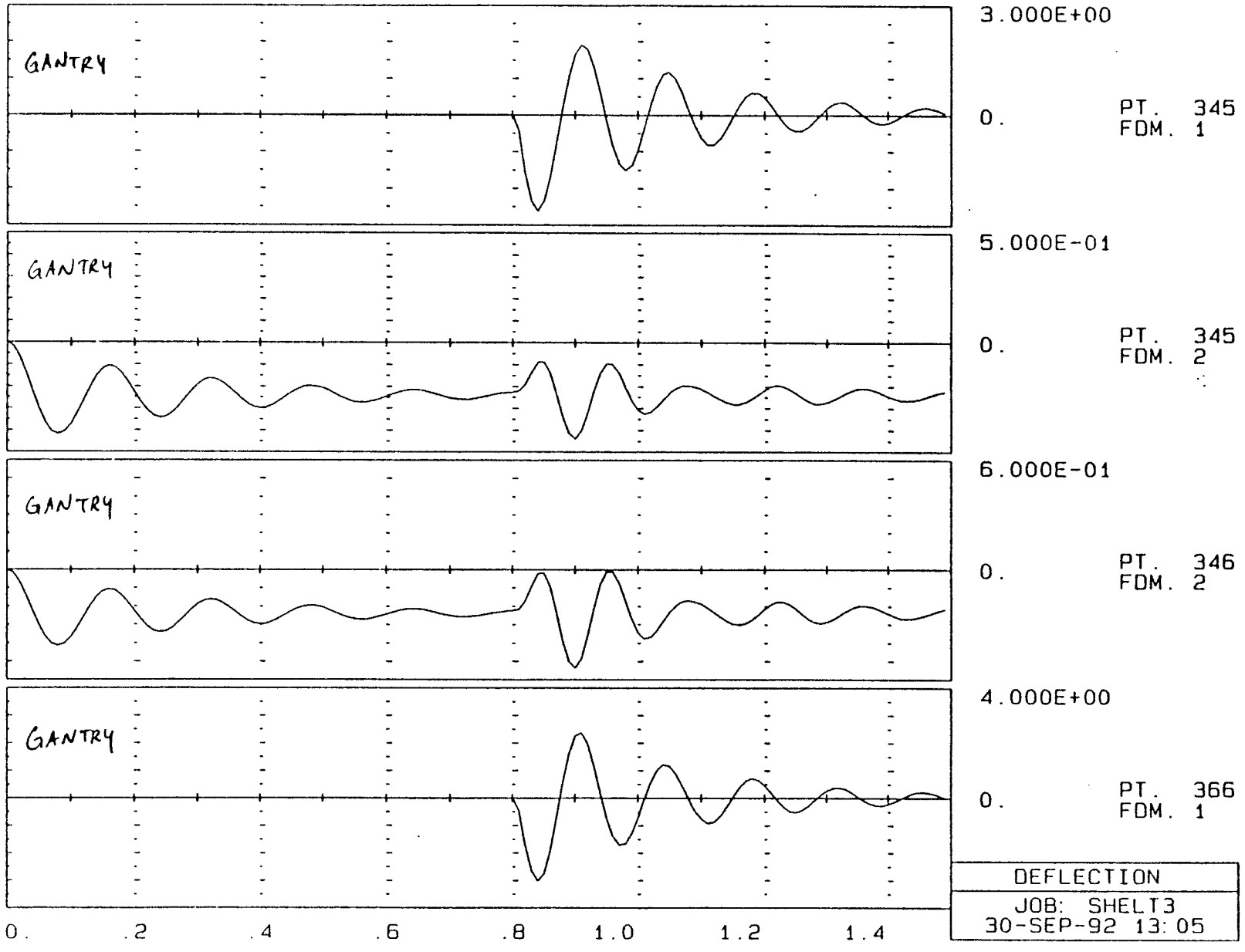
GANTRY
3.000E+00
0.
PT. 345
FDM. 1
GANTRY
5.000E-01
0.
PT. 345
FDM. 2
GANTRY
6.000E-01
0.
PT. 346
FDM. 2
GANTRY
4.000E+00
0.
PT. 366
FDM. 1
0.
.2
.4
.6
.8
1.0
1.2
1.4
DEFLECTION
JOB: SHELT3
30-SEP-92 13:05

Figure 75

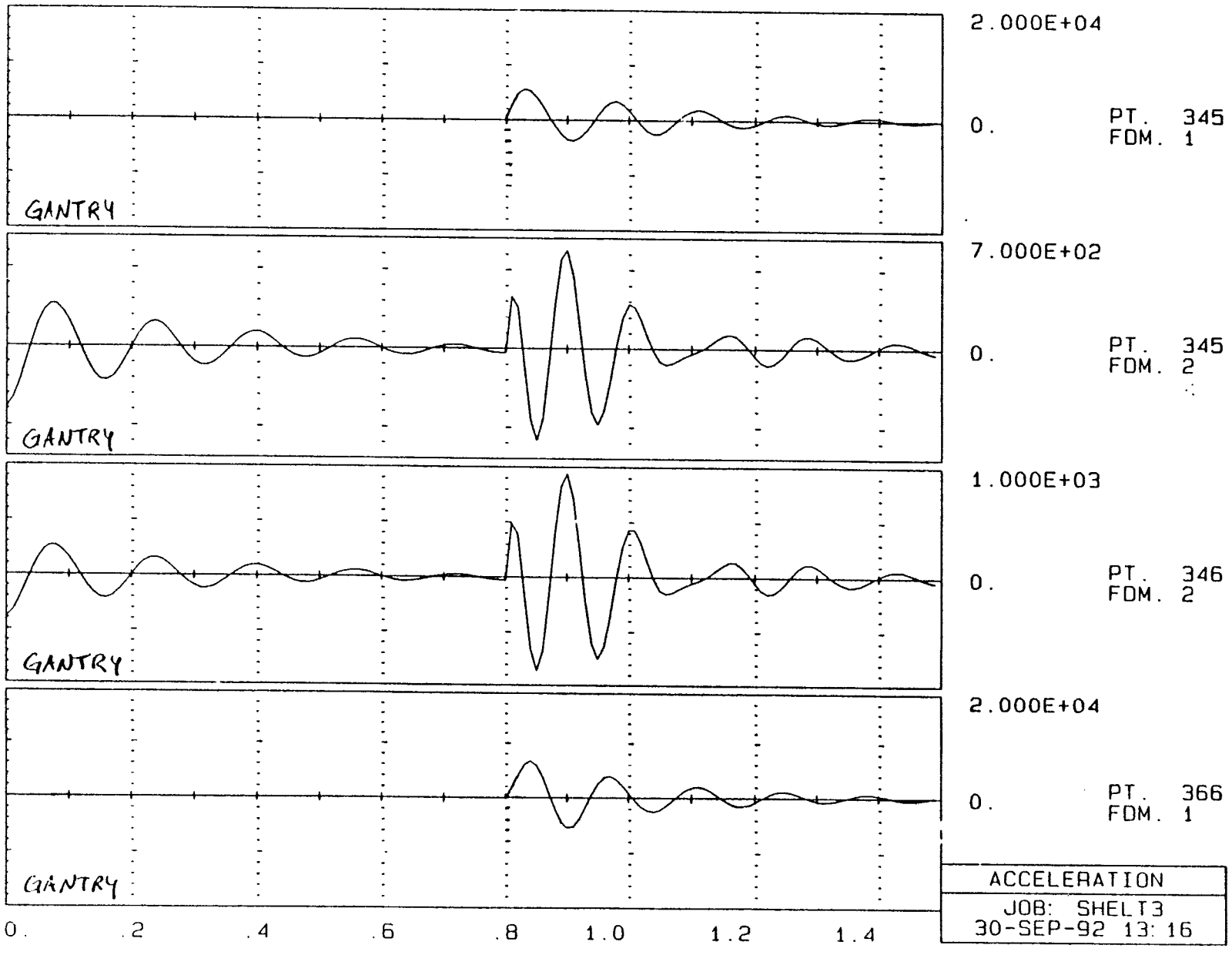
2.000E+04
0.
PT. 345
FDM. 1
GANTRY
7.000E+02
0.
PT. 345
FDM. 2
GANTRY
1.000E+03
0.
PT. 346
FDM. 2
GANTRY
2.000E+04
0.
PT. 366
FDM. 1
GANTRY
0.
.2
.4
.6
.8
1.0
1.2
1.4
ACCELERATION
JOB: SHELT3
30-SEP-92 13:16

Figure 76

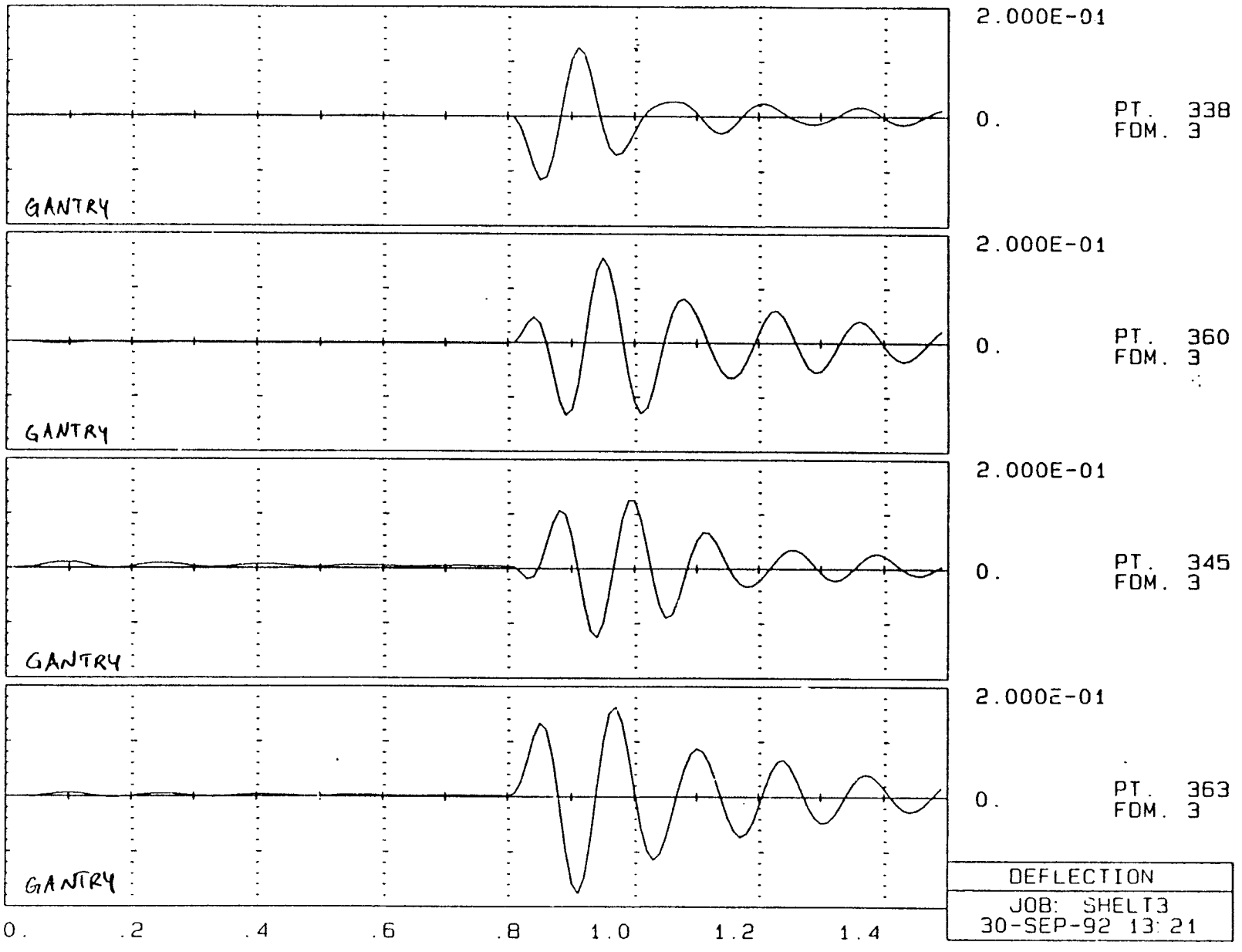
2.000E-01
0.
PT. 338
FDM. 3
GANTRY
2.000E-01
0.
PT. 360
FDM. 3
GANTRY
2.000E-01
0.
PT. 345
FDM. 3
GANTRY
2.000E-01
0.
PT. 363
FDM. 3
GANTRY
0.
.2
.4
.6
.8
1.0
1.2
1.4
DEFLECTION
JOB: SHELT3
30-SEP-92 13:21

Figure 77

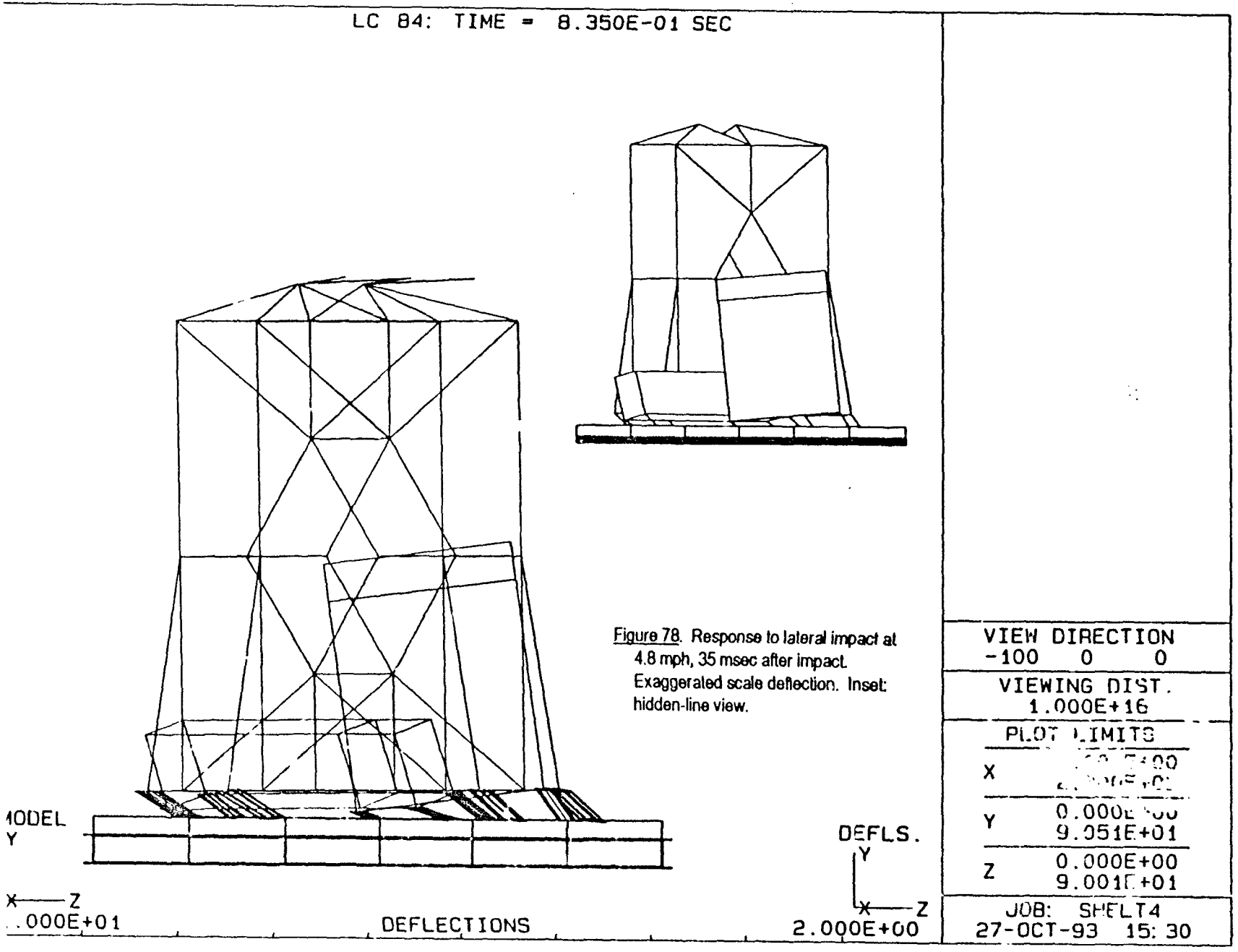

Figure 78. Response to lateral impact at 4.8 mph, 35 msec after impact. Exaggerated scale deflection. Inset: hidden-line view.

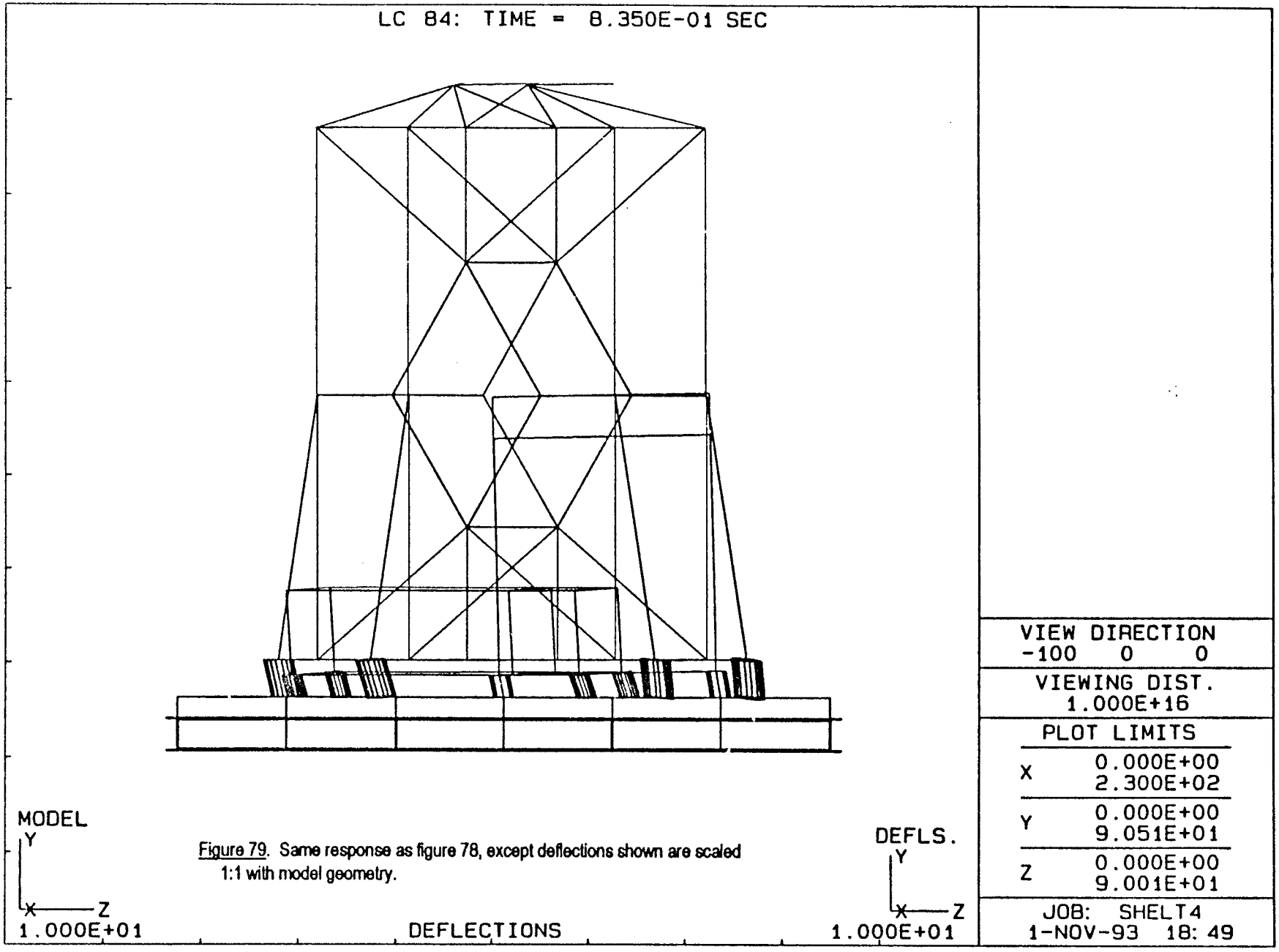

Figure 79. Same response as figure 78, except deflections shown are scaled 1:1 with model geometry.

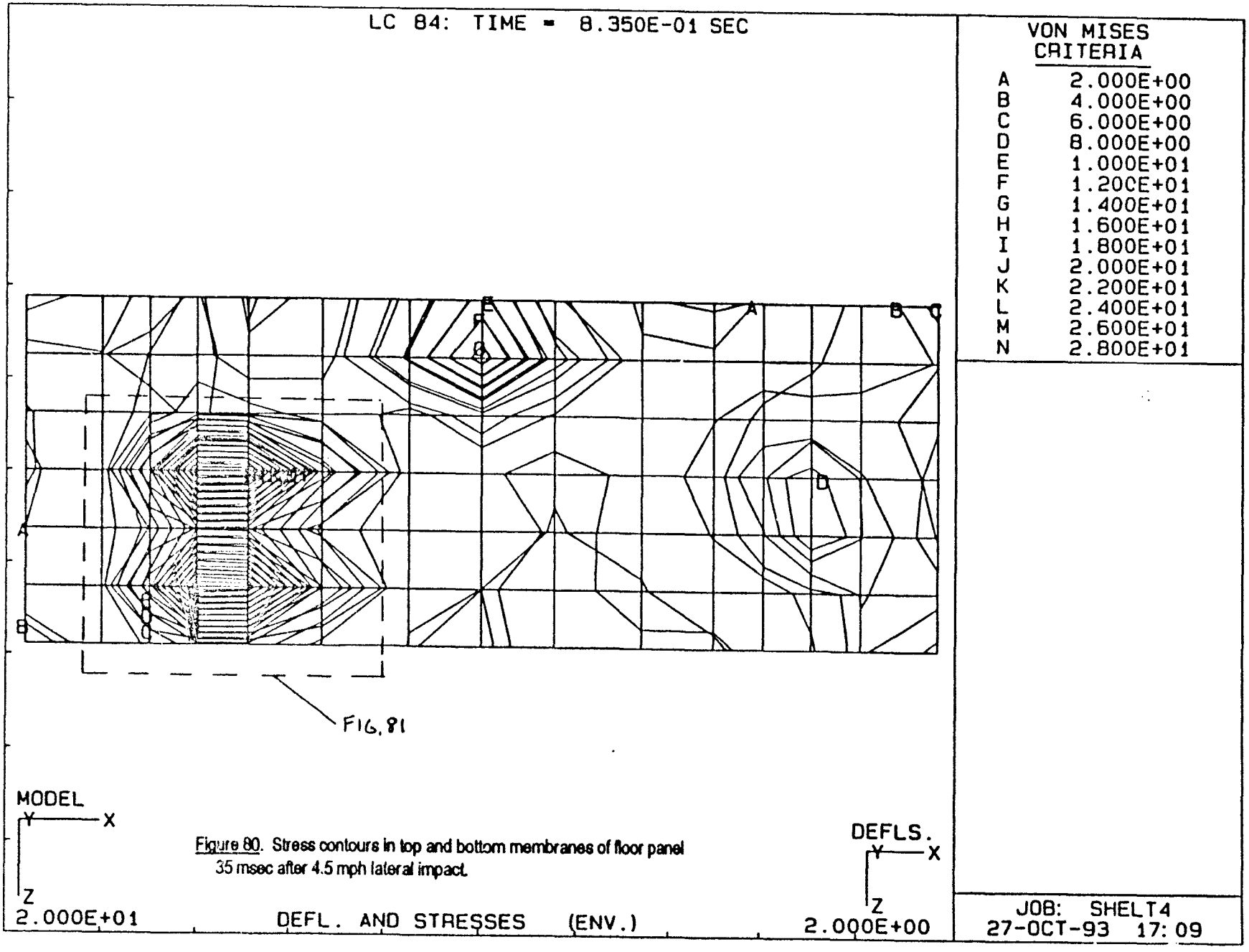

Figure 80. Stress contours in top and bottom membranes of floor panel 35 msec after 4.5 mph lateral impact.

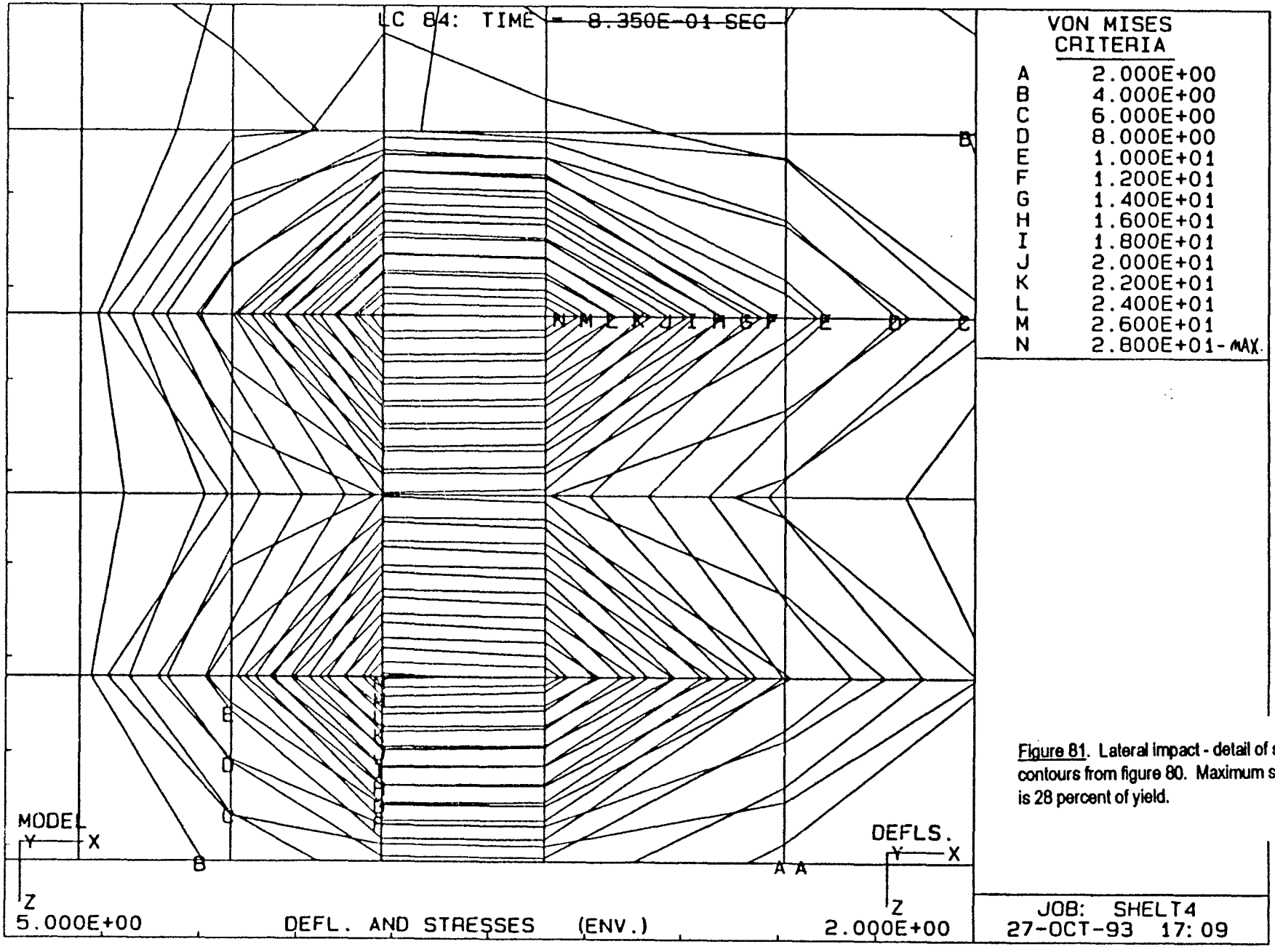

Figure 81. Lateral impact - detail of stress contours from figure 80. Maximum stress is 28 percent of yield.

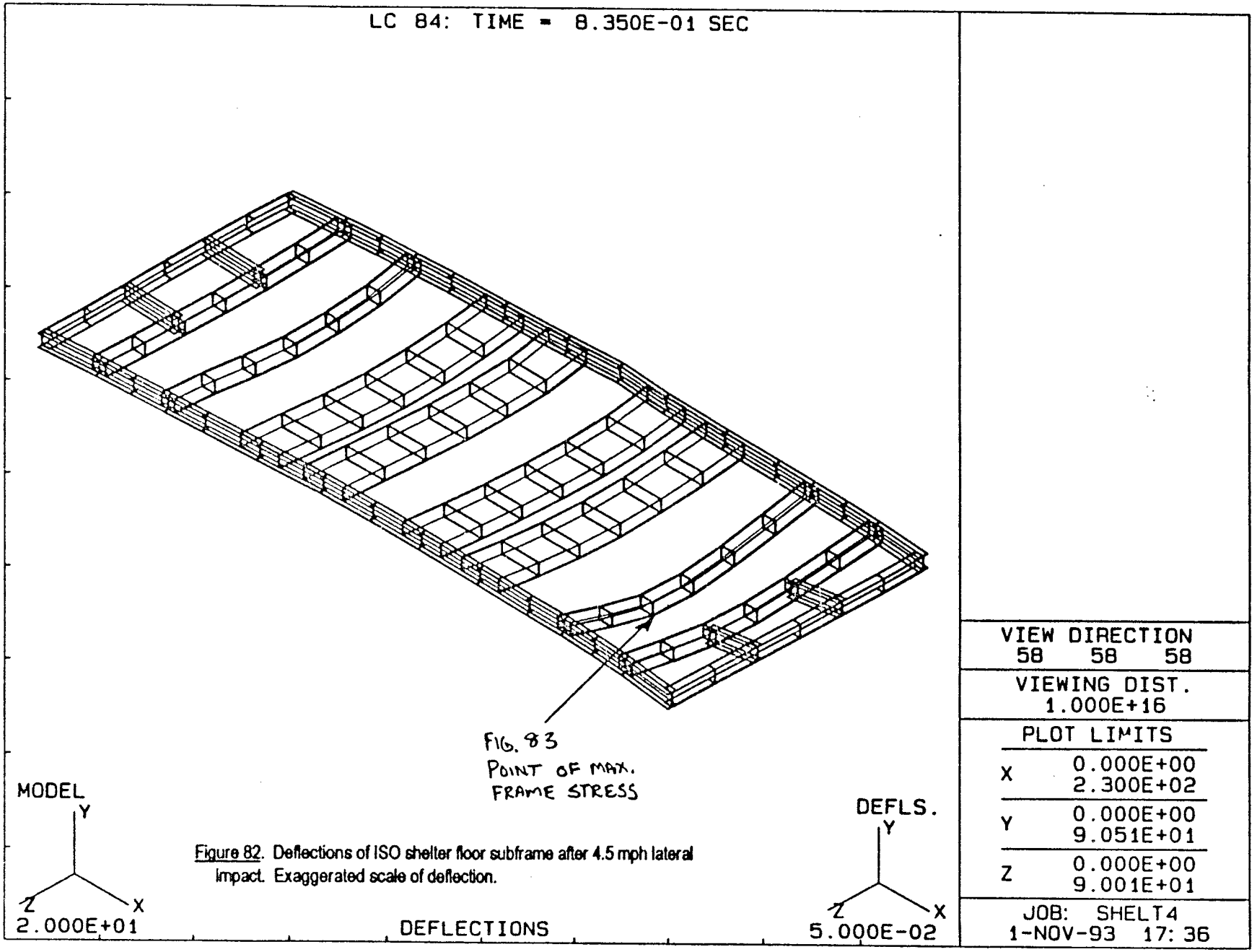

Figure 82. Deflections of ISO shelter floor subframe after 4.5 mph lateral impact. Exaggerated scale of deflection.

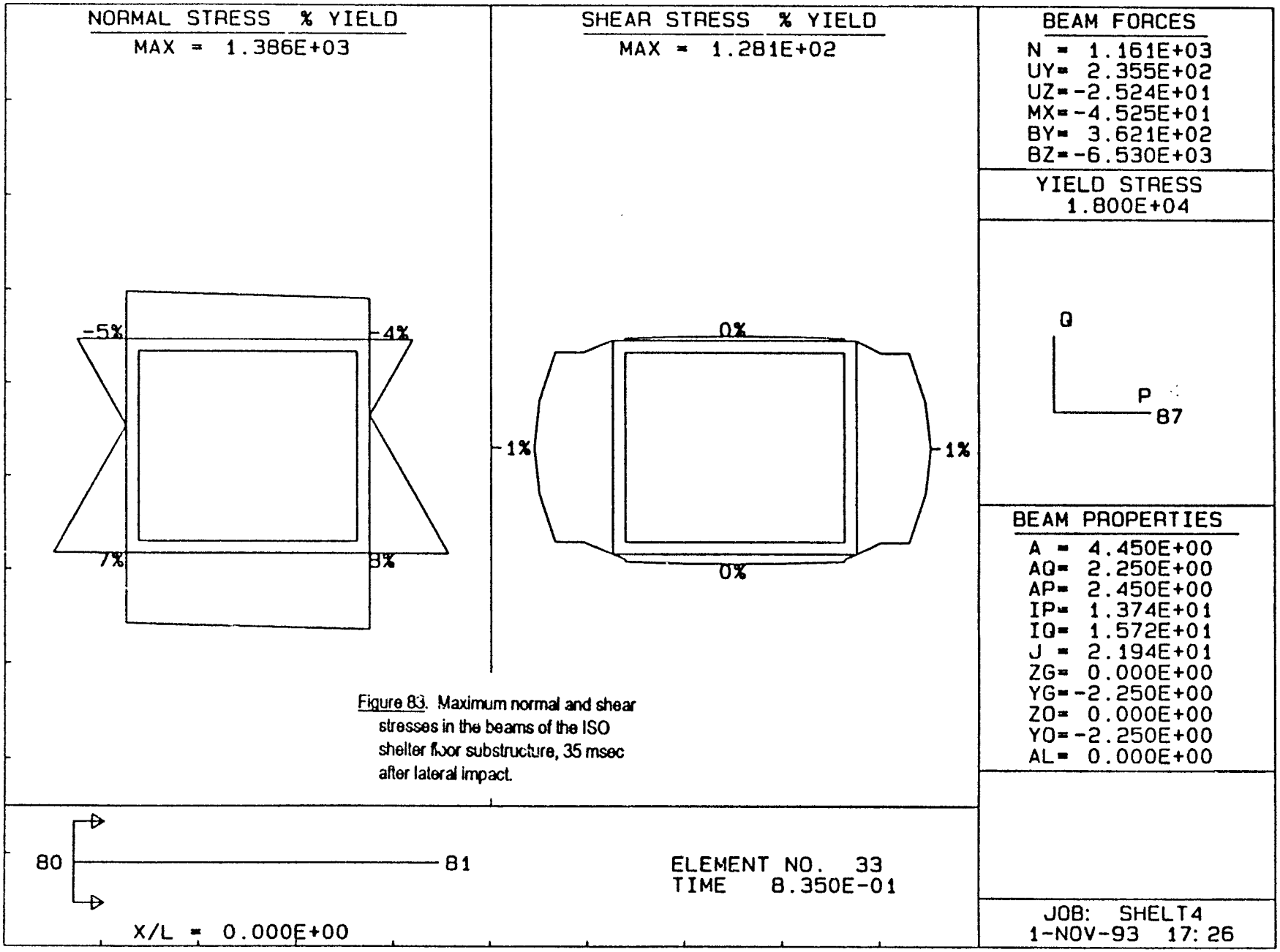

Figure 83. Maximum normal and shear stresses in the beams of the ISO shelter floor substructure, 35 msec after lateral impact.

Figure 84

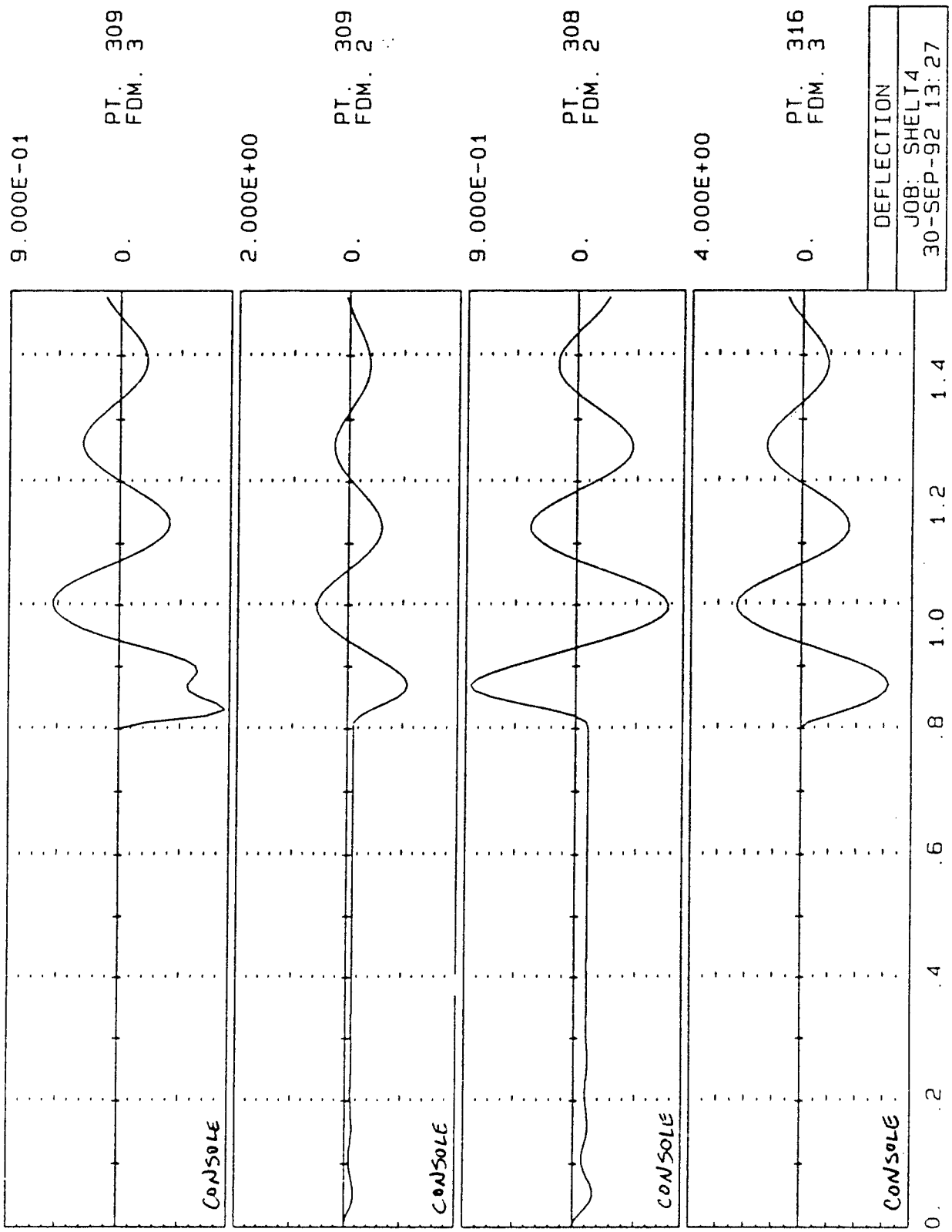
DEFLECTION
JOB: SHELT4
30-SEP-92 13:27
9.000E-01
0.
PT. 309
FOM. 3
CONSOLE
2.000E+00
0.
PT. 309
FOM. 2
CONSOLE
9.000E-01
0.
PT. 308
FOM. 2
CONSOLE
4.000E+00
0.
PT. 316
FOM. 3
CONSOLE
0. .2 .4 .6 .8 1.0 1.2 1.4

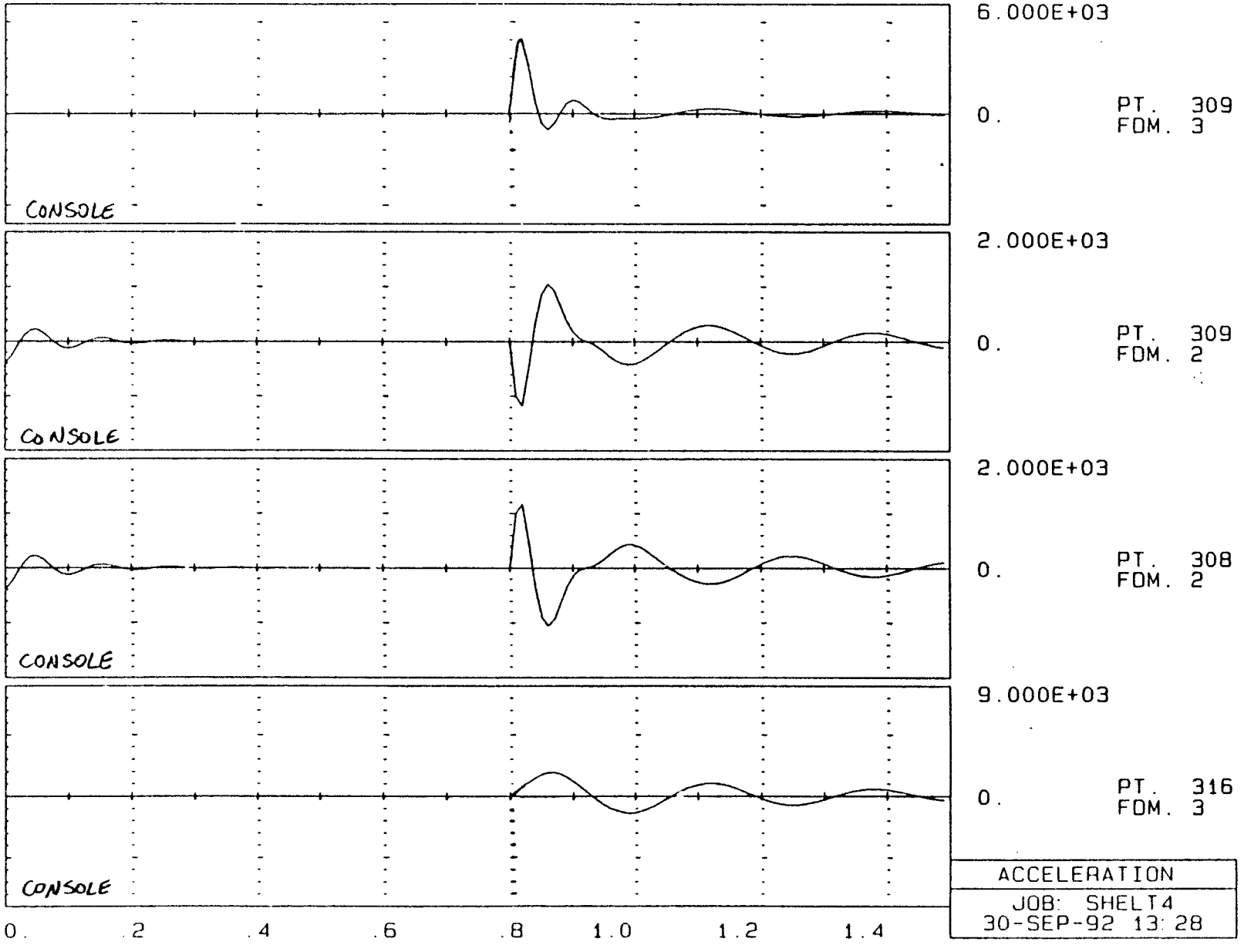
6.000E+03
0.
PT. 309
FDM. 3
CONSOLE
2.000E+03
0.
PT. 309
FDM. 2
CONSOLE
2.000E+03
0.
PT. 308
FDM. 2
CONSOLE
9.000E+03
0.
PT. 316
FDM. 3
CONSOLE
0.
.2
.4
.6
.8
1.0
1.2
1.4
ACCELERATION
JOB: SHELT4
30-SEP-92 13:28

Figure 85

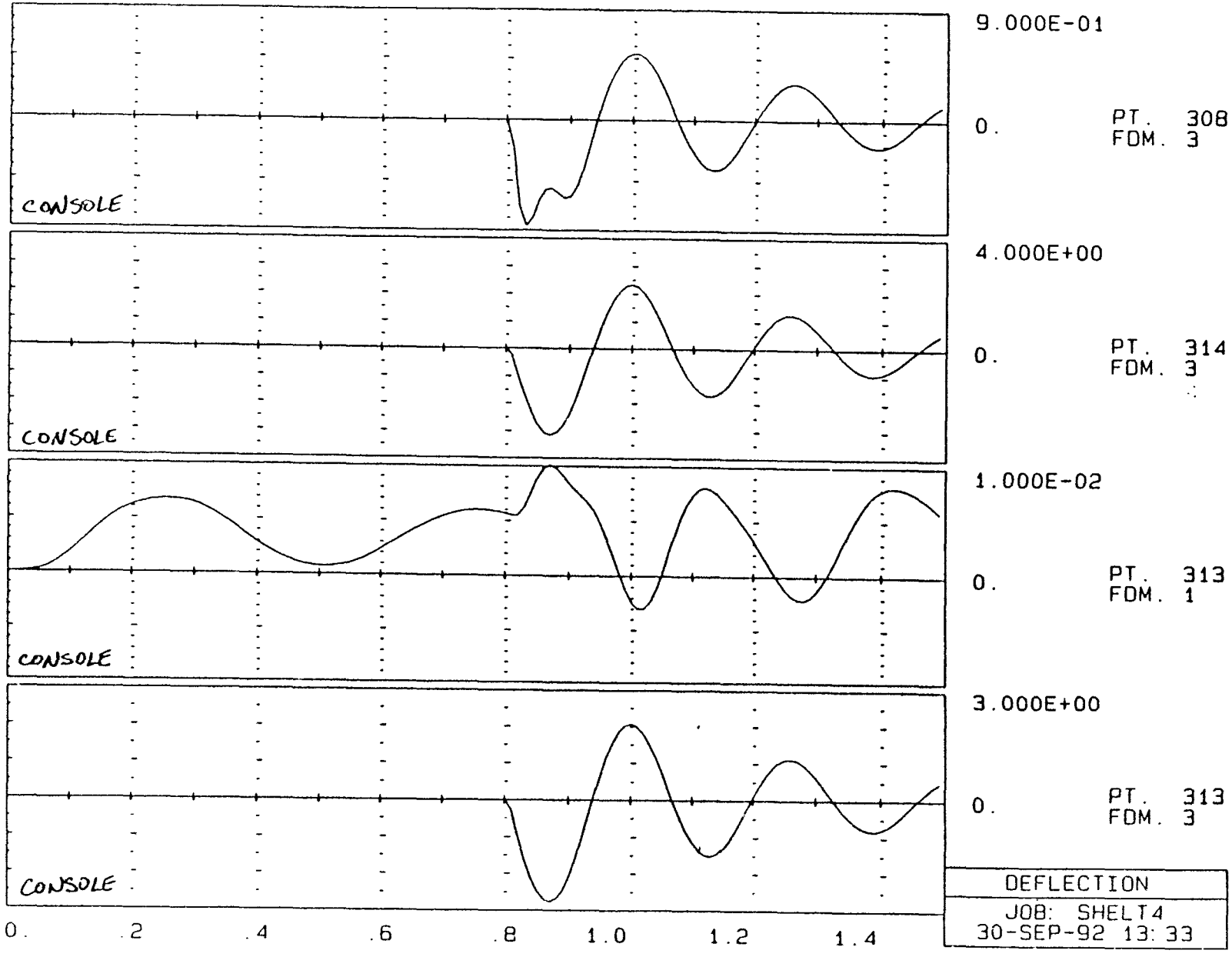
9.000E-01
0.
PT. 308
FDM. 3
CONSOLE
4.000E+00
0.
PT. 314
FDM. 3
CONSOLE
1.000E-02
0.
PT. 313
FDM. 1
CONSOLE
3.000E+00
0.
PT. 313
FDM. 3
CONSOLE
0.
.2
.4
.6
.8
1.0
1.2
1.4
DEFLECTION
JOB: SHELT4
30-SEP-92 13:33

Figure 86

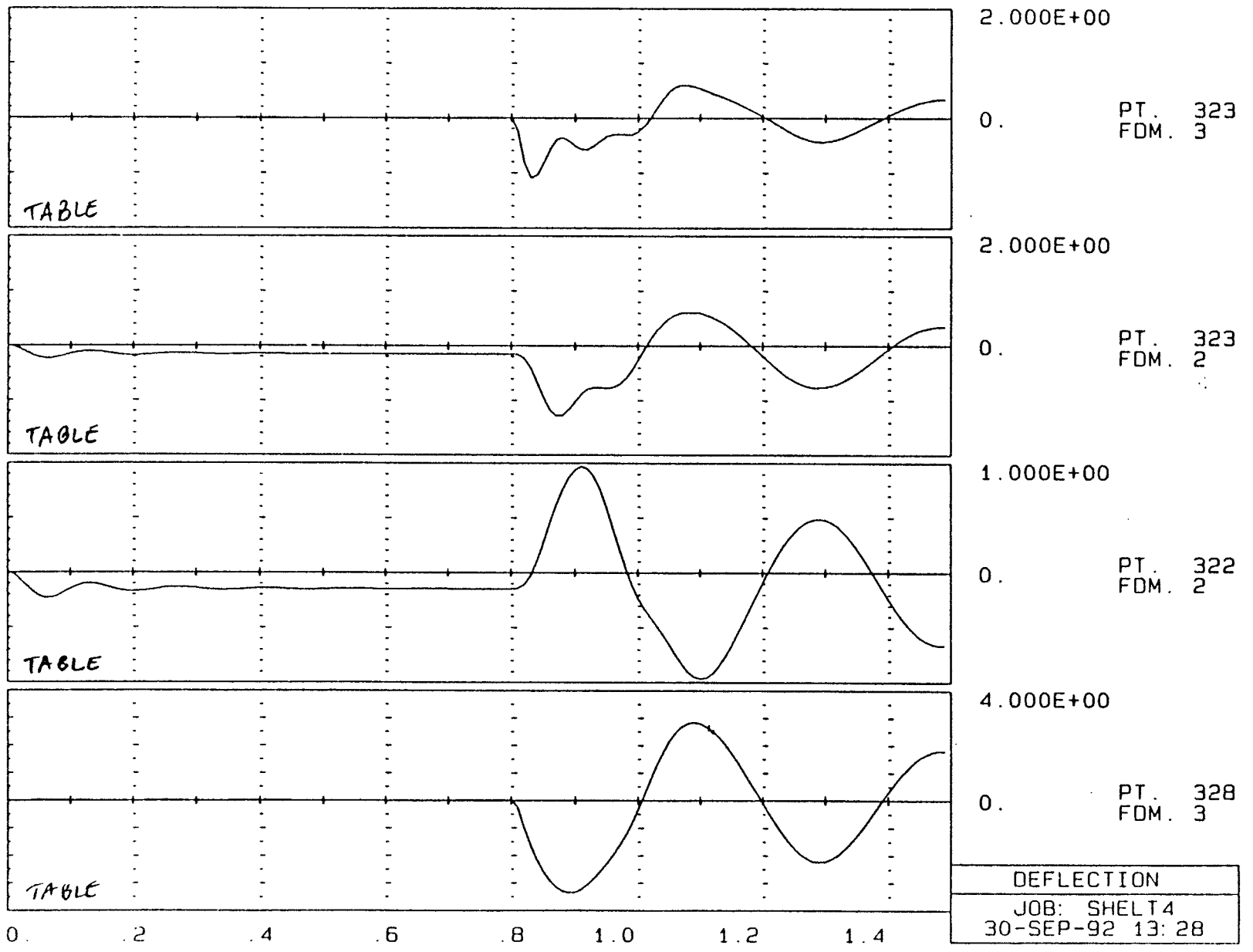
2.000E+00
0.
PT. 323
FDM. 3
TABLE
2.000E+00
0.
PT. 323
FDM. 2
TABLE
1.000E+00
0.
PT. 322
FDM. 2
TABLE
4.000E+00
0.
PT. 328
FDM. 3
TABLE
0.
.2
.4
.6
.8
1.0
1.2
1.4
DEFLECTION
JOB: SHELT4
30-SEP-92 13:28

Figure 87

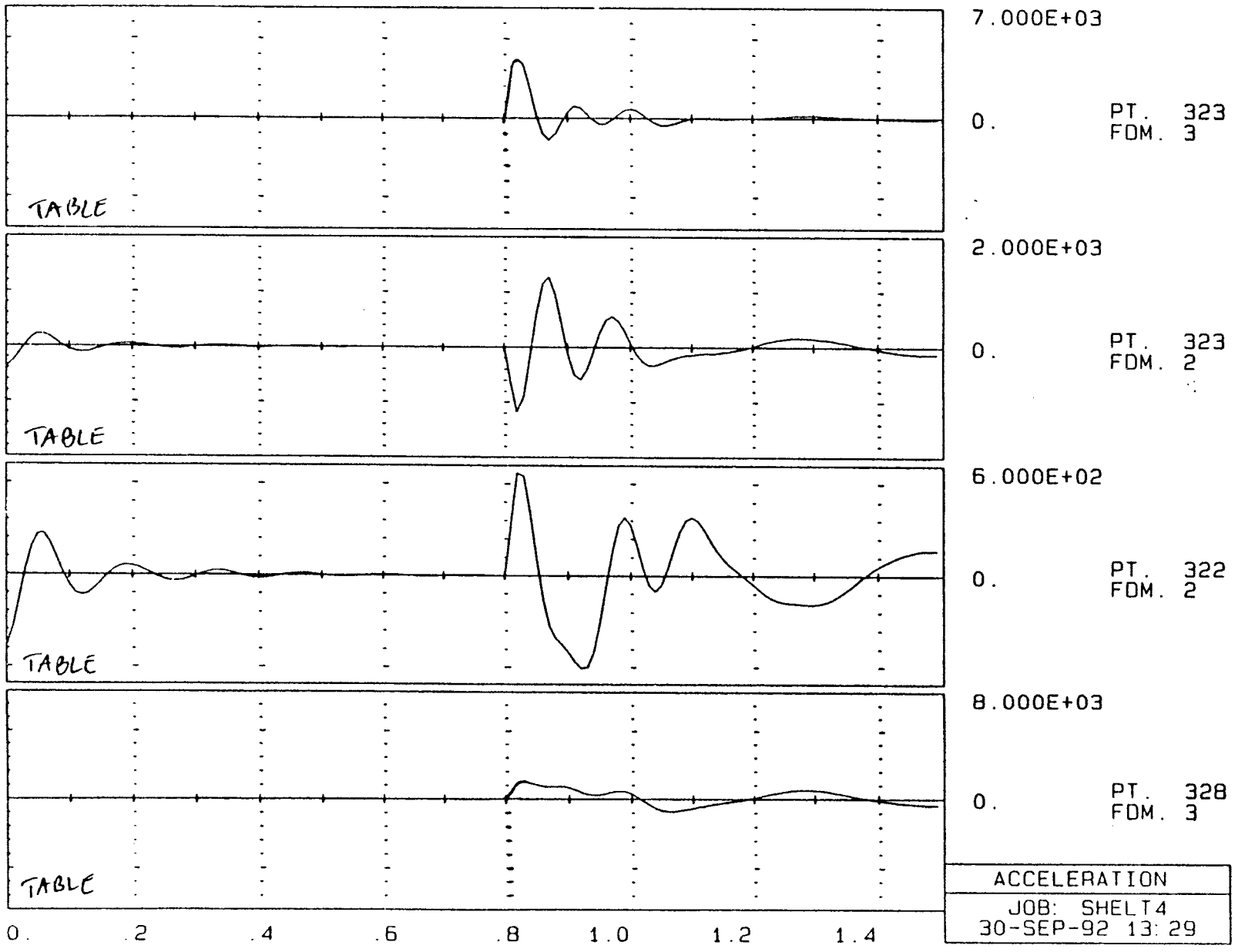
7.000E+03
0.
PT. 323
FDM. 3
TABLE
2.000E+03
0.
PT. 323
FDM. 2
TABLE
6.000E+02
0.
PT. 322
FDM. 2
TABLE
8.000E+03
0.
PT. 328
FDM. 3
TABLE
0.
.2
.4
.6
.8
1.0
1.2
1.4
ACCELERATION
JOB: SHELT4
30-SEP-92 13:29

Figure 88

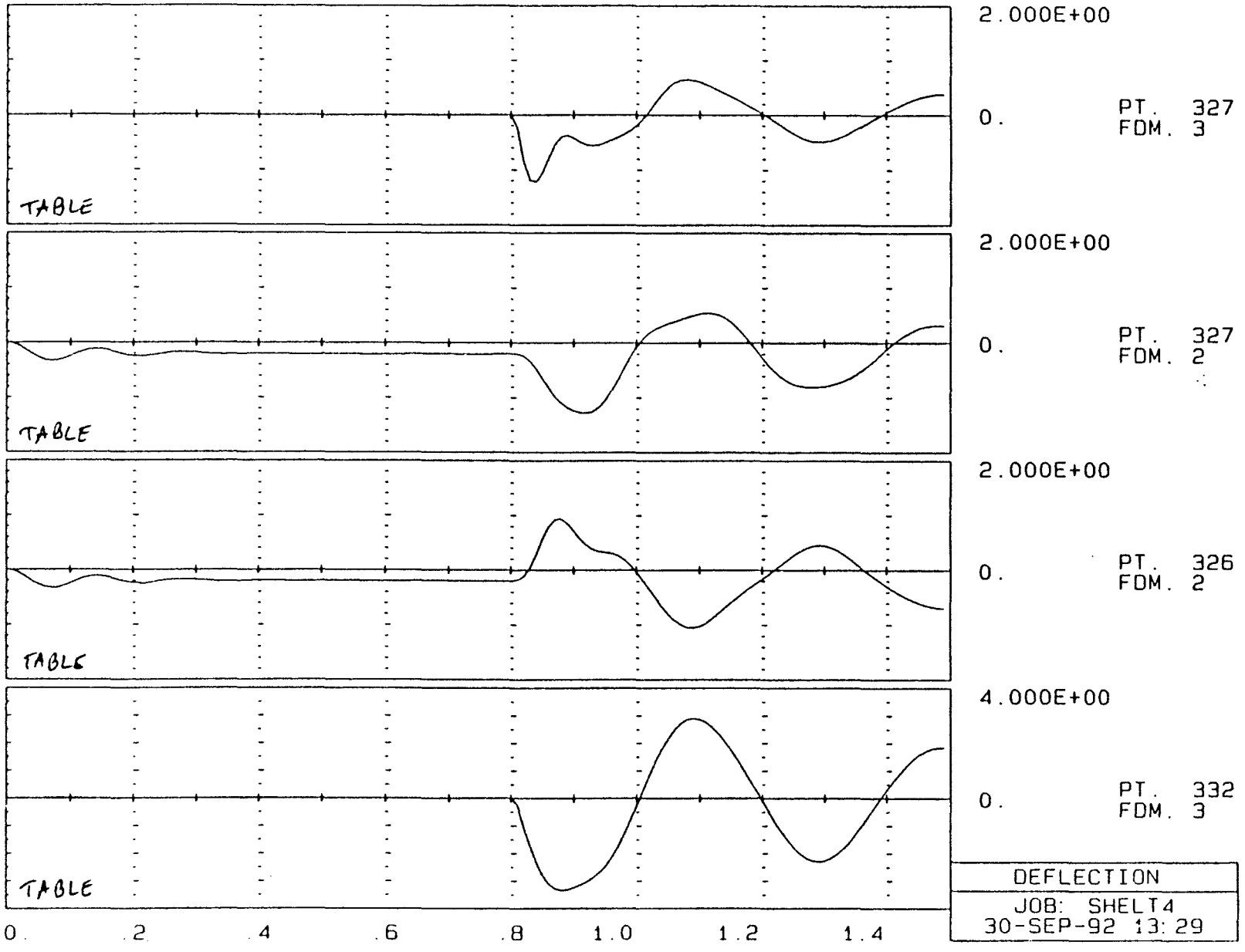
2.000E+00
0.
PT. 327
FDM. 3
TABLE
2.000E+00
0.
PT. 327
FDM. 2
TABLE
2.000E+00
0.
PT. 326
FDM. 2
TABLE
4.000E+00
0.
PT. 332
FDM. 3
TABLE
DEFLECTION
JOB: SHELT4
30-SEP-92 13:29
0.
.2
.4
.6
.8
1.0
1.2
1.4

Figure 89

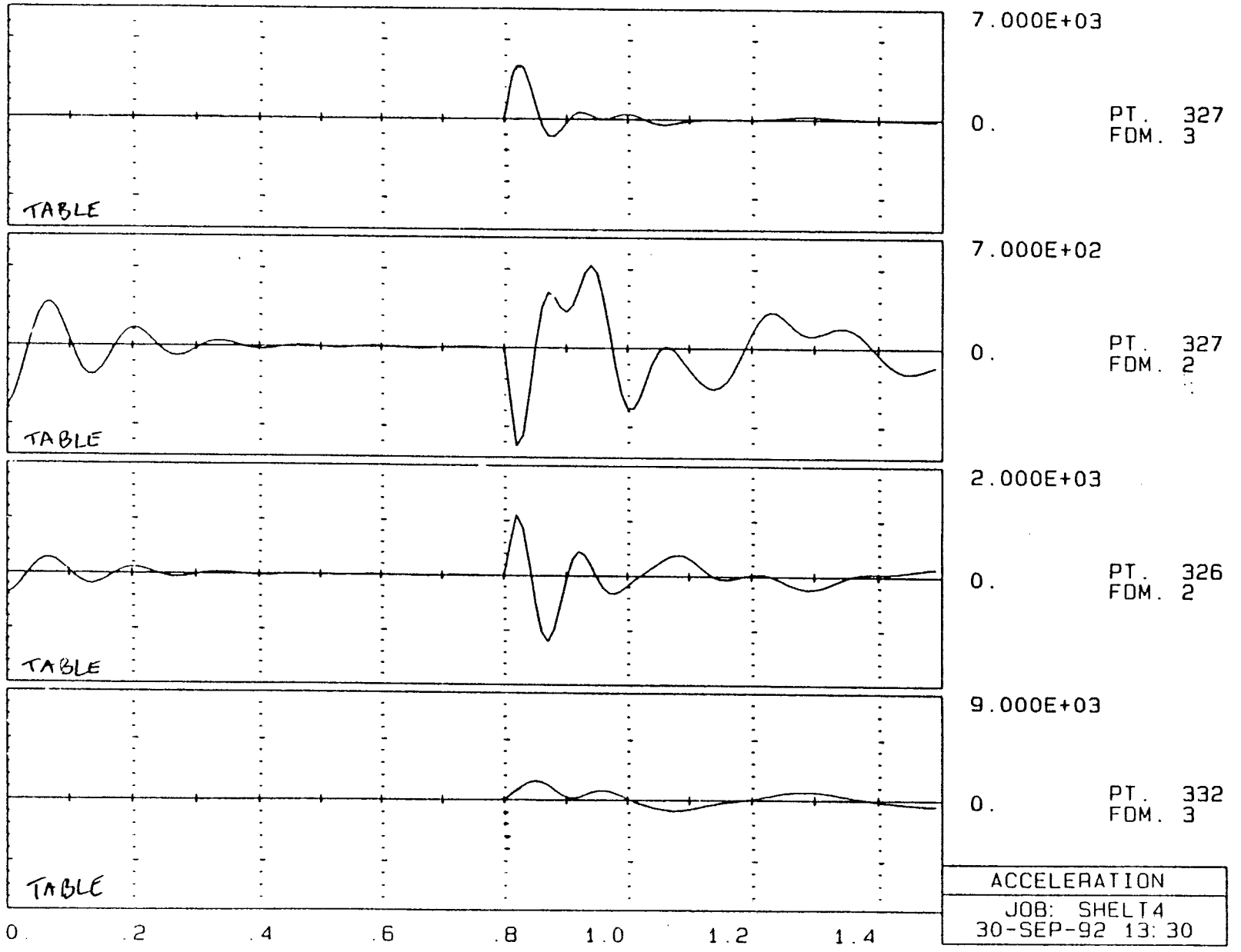
7.000E+03
0.
PT. 327
FDM. 3
TABLE
7.000E+02
0.
PT. 327
FDM. 2
TABLE
2.000E+03
0.
PT. 326
FDM. 2
TABLE
9.000E+03
0.
PT. 332
FDM. 3
TABLE
0
.2
.4
.6
.8
1.0
1.2
1.4
ACCELERATION
JOB: SHELT4
30-SEP-92 13:30

Figure 90

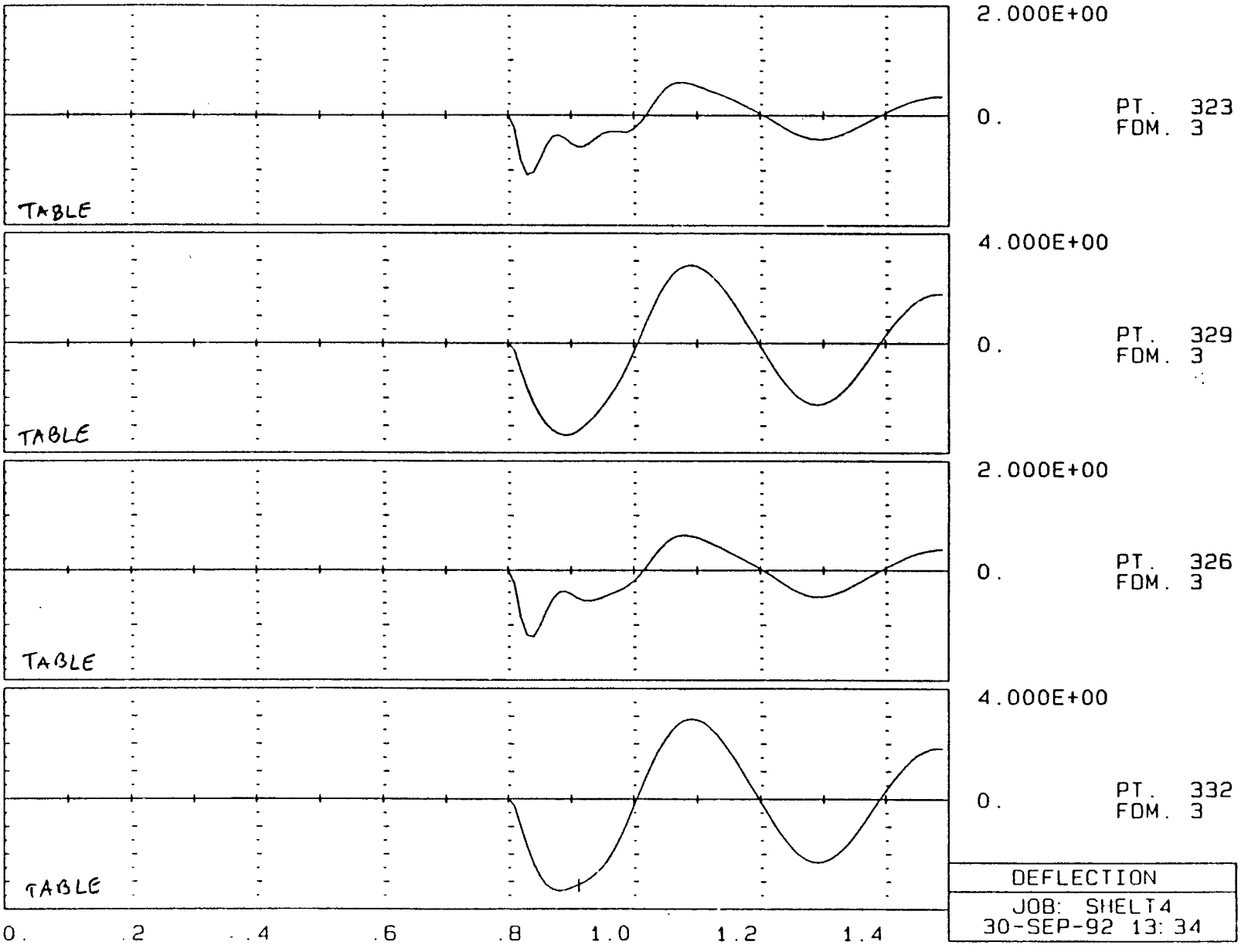
2.000E+00
0.
PT. 323
FDM. 3
TABLE
4.000E+00
0.
PT. 329
FDM. 3
TABLE
2.000E+00
0.
PT. 326
FDM. 3
TABLE
4.000E+00
0.
PT. 332
FDM. 3
TABLE
0.
.2
.4
.6
.8
1.0
1.2
1.4
DEFLECTION
JOB: SHELT4
30-SEP-92 13:34

Figure 91

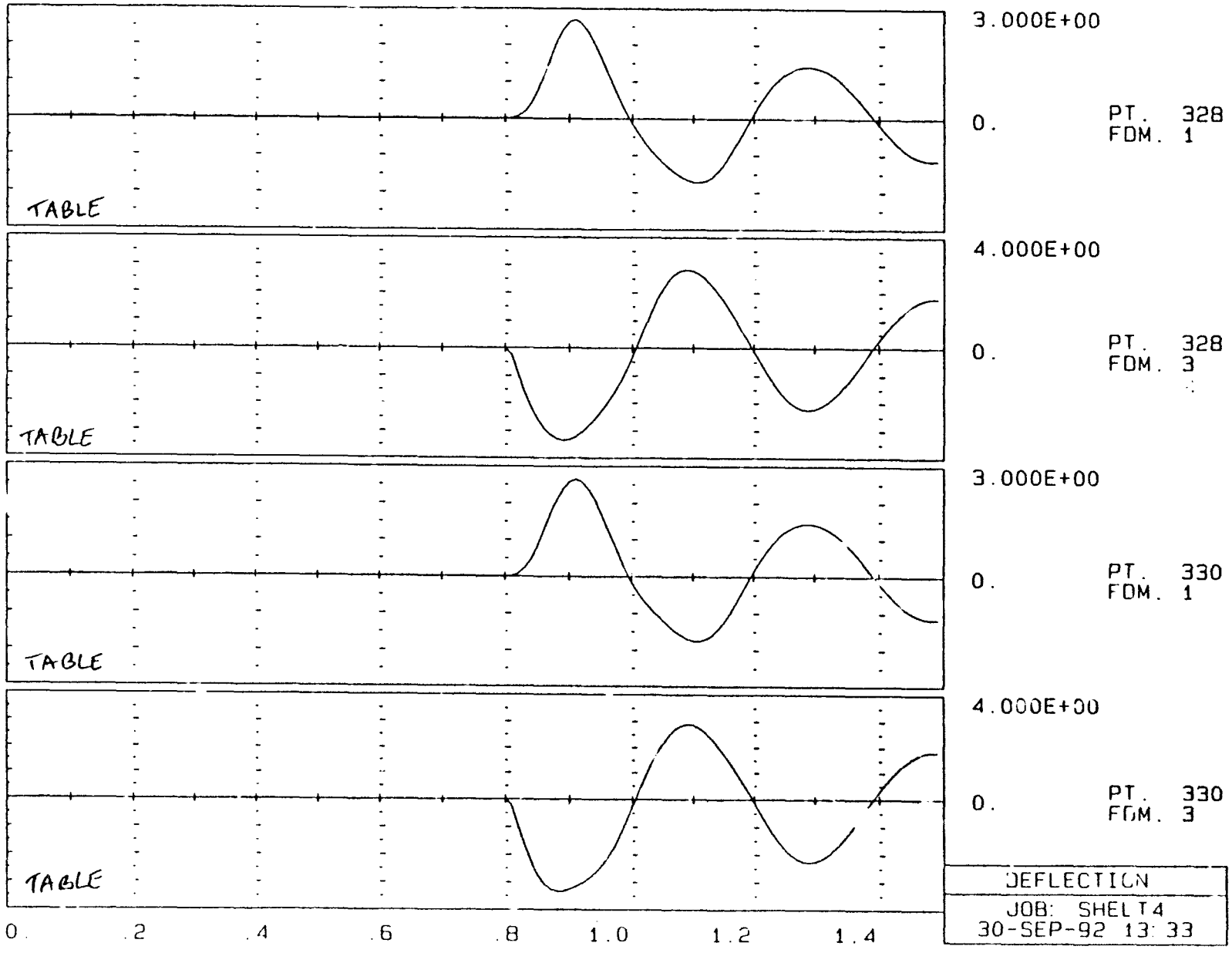
3.000E+00
0.
PT. 328
FDM. 1
TABLE
4.000E+00
0.
PT. 328
FDM. 3
TABLE
3.000E+00
0.
PT. 330
FDM. 1
TABLE
4.000E+00
0.
PT. 330
FDM. 3
TABLE
0.
.2
.4
.6
.8
1.0
1.2
1.4
DEFLECTION
JOB: SHELT4
30-SEP-92 13:33

Figure 92

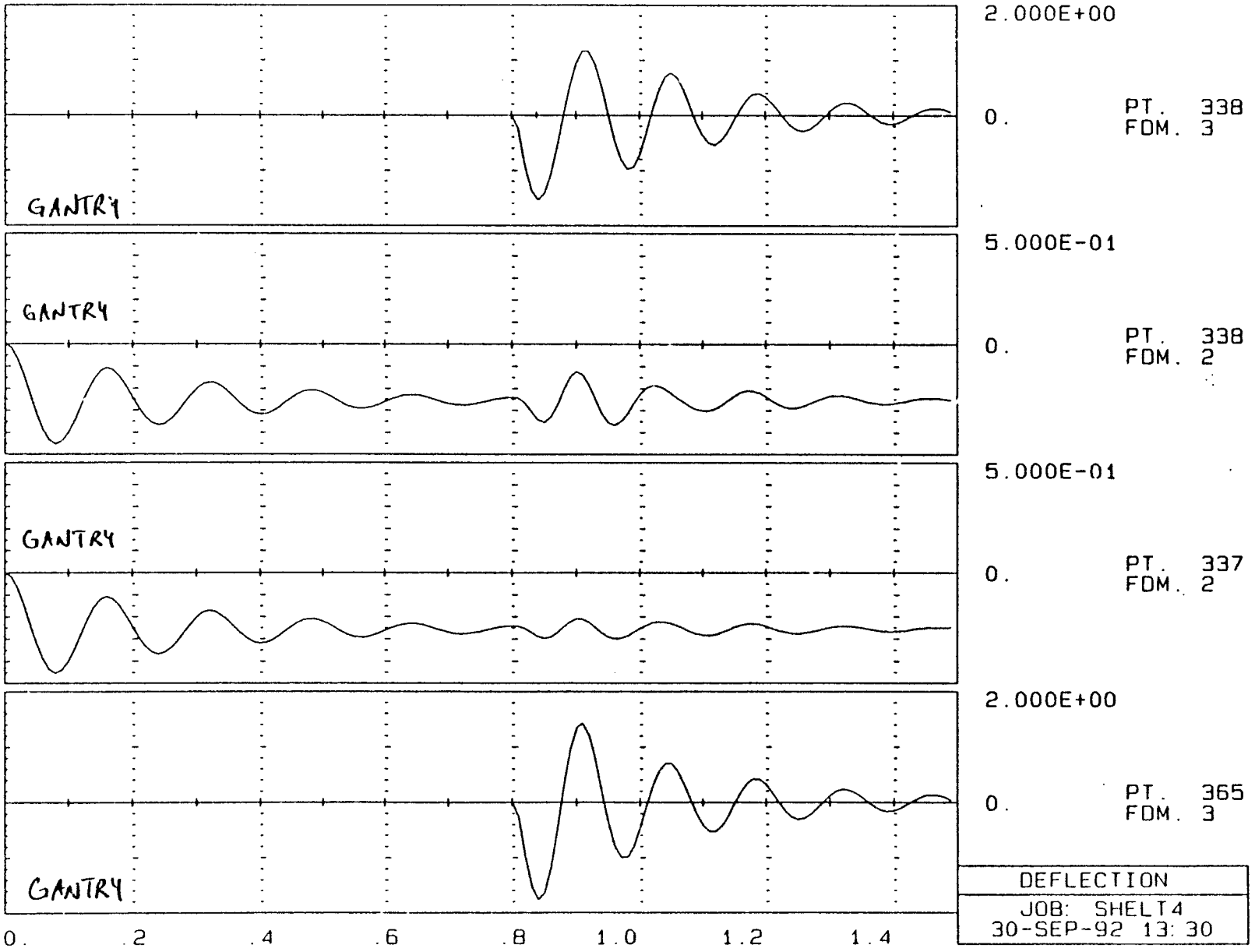
2.000E+00
0.
PT. 338
FDM. 3
GANTRY
5.000E-01
0.
PT. 338
FDM. 2
GANTRY
5.000E-01
0.
PT. 337
FDM. 2
GANTRY
2.000E+00
0.
PT. 365
FDM. 3
GANTRY
0.
.2
.4
.6
.8
1.0
1.2
1.4
DEFLECTION
JOB: SHELT4
30-SEP-92 13:30

Figure 94

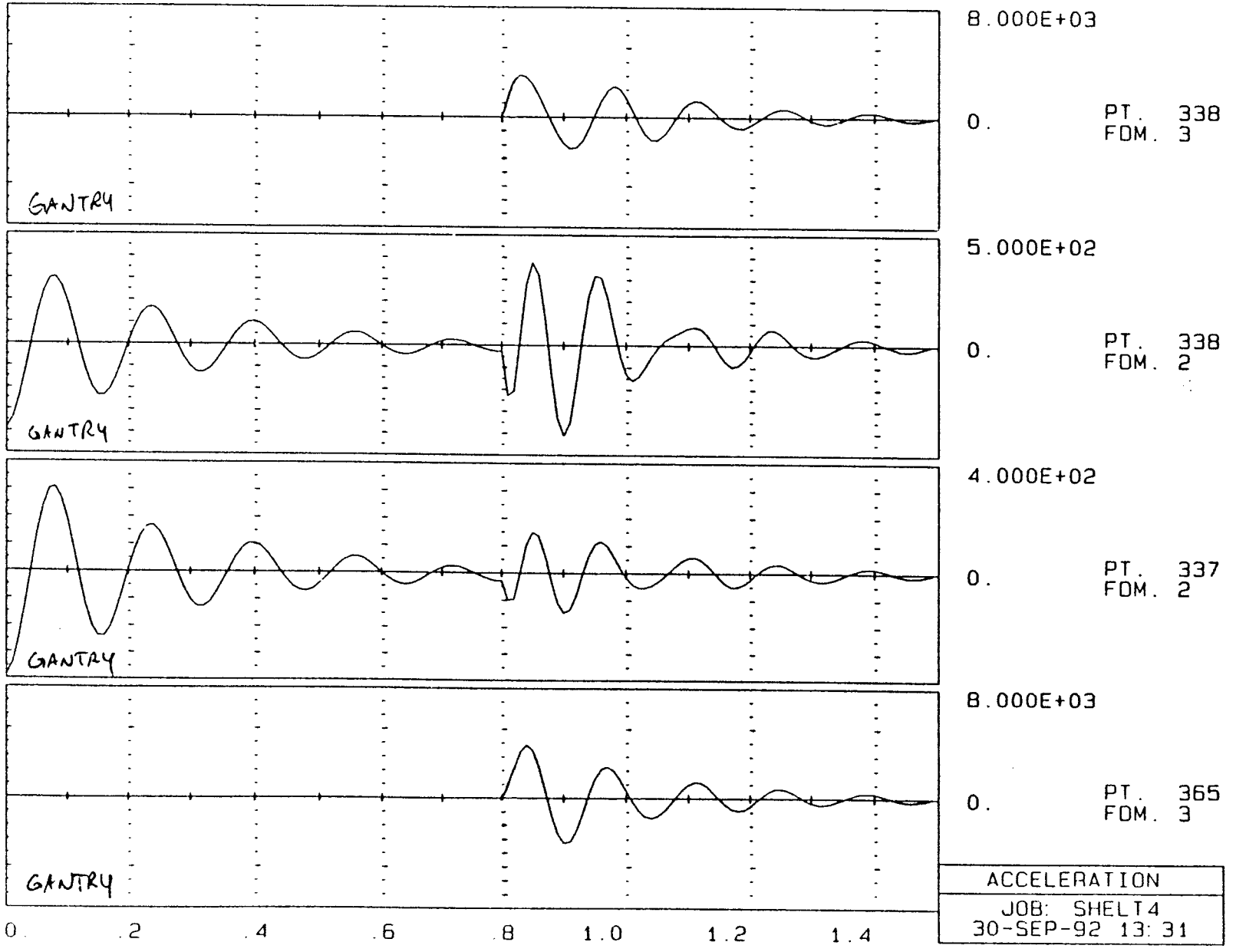
8.000E+03
0.
PT. 338
FDM. 3
GANTRY
5.000E+02
0.
PT. 338
FDM. 2
GANTRY
4.000E+02
0.
PT. 337
FDM. 2
GANTRY
8.000E+03
0.
PT. 365
FDM. 3
GANTRY
0
.2
.4
.6
.8
1.0
1.2
1.4
ACCELERATION
JOB: SHELT4
30-SEP-92 13:31

Figure 95

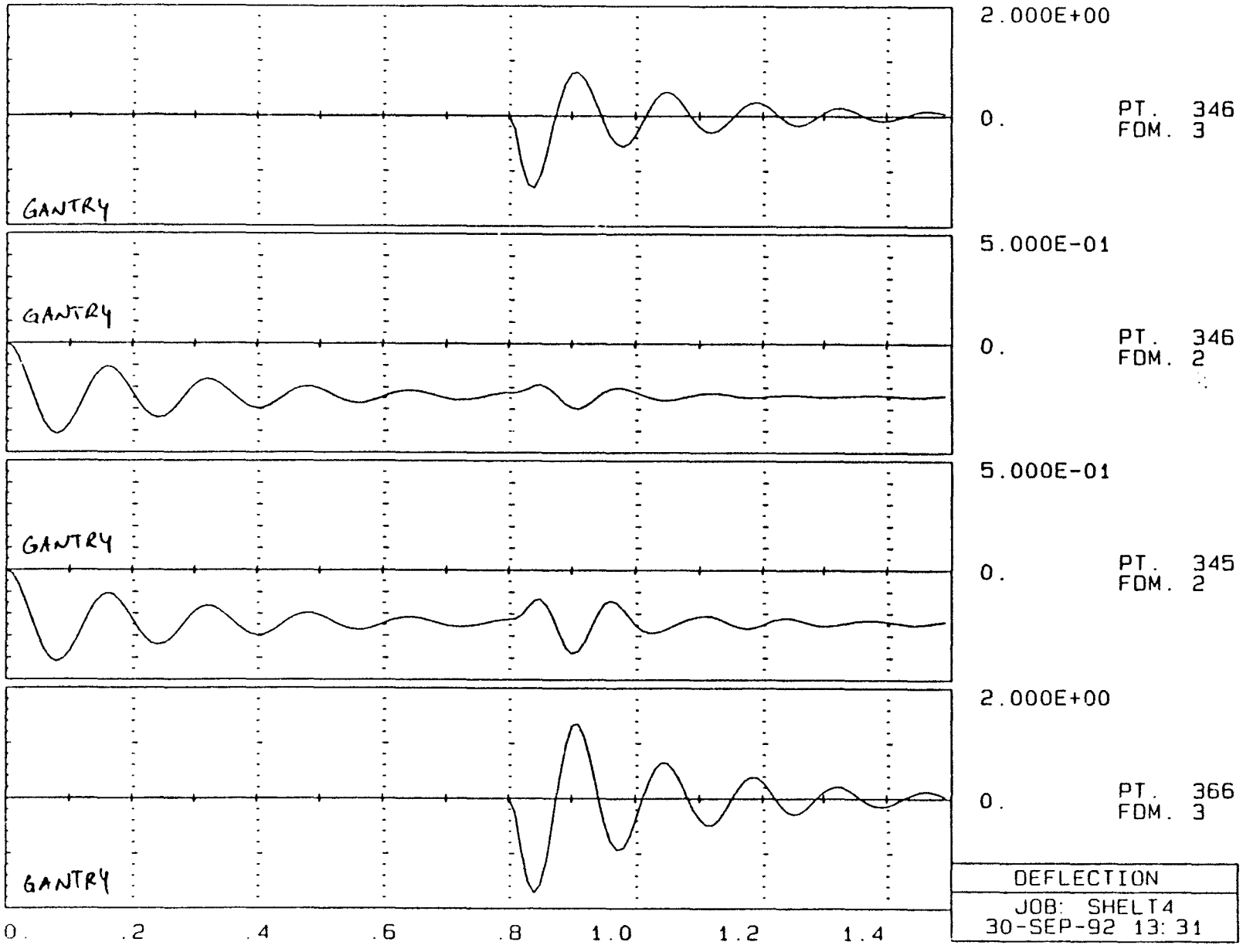
2.000E+00
0.
PT. 346
FDM. 3
GANTRY
5.000E-01
0.
PT. 346
FDM. 2
GANTRY
5.000E-01
0.
PT. 345
FDM. 2
GANTRY
2.000E+00
0.
PT. 366
FDM. 3
GANTRY
0.
.2
.4
.6
.8
1.0
1.2
1.4
DEFLECTION
JOB: SHELT4
30-SEP-92 13:31

Figure 96

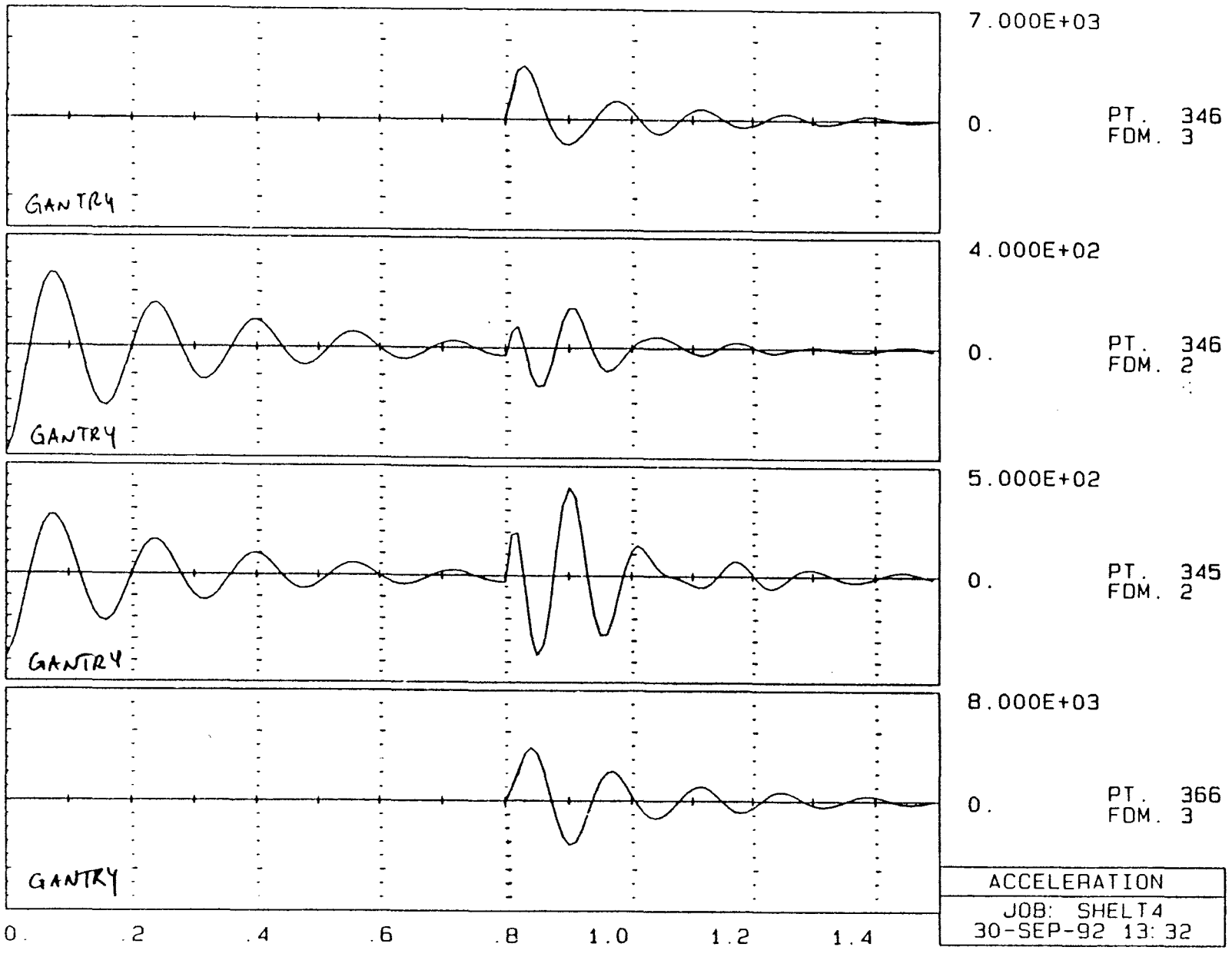
7.000E+03
0.
PT. 346
FDM. 3
GANTRY
4.000E+02
0.
PT. 346
FDM. 2
GANTRY
5.000E+02
0.
PT. 345
FDM. 2
GANTRY
8.000E+03
0.
PT. 366
FDM. 3
GANTRY
0.
.2
.4
.6
.8
1.0
1.2
1.4
ACCELERATION
JOB: SHELT4
30-SEP-92 13:32

Figure 97

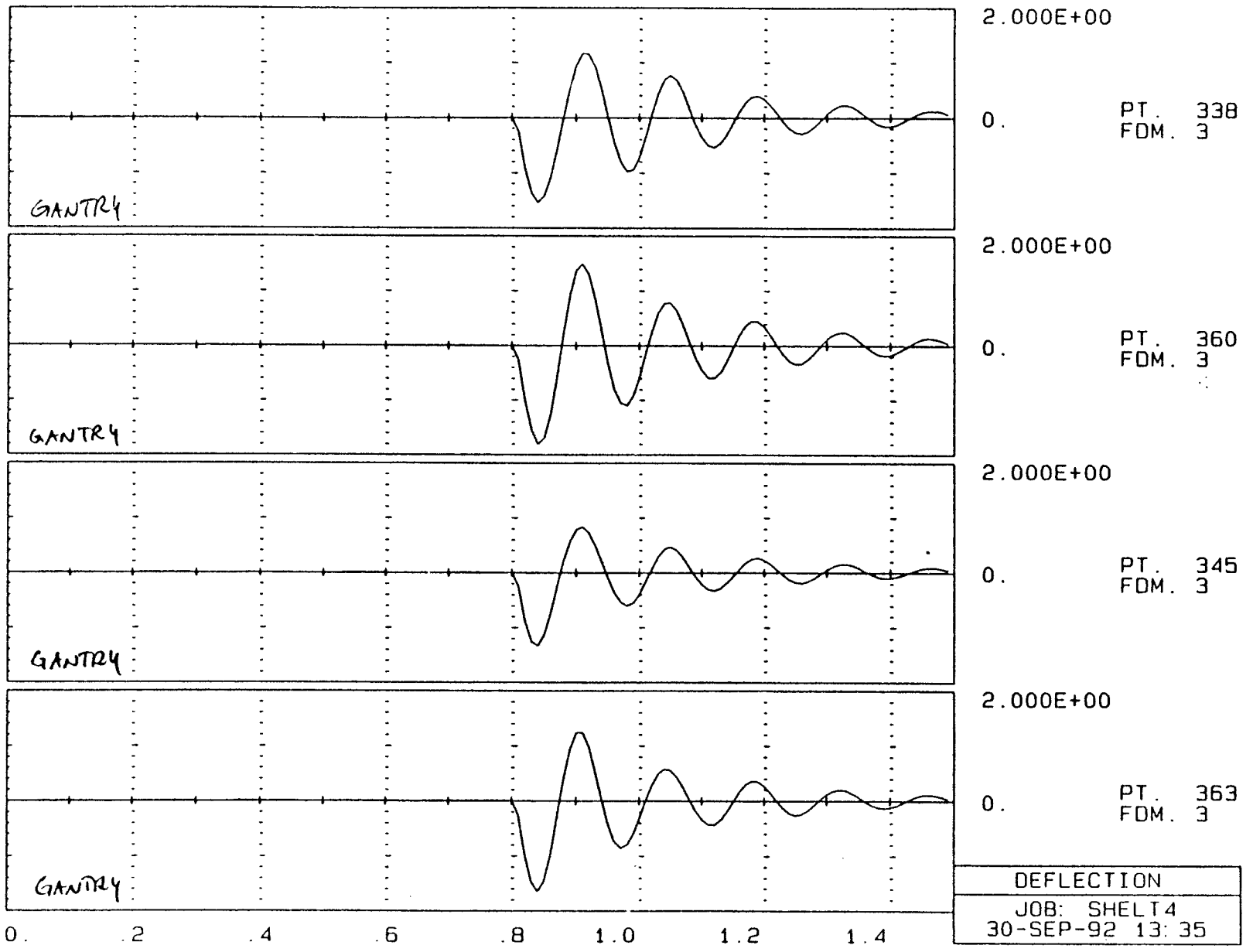
2.000E+00
0.
PT. 338
FDM. 3
GANTRY
2.000E+00
0.
PT. 360
FDM. 3
GANTRY
2.000E+00
0.
PT. 345
FDM. 3
GANTRY
2.000E+00
0.
PT. 363
FDM. 3
GANTRY
0.
.2
.4
.6
.8
1.0
1.2
1.4
DEFLECTION
JOB: SHELT4
30-SEP-92 13:35

Figure 98

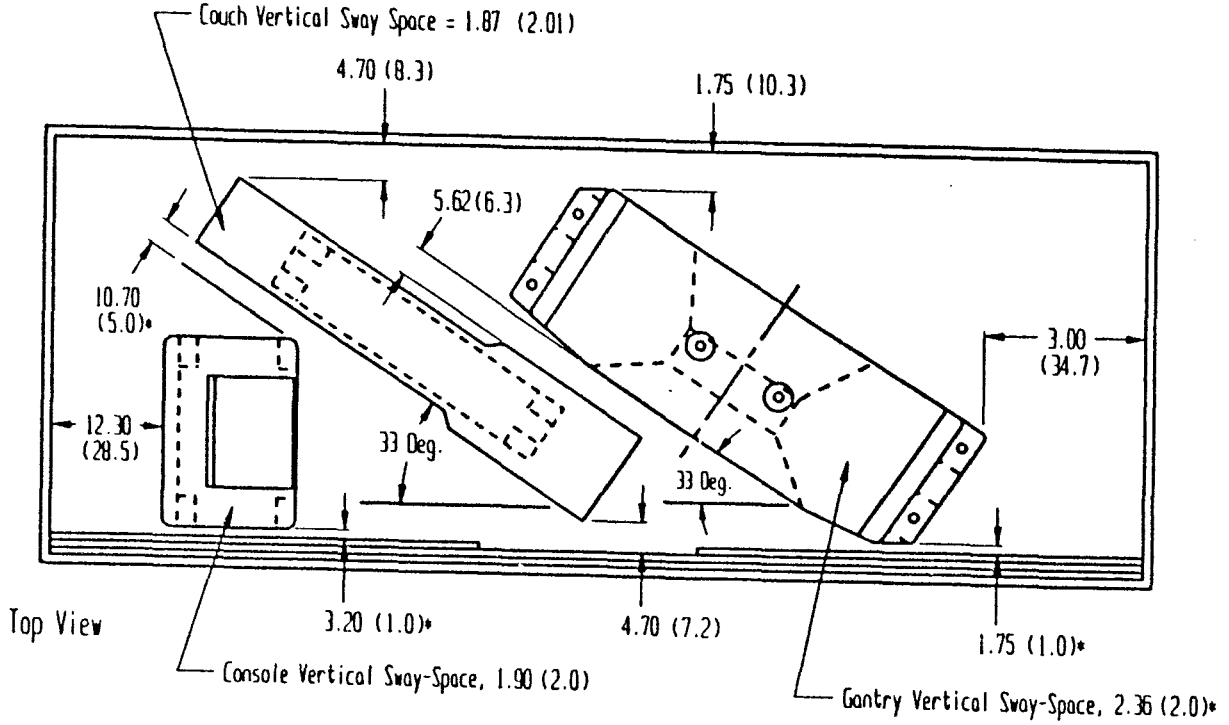

Figure 99. Calculated Mininun Required Sway-Space, Undeflected Position to Peak Displacenent, in inches. Ellipses Indicate Available Space, Based on Drawings. Asterisk Indicates Insufficient Sway Space in Prototype. Refer to Table 3.

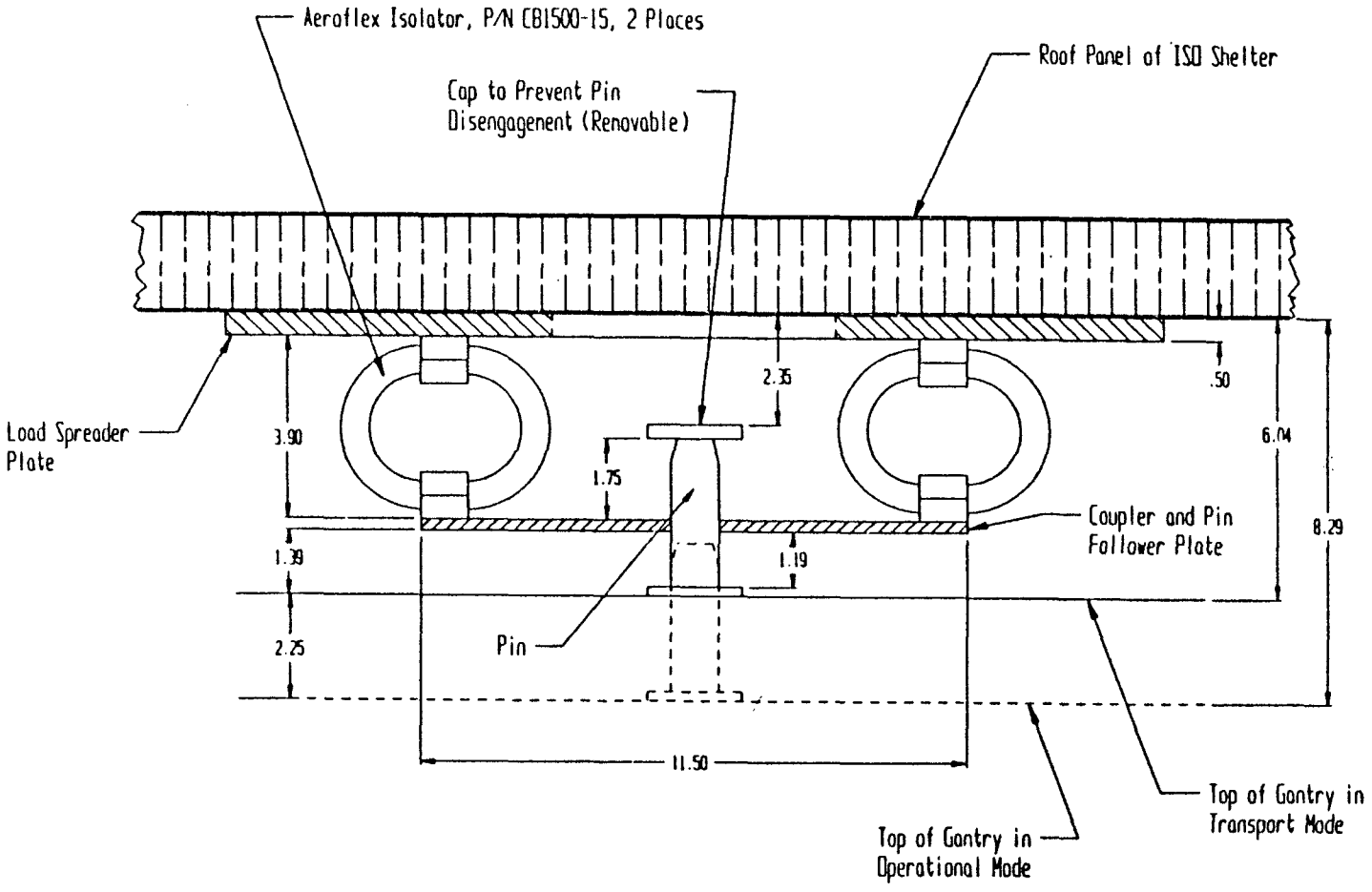

FIGURE 100. Proposed Concept to Replace Pin-In-Cup Design for Gantry Top Restraint, Prevents Pin Disengagenent and Inproves Restraint Characteristics.